ISSN 1756-1841 VOLUME 29 NUMBER 6 2026

International Journal of Rheumatic Diseases

Official journal of the Asia Pacific League of Associations for Rheumatology (APLAR)

WILEY

International Journal of Rheumatic Diseases

For submission instructions, subscription and all other information visit http://onlinelibrary.wiley.com/journal/10.1111/(ISSN)1756-185X

View this journal online at wileyonlinelibrary.com/journal/apl

International Journal of Rheumatic Diseases

WILEY

International Journal of Rheumatic Diseases

ORIGINAL ARTICLE

Outcomes of Vascular Interventions in Takayasu Arteritis and the Role of Biologic Therapy: A Multicenter Retrospective Study

Aysegul Avcu[1] | Sema Kaymaz-Tahra[2] | Rıza Can Kardas[3] | Fatma Basibuyuk[4] | Ömer Uludağ[5] | Duygu Kerim[6] | Senar San[7] | Hasan Kocaayan[8] | Zeliha Ademoglu[9] | Gokce Kenar Artin[4] | Burak Ince[5] | Hakan Emmungil[9] | Servet Akar[8] | Ayse Cefle[7] | Ayten Yazici[7] | Gokhan Keser[6] | Kenan Aksu[6] | Murat İnanc[5] | Fatos Onen[4] | Hamit Kucuk[3] | Haner Direskeneli[1] | Fatma Alibaz-Oner[1]

[1]Department of Internal Medicine, Division of Rheumatology, Marmara University, School of Medicine, Istanbul, Türkiye | [2]Department of Internal Medicine, Division of Rheumatology, Bahcesehir University, School of Medicine, Istanbul, Türkiye | [3]Department of Internal Medicine, Division of Rheumatology, Gazi University, School of Medicine, Ankara, Türkiye | [4]Department of Internal Medicine, Division of Rheumatology, Dokuz Eylul University, School of Medicine, Izmir, Türkiye | [5]Department of Internal Medicine, Division of Rheumatology, Faculty of Medicine, Istanbul University, Istanbul, Türkiye | [6]Department of Internal Medicine, Division of Rheumatology, Ege University, School of Medicine, Izmir, Türkiye | [7]Department of Internal Medicine, Division of Rheumatology, Kocaeli University, School of Medicine, Kocaeli, Türkiye | [8]Department of Internal Medicine, Division of Rheumatology, İzmir Katip Celebi University, School of Medicine, Izmir, Türkiye | [9]Department of Internal Medicine, Division of Rheumatology, Trakya University, School of Medicine, Edirne, Türkiye

Correspondence: Fatma Alibaz-Oner (falibaz@gmail.com)

Received: 20 December 2025 | **Revised:** 12 May 2026 | **Accepted:** 27 May 2026

Keywords: biologic therapy | restenosis | Takayasu arteritis | vascular intervention

ABSTRACT

Objectives: Takayasu arteritis (TAK) may lead to arterial stenosis/occlusion and aneurysms, occasionally requiring vascular interventions. We evaluated outcomes, restenosis, and complications after vascular interventions in TAK and explored factors associated with restenosis.

Methods: We retrospectively included TAK patients who underwent extracardiac endovascular or surgical vascular interventions before or after TAK diagnosis across eight tertiary centers (1995–2024). Indications, disease activity status at the time of intervention, procedural characteristics, early/late outcomes, major complications, and restenosis were recorded. Restenosis was defined as > 70% stenosis on follow-up imaging performed ≥ 3 months after the procedure. Restenosis analyses were restricted to steno-occlusive lesions.

Results: We included 119 patients with 201 treated lesions (185 steno-occlusive lesions; 16 aneurysms/dissections). Of all procedures, 61.2% ($n = 123$) were performed after TAK diagnosis under immunosuppressive therapy. Follow-up imaging was available for 170/185 steno-occlusive procedures, and restenosis status was evaluable in 168 procedures; restenosis occurred in 82/168 (48.8%) with a median time to restenosis of 19.5 months. In exploratory Kaplan–Meier analysis, 1-, 3-, and 5-year restenosis-free patency rates were 76.8%, 63.6%, and 56.5%, respectively. In analyses restricted to post-diagnosis steno-occlusive procedures, crude restenosis was significantly less frequent under biologic therapy than without biologic therapy (30.8% vs. 53.1%; Fisher's exact $p = 0.040$); however, biologic therapy was not associated with time to restenosis in Cox regression (HR 1.01, 95% CI 0.51–1.99; $p = 0.97$) or patient-clustered Cox analysis (HR 1.01, 95% CI 0.47–2.18; $p = 0.98$). Major complication rates were 3.9% for endovascular procedures and 12.5% for surgical procedures. Overall mortality was 11.8%, with two deaths attributed to procedure-related complications.

Conclusions: Vascular interventions in selected patients with Takayasu arteritis were associated with acceptable major complication rates. Among post-diagnosis steno-occlusive procedures, biologic therapy was associated with lower restenosis rates in crude analyses; however, this association was not sustained after accounting for restenosis timing. Therefore, the potential role of biologic therapy in improving post-interventional vascular outcomes should be interpreted cautiously and requires confirmation in prospective studies with standardized imaging surveillance.

1 | Introduction

Takayasu arteritis (TAK) is a large vessel vasculitis characterized by granulomatous inflammation, although its etiopathogenesis remains incompletely understood [1]. The disease primarily affects the aorta and its major branches and is most commonly observed in young women aged 20 to 30. While TAK is a global disorder, its prevalence is remarkably higher in Asian populations—with Japan reporting up to 40 cases per million compared to only 0.9 cases per million in the United States [2].

The clinical presentation of TAK is highly variable. Some patients may remain asymptomatic, while others develop serious complications such as hypertension, myocardial infarction, or stroke [3]. Traditionally, TAK is considered to progress through three distinct phases. The initial phase is marked by systemic inflammation and pre-stenotic changes; the second phase is characterized by the development of stenotic or aneurysmal arterial damage; and the final phase is a fibrotic, "burnt-out" stage. However, a pronounced systemic inflammatory response is not always evident, which can complicate a clear delineation of these phases. Consequently, diagnosis often occurs during the stenotic/aneurysmal phase or, in some cases, during the fibrotic phase, leading to a delay in identifying significant arterial damage [4].

Recent advances in non-invasive imaging techniques and the adoption of combined immunosuppressive treatment strategies have facilitated earlier diagnosis and more effective disease management [5, 6]. Early detection and appropriate treatment can significantly curb disease progression and minimize vascular complications. Glucocorticoids form the cornerstone of TAK treatment, while non-biologic disease-modifying antirheumatic drugs (DMARDs) are commonly used as steroid-sparing agents. In patients with relapsing or refractory disease despite conventional DMARD therapy, biologic agents such as tocilizumab or TNF inhibitors may be considered. Interventional or surgical procedures, including endovascular or open techniques, are indicated for symptomatic vascular lesions that persist despite medical therapy (for instance, arterial stenosis leading to limb claudication) or in scenarios where there is a risk of severe complications over time (e.g., a rapidly expanding aortic aneurysm) [7]. Nonetheless, the long-term outcomes and complication rates associated with these interventions continue to be a matter of debate. Contemporary studies continue to show substantial heterogeneity in post-interventional outcomes in TAK, with restenosis and long-term patency varying according to vascular territory, procedure type, disease activity, and follow-up duration. Recent cohorts, including large percutaneous intervention series and open/endovascular surgical cohorts, have emphasized that restenosis remains a major determinant of long-term outcome despite high early technical success rates [8–10].

This study aimed to retrospectively evaluate the outcomes of vascular interventions performed in patients with Takayasu arteritis, with particular emphasis on restenosis, procedure-related complications, and long-term efficacy. In addition, we aimed to assess factors associated with restenosis, including the potential impact of biologic therapies on post-interventional vascular outcomes. These findings may help clarify optimal interventional and medical strategies to improve long-term vascular outcomes in patients with TAK.

2 | Materials and Methods

2.1 | Study Population

This retrospective cohort study included 119 patients with Takayasu arteritis who fulfilled the 1990 ACR and/or 2022 ACR/EULAR classification criteria between 1995 and 2024, with a minimum post-intervention follow-up of at least 3 months. Patients with a history of extracardiac endovascular or surgical vascular interventions before or after diagnosis were enrolled from eight tertiary centers. The study was approved by the Marmara University Ethics Committee (Approval No: 09.2024.1330) and conducted in accordance with the Declaration of Helsinki.

Medical records were reviewed to document demographic characteristics, angiographic subtype according to the Numano classification [11], disease activity status, and inflammatory markers [erythrocyte sedimentation rate (ESR) and C-reactive protein (CRP)] at the time of intervention. Disease activity status at the time of intervention was retrospectively recorded as active or inactive based on physician global assessment (PGA) documented in the medical records. PGA reflected the treating physician's assessment and incorporated clinical findings, inflammatory markers, and available imaging information when documented.

Comorbidities, including hypertension (HT), diabetes mellitus (DM), hyperlipidemia (HL), coronary artery disease (CAD), and cerebrovascular disease (CVD), were recorded. Treatment regimens at the time of intervention included conventional synthetic DMARDs, such as methotrexate, azathioprine, and leflunomide, and biologic agents, such as infliximab, tocilizumab, and adalimumab. Glucocorticoid therapy before and during the intervention was classified by prednisone-equivalent dose as low (<7.5 mg/day), medium (≥ 7.5 to <30 mg/day), and high (≥ 30 mg/day). Post-intervention antithrombotic therapy, including antiplatelet therapy such as

acetylsalicylic acid and clopidogrel, and anticoagulant therapy, was also documented.

2.2 | Procedures

Intervention indications were based on clinical and radiological findings, including limb claudication, uncontrolled hypertension, neurological symptoms, aneurysm formation, and arterial dissection. Procedures included balloon angioplasty, stent placement, bypass grafting, endarterectomy, and thoracic or abdominal endovascular aneurysm repair (TEVAR/EVAR). Treated vessels were categorized as the aorta, renal arteries, subclavian arteries, carotid arteries, iliofemoral arteries, and other major vascular territories.

Early technical success for steno-occlusive lesions was defined as residual stenosis < 30%, in line with Society for Vascular Surgery reporting standards for endovascular arterial interventions [12]. For aneurysm or dissection procedures, early success was defined as complete exclusion of the aneurysm or false lumen without endoleak. Late procedural outcomes for steno-occlusive lesions were evaluated using vascular patency and restenosis outcomes. Restenosis was defined as > 70% stenosis detected on follow-up imaging, including CT angiography, MR angiography, or Doppler ultrasonography, performed ≥ 3 months after intervention. The > 70% threshold was selected to capture severe and clinically relevant restenosis, consistent with vascular practice in which ≥ 70% diameter narrowing is generally considered hemodynamically significant [13]. Restenosis analyses were restricted to steno-occlusive lesions; aneurysm and dissection procedures were excluded from these analyses. Follow-up imaging was performed according to symptoms, clinical suspicion, or physician decision rather than a standardized surveillance protocol. Therefore, restenosis outcomes represent clinically assessed restenosis in routine practice rather than protocol-driven imaging surveillance.

Repeat procedures were assessed using the complete procedural dataset. A repeat procedure was defined as a vascular intervention performed in a subsequent session after a previous intervention in the same patient. Repeat procedures were classified as same-territory or different-territory interventions according to the recorded vascular territory.

2.3 | Complications

In this study, minor complications were defined as events manageable with short-term observation or conservative medical treatment, such as mild bleeding, hematoma formation, or transient blood pressure changes. Major complications were defined as those requiring prolonged hospitalization, interventional or surgical management, or those potentially resulting in permanent sequelae or death. This category included perforation, thromboembolic events, severe bleeding, infarction, vascular occlusion, and organ failure.

Because minor complications could not be comprehensively identified from retrospective patient records, only major complication rates were reported. Complication rates for endovascular and surgical procedures were analyzed separately to compare profiles between the intervention types.

2.4 | Statistical Analysis

All statistical analyses were performed using SPSS version 28.0. Continuous variables are presented as mean ± standard deviation (SD) or median (IQR 25–75), and categorical variables are presented as frequencies and percentages. Normality of distribution was assessed using the Kolmogorov–Smirnov or Shapiro–Wilk tests. Student's *t*-test was used for group comparisons of normally distributed continuous variables, whereas the Mann–Whitney U test was applied for non-normally distributed variables. Categorical variables, including restenosis, intervention timing (pre- vs. post-diagnosis), disease activity status, and biologic therapy use, were compared using Chi-square or Fisher's exact tests, as appropriate. Treatment-related analyses, including glucocorticoid, conventional synthetic DMARD, and biologic DMARD exposure, were restricted to procedures performed after the diagnosis of Takayasu arteritis. Analyses assessing the association between biologic therapy and restenosis were further restricted to post-diagnosis steno-occlusive procedures with available restenosis status. Because restenosis is a time-dependent outcome, exploratory time-to-event analyses were performed for steno-occlusive procedures with available restenosis status and analyzable follow-up or restenosis time. Restenosis-free patency was estimated using Kaplan–Meier analysis, and 1-, 3-, and 5-year patency rates were calculated. Cox proportional hazards regression was used to evaluate the association between biologic therapy and time to restenosis. Cox proportional hazards models evaluating biologic therapy were first performed as univariable exploratory analyses. Additional parsimonious adjusted Cox models were constructed using selected clinically relevant covariates, including age, sex, disease activity at intervention, Numano type V disease, and atherosclerotic risk factors. Because some patients underwent more than one vascular procedure, an exploratory Cox model with patient-clustered robust standard errors was also performed to account for intra-patient correlation. These time-to-event analyses were considered exploratory because of the retrospective design, heterogeneous imaging intervals, and incomplete time-to-event information in some procedures. A two-sided p value < 0.05 was considered statistically significant.

3 | Results

3.1 | Patient Characteristics

The study included 119 patients, consisting of 101 females and 18 males. Patient demographics, comorbidities, and angiographic subtypes are summarized in Table 1. The median age at vascular intervention was 39 years (27–49), and the median age at diagnosis was 33 years (23–47). The median follow-up duration was 105 months (39–163), and the median diagnostic delay was 15.5 months (6–48). Patients who underwent interventions before diagnosis had significantly longer diagnostic delays than those treated after diagnosis (27 vs. 12 months, $p < 0.001$).

TABLE 1 | Characteristics of patients with Takayasu arteritis ($n = 119$).

Female/Male (*n*/*n*)	101/18
Age at procedure, years, median (Q1–Q3)	39 (27–49)
Age at onset, years, median (Q1–Q3)	28 (20.8–41.3)
Age at diagnosis, *years*, median (Q1–Q3)	33 (23–47)
Comorbidity, *n* (%)	
HT	75 (63%)
HL	22 (18.5%)
CVD	11 (9.2%)
DM	7 (5.9%)
CAD	7 (5.9%)
Type of vascular involvement, *n* (%) (Numano classification)	
Type 1	21 (17.6%)
Type 2	12 (10.1%)
Type 3	8 (6.7%)
Type 4	12 (10.1%)
Type 5	66 (55.5%)

Abbreviations: CAD, coronary artery disease; CVD, cerebrovascular disease; DM, diabetes mellitus; HL, hyperlipidemia; HT, hypertension; IQR, interquartile range.

According to the Numano classification, Type 5 was the most common angiographic subtype (55.5%). Hypertension was the most frequent comorbidity, and at least one coexisting atherosclerotic risk factor or disease was identified in 72% of patients. Current or former smoking was documented in 32.8%.

Among the 123 procedures performed after TAK diagnosis, most were performed under ongoing immunosuppressive therapy. At the time of post-diagnosis procedures, 88 procedures (71.5%) were performed under glucocorticoids, 103 (83.7%) under conventional synthetic DMARDs, and 44 (35.8%) under biologic DMARDs. Post-procedure antiplatelet, anticoagulant, and statin treatments are summarized in Table 2. Median laboratory values at the time of intervention were CRP 3.4 mg/L (2.7–7.85) and ESR 19 mm/h (8.7–29).

3.2 | Procedures

A total of 201 vascular lesions were included: 185 stenotic/occlusive lesions and 16 aneurysm/dissection lesions. Overall, 123 procedures (61.2%) were performed after TAK diagnosis. The most common indications for vascular intervention were limb claudication, uncontrolled hypertension, neurologic symptoms, aneurysm formation, and abdominal pain (Figure 1).

The distribution of procedure types and treated vascular territories is shown in Table 3. Endovascular procedures were more frequent than surgical procedures, with stent placement being the most common intervention. The overall early technical success rate was 91.5% ($n = 184$).

TABLE 2 | Medical treatment at the time of procedure and post-procedure antiplatelet/statin treatment.

Immunosuppressive therapy at the time of post-diagnosis procedures ($n = 123$)	
Treatment, *n* (%)	
Glucocorticoids (prednisone-equivalent)	88 (71.5%)
Low dose (< 7.5 mg/day)	59 (48%)
Medium dose (≥ 7.5 to < 30 mg/day)	17 (14%)
High dose (≥ 30 mg/day)	12 (10%)
csDMARD	103 (83.7%)
bDMARD	44 (35.8%)
Post-procedure antiplatelet/statin treatment in steno-occlusive procedures **($n = 185$)**	
Statin	82 (44%)
ASA monotherapy	85 (46%)
Clopidogrel monotherapy	7 (4%)
Dual antiplatelet therapy (ASA plus clopidogrel)	82 (44%)

Abbreviations: ASA, acetylsalicylic acid; bDMARD, biologic disease-modifying antirheumatic drug; csDMARD, conventional synthetic disease-modifying antirheumatic drug.

Twenty-eight patients underwent vascular interventions in more than one procedural session. After excluding same-session interventions, 49 later-session repeat procedures were identified, including 34 same-territory and 15 different-territory interventions. Repeat procedures most commonly involved the iliofemoral, renal, subclavian, and carotid territories.

3.3 | Follow-Up and Restenosis

The median post-procedural follow-up duration was 106 months (34–165.5). Follow-up imaging was available for 170/185 (91.9%) steno-occlusive procedures, and restenosis status was evaluable in 168 procedures. Restenosis occurred in 82/168 procedures (48.8%), with a median time to restenosis of 19.5 months (6.0–53.5). In exploratory Kaplan–Meier analysis including 161 steno-occlusive procedures with analyzable time-to-event data, 1-, 3-, and 5-year restenosis-free patency rates were 76.8%, 63.6%, and 56.5%, respectively. The median restenosis-free patency time was 87 months.

Restenosis rates were comparable between procedures performed before and after diagnosis (55% vs. 44%; $p = 0.20$) and between endovascular and surgical interventions (46% vs. 58%; $p = 0.25$). Restenosis varied by Numano angiographic subtype, as shown in Figure 2.

Among post-diagnosis steno-occlusive procedures with evaluable restenosis status and available disease activity data, 22/103 (21.4%) were performed during physician-assessed active disease. Restenosis rates were comparable between procedures performed during active and inactive disease (10/22, 45.5% vs. 36/81, 44.4%; Fisher's exact $p = 1.000$). Restenosis rates were also

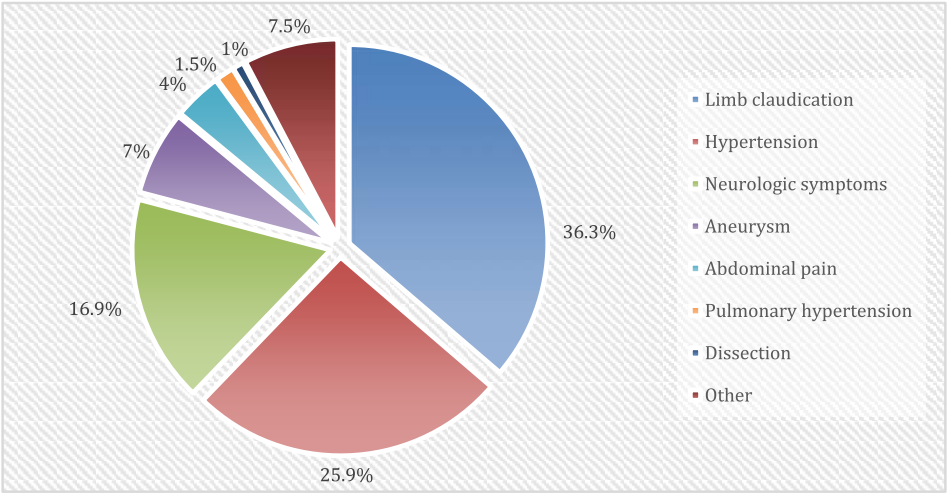

FIGURE 1 | Distribution of indications for vascular interventions ($n = 201$ procedures). Distribution of indications for vascular interventions ($n = 201$ procedures). The most frequent indication was limb claudication (36.3%; $n = 73$), followed by uncontrolled hypertension (25.9%; $n = 52$), neurologic symptoms (16.9%; $n = 34$), aneurysm (7.0%; $n = 14$), abdominal pain (4.0%; $n = 8$), other indications (7.5%; $n = 15$), pulmonary hypertension (1.5%; $n = 3$), and dissection (1.0%; $n = 2$).

TABLE 3 | Distribution of arterial lesions and vascular interventions.

Arterial lesion type, *n* (%)	
Stenosis	185 (92%)
Aneurysm/dissection	16 (8%)
Arterial territory, *n*(%)	
Renal artery	52 (25.9%)
Subclavian artery	30 (14.9%)
Carotid artery	28 (13.9%)
Aorta	28 (13.9%)
Iliofemoral artery	27 (13.4%)
Mesenteric artery	8 (3.9%)
Pulmonary artery	3 (1.5%)
Brachial artery	3 (1.5%)
Axillary artery	3 (1.5%)
Truncus brachiocephalicus	2 (1%)
Other	17 (8.5%)
Type of procedure, *n* (%)	
Stent	116 (57.7%)
Balloon angioplasty	33 (16.4%)
Bypass grafting	44 (21.9%)
Endarterectomy	4 (2%)
TEVAR/EVAR	4 (2%)

Abbreviation: TEVAR/EVAR, thoracic or abdominal endovascular aneurysm repair.

comparable according to atherosclerotic risk factors, including hypertension, diabetes mellitus, hyperlipidemia, coronary artery disease, and cerebrovascular disease.

Among post-diagnosis steno-occlusive procedures with available restenosis and biologic treatment data, crude restenosis was significantly less frequent in procedures performed under biologic therapy than in those performed without biologic therapy (12/39, 30.8% vs. 34/64, 53.1%; Fisher's exact $p = 0.040$) (Figure 3). Kaplan–Meier curves according to biologic therapy status are shown in Figure 4. However, this crude association was not confirmed in exploratory time-to-event analyses. Of the 103 post-diagnosis steno-occlusive procedures with available restenosis and biologic treatment data, 100 had analyzable time-to-event information and were included in the Kaplan–Meier and Cox analyses. In univariable exploratory Cox regression analysis, biologic therapy was not significantly associated with time to restenosis (HR 1.01, 95% CI 0.51–1.99; $p = 0.97$). Similar findings were obtained in the patient-clustered robust Cox model (HR 1.01, 95% CI 0.47–2.18; $p = 0.98$). In parsimonious exploratory adjusted Cox models including selected demographic and clinically relevant covariates, biologic therapy remained unassociated with time to restenosis (Table S2). Exploratory analyses did not show statistically significant associations between restenosis and glucocorticoid or conventional synthetic DMARD use in post-diagnosis procedures.

To address potential confounding by indication, baseline and procedural characteristics were compared between post-diagnosis steno-occlusive procedures performed with and without biologic therapy at the time of intervention. Procedures performed under biologic therapy had longer disease duration at intervention, more frequent prior vascular intervention, shorter post-procedural follow-up, and a different Numano angiographic distribution compared with procedures performed without biologic therapy (Table S1).

3.4 | Complications and Mortality

The major complication rate was 3.9% ($n = 6$) for endovascular procedures and 12.5% ($n = 6$) for surgical procedures.

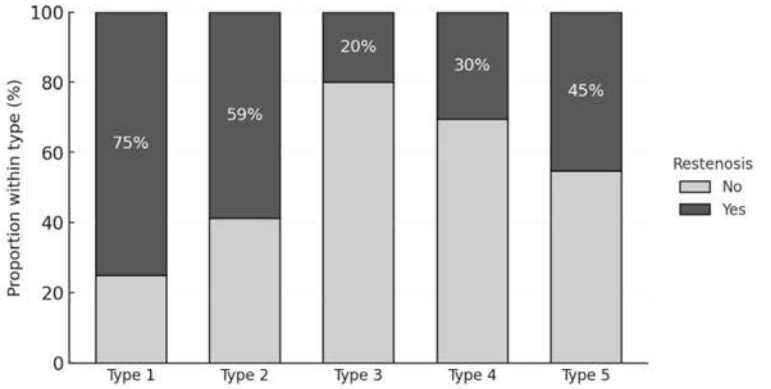

Type 1: 21/28 (75%, 95% CI 57%–87%); Type 2: 10/17 (59%, 95% CI 36%–78%); Type 3: 1/5 (20%, 95% CI 4%–62%); Type 4: 7/23 (30%, 95% CI 16%–51%); Type 5: 43/95 (45%, 95% CI 36%–55%).

FIGURE 2 | Restenosis rates by angiographic type in Takayasu arteritis. Stacked bar chart showing, for each angiographic type, the proportion of steno-occlusive procedures with restenosis (dark gray) and without restenosis (light gray). Percentages within the bars indicate the restenosis rate for each type; values are shown as n/N (%), and corresponding 95% confidence intervals are provided in the figure.

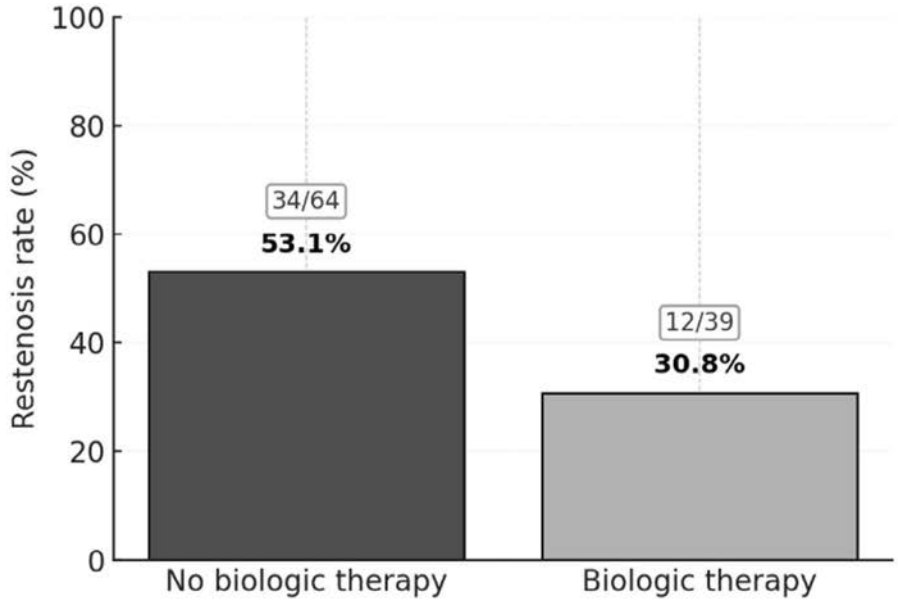

No biologic: 34/64 (53.1%, 95% CI 41.1%–64.8%); Biologic: 12/39 (30.8%, 95% CI 18.6%–46.4%). Fisher's exact p = 0.040.

FIGURE 3 | Restenosis rates in post-diagnosis steno-occlusive procedures with and without biologic therapy. Restenosis occurred in 53.1% of procedures not receiving biologic therapy versus 30.8% of procedures receiving biologic therapy (Fisher's exact $p = 0.040$).

Endovascular complications included femoral artery pseudoaneurysm, femoral artery dissection, hypotension requiring vasopressor support in the intensive care unit, and femoral artery embolism. Major surgical complications included graft leakage, graft infection, pericardial tamponade, gastrointestinal bleeding associated with antiplatelet use, and graft separation.

The overall mortality rate was 11.8% (14/119 patients), with two deaths attributed to intervention-related complications. One death occurred following abdominal aortic bypass, and another was due to intracranial hemorrhage after stent placement.

4 | Discussion

Previous studies have reported heterogeneous results regarding the efficacy and durability of surgical and endovascular interventions in Takayasu arteritis. In this multicenter retrospective cohort, we evaluated early technical success, long-term restenosis-free patency, treatment-related factors, and major

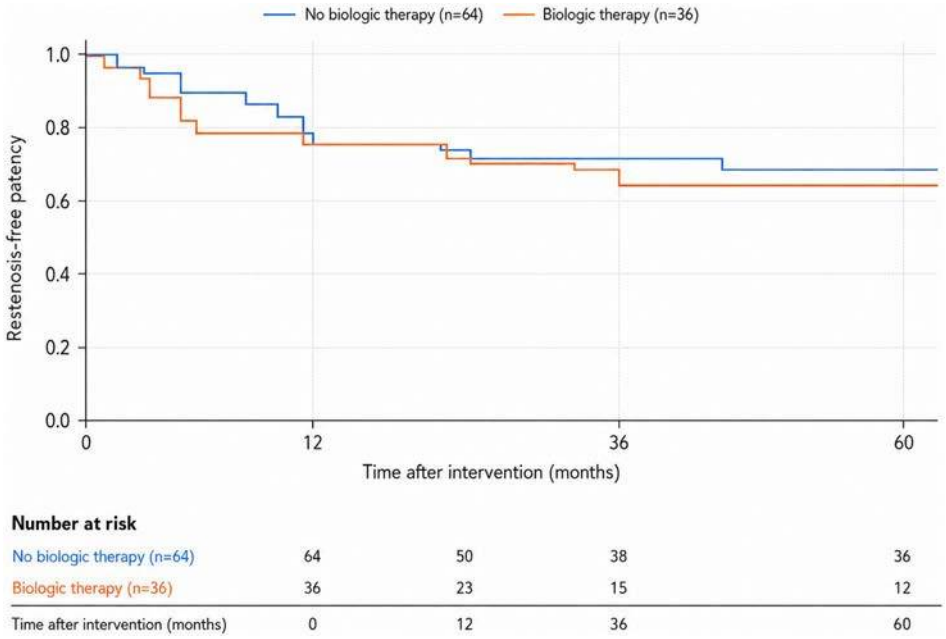

FIGURE 4 | Kaplan–Meier curves for restenosis-free patency after vascular intervention according to biologic therapy exposure. The analysis included 100 post-diagnosis steno-occlusive procedures with analyzable time-to-event data: 64 without biologic therapy and 36 with biologic therapy. Number-at-risk values are shown below the x-axis. Biologic therapy was not significantly associated with time to restenosis in the univariable exploratory Cox proportional hazards model.

complications after vascular interventions in TAK. Given the limited long-term data on vascular interventions in this disease, our findings contribute to the real-world evidence on post-interventional vascular outcomes in TAK.

Restenosis remains a major limitation after vascular interventions despite advances in endovascular techniques. In peripheral artery disease, particularly involving the femoropopliteal region, primary vessel patency rates range between 30% and 80% within 1–2 years depending on lesion complexity and procedural technique [14]. Similarly, long-term patency after revascularization in TAK is variable and appears to be influenced by vascular territory, lesion characteristics, disease activity, and intervention type. Our 1-, 3-, and 5-year restenosis-free patency estimates highlight the need for long-term vascular surveillance after intervention.

Restenosis was numerically higher after surgery than after endovascular intervention, without a statistically significant difference. Although several studies suggest superior long-term patency with surgery, the lack of a clear advantage in our cohort may relate to the smaller surgical sample and heterogeneity in lesion characteristics. In a 10-year retrospective analysis, Diao et al. reported patency rates of 48.8% in surgically treated patients compared with 31.8% in those undergoing endovascular intervention, favoring surgery [15]. Likewise, a recently published study demonstrated markedly improved patency rates after surgical intervention during the first three years of follow-up [9].

Patency outcomes also differed substantially across vascular territories, supporting the concept that outcomes in TAK are influenced not only by intervention type but also by local vascular anatomy, lesion characteristics, and follow-up strategy. In our cohort, restenosis was most frequent in the brachiocephalic artery, followed by the subclavian, mesenteric, and iliofemoral arteries. Joseph et al. showed that repeat percutaneous interventions may improve overall success in patients with restenosis, although long subclavian artery lesions had lower initial success and higher reintervention rates [10]. Similarly, Gülcü et al. emphasized the importance of close surveillance and repeat interventions to maintain patency [16]. The concentration of repeat procedures in the iliofemoral territory in our cohort further supports the need for territory-specific long-term follow-up.

Beyond procedural approach, disease activity at the time of intervention is an important consideration in TAK. Elective vascular interventions are generally recommended during quiescent disease whenever feasible; however, intervention may be necessary in selected patients with life-, organ-, or limb-threatening vascular lesions. Urgent interventions were uncommon in this series, consistent with previous reports indicating that critical ischemic manifestations, such as digital gangrene, are rare in TAK [17]. Glucocorticoid treatment is recommended in active or suspected active disease during the perioperative period [18]. Among post-diagnosis procedures, most were performed under ongoing medical treatment, with glucocorticoid use in 71.5% of interventions. In the analysis restricted to post-diagnosis steno-occlusive procedures with available disease activity data, restenosis rates were comparable between active and inactive disease. This finding is consistent with Joseph et al., who reported that restenosis was not directly related to baseline disease activity, although persistent disease activity during follow-up was associated with restenosis [10]. Given the difficulty of assessing disease activity in TAK and the possibility of angiographic progression despite apparent clinical remission, this negative finding does not override the recommendation to perform elective interventions during quiescent disease whenever feasible [19].

Early use of biologic therapies may reduce the subsequent need for surgical intervention in selected patients with TAK [5]. Porter et al. also reported that early combined immunosuppression and timely transition to biologic therapy improved outcomes in patients with supra-aortic TAK presenting with cerebral ischemia [20]. Biologic therapy was associated with a significantly lower crude restenosis rate in post-diagnosis steno-occlusive procedures; however, this association was not sustained in Cox models incorporating the timing of restenosis. This discrepancy may reflect confounding by treatment era, follow-up intensity, lesion characteristics, disease severity, or timing of biologic initiation rather than a direct treatment effect. Although post-interventional restenosis is partly driven by vascular remodeling and neointimal hyperplasia [21], our findings do not establish an independent protective effect of biologic therapy on restenosis.

Major complication rates were acceptable, particularly for endovascular procedures. In the present study, major complications occurred in 3.9% of endovascular procedures and 12.5% of surgical procedures. In the general population, major complications after elective percutaneous peripheral revascularization are reported at approximately 2.1% [22], whereas peripheral vascular surgery has been associated with complication rates of around 30% [23]. Because TAK typically affects younger patients, age-related surgical risks may be lower than in atherosclerotic vascular disease; however, vascular inflammation, complex anatomy, and previous interventions may increase procedural risk [24]. The presence of acute-phase elevation during intervention has also been reported as an important risk factor for post-intervention complications [25], supporting the importance of inflammatory control before elective procedures.

Antiplatelet therapy has been proposed as part of peri-interventional management to support patency after endovascular procedures in TAK [24]. In the present study, dual antiplatelet therapy was prescribed in about half of the procedures performed for steno-occlusive lesions, reflecting variation in practice across centers. However, the optimal antithrombotic strategy after endovascular or surgical procedures remains insufficiently defined [26]. Furthermore, atherosclerotic comorbidities were common in this cohort. Chronic inflammation in TAK may accelerate atherosclerosis in the aorta and major branches [27]. Although traditional atherosclerotic risk factors were not significantly associated with restenosis, numerically higher rates among patients with coronary artery disease, diabetes mellitus, or cerebrovascular disease suggest that coexisting atherosclerosis may still influence long-term vascular outcomes.

Our study has several limitations. Its retrospective multicenter design may have introduced missing data, observational bias, and heterogeneity in procedural techniques, medical treatment, and timing of revascularization. Follow-up imaging was not performed according to a standardized surveillance protocol but was driven by symptoms, clinical need, or physician decision, which may have caused detection bias and underestimation of asymptomatic restenosis. Disease activity was assessed retrospectively using physician global assessment rather than uniformly available ITAS2010 or Kerr's criteria, limiting standardization across centers. Treatment-related analyses, including exploratory adjusted Cox models, are limited by potential residual confounding related to disease severity, lesion characteristics, treatment era, and follow-up intensity, as well as by the limited number of events, missing covariate data, repeated procedures within patients, and heterogeneous follow-up imaging.

In conclusion, vascular interventions in selected patients with Takayasu arteritis were associated with high early technical success and acceptable major complication rates, but restenosis remained common during long-term follow-up. Restenosis-free patency varied across vascular territories, supporting the need for individualized intervention planning and long-term vascular surveillance. Although biologic therapy was associated with lower crude restenosis rates in post-diagnosis steno-occlusive procedures, this association was not confirmed in time-to-event analyses. Prospective studies with standardized imaging follow-up are needed to clarify whether biologic therapy improves post-interventional vascular outcomes.

Author Contributions

Aysegul Avcu and Fatma Alibaz-Oner contributed to the conception and design of the study. Aysegul Avcu, Sema Kaymaz-Tahra, Rıza Can Kardas, Fatma Basibuyuk, Ömer Uludağ, Duygu Kerim, Senar San, Hasan Kocaayan, Zeliha Ademoglu, Gokce Kenar Artin, Burak Ince, Hakan Emmungil, Servet Akar, Ayse Cefle, Ayten Yazici, Gokhan Keser, Kenan Aksu, Murat İnanc, Fatos Onen, Hamit Kucuk, Haner Direskeneli, and Fatma Alibaz-Oner contributed to data acquisition, clinical data collection, and/or interpretation of the data. Aysegul Avcu drafted the manuscript. Fatma Alibaz-Oner and Haner Direskeneli critically revised the manuscript for important intellectual content. All authors reviewed and approved the final version of the manuscript and agree to be accountable for all aspects of the work.

Acknowledgments

The authors have nothing to report.

Funding

The authors have nothing to report.

Conflicts of Interest

The authors declare no conflicts of interest.

Data Availability Statement

The data that support the findings of this study are available from the corresponding author upon reasonable request.

References

1. G. Keser, K. Aksu, and H. Direskeneli, "Takayasu Arteritis: An Update," *Turkish Journal of Medical Sciences* 48, no. 4 (2018): 681–697.

2. D. Alnabwani, P. Patel, P. Kata, V. Patel, A. Okere, and P. Cheriyath, "The Epidemiology and Clinical Manifestations of Takayasu Arteritis: A Descriptive Study of Case Reports," *Cureus* 13, no. 9 (2021): e17998.

3. S. R. Sparks, A. Chock, S. Seslar, J. J. Bergan, and E. L. Owens, "Surgical Treatment of Takayasu's Arteritis: Case Report and Literature Review," *Annals of Vascular Surgery* 14, no. 2 (2000): 125–129.

4. E. Tombetti and J. C. Mason, "Takayasu Arteritis: Advanced Understanding Is Leading to New Horizons," *Rheumatology (Oxford, England)* 58, no. 2 (2019): 206–219.

5. J. C. Mason, "Surgical Intervention and Its Role in Takayasu Arteritis," *Best Practice & Research. Clinical Rheumatology* 32, no. 1 (2018): 112–124.

6. C. Dejaco, S. Ramiro, M. Bond, et al., "EULAR Recommendations for the Use of Imaging in Large Vessel Vasculitis in Clinical Practice: 2023 Update," *Annals of the Rheumatic Diseases* 83, no. 6 (2024): 741–751, https://doi.org/10.1136/ard-2023-224543.

7. B. Hellmich, A. Agueda, S. Monti, et al., "2018 Update of the EULAR Recommendations for the Management of Large Vessel Vasculitis," *Annals of the Rheumatic Diseases* 79, no. 1 (2020): 19–30.

8. X. Zhang, L. Gui, R. Li, et al., "Clinical Characteristics of Patients With Takayasu Arteritis Undergoing Open or Endovascular Operations in China," *Reviews in Cardiovascular Medicine* 25, no. 10 (2024): 373, https://doi.org/10.31083/j.rcm2510373.

9. J. Shin, A. Cho, A. Han, S. Ahn, S. Min, and S. K. Min, "Long-Term Patency and Complications of Endovascular and Surgical Revascularization for Takayasu Arteritis," *Vascular Specialist International* 40 (2024): 46, https://doi.org/10.5758/vsi.240090.

10. G. Joseph, V. S. Thomson, T. V. Attumalil, et al., "Outcomes of Percutaneous Intervention in Patients With Takayasu Arteritis," *Journal of the American College of Cardiology* 81, no. 1 (2023): 49–64.

11. A. Hata, M. Noda, R. Moriwaki, and F. Numano, "Angiographic Findings of Takayasu Arteritis: New Classification," *International Journal of Cardiology* 54, no. Suppl (1996): S155–S163.

12. M. C. Stoner, K. D. Calligaro, R. A. Chaer, et al., "Reporting Standards of the Society for Vascular Surgery for Endovascular Treatment of Chronic Lower Extremity Peripheral Artery Disease," *Journal of Vascular Surgery* 64, no. 1 (2016): e1–e21.

13. S. R. Bailey, J. A. Beckman, T. D. Dao, et al., "ACC/AHA/SCAI/SIR/SVM 2018 Appropriate Use Criteria for Peripheral Artery Intervention," *Journal of the American College of Cardiology* 73, no. 2 (2019): 214–237, https://doi.org/10.1016/j.jacc.2018.10.002.

14. J. A. Beckman, P. A. Schneider, and M. S. Conte, "Advances in Revascularization for Peripheral Artery Disease," *Circulation Research* 128, no. 12 (2021): 1885–1912.

15. Y. Diao, S. Yan, S. Premaratne, et al., "Surgery and Endovascular Management in Patients With Takayasu's Arteritis: A Ten-Year Retrospective Study," *Annals of Vascular Surgery* 63 (2020): 34–44.

16. A. Gülcü, N. S. Gezer, S. Akar, N. Akkoç, F. Önen, and A. Y. Göktay, "Long-Term Follow-Up of Endovascular Repair in the Management of Arterial Stenosis Caused by Takayasu's Arteritis," *Annals of Vascular Surgery* 42 (2017): 93–100.

17. M. M. Khan, A. K. Azad, M. K. Yadav, et al., "Digital Gangrene Is a Rare Presentation of Takayasu's Arteritis," *Mymensingh Medical Journal* 32, no. 4 (2023): 1208–1213.

18. M. Maz, S. A. Chung, A. Abril, et al., "2021 American College of Rheumatology/Vasculitis Foundation Guideline for the Management of Giant Cell Arteritis and Takayasu Arteritis," *Arthritis & Rhematology* 73, no. 8 (2021): 1349–1365.

19. G. S. Kerr, C. W. Hallahan, J. Giordano, et al., "Takayasu Arteritis," *Annals of Internal Medicine* 120, no. 11 (1994): 919–929, https://doi.org/10.7326/0003-4819-120-11-199406010-00004.

20. A. Porter, T. Youngstein, E. Tombetti, and J. C. Mason, "Biologic Therapy in Supra-Aortic Takayasu Arteritis Can Improve Symptoms of Cerebral Ischaemia Without Surgical Intervention," *Rheumatology (Oxford, England)* 59, no. Suppl 3 (2020): iii28–iii32.

21. T. Donisan, L. Madanat, D. V. Balanescu, A. Mertens, and S. Dixon, "Drug-Eluting Stent Restenosis: Modern Approach to a Classic Challenge," *Current Cardiology Reviews* 19, no. 3 (2023): e030123212355.

22. S. Malekzadeh, T. Rolf, F. Doenz, A. Chouiter, A. M. Jouannic, and S. D. Qanadli, "Safety of Elective Percutaneous Peripheral Revascularization in Outpatients: A 10-Year Single-Center Experience," *Diagnostic and Interventional Imaging* 100, no. 6 (2019): 347–352.

23. M. Kehlet, L. P. Jensen, and T. V. Schroeder, "Risk Factors for Complications After Peripheral Vascular Surgery in 3,202 Patient Procedures," *Annals of Vascular Surgery* 36 (2016): 13–21.

24. J. H. Jung, Y. H. Lee, G. G. Song, H. S. Jeong, J. H. Kim, and S. J. Choi, "Endovascular Versus Open Surgical Intervention in Patients With Takayasu's Arteritis: A Meta-Analysis," *European Journal of Vascular and Endovascular Surgery* 55, no. 6 (2018): 888–899.

25. D. Saadoun, M. Lambert, T. Mirault, et al., "Retrospective Analysis of Surgery Versus Endovascular Intervention in Takayasu Arteritis: A Multicenter Experience," *Circulation* 125, no. 6 (2012): 813–819.

26. V. Aboyans, R. Bauersachs, L. Mazzolai, et al., "Antithrombotic Therapies in Aortic and Peripheral Arterial Diseases in 2021: A Consensus Document," *European Heart Journal* 42, no. 39 (2021): 4013–4024.

27. F. Numano, Y. Kishi, A. Tanaka, M. Ohkawara, T. Kakuta, and Y. Kobayashi, "Inflammation and Atherosclerosis. Atherosclerotic Lesions in Takayasu Arteritis," *Annals of the New York Academy of Sciences* 902 (2000): 65–76, https://doi.org/10.1111/j.1749-6632.2000.tb06301.x.

Supporting Information

Additional supporting information can be found online in the Supporting Information section. **Table S1:** Baseline and procedural characteristics of post-diagnosis steno-occlusive procedures according to biologic therapy status at intervention. **Table S2:** Exploratory Cox models evaluating the association between biologic therapy and time to restenosis.

International Journal of Rheumatic Diseases

WILEY

International Journal of Rheumatic Diseases

LETTER TO THE EDITOR

Calcinosis Cutis in Sjögren's Syndrome With Interstitial Lung Disease

Norwin Philip L. Bation | Jan Mark T. Antenor | Sandra V. Navarra

Section of Rheumatology, University of Santo Tomas Hospital, Manila, Philippines

Correspondence: Norwin Philip L. Bation (nplbation@gmail.com)

Received: 14 April 2026 | **Revised:** 10 May 2026 | **Accepted:** 26 May 2026

Dear Editor,

Calcinosis cutis is characterized by the deposition of insoluble calcium salts in the skin and subcutaneous tissues and is most commonly associated with autoimmune connective tissue diseases (CTDs), particularly systemic sclerosis, and dermatomyositis [1]. In contrast, its occurrence in primary Sjögren's syndrome (pSS) is exceedingly rare and remains poorly characterized [2]. This rarity presents a critical gap in understanding its clinical spectrum, pathogenesis, and management. Here, we report a case of calcinosis cutis in pSS with concomitant interstitial lung disease (ILD), highlighting a potentially underrecognized association.

A 69-year-old woman presented with inflammatory arthritis, sicca symptoms, and fatigue. Serologic evaluation demonstrated strongly positive anti-SSA/Ro antibodies (> 600 U/mL; ULN 7), while antinuclear antibody, anti-dsDNA, anti-Smith, anti-RNP, rheumatoid factor, and anti-cyclic citrullinated peptide antibodies were negative. A diagnosis of pSS was established, and she was treated with hydroxychloroquine, tapering doses of prednisone, and azathioprine, resulting in partial clinical improvement and subsequent prednisone discontinuation.

Three years later, she developed a nonproductive cough and exertional dyspnea. Pulmonary function tests and high-resolution computed tomography (HRCT) demonstrated interstitial lung disease (ILD) with a usual interstitial pneumonia (UIP) pattern (Figure 1). Around this period, she also developed progressively enlarging, firm subcutaneous nodules over the left elbow, both wrists, hands, and upper back. Radiographs demonstrated extensive soft tissue calcifications in these areas (Figure 2), consistent with calcinosis cutis. With disease progression and development of ILD, azathioprine was switched to mycophenolate mofetil (MMF), with reintroduction of low-dose prednisone. Alendronate was initiated for osteoporosis prevention. Over 2 years of follow-up, both ILD and calcinosis cutis remained clinically stable without significant progression, likely reflecting stabilization of the underlying autoimmune disease following adjustment of immunosuppressive therapy.

Calcinosis cutis is a recognized complication of CTDs, most frequently observed in systemic sclerosis, dermatomyositis, and overlap syndromes. Calcium deposition within the skin, subcutaneous tissue, and periarticular structures, often over bony prominences, may result in pain, ulceration, recurrent infection,

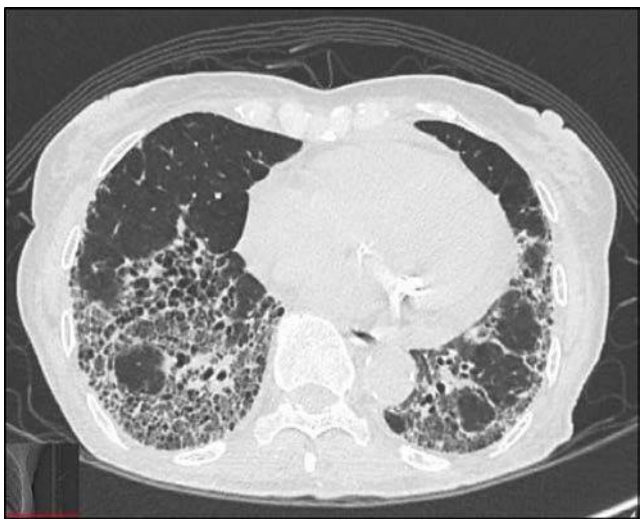

FIGURE 1 | Chest CT scan with contrast showing subpleural reticular densities with honeycombing of both lungs consistent with bilateral interstitial lung disease with Usual Interstitial Pneumonia (UIP) pattern.

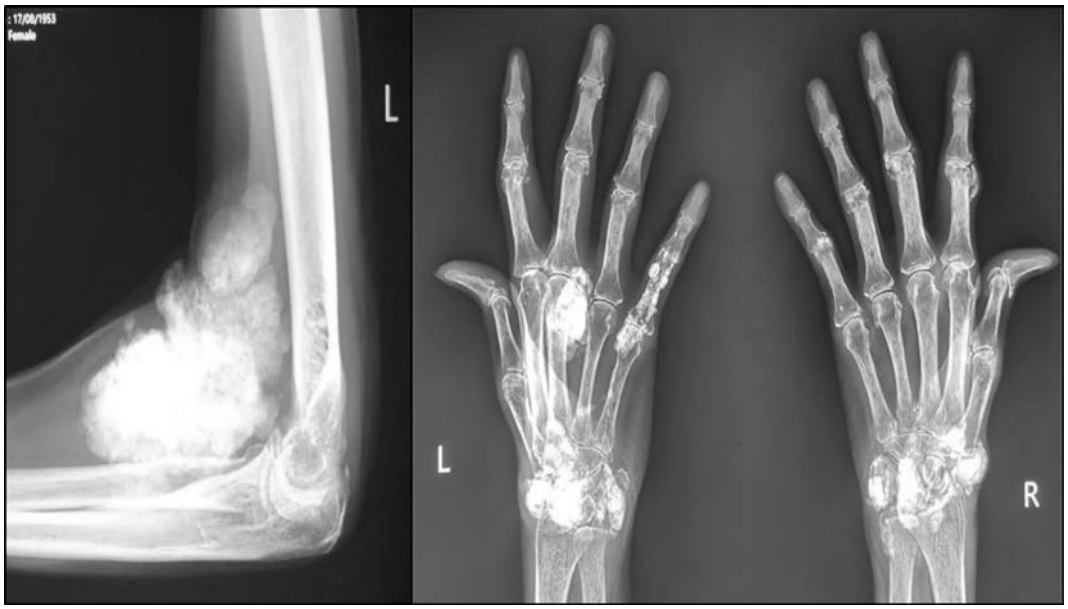

FIGURE 2 | Lateral radiographs of the left elbow and both hands showing numerous calcifications in the subcutaneous tissue.

and functional impairment, significantly affecting quality of life [1].

The occurrence of calcinosis cutis varies widely across autoimmune disorders. It is reported in 18%–49% of patients with systemic sclerosis, 30%–37% in adult dermatomyositis (and up to 70% in juvenile dermatomyositis), and 3%–40% in systemic lupus erythematosus. In contrast, calcinosis cutis remains exceptionally rare in pSS with only seven reported cases in the literature to date [2–8].

This case highlights calcinosis cutis as a potentially underrecognized manifestation of pSS occurring in association with ILD. The temporal relationship between onset of ILD and subsequent development of calcinosis cutis raises the possibility that calcinosis may reflect heightened systemic inflammatory activity or evolving disease severity in selected patients.

The clinical presentation of calcinosis cutis is heterogeneous. It may be localized (calcinosis circumscripta), typically confined to an extremity or periarticular region, or diffuse (calcinosis universalis), involving muscles and tendons [9]. In our patient, calcifications predominantly involved the upper extremities and upper back, consistent with the distribution described in previously reported pSS-associated cases [2–6]. However, more extensive involvement, including the elbows, knees, gluteal–pelvic region, and thighs, has also been reported [7, 8].

The pathophysiology of dystrophic calcification remains incompletely understood. Proposed mechanisms include chronic inflammation, tissue hypoxia, recurrent microtrauma, dysregulation of bone matrix proteins, and persistent tissue injury promoting aberrant calcium deposition [10, 11].

Management remains challenging because evidence is limited primarily to case reports and small case series, with variable responses reported across therapies. Medical treatments including diltiazem, colchicine, bisphosphonates, probenecid, warfarin, minocycline, salicylates, aluminum hydroxide, carbon dioxide laser therapy, systemic glucocorticoids, as well as immunosuppressants such as methotrexate and MMF, and other immunomodulatory/targeted therapies such as intravenous immunoglobulin, rituximab, JAK inhibitors, and TNF inhibitors have demonstrated benefit in selected patients, although consistent efficacy has not been established. Surgical excision may be considered for large, localized lesions associated with recurrent infection, ulceration, functional impairment, or cosmetic concerns [1, 11]. In the absence of validated guidelines supporting the preferential use of one agent over another or identifying patients most likely to benefit from specific therapies, clinical management should primarily focus on controlling the underlying autoimmune disease and systemic inflammatory activity [12].

This case adds to the limited body of literature describing this rare association, particularly in the presence of interstitial lung disease. The paucity of data on its prevalence, clinical course, pathogenesis, and treatment underscores the need for further studies. Early recognition and individualized management are essential to prevent morbidity and improve patient outcomes.

Author Contributions

All authors were involved in the clinical care of the patient, collection and interpretation of clinical data, preparation and critical revision of the manuscript, and approved the final version for publication.

Consent

Written informed consent was obtained from the patient for publication of this case report and accompanying images. All identifying information has been removed to ensure patient confidentiality.

Conflicts of Interest

The authors declare no conflicts of interest.

Data Availability Statement

The data that support the findings of this study are available from the corresponding author upon reasonable request.

References

1. I. Mormile, F. Mosella, P. Turco, F. Napolitano, A. de Paulis, and F. W. Rossi, "Calcinosis Cutis and Calciphylaxis in Autoimmune Connective Tissue Diseases," *Vaccines (Basel)* 11, no. 5 (2023): 898, https://doi.org/10.3390/vaccines11050898.

2. M. Llamas-Velasco, C. Eguren, D. Santiago, C. García-García, J. Fraga, and A. García-Diez, "Calcinosis Cutis and Sjögren's Syndrome," *Lupus* 19, no. 6 (2010): 762–764, https://doi.org/10.1177/0961203309355298.

3. K. Gonzalez-Ramos, K. Ramsubeik, and G. Kaeley, "Case of Calcinosis Cutis Associated With Sjögren's Syndrome," *Clinical Case Reports* 11, no. 6 (2023): e7628, https://doi.org/10.1002/ccr3.7628.

4. P. L. Wasserman, C. Wiesler, C. Kurra, R. Omman, K. Taylor, and R. Puri, "MR Imaging Findings of Calcinosis Cutis in Primary Sjögren Syndrome, a Rare Manifestation," *Radiology Case Reports* 15, no. 7 (2020): 1029–1038, https://doi.org/10.1016/j.radcr.2020.04.025.

5. H. Fueki, R. Hino, M. Yoshioka, M. Nakamura, and Y. Tokura, "Calcinosis Cutis Associated With Primary Sjögren's Syndrome: Strong Expression of Osteonectin and Matrix Gla Protein," *Rheumatology (Oxford, England)* 50, no. 12 (2011): 2318–2320, https://doi.org/10.1093/rheumatology/ker304.

6. A. P. V. Akhila, J. Massiel, and K. Aaradhana, "A Case of Calcinosis Cutis in a Patient With Sjögren Syndrome," *AIM Clinical Cases* 3 (2024): e231411, https://doi.org/10.7326/aimcc.2023.1411.

7. Y. Tsuchida, S. Sumitomo, K. Fujio, and K. Yamamoto, "Massive Calcinosis Cutis Associated With Primary Sjögren's Syndrome," *BMJ Case Reports* 2016 (2016): bcr2015214006, https://doi.org/10.1136/bcr-2015-214006.

8. C. H. Yang ang, C. W. Chang, Y. R. Kuo, and S. H. Huang, "Widespread Dystrophic Calcinosis Cutis in Both Thighs Associated With Sjögren's Syndrome: A Case of 20-Year Follow-Up," *Kaohsiung Journal of Medical Sciences* 35, no. 10 (2019): 648–650, https://doi.org/10.1002/kjm2.12103.

9. C. Le and P. M. Bedocs, "Calcinosis Cutis," in *StatPearls* (StatPearls Publishing, 2024), https://www.ncbi.nlm.nih.gov/books/NBK448127/.

10. N. Reiter, L. El-Shabrawi, B. Leinweber, A. Berghold, and E. Aberer, "Calcinosis Cutis: Part I. Diagnostic Pathway," *Journal of the American Academy of Dermatology* 65, no. 1 (2011): 1–12, https://doi.org/10.1016/j.jaad.2010.08.038.

11. H. Elahmar, B. M. Feldman, and S. R. Johnson, "Management of Calcinosis Cutis in Rheumatic Diseases," *Journal of Rheumatology* 49, no. 9 (2022): 980–989, https://doi.org/10.3899/jrheum.211393.

12. A. Dima, P. Balanescu, and C. Baicus, "Pharmacological Treatment in Calcinosis Cutis Associated With Connective-Tissue Diseases," *Romanian Journal of Internal Medicine* 52, no. 2 (2014): 55–67.

International Journal of Rheumatic Diseases

WILEY

International Journal of Rheumatic Diseases

EDITORIAL

Deconstructing the Synovium: A New Era of Precision Medicine in Rheumatoid Arthritis

Tang-Kai Cheng[1] | Wei-Che Hsu[2,3] | James Cheng-Chung Wei[4,5,6]

[1]Department of Rheumatology, Chung Shan Medical University Hospital, Taichung, Taiwan | [2]Department of Anesthesiology, Chung Shan Medical University Hospital, Taichung, Taiwan | [3]Department of Anesthesiology, School of Medicine, Chung Shan Medical University, Taichung, Taiwan | [4]Department of Allergy, Immunology & Rheumatology, Chung Shan Medical University Hospital, Taichung, Taiwan | [5]Institute of Medicine, Chung Shan Medical University, Taichung, Taiwan | [6]Graduate Institute of Integrated Medicine, China Medical University, Taichung City, Taiwan

Correspondence: James Cheng-Chung Wei (jccwei@gmail.com)

Received: 27 November 2025 | **Revised:** 25 May 2026 | **Accepted:** 27 May 2026

Rheumatoid arthritis (RA) has long been treated as a single disease, yet its clinical heterogeneity is a daily challenge for rheumatologists. The current trial-and-error approach to therapy, often escalating from methotrexate to biologic agents, fails a significant portion of patients, leading to delays in disease control and irreversible joint damage. This therapeutic gap stems from a fundamental disconnect: our common clinical measures of systemic inflammation often fail to reflect the complex and varied molecular processes occurring within the diseased synovial tissue. The field is now at a crucial inflection point, moving away from a systemic-only view and toward a new era of precision medicine guided by the synovium itself.

Recent advancements in single-cell technology have allowed us to deconstruct the synovial ecosystem, revealing that RA is not one disease, but several distinct "pathotypes." This tissue-centric view is critical. For instance, recent work has highlighted that stromal cells, particularly distinct synovial fibroblast subtypes—such as PRIME (CD45−CD31−PDPN+ preinflammatory mesenchymal) cells—are not passive bystanders but can actively drive a refractory, pro-fibrotic disease pathotype that is less responsive to traditional immune-suppressing biologics [1]. Concurrently, other studies focusing on T and B cell interactions have reinforced the idea of a "lymphomyeloid" pathotype, characterized by ectopic lymphoid structures and a strong adaptive immune signature [2]. Understanding which pathotype dominates a patient's joint is key to selecting the right therapy.

In this context, a pivotal study by Rivellese et al. in *Arthritis & Rheumatology* provides a critical piece of the puzzle [3]. By performing a comparative analysis of immune cells from both peripheral blood (PB) and matched synovial biopsies in early, treatment-naive RA patients, the authors highlight this systemic-synovial divergence. They observed that circulating B cell levels, for example, showed a significant *inverse* correlation with markers of inflammation and disease activity, a paradox when compared to the B-cell-rich inflammation seen in many RA joints.

Most compellingly, the study by Rivellese et al. identifies T peripheral helper (Tph) cells as a unique subset that bridges this gap [3]. Tph cells were the only circulating immune cell type found to be positively correlated with *both* systemic inflammatory markers and the local synovial inflammation score. Furthermore, high circulating Tph levels were strongly associated with the lymphomyeloid synovial pathotype. This is a crucial finding: it suggests that Tph cells could function as a "liquid biopsy," allowing us to infer the underlying molecular pathology of the joint—a specific, T/B cell-driven inflammation—from a simple blood test.

The way forward now lies in integrating these insights. While multi-omics analysis of synovial tissue is powerful for *defining* these pathotypes [4], it is not clinically scalable for routine use. The true challenge is translating this tissue-level knowledge into actionable, non-invasive biomarkers. The Tph cell identified by Rivellese et al. is a prime candidate [3]. Other circulating markers, such as specific microRNA profiles, are also showing promise in predicting therapeutic response [5]. The future of RA care will likely involve classifying patients not by their clinical

Tang-Kai Cheng and Wei-Che Hsu contributed equally to this work.

symptoms alone, but by their dominant synovial pathotype. The work of Rivellese and colleagues is a vital step toward achieving this, providing a tangible biomarker that may 1 day allow us to bypass the biopsy and deliver the right drug to the right patient at the right time.

Author Contributions

Tang-Kai Cheng: conceptualization, writing – original draft, and writing – review and editing. **Wei-Che Hsu:** writing – review and editing. **James Cheng-Chung Wei:** conceptualization, supervision, and writing – review and editing. All authors have read and approved the final manuscript, and meet the ICMJE criteria for authorship.

Conflicts of Interest

The authors declare no conflicts of interest.

Data Availability Statement

The data that support the findings of this study are available on request from the corresponding author. The data are not publicly available due to privacy or ethical restrictions.

References

1. Y. J. Lin, J. An, and X. Feng, "The Role of Synovial Fibroblast Subtypes in the Persistence of Rheumatoid Arthritis: A New Therapeutic Frontier," *Lancet Rheumatology* 6, no. 5 (2024): e315–e327.

2. N. Al-Saadi, J. Bakshi, C. Mauri, and C. Pitzalis, "B-Cell and T-Cell Interactions in Rheumatoid Arthritis: New Insights and Therapeutic Opportunities," *Nature Reviews Rheumatology* 20, no. 4 (2024): 207–221.

3. F. Rivellese, E. Pontarini, L. Fossati-Jimack, et al., "Comparative Analysis of Circulating and Synovial Immune Cells in Early Untreated Rheumatoid Arthritis and Their Relationship With Molecular Pathology and Disease Outcomes," *Arthritis and Rheumatology* 77, no. 10 (2025): 1349–1361.

4. S. Yoshida, S. Nakagawa, and Y. Kaneko, "The Clinical Utility of Multi-Omics Approaches in Defining and Predicting Synovial Pathotypes in Rheumatoid Arthritis," *International Journal of Rheumatic Diseases* 28, no. 1 (2025): 15–24.

5. L. Wang, S. Chen, and Z. G. Li, "Circulating microRNA Profiles as Prognostic Biomarkers for Methotrexate Response in Early Rheumatoid Arthritis," *International Journal of Rheumatic Diseases* 27, no. 3 (2024): e14987.

International Journal of Rheumatic Diseases

WILEY

International Journal of Rheumatic Diseases

EDITORIAL

Treat-to-Target in the New Era of Systemic Lupus Erythematosus Management: Targets, Tools, and Therapeutics

Teng-Chieh Hsu[1,2] | An-Ping Huo[3,4] | Pui-Ying Leong[3,4,5,6]

[1]Department of Allergy, Immunology & Rheumatology, Wuri Lin Shin Hospital, Taichung, Taiwan | [2]College of Health Care and Management, Chung Shan Medical University, Taichung, Taiwan | [3]Institute of Medicine, Chung Shan Medical University, Taichung, Taiwan | [4]Divison of Allergy, Immunology and Rheumatology, Department of Internal Medicine, Chung Shan Medical University Hospital, Taichung, Taiwan | [5]School of Medicine, Chung Shan Medical University, Taichung, Taiwan | [6]Feng Chia University, Taichung, Taiwan

Correspondence: Pui-Ying Leong (fiona.leong@gmail.com)

Received: 25 January 2026 | **Revised:** 17 May 2026 | **Accepted:** 26 May 2026

Systemic lupus erythematosus (SLE) has long been regarded as the prototype of complex autoimmune diseases, characterized by protean manifestations and an unpredictable course. Over recent decades, improved survival has shifted the focus of SLE management from preventing mortality alone to achieving sustained disease control while minimizing long-term treatment-related harm. In this context, treat-to-target (T2T) has emerged as a guiding principle, yet its translation into routine clinical practice remains incomplete.

Despite its conceptual appeal, implementation of T2T in SLE remains more challenging than in rheumatoid arthritis, largely because of disease heterogeneity and the absence of a single unifying target. More importantly, a critical gap persists between theoretical targets and real-world practice. Chronic glucocorticoid (GC) exposure continues to be accepted as part of routine disease control in many patients, even though GC exposure is independently associated with irreversible damage accrual in SLE [1]. This disconnect underscores the need to reexamine how T2T is interpreted and applied in contemporary SLE care.

1 | The Targets: LLDAS and DORIS

Two major definitions have been developed to operationalize T2T in SLE: the lupus low disease activity state (LLDAS) and the Definition of Remission in SLE (DORIS).

DORIS remission, defined by clinical SLEDAI-2K = 0, Physician Global Assessment (PGA) < 0.5, stable background therapy, and low-dose glucocorticoids (prednisolone ≤ 5 mg/day), represents the ideal target [2]. However, this state remains difficult to achieve and sustain in a substantial proportion of patients in routine practice.

LLDAS has therefore emerged as a more pragmatic and attainable target. Defined by SLEDAI-2K ≤ 4 without major organ activity, no new disease activity, PGA ≤ 1, and prednisolone ≤ 7.5 mg/day, LLDAS has been validated across multiple cohorts, including landmark studies from the Asia-Pacific Lupus Collaboration (APLC). Patients who spend a greater proportion of time in LLDAS have a significantly reduced risk of damage accrual [3, 4].

Importantly, the glucocorticoid thresholds embedded within LLDAS and DORIS should be interpreted as upper limits rather than long-term therapeutic goals. In clinical practice, these thresholds are sometimes misconstrued as acceptable maintenance doses, which may inadvertently perpetuate chronic steroid exposure. In line with the 2023 EULAR update, glucocorticoids should be minimized to the lowest feasible dose, with maintenance treatment ideally ≤ 5 mg/day prednisone equivalent and, whenever feasible, withdrawal [5]. In this sense, LLDAS should be viewed as a transitional target rather than a justification for indefinite exposure to 7.5 mg/day.

2 | The Therapeutics: Beyond Non-Specific Immunosuppression

Achieving these targets requires moving beyond the historical reliance on high-dose glucocorticoids and broad-spectrum immunosuppressive agents. The past decade has witnessed major advances in lupus therapeutics, with targeted therapies offering improved efficacy and a clearer steroid-sparing rationale.

Belimumab, a BLyS inhibitor, was the first biologic approved for SLE and has demonstrated additional benefit in lupus nephritis in the BLISS-LN trial, including improved renal response and a lower risk of renal-related events [6]. From a T2T perspective, the value of belimumab extends beyond disease control alone, as it may facilitate earlier and more sustained reduction in glucocorticoid exposure.

Anifrolumab, a monoclonal antibody targeting the type I interferon receptor, addresses a key pathogenic pathway in SLE. In TULIP-2, anifrolumab improved disease activity using the BICLA endpoint and supported glucocorticoid tapering [7]. These findings highlight its role not only in suppressing disease activity but also in enabling steroid-sparing treatment strategies.

Voclosporin, a novel calcineurin inhibitor, has expanded the treatment armamentarium for lupus nephritis. The AURORA 1 and AURORA 2 studies demonstrated more rapid and sustained reductions in proteinuria when voclosporin was added to standard therapy, without a detrimental long-term signal for renal function [8, 9]. This approach may also support earlier reduction of glucocorticoid exposure, which remains a central objective in T2T strategies.

3 | The Frontier: CAR-T Cell Therapy

An emerging and potentially transformative approach in SLE is chimeric antigen receptor (CAR) T-cell therapy. Early reports of anti-CD19 CAR-T therapy in refractory SLE have shown remarkable outcomes, including drug-free remission and disappearance of autoantibodies [10, 11]. These findings raise the possibility of an "immunological reset" and suggest a therapeutic paradigm fundamentally different from chronic suppression. Although questions remain regarding safety, cost, and scalability, CAR-T therapy may represent a future strategy aimed at sustained remission without ongoing immunosuppression in highly selected patients.

4 | The Challenge: Access and Implementation

Despite therapeutic advances, a substantial gap remains between treatment recommendations and real-world practice. Access to biologic and targeted therapies is uneven, and in many settings, these agents are still reserved for refractory disease rather than used earlier as steroid-sparing interventions.

This gap is particularly pronounced in the Asia-Pacific region. APLAR consensus statements and region-specific literature have emphasized that SLE in Asia-Pacific is shaped by substantial variation in disease burden, healthcare access, tolerability, adherence, reimbursement systems, and availability of specialist care [12, 13]. These constraints may further limit the implementation of evidence-based care. As a result, many patients continue to rely on prolonged glucocorticoid therapy to maintain disease control, reflecting not only clinical need but also structural limitations within healthcare systems.

Addressing this gap requires a more pragmatic approach to T2T implementation. In our view, T2T in SLE should not be applied as a uniform framework, but rather adapted to local healthcare contexts. In resource-variable settings, prioritizing glucocorticoid tapering as an early treatment objective may be more feasible, even when access to biologic therapies is limited.

We propose that a stepwise approach to T2T may be more practical in the Asia-Pacific region, in which initial disease control is achieved with available therapies, followed by progressive reduction of glucocorticoids and, where possible, introduction of steroid-sparing agents. In parallel, strengthening referral pathways, clinician education, and longitudinal monitoring are essential to improve implementation.

T2T should therefore be understood not as a rigid framework, but as a flexible strategy that balances ideal targets with real-world constraints, while preserving its central aim: disease control with the least possible cumulative treatment toxicity.

5 | Conclusion

The management of SLE has evolved substantially, with clearer treatment targets, better assessment tools, and an expanding range of therapeutic options. However, achieving these targets in practice requires more than formal endorsement of LLDAS or remission.

In contemporary SLE care, T2T should no longer be defined by stabilization on chronic low-dose glucocorticoids. Rather, successful T2T must explicitly incorporate glucocorticoid minimization and, where possible, complete withdrawal as a central therapeutic objective. In this context, the true value of emerging therapies lies not only in improving disease control, but also in enabling a transition away from long-term steroid dependence. Bridging the gap between targets and practice, particularly in resource-variable settings such as the Asia-Pacific region, will be essential to improving long-term outcomes for patients with SLE.

Author Contributions

Teng-Chieh Hsu contributed to the conceptualization, literature review, and drafting of the manuscript. An-Ping Huo assisted with the literature review and provided intellectual input during manuscript preparation. Pui-Ying Leong, as the corresponding author, supervised the work and critically reviewed and revised the manuscript. All authors reviewed and approved the final version of the manuscript and agree to be accountable for all aspects of the work.

Conflicts of Interest

The authors declare no conflicts of interest.

Data Availability Statement

The authors have nothing to report.

References

1. D. Apostolopoulos, R. Kandane-Rathnayake, W. Louthrenoo, et al., "Independent Association of Glucocorticoids With Damage Accrual in SLE," *Lupus Science & Medicine* 3, no. 1 (2016): e000157, https://doi.org/10.1136/lupus-2016-000157.

2. R. F. van Vollenhoven, G. Bertsias, A. Doria, et al., "2021 DORIS Definition of Remission in Systemic Lupus Erythematosus: Final Recommendations From an International Task Force," *Lupus Science & Medicine* 8, no. 1 (2021): e000538, https://doi.org/10.1136/lupus-2021-000538.

3. K. Franklyn, C. S. Lau, S. V. Navarra, et al., "Definition and Initial Validation of a Lupus Low Disease Activity State (LLDAS)," *Annals of the Rheumatic Diseases* 75, no. 9 (2016): 1615–1621, https://doi.org/10.1136/annrheumdis-2015-207726.

4. V. Golder, R. Kandane-Rathnayake, M. Huq, et al., "Lupus Low Disease Activity State as a Treatment Endpoint for Systemic Lupus Erythematosus: A Prospective Validation Study," *Lancet Rheumatology* 1, no. 2 (2019): e95–e102, https://doi.org/10.1016/S2665-9913(19)30037-2.

5. A. Fanouriakis, M. Kostopoulou, K. Cheema, et al., "EULAR Recommendations for the Management of Systemic Lupus Erythematosus: 2023 Update," *Annals of the Rheumatic Diseases* 83, no. 1 (2024): 15–29, https://doi.org/10.1136/ard-2023-224762.

6. R. Furie, B. H. Rovin, F. Houssiau, et al., "Two-Year Randomized Controlled Trial of Belimumab in Lupus Nephritis," *New England Journal of Medicine* 383, no. 12 (2020): 1117–1128, https://doi.org/10.1056/NEJMoa2001180.

7. E. F. Morand, R. Furie, Y. Tanaka, et al., "Trial of Anifrolumab in Active Systemic Lupus Erythematosus," *New England Journal of Medicine* 382, no. 3 (2020): 211–221, https://doi.org/10.1056/NEJMoa1912196.

8. B. H. Rovin, Y. K. O. Teng, E. M. Ginzler, et al., "Efficacy and Safety of Voclosporin Versus Placebo for Lupus Nephritis (AURORA 1): A Double-Blind, Randomised, Multicentre, Placebo-Controlled, Phase 3 Trial," *Lancet* 397, no. 10289 (2021): 2070–2080, https://doi.org/10.1016/S0140-6736(21)00578-X.

9. A. Saxena, E. M. Ginzler, K. Gibson, et al., "Safety and Efficacy of Long-Term Voclosporin Treatment for Lupus Nephritis in the Phase 3 AURORA 2 Clinical Trial," *Arthritis & Rhematology* 76, no. 1 (2024): 59–67, https://doi.org/10.1002/art.42657.

10. A. Mackensen, F. Müller, D. Mougiakakos, et al., "Anti-CD19 CAR T-Cell Therapy for Refractory Systemic Lupus Erythematosus," *Nature Medicine* 28, no. 10 (2022): 2124–2132, https://doi.org/10.1038/s41591-022-02017-5.

11. F. Müller, J. Taubmann, L. Bucci, et al., "CD19 CAR T-Cell Therapy in Autoimmune Disease: A Case Series With Follow-Up," *New England Journal of Medicine* 390, no. 8 (2024): 687–700, https://doi.org/10.1056/NEJMoa2308917.

12. C. C. Mok, L. Hamijoyo, N. Kasitanon, et al., "The Asia-Pacific League of Associations for Rheumatology Consensus Statements on the Management of Systemic Lupus Erythematosus," *Lancet Rheumatology* 3, no. 7 (2021): e517–e531, https://doi.org/10.1016/S2665-9913(21)00009-6.

13. Y. Tanaka, S. O'Neill, M. Li, I. C. Tsai, and Y. W. Yang, "Systemic Lupus Erythematosus: Targeted Literature Review of the Epidemiology, Current Treatment, and Disease Burden in the Asia Pacific Region," *Arthritis Care and Research* 74, no. 2 (2022): 187–198, https://doi.org/10.1002/acr.24431.

International Journal of Rheumatic Diseases

WILEY

International Journal of Rheumatic Diseases

LETTER TO THE EDITOR

Case Report: Allergic Bronchopulmonary Aspergillosis and Eosinophilic Granulomatosis With Polyangiitis Complicated by Lymphedema

Haodong Huang | Yuhua Wang

Department of Rheumatology and Immunology, Beijing Shijitan Hospital, Capital Medical University, Beijing, China

Correspondence: Yuhua Wang (wyhxxtt@163.com)

Received: 26 November 2025 | **Revised:** 25 February 2026 | **Accepted:** 11 May 2026

Dear Editor,

We report a rare case of eosinophilic granulomatosis with polyangiitis (EGPA) combined with allergic bronchopulmonary aspergillosis (ABPA), which started with purpura and edema of the lower limbs, with significant pleural effusion and gastrointestinal (GI) involvement, and edema of the lower limbs manifested as lymphedema. This case highlights the diagnostic and management challenges and extends the known clinical spectrum of EGPA.

A 78-year-old male, with a history of bronchial asthma and ABPA diagnosed in 2019 (eosinophilia 13.2%, IgE 3550–3930 IU/mL, *Aspergillus fumigatus*-specific IgE positive), was admitted on June 25, 2021. He presented with a 2-week history of limb edema, cutaneous purpura, fatigue, and progressive dyspnea. Emergency evaluation revealed striking peripheral eosinophilia (WBC 14.67×10^9/L, 58.1% eosinophils). Initial CT scans showed bronchiectasis and left lower lobe infiltrates. Cardiac color Doppler ultrasonography indicated normal pulmonary artery pressure (35 mmHg) and cardiac chamber diameter, along with normal B—type natriuretic peptide (BNP) levels, thereby excluding cardiogenic edema. Biochemical examinations revealed normal creatinine, urea, and electrolyte levels, ruling out nephrogenic edema. Vascular ultrasonography definitively excluded lower—extremity venous thrombosis. PET/CT characteristics: The "multiple reticular shadows" in the subcutaneous fat space within the scanning scope represent the direct imaging manifestations of lymphatic stasis, ruling out the transient interstitial edema induced by simple cardiac factors or hypoproteinemia. Lymphoscintigraphy revealed sluggish lymphatic drainage in both lower extremities, along with continuous development of bilateral venous angles, indicating mechanical or inflammatory obstruction at the outlet level of the thoracic duct. Lymphatic surgery consultation posited that the edema was not merely a solitary reflux disorder but rather a manifestation of systemic lymphatic involvement within the context of vasculitis. Elucidation of ANCA status laboratory examinations indicated the presence of ANA and the absence of ANCA; specifically, both MPO—ANCA (p—ANCA) and PR3—ANCA (c—ANCA) were negative. Upon admission, the patient's condition deteriorated, accompanied by the emergence of new bilateral pleural effusions and atelectasis (Figure 1A).

The complex presentation, characterized by new systemic symptoms, pronounced hypereosinophilia, and pre-existing ABPA, necessitated a broad differential diagnosis. Initial considerations included ABPA exacerbation, other hypereosinophilic syndromes, drug-induced eosinophilia, and systemic vasculitis. Ultimately, Eosinophilic Granulomatosis with Polyangiitis (EGPA) was diagnosed. The rationale was based on persistent hypereosinophilia (peak 6.36×10^9/L), obstructive lung disease, nasal polyps, and bone marrow eosinophil infiltration, fulfilling the 2022 ACR/EULAR EGPA classification criteria (score = 11) [1]. It was considered that cutaneous purpura was caused by microvascular disease, but it was difficult to exclude the influence of ABPA in pleural effusion and lung involvement. Notably, ABPA preceded EGPA by two years. During the patient's hospitalization, acute subxiphoid pain emerged. Colonoscopy revealed only mild chronic inflammation. Nevertheless, the patient presented evident imaging findings of "incomplete intestinal obstruction"

(air—fluid levels on PET/CT) and diffuse thickening of the peritoneum. After excluding other etiologies, this was ascribed to EGPA—related gastrointestinal involvement.

Treatment with intravenous methylprednisolone (40 mg) rapidly resolved abdominal pain and induced disease remission, evidenced by normalized eosinophils (0.06×10^9/L), resolved rash/effusions, and abated edema. Although a skin biopsy was not conducted in this case [2], the diagnosis of EGPA was assigned a score as high as 11 according to the 2022 ACR/EULAR criteria. Moreover, the therapeutic response was prompt: the abdominal pain and rash subsided rapidly within 24 h subsequent to treatment with intravenous methylprednisolone, a notable diagnostic response that strongly implies a vasculitis etiology. Immunosuppression was transitioned to cyclophosphamide (1.0 g/month) plus oral steroids. At the same time, the anti-aspergillus treatment of ABPA should be strengthened. During 2021–2025 follow-up, sustained remission was achieved with step-down therapy, demonstrating complete biochemical normalization and radiographic resolution of effusions (Figure 1B). No significant complications occurred. Table 1 presents a summary of the alterations in the crucial indicators of this patient throughout these six years.

Eosinophilic granulomatosis with polyangiitis (EGPA) is a rare anti-neutrophil cytoplasmic antibody (ANCA) associated vasculitis with a prevalence of 10.7–17.8 per million population [1]. The clinical manifestations are complex and diverse, often starting with prodromal symptoms such as asthma, allergic rhinitis and nasal polyps, and then may develop a variety of clinical manifestations such as pulmonary infiltrates, cardiac involvement, gastrointestinal symptoms, peripheral neuropathy and skin manifestations such as purpura. Nevertheless, the incidence of concurrent ABPA in clinical practice is exceedingly low. Its clinical manifestations, particularly bronchial asthma and pulmonary radiological findings, often significantly overlap with those of other pulmonary diseases, thereby posing a considerable challenge to accurate diagnosis [2]. The co-occurrence of ABPA and EGPA, particularly with severe GI involvement and generalized lymphedema, is rare and poses significant diagnostic and therapeutic challenges [2, 3]. This case suggests that chronic fungal antigen exposure in ABPA may act as a catalyst

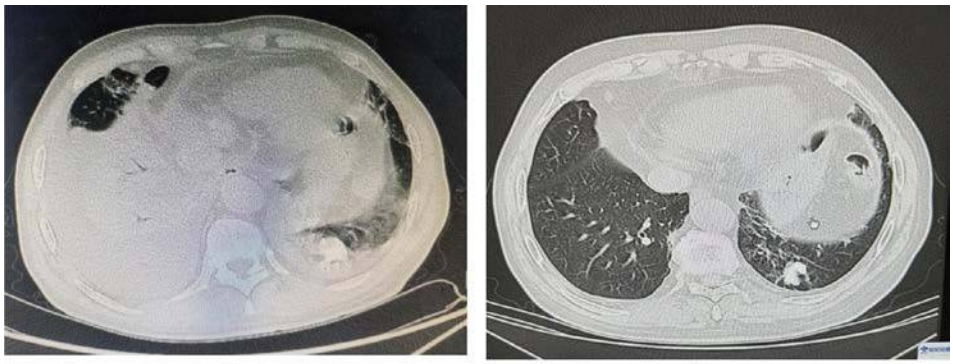

FIGURE 1 | (A) Pulmonary imaging of the case at initial diagnosis. (B) Changes in pulmonary lesions after three years of standard treatment.

TABLE 1 | Variations in key indicators for this case over the past six years.

Time point	Clinical symptoms and diagnosis	Peripheral blood eosinophils	Key laboratory tests/imaging
2019.08	Initial diagnosis of ABPA	0.67×10^9/L	Bronchiectasis, high-attenuation mucus plugs, Af-IgE(+)
2020.01–08	Symptom fluctuation, itraconazole maintenance	Fluctuating increase	CT showed bronchial wall thickening and slight progression of pulmonary nodules
2021.06.25	Admission for acute EGPA onset	8.53×10^9/L	Cutaneous purpura, severe abdominal pain, bilateral pleural effusion
2021.06.30	EGPA confirmed (ACR score: 11)	6.36×10^9/L	ANCA negative; Bone marrow eosinophil infiltration
2021.07.06	Lymphatic function assessment	Began to decrease post-treatment	Lymphoscintigraphy showed slow drainage and thoracic duct outlet obstruction
After 2021.08	Induction of remission and maintenance therapy	Gradually normalized	Abdominal pain relieved by methylprednisolone pulse, followed by CTX 1.0 g/month maintenance
2025.07	Follow-up for sustained clinical remission	0.06×10^9/L	Re-examination showed full normalization of IgE, ESR, CRP, and Alb

TABLE 2 | Radiological features and distinctions between ABPA and EGPA.

Radiological signs	ABPA [11]	EGPA [12]	Manifestations in this case
Lesion location	Central bronchiectasis	Peripheral/subpleural infiltrates	Bronchiectasis in 2019; peripheral ground-glass opacities in 2021
Mucus plugs	High-attenuation mucus plugs (HAM) [13]	Iso-attenuating mucus plugs	HAM calcifications visible in 2019
Vascular signs	Normal vessel diameter	Increased pulmonary small vessel shadows	Subpleural small vessel dilation visible in 2021
Pleural effusion	Rare	Common (mostly bilateral)	Massive bilateral pleural effusion appeared in 2021

for ANCA-negative EGPA, potentially via shared Th2/Th17 immune dysregulation and eosinophil activation [4]. Fungal spores have the capacity to induce a Th17 response. The IL-17 secreted by Th17 cells synergizes with Th2 cytokines to exacerbate vascular endothelial damage [5]. In patients with IL-5 ABPA, the airway continuously generates high levels of IL-5. This cytokine stimulates the production of a substantial quantity of eosinophils (Eos) in the bone marrow and extends their peripheral survival time [6], subsequently leading to systemic vasculitis. The lymphedema, a rare EGPA complication. It is hypothesized that EGPA complicated by lymphedema is attributable to eosinophilic lymphangitis [7]. Eosinophils exert direct toxicity on the lymphatic endothelium by releasing major basic protein (MBP) and eosinophil cationic protein (ECP) via degranulation [8, 9]. Moreover, the IL-4/IL-13 produced in a Th2-polarized environment promotes perilymphatic fibrosis, resulting in mechanical occlusion of lymphatic vessels [10]. In this particular case, the obstruction at the thoracic duct outlet may be associated with EGPA inflammation in the mediastinal region, further expanding the clinical spectrum and highlighting the need for early recognition and aggressive treatment of the underlying inflammatory condition [5]. Our findings underscore the complex interplay between allergic and autoimmune pathologies and emphasize the importance of vigilant monitoring for systemic symptoms in ABPA patients.

Conversely, the radiological features presented in Table 2 explicitly illustrate the dynamic progression of pulmonary imaging characteristics, commencing from ABPA and gradually overlapping with those of EGPA.

We report a rare case of eosinophilic granulomatosis with polyangiitis (EGPA) co-occurring with allergic bronchopulmonary aspergillosis (ABPA), characterized by severe gastrointestinal involvement and generalized lymphedema. This challenging presentation underscores the diagnostic complexities and suggests that chronic fungal antigen exposure in ABPA may catalyze ANCA-negative EGPA. Our findings emphasize the importance of vigilant monitoring for systemic vasculitis in ABPA patients, thereby expanding the known clinical spectrum of EGPA.

Author Contributions

Haodong Huang: methodology, investigation, data curation, formal analysis, writing – original draft. **Yuhua Wang:** conceptualization, resources, supervision, project administration, funding acquisition, writing – review and editing.

Ethics Statement

As a case report, ethics committee approval was not required. The study adheres to the Declaration of Helsinki.

Consent

The patient provided written informed consent to publish their de-identified clinical data and images.

Conflicts of Interest

The authors declare no conflicts of interest.

Data Availability Statement

The data that support the findings of this study are available from the corresponding author upon reasonable request.

References

1. G. Emmi, A. Bettiol, E. Gelain, et al., "Evidence-Based Guideline for the Diagnosis and Management of Eosinophilic Granulomatosis With Polyangiitis," *Nature Reviews Rheumatology* 19, no. 6 (2023): 378–393, https://doi.org/10.1038/s41584-023-00958-w.

2. T. Kawakami, K. Yokoyama, T. Ikeda, H. Tomizawa, and S. Ueki, "Presence of Eosinophil Extracellular Trap Cell Death in the Affected Skin of Eosinophilic Granulomatosis With Polyangiitis," *Journal of Dermatology* 50, no. 4 (2023): 551–555, https://doi.org/10.1111/1346-8138.16656.

3. A. M. Marra, P. Curci, G. Franco, et al., "Coexistence of Eosinophilic Granulomatosis With Polyangiitis and Allergic Bronchopulmonary Aspergillosis: A Fascinating Relationship," *Cureus* 16 (2024): e57917, https://doi.org/10.7759/cureus.57917.

4. G. Trivioli, B. Terrier, and A. Vaglio, "Eosinophilic Granulomatosis With Polyangiitis: Understanding the Disease and Its Management," *Rheumatology* 59, no. Suppl 3 (2020): iii84–iii94, https://doi.org/10.1093/rheumatology/kez570.

5. R. G. Luo, Y. F. Wu, H. W. Lu, et al., "TH2-Skewed Peripheral T-Helper Cells Drive B-Cells in Allergic Bronchopulmonary Aspergillosis," *European Respiratory Journal* 63, no. 5 (2024): 2400386, https://doi.org/10.1183/13993003.00386-2024.

6. L. Hua and M. Xie, "Heterogeneity and Individualized Therapy for Eosinophilic Granulomatosis With Polyangiitis," *Therapeutic Advances in Respiratory Disease* 19 (2025): 17534666251318615, https://doi.org/10.1177/17534666251318615.

7. S. G. Rockson, "Advances in Lymphedema," *Circulation Research* 128, no. 12 (2021): 2003–2016, https://doi.org/10.1161/CIRCRESAHA.121.318307.

8. M. López Paraja, G. Starita Fajardo, I. Donate Velasco, et al., "Molecular Pathogenesis and Targeted Therapies in Eosinophilic Granulomatosis With Polyangiitis: An Updated Review," *International Journal of Molecular Sciences* 26, no. 22 (2025): 11141, https://doi.org/10.3390/ijms262211141.

9. P. Esterre, C. Plichart, M. O. Huin-Blondey, et al., "Circulating Fibrosis Markers, Eosinophil Cationic Protein and Eosinophil Protein X in Patients With *Wuchereria bancrofti* Infection: Association With Clinical Status," *Parasite* 13, no. 2 (2006): 165–170, https://doi.org/10.1051/parasite/2006132165.

10. S. O. Lee and I. K. Kim, "Molecular Pathophysiology of Secondary Lymphedema," *Frontiers in Cell and Development Biology* 12 (2024): 1363811, https://doi.org/10.3389/fcell.2024.1363811.

11. R. Agarwal, I. S. Sehgal, V. Muthu, et al., "Revised ISHAM-ABPA Working Group Clinical Practice Guidelines for Diagnosing, Classifying and Treating Allergic Bronchopulmonary Aspergillosis/Mycoses," *European Respiratory Journal* 63, no. 4 (2024): 2400061, https://doi.org/10.1183/13993003.00061-2024.

12. F. Delestre, A. L. Brun, B. Thoreau, et al., "Clinico-Radiological Correlation and Prognostic Value of Baseline Chest Computed Tomography in Eosinophilic Granulomatosis With Polyangiitis," *Rheumatology* 62, no. 10 (2023): 3351–3357, https://doi.org/10.1093/rheumatology/kead077.

13. R. Agarwal, "High Attenuation Mucoid Impaction in Allergic Bronchopulmonary Aspergillosis," *World Journal of Radiology* 2, no. 1 (2010): 41–43, https://doi.org/10.4329/wjr.v2.i1.41.

International Journal of Rheumatic Diseases

WILEY

International Journal of Rheumatic Diseases

LETTER TO THE EDITOR

Case Report: Successful Treatment of Refractory Palmoplantar Pustulosis With Spesolimab and Apremilast

Lin Jiang | Zhipeng Lin | Jiawen Guo | Zhendong Wei | Aoxue Wang

Department of Dermatology, The Second Hospital of Dalian Medical University, Dalian, China

Correspondence: Aoxue Wang (wangaxdl@163.com)

Received: 25 June 2025 | **Revised:** 26 June 2025 | **Accepted:** 11 May 2026

Keywords: apremilast | IL-36 inhibitor | palmoplantar pustulosis | phosphodiesterase 4 inhibitor | spesolimab

Dear Editor,

Palmoplantar pustulosis (PPP) is a chronic and rare inflammatory dermatosis, recognized as a subtype of pustular psoriasis [1]. The pathogenesis of PPP remains incompletely elucidated. Inherent heterogeneity of PPP often makes patients with the same diagnosis respond differently to agents. Here we report a case of refractory PPP triggered and exacerbated by the COVID-19 vaccine, which showed significant improvement with combination therapy using the IL-36 receptor antagonist (IL-36Ra) spesolimab and the oral phosphodiesterase 4 (PDE4) inhibitor apremilast.

A 43-year-old male developed painful pustules, crusting, and scaling on the palms and soles after receiving his third dose of the inactivated COVID-19 vaccine. He also experienced persistent pain in multiple areas, including the chest, ribs, lower back, and sacroiliac joints. Treatments with acitretin, corticosteroids, tripterygium glycosides, and topical corticosteroid ointment were ineffective. In May 2023, the patient was diagnosed with PPP following a pathological examination (Figure S1). The detailed clinical timeline is presented in Figure 1. He had a generalized pustular psoriasis physician global assessment (GPPGA) score of 3.0 and a generalized pustular psoriasis area and severity index (GPPASI) score of 10.9. After 5 weeks of secukinumab (300 mg weekly), pustules on the hands and feet persisted and arthralgia did not improve. A skin biopsy revealed eczema-like changes, leading to secukinumab discontinuation due to suspected immune shift (Figure S2).

In July 2023, the patient was admitted to the hospital due to recurrent exacerbations of pustules on the hands and feet, along with multiple nails showing irregular pitting, thickening, discoloration, and oil-drop changes (Figure 2A). Laboratory tests revealed elevated blood glucose (8.81 mmol/L), glycated hemoglobin (HbA1c: 7.7%), and immunoglobulin E (206 IU/mL). He started spesolimab (900 mg IV), but after initial symptom relief, the pustules worsened on the palms and soles, and there was no improvement in nail damage (Figure 2B), while arthralgia improved. In consideration of the fact that spesolimab demonstrated a slower onset of efficacy and the patient required rapid disease control, oral apremilast was initiated on August 9 using a dose-escalation protocol (starting at 10 mg daily, increasing incrementally to a maintenance dose of 60 mg daily).

By November 2023, fewer pustules appeared, and nail improvement was observed (Figure 2C). During the follow-up in August 2024, the patient reported mild arthralgia and five to eight new pustules daily. However, erythema and scaling had largely resolved, and the nails had returned to their normal appearance (Figure 2D). The GPPGA and GPPASI scores were 1.0 and 1.1, respectively, with further improvement following the third infusion of spesolimab.

PPP is a clinically and molecularly heterogeneous condition, often resistant to conventional treatments. Moreover, the patient's prolonged smoking habit may have contributed to aggravating the disease refractoriness. In this case, secukinumab induced eczema-like lesions, highlighting the complexity of managing refractory PPP. Spesolimab can rapidly modulate dysregulated molecular pathways in generalized pustular psoriasis by blocking IL-36R and significantly reducing IL-36 pathway-related markers within 1 week. It decreases

Lin Jiang and Zhipeng Lin are co-first authors.

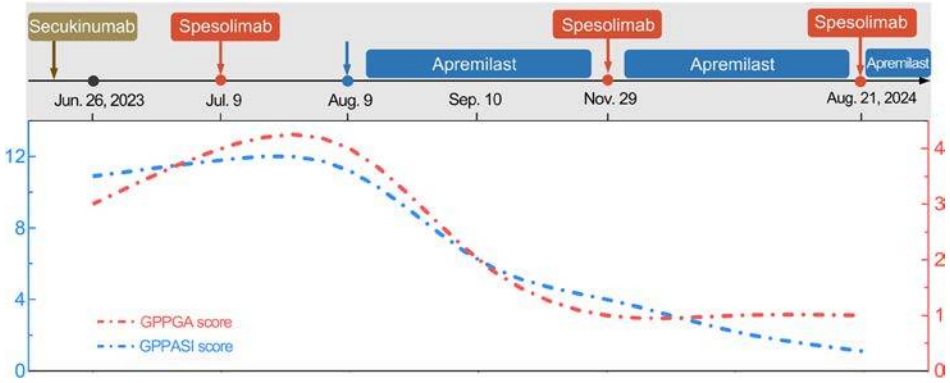

FIGURE 1 | The timeline of the GPPGA and GPPASI scores showed a progressive improvement in the patient's condition. GPPASI, generalized pustular psoriasis area and severity index; GPPGA, generalized pustular psoriasis physician global assessment.

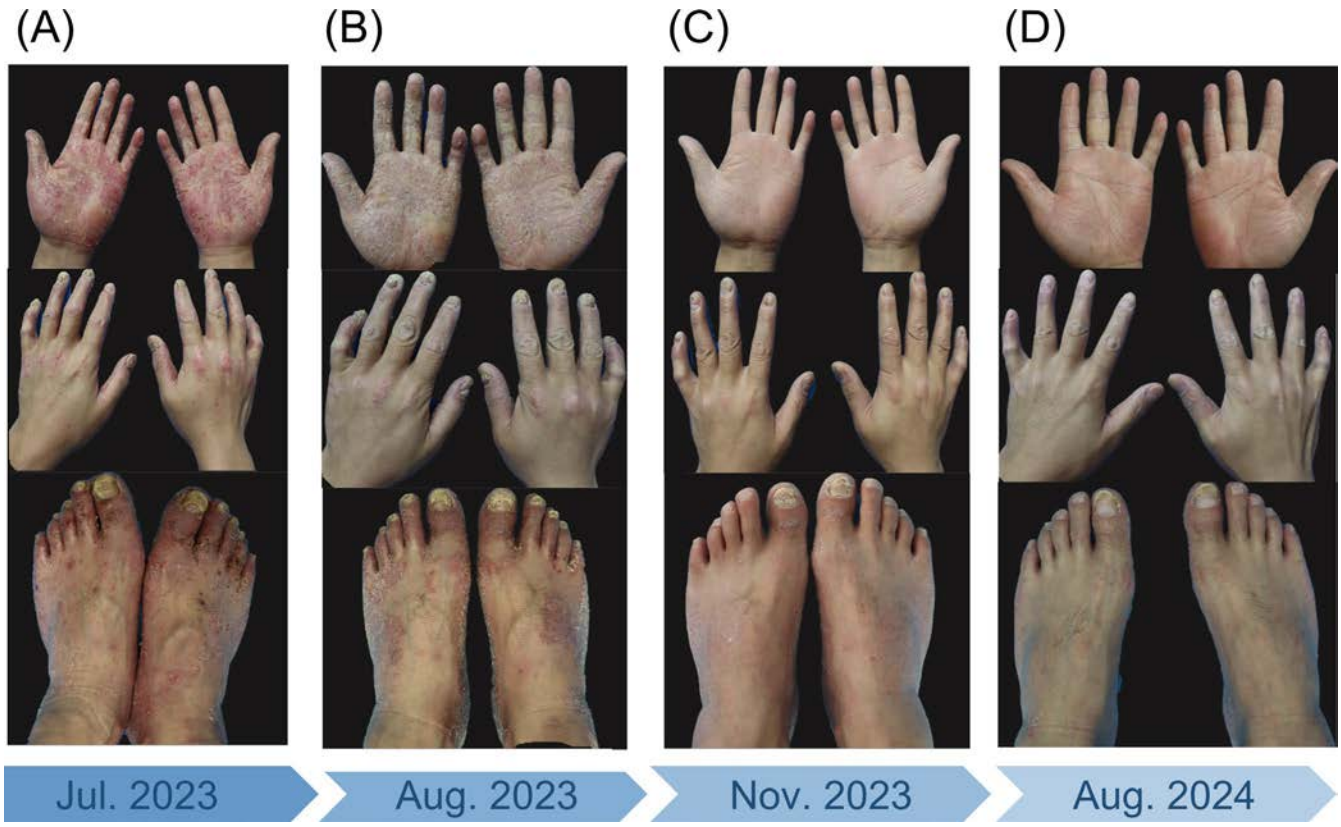

FIGURE 2 | Clinical images before and after initiation of therapy with spesolimab and apremilast in refractory palmoplantar pustulosis. (A) Before treatment with spesolimab, the palms and soles exhibited pronounced erythema, pustules, hyperkeratosis, and scaling. (B) After 4 weeks of spesolimab treatment, there was minimal improvement in the skin lesions. (C) After 3 months of combined oral apremilast, erythema, pustules, and scaling of the palms and soles improved. (D) Skin lesions on the palms and soles completely resolved after 1 year of combined spesolimab and apremilast treatment.

$CD3^+$ T cells, $CD11c^+$ cells, and IL-36γ^+ cells in lesions, ameliorates Th1/Th17 inflammatory responses, and suppresses neutrophil-mediated inflammation [2]. A Phase IIa clinical trial investigating spesolimab for the treatment of PPP suggested potential efficacy; however, it was unsuccessful in meeting its primary endpoints [3]. Furthermore, another phase IIb clinical trial demonstrated that spesolimab provides modest improvements and exhibits favorable tolerability in the treatment of moderate-to-severe PPP [4]. Apremilast indicated efficacy in reducing GPPASI scores and alleviating pruritus and pain, especially with long-term treatment [5]. The combination of spesolimab and apremilast resulted in substantial symptom relief, with reduced pustule formation and improved nail appearance. It is hypothesized that spesolimab and apremilast target distinct pathways—antagonizing IL-36R and PDE4, respectively—and synergistically regulate inflammatory signaling in PPP. This therapeutic approach aligns with other studies reporting favorable outcomes using combination therapies for recalcitrant PPP, such as TNF blockers with ustekinumab [6].

Our case demonstrates the excellent efficacy of spesolimab combined with apremilast in a patient with severe PPP, who had not responded adequately to treatments with acitretin, secukinumab, topical steroids, and systemic therapies. Thus, the combination therapy may be a promising therapeutic option for refractory PPP that warrants further study.

Author Contributions

A.W. designed the report. L.J., Z.L., J.G., and Z.W. contributed to the writing of the original draft of the paper. A.W. contributed to the revision of the draft and served as the published correspondence author. L.J., Z.L., J.G., Z.W., and A.W. reviewed and approved the final manuscript.

Acknowledgments

The authors have nothing to report.

Funding

The authors have nothing to report.

Consent

Written informed consent was obtained from the patient at The Second Hospital of Dalian Medical University in Dalian, China, on December 29, 2023, for purposes of authorship and publication of this case report.

Conflicts of Interest

The authors declare no conflicts of interest.

Data Availability Statement

The data that support the findings of this study are available from the corresponding author upon reasonable request. The data are not publicly available due to privacy or ethical restrictions.

References

1. M. Murakami and T. Terui, "Palmoplantar Pustulosis: Current Understanding of Disease Definition and Pathomechanism," *Journal of Dermatological Science* 98, no. 1 (2020): 13–19, https://doi.org/10.1016/j.jdermsci.2020.03.003.

2. P. Baum, S. Visvanathan, S. Garcet, et al., "Pustular Psoriasis: Molecular Pathways and Effects of Spesolimab in Generalized Pustular Psoriasis," *Journal of Allergy and Clinical Immunology* 149, no. 4 (2022): 1402–1412, https://doi.org/10.1016/j.jaci.2021.09.035.

3. U. Mrowietz, A. D. Burden, A. Pinter, et al., "Spesolimab, an Anti-Interleukin-36 Receptor Antibody, in Patients With Palmoplantar Pustulosis: Results of a Phase IIa, Multicenter, Double-Blind, Randomized, Placebo-Controlled Pilot Study," *Dermatol. Ther. (Heidelb.)* 11, no. 2 (2021): 571–585, https://doi.org/10.1007/s13555-021-00504-0.

4. A. D. Burden, R. Bissonnette, A. A. Navarini, et al., "Spesolimab Efficacy and Safety in Patients With Moderate-To-Severe Palmoplantar Pustulosis: A Multicentre, Double-Blind, Randomised, Placebo-Controlled, Phase IIb, Dose-Finding Study," *Dermatol. Ther. (Heidelb.)* 13, no. 10 (2023): 2279–2297, https://doi.org/10.1007/s13555-023-01002-1.

5. T. Terui, Y. Okubo, S. Kobayashi, et al., "Efficacy and Safety of Apremilast for the Treatment of Japanese Patients With Palmoplantar Pustulosis: Results From a Phase 2, Randomized, Placebo-Controlled Study," *American Journal of Clinical Dermatology* 24, no. 5 (2023): 837–847, https://doi.org/10.1007/s40257-023-00788-2.

6. B. Husson, C. Barbe, S. Hegazy, et al., "Efficacy and Safety of TNF Blockers and of Ustekinumab in Palmoplantar Pustulosis and in Acrodermatitis Continua of Hallopeau," *Journal of the European Academy of Dermatology and Venereology* 34, no. 10 (2020): 2330–2338, https://doi.org/10.1111/jdv.16265.

Supporting Information

Additional supporting information can be found online in the Supporting Information section. **Figure S1:** Pathological images of the skin lesion upon admission. (A) Psoriatic hyperplasia showed Kogoj's micro-abscesses, basket-weave hyperkeratosis, and lymphocyte infiltration around superficial dermal blood vessels (50×). (B) Kogoj's micro-abscesses were polymorphonuclear neutrophil aggregates in the necrotic epidermis beneath the basket-weave hyperkeratosis, forming a sponge-like pattern (100×). **Figure S2:** Histopathological examination of skin lesions after five doses of secukinumab revealed eczematous changes, which were characterized by mild cellular swelling and inflammatory cell infiltration, predominantly in the perivascular region and superficial dermis. (A) 50×; (B) 100×.

International Journal of Rheumatic Diseases

WILEY

International Journal of Rheumatic Diseases

LETTER TO THE EDITOR

Beyond Incidental Findings: Schmorl's Nodes in the Diagnosis of Osteoporotic Vertebral Compression Fractures

Harun Kürşat Karademir | Beytullah Yazar | Ahmet Furkan Çolak | Hilmi Berkan Abacıoğlu | Murat Kara

Department of Physical and Rehabilitation Medicine, Hacettepe University Medical School, Ankara, Turkey

Correspondence: Hilmi Berkan Abacıoğlu (hilmiberkanabacoglu@gmail.com)

Received: 11 November 2025 | **Revised:** 26 May 2026 | **Accepted:** 1 June 2026

Keywords: bone mineral density | degeneration | spine | vitamin D

Dear Editor,

A 73-year-old man presented with gait disturbance and low back pain that had persisted for about 26 years. His symptoms began following a trauma to the vertebral column and spinal cord after being trapped under rubble during an earthquake. At that time, a vertebral fracture was diagnosed, although the specific level was not documented. He was treated conservatively with a brace and did not undergo surgical intervention.

Lumbar magnetic resonance imaging (MRI) revealed diffuse vertebral degeneration with approximately 50% height loss of vertebral height at the L1-L4 levels and multiple Schmorl's nodes (SNs) in the same region (Figure 1). Degenerative and inflammatory changes were also noted around these nodes (Figure 1B). Previous brain MRI had revealed findings consistent with ependymoma and right lateral ventricular enlargement, which were considered clinically stable during follow-up. Despite these findings, the patient remained ambulatory with a walker and independent in daily activities.

On physical examination, vertebral tenderness was not observed. Neurological evaluation revealed weaknesses in muscle strength of 1/5 in the left ankle and 1st toe dorsiflexion, and 3/5 in the left hip abduction, with a positive Babinski sign on the left side. Osteoporosis risk factors were otherwise unremarkable. Bone mineral densitometry (BMD) results demonstrated a T-score of 0.0 at the lumbar spine (L1-L4) and −1.0 at the left femoral neck. FRAX analysis estimated a 10-year probability of 7.8% for a major osteoporotic fracture and 3.4% for a hip fracture. As quantitative computed tomography (QCT) for BMD assessment was not available at our institution, we were unable to perform this evaluation. Based on these findings and FRAX score, intravenous zoledronic acid 5 mg for a year and daily vitamin D supplementation were initiated.

Osteoporosis is a progressive metabolic disease characterized by decreased bone mass and deterioration of bone microarchitecture, leading to increased fracture risk. Early diagnosis and treatment are essential to prevent fragility fractures. Dual-energy X-ray absorptiometry (DXA) is the gold standard for BMD assessment; however, its accuracy at the lumbar spine (L1–L4) can be compromised by degenerative changes, orthopedic implants, or—most notably in our patient—vertebral fractures [1–3].

Schmorl's nodes (SNs), defined as herniations of the nucleus pulposus through the cartilaginous and bony endplates into the adjacent vertebral body, are often asymptomatic and detected incidentally [4]. However, they can be associated with back pain and impairment of quality of life. In our patient, although overt symptoms were absent, MRI revealed multiple SNs and advanced vertebral degeneration accompanied by pronounced endplate inflammation.

Previous studies have shown a strong association between SNs and osteoporosis [5, 6]. Their presence should prompt further investigation for bone fragility [1, 2]. Large SNs, particularly when accompanied by inflammatory changes, may resemble osteoporotic compression fractures, complicating the differential diagnosis. However, SNs typically appear as localized endplate depressions with preserved vertebral height, distinguishing them from true compression fractures [7]. Nevertheless, due to their association with endplate fragility, multiple SNs may indicate increased susceptibility to osteoporotic vertebral fractures.

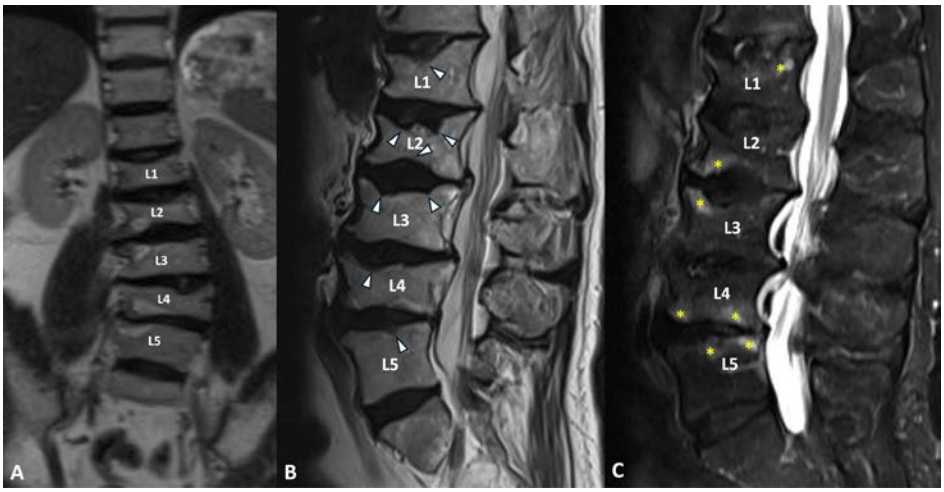

FIGURE 1 | Coronal magnetic resonance imaging (MRI) using Half Fourier Single-shot Turbo spin-Echo (HASTE) sequence reveals height loss at L1–4 vertebrae (A). T2-weighted Turbo Spin Echo (TSE) MRI demonstrates wedge-type osteoporotic fractures at L1–2 vertebrae and a biconcave deformity at L4 vertebra, along with multiple Schmorl's nodes *(arrowheads)* (B). Spectral Attenuated Inversion Recovery (SPAIR) sequence illustrates associated inflammatory signals at the vertebral endplates *(asterisks)* (C).

This highlights the importance of comprehensive clinical and radiological evaluation. In our case, the coexistence of vertebral height loss and multiple SNs supported the diagnosis of osteoporotic compression fractures.

In conclusion, degenerative spinal changes can significantly reduce the reliability of lumbar BMD measurements. Therefore, a holistic evaluation integrating clinical, radiological, and laboratory data is warranted. Asymptomatic or "silent" osteoporosis can easily be overlooked, yet it carries significant risks for diminished quality of life and increased morbidity. Needless to say, the identification of SNs should prompt clinicians to consider underlying osteoporosis and possible vertebral compression fractures.

Author Contributions

Harun Kürşat Karademir: investigation, writing – original draft preparation. **Beytullah Yazar:** investigation, writing – original draft preparation. **Ahmet Furkan Çolak:** investigation, writing – original draft preparation. **Hilmi Berkan Abacıoğlu:** conceptualization, investigation, writing – original draft preparation. **Murat Kara:** supervision, writing – review and editing. All authors contributed to the study conception and design, critically reviewed the manuscript, approved the final version for publication, and meet the ICMJE criteria for authorship.

Acknowledgments

The authors have nothing to report.

Funding

The authors have nothing to report.

Consent

Informed consent was obtained from the patient.

Conflicts of Interest

The authors declare no conflicts of interest.

Data Availability Statement

Data sharing not applicable to this article as no datasets were generated or analysed during the current study.

References

1. B. Çulha, H. B. Abacıoğlu, and M. Kara, "Schmorl's Nodes: A Clinical Clue for Disguised Osteoporosis," *Geriatrics & Gerontology International* 25 (2025): 1427–1428.

2. H. B. Abacıoğlu, P. Analay, M. Kara, and L. Özçakar, "Diagnosing Osteoporosis Despite Schmorl's Nodes and Ankylosing Spondylitis," *Journal of Clinical Densitometry* 28 (2025): 101608, https://doi.org/10.1016/j.jocd.2025.101608.

3. J. H. Krege, P. D. Miller, L. Lenchik, D. A. Misurski, and P. Chen, "New or Worsening Lumbar Spine Vertebral Fractures Increase Lumbar Spine Bone Mineral Density and Falsely Suggest Improved Skeletal Status," *Journal of Clinical Densitometry* 9 (2006): 144–149.

4. K. A. Kyere, K. D. Than, A. C. Wang, et al., "Schmorl's Nodes," *European Spine Journal* 21 (2012): 2115–2121.

5. M. Othman and V. K. Menon, "The Prevalence of Schmorl's Nodes in Osteoporotic vs Normal Patients: A Middle Eastern Population Study," *Osteoporosis International* 33 (2022): 1493–1499.

6. Y. X. J. Wáng, X. R. Wang, J. C. S. Leung, B. W. M. Yu, J. F. Griffith, and T. C. Y. Kwok, "Schmorl's Nodes Are Associated With Prevalent Osteoporotic Vertebral Fracture and Low Bone Mineral Density: A Population-Based Thoracic Spine MRI Study in Older Men and Women," *Quantitative Imaging in Medicine and Surgery* 13 (2023): 1914–1926.

7. Y. X. J. Wáng, F. R. Santiago, M. Deng, and M. H. Nogueira-Barbosa, "Identifying Osteoporotic Vertebral Endplate and Cortex Fractures," *Quantitative Imaging in Medicine and Surgery* 7 (2017): 555–591.

International Journal of Rheumatic Diseases

WILEY

International Journal of Rheumatic Diseases

LETTER TO THE EDITOR

Circulating Mucosal-Associated Invariant T Cells in Takayasu Arteritis

Yanmei Li[1,2] | Jun Du[1,2] | Na Zhang[1,2] | Hou Hou[1,2] | Wei Wei[1,2]

[1]Department of Rheumatology and Immunology, Tianjin Medical University Tianjin General Hospital, Tianjin, China | [2]Tianjin Medical University General Hospital Medical Center for Rheumatology and Immunology, Tianjin, China

Correspondence: Hou Hou (houhou8@163.com) | Wei Wei (tjweiwei2003@163.com)

Received: 3 January 2026 | **Revised:** 21 May 2026 | **Accepted:** 24 May 2026

Dear Editor,

Takayasu arteritis (TAK) is a rare type of large vessel vasculitis that involves the aorta, its main branches, and the pulmonary artery. Inflammatory lesions are characterized by arterial wall thickening and subsequent luminal stenosis, occlusion, dilatation, or aneurysm formation. Although the exact etiology of TAK remains unknown, genetic factors, environmental influences, infections, and autoimmune reactions are believed to play a role in its development. T cells, NK cells and γδ T cells have been implicated in TA pathophysiology because of their infiltration within arteries [1, 2]. Mucosa-associated invariant T (MAIT) cells are an innate-like subset of T cells that express the evolutionarily conserved semi-invariant T cell antigen receptor (TCR) α-chain Vα7.2-Jα33/Jα20/Jα12 in humans [3]. Mature MAIT cells are predominantly found in peripheral blood, intestinal lamina propria lymphoid tissue, liver, and lungs and are restricted by major histocompatibility complex-like molecules (MR1) [4]. Human MAIT cells can be identified by specific MR1 tetramers as well as surface markers such as TCR Vα7.2 and CD161 [5, 6]. Additionally, MAIT cells can be activated by multiple cytokines, including IL-2, IL-12, IL-15, and IL-18, independent of their TCRs, leading to the release of interferon-gamma (IFNγ), tumor necrosis factor-alpha (TNFα), and IL-17, as well as inflammatory and cytotoxic molecules such as granzyme B and perforin, to rapidly mediate immune responses and provide protection against infection [7]. MAIT cells play important roles in infectious and autoimmune diseases [8]. However, there have been no studies on the changes of MAIT cells in TAK. In this study, we explored alterations in the frequency and phenotype of MAIT cells in patients with TAK to clarify their role in disease.

The study included 14 treatment-naive active patients, 8 inactive TAK patients, and 22 healthy controls (HCs) (Table 1). Patients with active TAK had a shorter disease duration and elevated Indian Takayasu Clinical Activity Score (ITAS) 2010. Peripheral blood mononuclear cells (PBMCs) were obtained via Ficoll-Paque (GE Healthcare, USA) gradient centrifugation. PBMCs were first stained with a Zombie NIR Fixable Viability Kit (BioLegend, USA) to remove dead cells. Cell surface and intracellular staining were performed with the following monoclonal antibodies (Abs): anti-TCR-Vα7.2, anti-CD3, anti-CD161, anti-CD69, anti-PD-1, anti-TNFα, anti-IFNγ, anti-IL-17, anti-CCR2 (BioLegend, USA), and 5-OP-RU tetramer (NIH, USA). To detect cytokine production, PBMCs were cultured in RPMI medium supplemented with 10% fetal bovine serum and stimulated with Leukocyte Activation Cocktail (BD Biosciences, USA) according to the manufacturer's instructions. Data were acquired via flow cytometry (BD LSR-Fortessa, USA) and analyzed with FlowJo software version 10.8 (Ashland, OR, USA).

Statistical evaluations were performed with GraphPad Prism 9.0 (GraphPad Software Inc., USA). Data are expressed as medians with interquartile ranges. The Kruskal–Wallis test with Dunn's correction was used for multiple comparisons. Correlations were assessed with Pearson correlation. Differences at $p < 0.05$ were considered statistically significant.

MAIT cells were defined as CD3+ 5-OP-RU tetramer+ cells (Figure 1A). We found that the frequency of circulating MAIT cells (among CD3+ T cells) in the active TAK group was significantly higher than that in the inactive TAK group ($p = 0.002$)

Yanmei Li and Jun Du contributed equally to this study.

TABLE 1 | Characteristics of TAK patients and healthy controls.

	HC ($n=22$)	Active TAK ($n=14$)	Inactive TAK ($n=8$)
Age (years, range)	43.5 (25–62)	39 (25–63)	42.5 (17–59)
Sex (male/female)	2/20	1/13	1/7
Duration (months, range)	NA	6 (1–72)	60 (12–360)***
ITAS2010	NA	4.5 (2-6)	1 (0–1)****
CRP (mg/dL, range)	NA	2.02 (0.20–7.68)	0.3 (0.1–0.62)*
ESR (mm/h)	NA	45 (10–68)	16 (3–25)**
Corticosteroids Immunosuppressant	NA	No	Yes
Cyclosporine A			1
Methotrexate			4
Mycophenolate Mofetil			4
Cyclophosphamide			1
Tocilizumab			1

Abbreviations: CRP, C reactive protein; ESR, erythrocyte sedimentation rate; HC, healthy controls; ITAS, Indian Takayasu Clinical Activity Score; NA, not applicable; TAK, Takayasu arteritis.
*$p<0.05$.
**$p<0.01$.
***$p<0.001$.
****$p<0.0001$.

and the HC group ($p=0.018$; Figure 1B). In all the TAK patients, the percentage of MAIT cells was positively correlated with ITAS 2010, but was not significantly correlated with erythrocyte sedimentation rate (ESR) or C reactive protein (CRP) level (Figure 1C). Next, we investigated the activation and chemokine receptor expression of circulating MAIT cells in TAK patients. The frequency of MAIT cells expressing CD69 (an early activation marker) was lower in inactive TAK patients than in active TAK patients ($p=0.003$) and HC ($p=0.026$), while the expression of PD-1 (a late activation marker) was not significantly different (Figure 1D). Compared with inactive patients, patients with active TAK had a higher frequency of C-C chemokine receptor type 2 (CC2R)-expressing MAIT cells ($p=0.0002$; Figure 1E), suggesting that MAIT cells exhibited weak chemotaxis after treatment. We subsequently examined the expression levels of IFNγ, TNFα, and IL-17 in TAK patients before and after treatment (Figure 1F). The results revealed that the percentages of MAIT cells that secreted these cytokines did not significantly differ among the three groups (Table 2).

This study explored alterations in immune dynamics and the potential function of MAIT cells in patients with TAK. We found that the frequency of circulating MAIT cells in active TAK patients was elevated, but their levels decreased following treatment. In fact, in most rheumatic diseases, including ANCA associated vasculitis and polymyalgia rheumatica, the frequency of MAIT cells in the peripheral blood is decreased, possibly because of recruitment to affected organs and overactivation-induced exhaustion [9–12]. A previous study revealed that in giant cell arteritis (GCA), another type of large-vessel vasculitis, MAIT cells are not significantly altered in peripheral blood but are detected in affected temporal arteries [13]. In patients with GCA, MAIT cells are present in a higher proportion in the arterial wall than in the blood [13]. However, our study revealed that the frequency of MAIT cells is increased in patients with active TAK. Furthermore, the expression of the late activation marker PD-1 did not significantly differ among the three groups, suggesting that MAIT cells do not exhibit an exhausted phenotype in TAK. Additionally, we observed a trend toward increased CCR2 expression on MAIT cells before treatment, which decreased after treatment. Previous studies have shown that CCL2 is elevated in the serum of patients with Takayasu arteritis [14, 15]. These findings indicate that MAIT cells might be chemotactically attracted to the involved arterial wall in TAK. However, this needs to be verified by quantifying MAIT cells at arteritis sites. The observed alterations of MAIT cells in TAK necessitate further verification through larger-scale sample and longitudinal cohort studies.

CD69 expression of MAIT cells is reduced in inactive TAK patients than in active TAK patients and HCs. We speculate that the downregulation of CD69 expression on MAIT cells following treatment may be associated with glucocorticoid and immunosuppressant therapy. Serum TNFα, IFNγ, and IL-17 levels are elevated in patients with Takayasu arteritis [16]. However, compared with those in HCs, the expression of activation markers and cytokines in MAIT cells in TAK patients did not significantly differ, suggesting that MAIT cells do not exhibit increased activation characteristics in disease. Another possibility is that the small sample size was insufficient to achieve statistical power. In rheumatic diseases such as rheumatoid arthritis, systemic lupus erythematosus, systemic sclerosis, primary Sjögren's syndrome, and psoriatic arthritis, activated MAIT cells exhibit a distinct cytokine secretion profile [12]. MAIT cell activation can be achieved through either a TCR-dependent mechanism or stimulation by cytokines such as IL-6, IL-18, and IFNα [17]. Larger sample sizes and further investigations into the function of MAIT cells in TAK are needed in future studies.

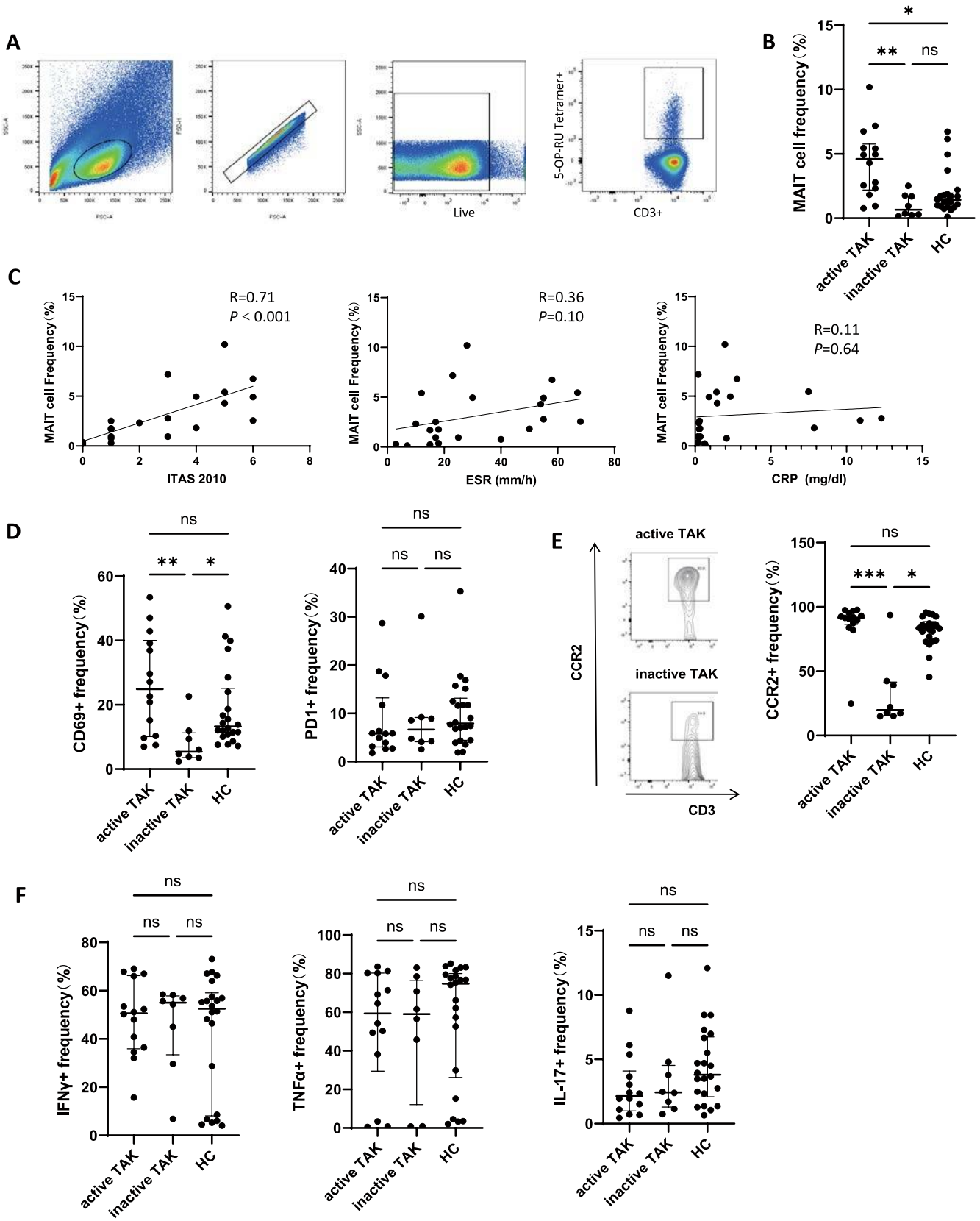

FIGURE 1 | Changes of peripheral blood MAIT cell frequency in TAK patients. (A) Gating strategy for MAIT cells. (B) MAIT cell frequency comparison among HC, active and inactive TAK patients. (C) Correlations between the MAIT cell frequency and clinical parameters (ITAS 2010, ESR, CRP) in TAK patients. (D) CD69 and PD-1 expression on MAIT cells in three groups. (E) Representative plot of CCR2 expression on MAIT cells, and comparison among HC, active as well as inactive TAK patients. (F) Cytokines production by MAIT cells from TAK patients, PMA plus ionomycin for 5 h. $^{*}p < 0.05$, $^{**}p < 0.01$, $^{***}p < 0.001$, ns = not significant. (active: $N = 14$, inactive: $N = 8$; HC: $N = 22$). The Kruskal–Wallis test with Dunn's correction was used for multiple comparisons. Correlations were analyzed using Spearman's correlation analysis.

TABLE 2 | Changes in the percentage of circulating MAIT cells in the three groups.

	HC ($n=22$)	Active TAK ($n=14$)	Inactive TAK ($n=8$)
MAIT cell frequency (median, %)	1.42 (0.92–1.95)	4.61 (2.20–5.77)*	0.66 (0.25–1.74)##
CD69+ MAIT cell frequency (median, %)	13.25 (10.63–25.13)	24.85 (10.14–40.05)	5.42 (3.60–11.27)*,##
PD1+ MAIT cell frequency (median, %)	7.90 (4.42–13.15)	5.81 (3.05–13.23)	6.65 (4.13–9.15)
CCR2+ MAIT cell frequency (median, %)	83.35 (73.7–95.6)	91.65 (86.43–95.70)	19.80 (15.63–41.50)*,###
IFNγ+ MAIT cell frequency (median, %)	52.50 (8.09–59.13)	50.65 (35.93–66.25)	55.00 (33.45–51.57)
TNFα+ MAIT cell frequency (median, %)	74.80 (26.23–80.05)	59.35 (29.49–80.30)	59.00 (12.13–76.58)
IL17+ MAIT cell frequency (median, %)	3.81 (2.10–6.75)	2.15 (1.00–4.09)	2.43 (1.29–4.54)

Abbreviations: HC, healthy controls; MAIT, mucosa-associated invariant T; TAK, Takayasu arteritis.
*$p<0.05$ compared with the HC group.
##$p<0.01$ compared with the active TAK group.
###$p<0.001$ compared with the active TAK group.

In summary, we present the first investigation of MAIT cell alterations in the peripheral blood of TAK patients. However, the study has several limitations, including a small sample size and a lack of involvement of affected tissues. Further mechanistic studies are needed to elucidate the role of MAIT cells in TAK.

Author Contributions

Y.L. and J.D. primarily designed and performed the analysis, verified the data, and wrote the manuscript; N.Z. reviewed and revised the article; H.H. and W.W. supervised the entire project. All authors read the manuscript, provided critical feedback on the intellectual content, and approved the final version.

Acknowledgments

The MR1 tetramer technology was developed jointly by Dr. James McCluskey, Dr. Jamie Rossjohn, and Dr. David Fairlie, and the material was produced by the NIH Tetramer Core Facility as permitted to be distributed by the University of Melbourn.

Funding

This work is supported by Tianjin Health Research Project (TJWJ2023QN005, TJWJ2025ZK001), Tianjin Key Clinical Specialty and Tianjin Key Medical Discipline Construction Project (TJYXZDXK-3-011C).

Conflicts of Interest

The authors declare no conflicts of interest.

Data Availability Statement

The original data presented in the study can be directed to the corresponding authors.

References

1. B. Savioli, H. F. V. Torquato, E. J. Paredes-Gamero, et al., "Effector CD4+ T-Cell Subsets in Takayasu Arteritis-Differences Between the Peripheral Blood and the Aorta," *Clinical and Experimental Immunology* 217, no. 2 (2024): 183–194.

2. Y. Seko, S. Minota, A. Kawasaki, et al., "Perforin-Secreting Killer Cell Infiltration and Expression of a 65-kD Heat-Shock Protein in Aortic Tissue of Patients With Takayasu's Arteritis," *Journal of Clinical Investigation* 93, no. 2 (1994): 750–758.

3. D. I. Godfrey, A. P. Uldrich, J. McCluskey, J. Rossjohn, and D. B. Moody, "The Burgeoning Family of Unconventional T Cells," *Nature Immunology* 16, no. 11 (2015): 1114–1123.

4. C. Zhu, Q. Huai, Y. Du, et al., "Mucosal-Associated Invariant T Cells: Origins, Biological Functions, Diseases, and Therapeutic Targets," *MedComm (2020)* 6, no. 11 (2025): e70445.

5. A. Rahimpour, H. F. Koay, A. Enders, et al., "Identification of Phenotypically and Functionally Heterogeneous Mouse Mucosal-Associated Invariant T Cells Using MR1 Tetramers," *Journal of Experimental Medicine* 212, no. 7 (2015): 1095–1108.

6. E. Billerbeck, Y. H. Kang, L. Walker, et al., "Analysis of CD161 Expression on Human CD8+ T Cells Defines a Distinct Functional Subset With Tissue-Homing Properties," *Proceedings of the National Academy of Sciences of the United States of America* 107, no. 7 (2010): 3006–3011.

7. X. Z. Tang, J. Jo, A. T. Tan, et al., "IL-7 Licenses Activation of Human Liver Intrasinusoidal Mucosal-Associated Invariant T Cells," *Journal of Immunology* 190, no. 7 (2013): 3142–3152.

8. A. Toubal, I. Nel, S. Lotersztajn, and A. Lehuen, "Mucosal-Associated Invariant T Cells and Disease," *Nature Reviews. Immunology* 19, no. 10 (2019): 643–657.

9. C. Braudeau, K. Amouriaux, A. Néel, et al., "Persistent Deficiency of Circulating Mucosal-Associated Invariant T (MAIT) Cells in ANCA-Associated Vasculitis," *Journal of Autoimmunity* 70 (2016): 73–79.

10. B. Fazekas, A. Moreno-Olivera, Y. Kelly, et al., "Alterations in Circulating Lymphoid Cell Populations in Systemic Small Vessel Vasculitis Are Non-Specific Manifestations of Renal Injury," *Clinical and Experimental Immunology* 191, no. 2 (2018): 180–188.

11. S. Nakajima, A. Chiba, A. Makiyama, et al., "Association of Mucosal-Associated Invariant T Cells With Different Disease Phases of Polymyalgia Rheumatica," *Rheumatology (Oxford, England)* 59, no. 10 (2020): 2939–2946.

12. Y. Li, J. Du, and W. Wei, "Emerging Roles of Mucosal-Associated Invariant T Cells in Rheumatology," *Frontiers in Immunology* 13 (2022): 819992.

13. T. Ghesquière, M. Ciudad, A. Ramon, et al., "Mucosal-Associated Invariant T Cells in Giant Cell Arteritis," *Journal of Autoimmunity* 121 (2021): 102652.

14. X. Zhang, S. Li, W. Lason, M. Greco, P. Klenerman, and T. S. C. Hinks, "MAIT Cells Protect Against Sterile Lung Injury," *Cell Reports* 44, no. 2 (2025): 115275.

15. V. Dhawan, N. Mahajan, and S. Jain, "Role of C-C Chemokines in Takayasu's Arteritis Disease," *International Journal of Cardiology* 112, no. 1 (2006): 105–111.

16. B. Savioli, W. H. Abdulahad, E. Brouwer, C. G. M. Kallenberg, and A. W. S. de Souza, "Are Cytokines and Chemokines Suitable Biomarkers for Takayasu Arteritis?," *Autoimmunity Reviews* 16, no. 10 (2017): 1071–1078.

17. A. Chiba, N. Tamura, K. Yoshikiyo, et al., "Activation Status of Mucosal-Associated Invariant T Cells Reflects Disease Activity and Pathology of Systemic Lupus Erythematosus," *Arthritis Research & Therapy* 19, no. 1 (2017): 58.

International Journal of Rheumatic Diseases

WILEY

International Journal of Rheumatic Diseases

EDITORIAL

IL-18 as a Driver in Pathogenic Th17 Cell Responses: A Promising Therapeutic Target in Autoimmune Diseases

Ming Liu[1] | Yue Zhao[2] | Ligang Jie[3] | Mengna Zhao[2] | Yuan Tang[2] | Liwei Lu[2]

[1]Department of Rheumatology and Immunology, The First Affiliated Hospital of Shaoyang University, Shaoyang, China | [2]Department of Pathology, Shenzhen Institute of Research and Innovation, The University of Hong Kong, Hong Kong, China | [3]Department of Rheumatology and Immunology, Zhujiang Hospital, Southern Medical University, Guangzhou, China

Correspondence: Yuan Tang (yuantang@hku.hk) | Liwei Lu (liweilu@hku.hk)

Received: 15 January 2026 | **Revised:** 6 May 2026 | **Accepted:** 20 May 2026

Autoimmune diseases, such as primary Sjögren's syndrome (pSS) and systemic lupus erythematosus (SLE), pose a substantial global health burden due to aberrant immune attacks on self-tissues. Increasing evidence indicates a pivotal role of IL-17-producing CD4$^+$ T helper 17 (Th17) cells in the pathogenesis of autoimmune disorders, in which Th17 cells promote autoimmune inflammation and tissue injury through the production of various effector molecules. The inflammatory microenvironment critically governs Th17 cell plasticity, polarizing them into either pathogenic Th17 (pTh17) cells to produce potent effector molecules like IFN-γ and GM-CSF with highly inflammatory phenotypes or conventional Th17 (cTh17) cells that maintain tissue homeostasis via regulatory mediators such as IL-10. Functional studies demonstrate that pTh17 cells drive breakdown of immune tolerance and inflammatory tissue destruction in diseases such as multiple sclerosis and autoimmune arthritis [1]. Although inflammatory cytokines including IL-6, IL-23, and IL-1β have been extensively studied in Th17 biology and disease pathology [2], the involvement of interleukin-18 (IL-18), a potent inflammasome-associated cytokine, in autoimmune pathogenesis has remained incompletely defined.

In a newly published paper in Cellular & Molecular Immunology, Tang et al. report a pivotal role for IL-18 as a potent driver in pTh17 cell responses in pSS and SLE [3]. The authors demonstrate that IL-18 signaling stabilizes mRNA of the transcription factor basic helix–loop–helix family member e40 (Bhlhe40) in a Stat3-dependent manner, thereby promoting glycolytic reprogramming and production of GM-CSF and IL-17 (Figure 1). The identified IL-18/Stat3/Bhlhe40/glycolysis axis reprograms conventional "non-pathogenic" Th17 cells into highly proinflammatory effectors. Remarkably, neutralizing IL-18 markedly attenuated disease severity in murine models of experimental SS and lupus, providing robust preclinical evidence for IL-18 blockade as a therapeutic approach.

Over the past decades, IL-18 has been predominantly regarded as a proinflammatory cytokine favoring Th1 and natural killer (NK) cell responses, while its impact on Th17 cell biology has remained ambiguous, as indicated in previous studies that IL-18 exerts an inhibitory function in regulating homeostatic Th17 responses within the gut [4]. Tang and colleagues first observed that both human and murine Th17 cells express the highest levels of IL-18Rα among CD4$^+$ T cell subsets, rendering them uniquely responsive to IL-18. In culture, the addition of exogenous IL-18 to IL-6/TGF-β1-polarized cTh17 cells rapidly induced a pathogenic phenotype characterized by elevated GM-CSF production, a hallmark of encephalitogenic and arthritogenic Th17 subsets in autoimmune development [5]. Mechanistically, IL-18 induced Stat3 phosphorylation, leading to enhanced Bhlhe40 mRNA stability and expression. Bhlhe40, previously linked to circadian and hypoxic responses, has emerged as a critical mediator of Th17 pathogenicity [6], while its knockdown abolished IL-18-induced GM-CSF upregulation in Th17 cells. Furthermore, IL-18-primed pTh17 cells exhibited increased glucose uptake via glucose transporter 3 (GLUT3) and glycolytic flux, with Bhlhe40 directly controlling key glycolytic enzymes. These findings integrate transcriptional and metabolic reprogramming as intertwined features of Th17 pathogenicity.

In this study, the clinical relevance of these findings is further highlighted by the data from both plasma and saliva samples from patients. Levels of bioactive free IL-18 in saliva and plasma were elevated in pSS and SLE patients and associated closely

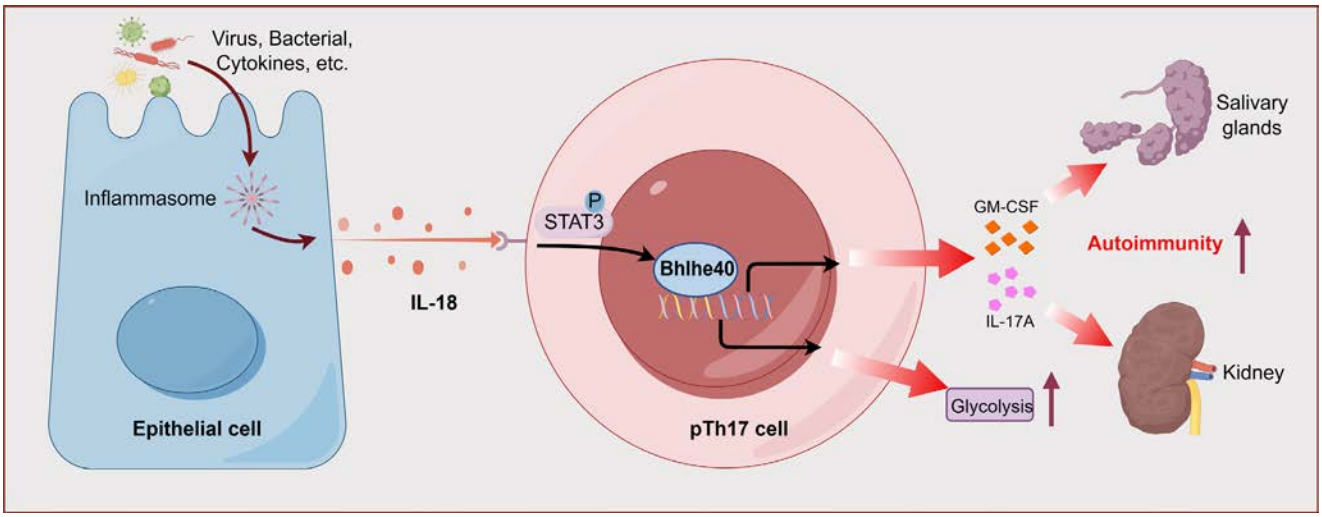

FIGURE 1 | Epithelial-derived IL-18 drives autoimmune development by amplifying pathogenic Th17 (pTh17) cell responses. Inflammatory triggers, such as viruses, bacteria, and cytokines, promote IL-18 release from epithelial cells. IL-18 drives phosphorylation of Stat3 in Th17 cells, resulting in increased expression of Bhlhe40, which promotes the proinflammatory functions of pTh17 cells through enhanced IL-17 and GM-CSF production and elevated glycolytic activity. These effector cytokines drive glandular inflammation in salivary glands and renal pathology in the kidney, leading to tissue damage and autoimmune disease progression in pSS and SLE.

with disease activity. IL-18 overexpression in salivary gland acinar and renal tubular epithelial cells suggested non-canonical IL-18 production from non-hematopoietic sources, possibly mediated by toll-like receptor and type I interferon signaling independently of classical inflammasome pathways in immune cells. In mice with experimental SS, both local and systemic IL-18 blockade by anti-IL-18 monoclonal antibody improved salivary function, reduced autoantibody titers, suppressed pTh17 infiltration, and ameliorated disease development. Similar effects of IL-18 neutralization were observed in lupus mice, showing significantly attenuated disease progression.

This work has several critical translational implications. Firstly, it positions IL-18 as a core cytokine alongside established drivers, such as IL-1β, IL-6, and IL-23, of Th17 pathogenicity, but through a distinct Bhlhe40-dependent metabolic axis. Moreover, the elevated salivary IL-18 level may serve as a promising, non-invasive and accessible biomarker for glandular involvement in pSS. Therapeutically, these findings strongly support the rapid repurposing of existing IL-18 inhibitors such as recombinant IL-18 binding protein (tadekinig alfa) [7] or anti-IL-18 antibodies [8] for potential clinical applications in treating pSS and SLE, particularly in Th17-dominant or treatment-refractory patients. As IL-18 signaling converges on Stat3, combining IL-18 blockade with the Janus kinase-signal transducer and activator of transcription (JAK–STAT) inhibitors may provide synergistic efficacy. Therefore, targeting IL-18 represents a promising upstream intervention with both biomarker-guided and combinatorial therapeutic potential.

However, certain limitations from this study warrant further investigation. While available murine models may recapitulate key features of pSS and SLE, interspecies differences in IL-18 signaling, such as human-specific isoforms or receptor affinities, may affect translatability. Although the investigation centers on $CD4^+$ T cells, the potential impact of IL-18 on IL-17 production by innate lymphoid cells or γδ T cells, an important alternative source in mucosal and peripheral tissues [9], remains unexamined. Additionally, the reliance on bulk RNA sequencing may obscure heterogeneity within Th17 populations, potentially averaging out subpopulation-specific signals, whereas single-cell analyses could more precisely define the Bhlhe40-driven transcriptional signature. Finally, while the efficacies of IL-18 blockade are evident in preclinical experiments, long-term risks such as impaired host defense against intracellular pathogens require careful monitoring in future studies. Prospective comparisons with approved agents targeting the IL-17 axis (e.g., secukinumab), noted for paradoxically aggravating inflammatory bowel diseases such as Crohn's disease [10], may facilitate further validation for IL-18-targeted interventions in autoimmune diseases and autoinflammatory disorders [11, 12].

In summary, these new findings have unveiled a pivotal role of the IL-18-Bhlhe40 axis in Th17 pathobiology, establishing IL-18 neutralization as an attractive upstream intervention for Th17-driven autoimmune diseases. With existing agents already in clinical use for other indications, targeting IL-18 offers a new venue from bench to bedside, potentially broadening treatment options for pSS, SLE, and related autoimmune disorders.

Author Contributions

Ming Liu: conceptualization, writing original draft. **Yue Zhao:** writing original draft. **Mengna Zhao:** writing original draft. **Ligang Jie:** writing original draft. **Yuan Tang:** review and editing. **Liwei Lu:** review and editing, supervision, management. All authors have read and agreed to the published version of the manuscript.

Funding

This work was supported by National Natural Science Foundation of China (U25A6004), Hunan Provincial Natural Science Foundation of China (2025JJ81119), the Scientific Research Project of Hunan Provincial Department of Education (Excellent Youth Project, 24B0700) and the Shaoyang Science and Technology Bureau (2024PT4053).

Conflicts of Interest

The authors declare no conflicts of interest.

Data Availability Statement

Data sharing not applicable to this article as no datasets were generated or analyzed during the current study.

References

1. X. Wu, J. Tian, and S. Wang, "Insight Into Non-Pathogenic Th17 Cells in Autoimmune Diseases," *Frontiers in Immunology* 9 (2018): 1112, https://doi.org/10.3389/fimmu.2018.01112.

2. Y. Lee, A. Awasthi, N. Yosef, et al., "Induction and Molecular Signature of Pathogenic TH17 Cells," *Nature Immunology* 13 (2012): 991–999, https://doi.org/10.1038/ni.2416.

3. Y. Tang, Y. Zhao, Z. Chen, et al., "IL-18 Drives the Bhlhe40-Mediated Pathogenic Th17 Cell Response and Exacerbates Autoimmune Disease Progression," *Cellular & Molecular Immunology* 22 (2025): 1581–1597, https://doi.org/10.1038/s41423-025-01356-w.

4. O. J. Harrison, N. Srinivasan, J. Pott, et al., "Epithelial-Derived IL-18 Regulates Th17 Cell Differentiation and Foxp3$^+$ Treg Cell Function in the Intestine," *Mucosal Immunology* 8 (2015): 1226–1236, https://doi.org/10.1038/mi.2015.13.

5. K. Ghoreschi, A. Laurence, X.-P. Yang, et al., "Generation of Pathogenic TH17 Cells in the Absence of TGF-β Signalling," *Nature* 467 (2010): 967–971, https://doi.org/10.1038/nature09447.

6. C.-C. Lin, T. R. Bradstreet, E. A. Schwarzkopf, et al., "IL-1–Induced Bhlhe40 Identifies Pathogenic T Helper Cells in a Model of Autoimmune Neuroinflammation," *Journal of Experimental Medicine* 213 (2016): 251–271, https://doi.org/10.1084/jem.20150568.

7. C. Gabay, B. Fautrel, J. Rech, et al., "Open-Label, Multicentre, Dose-Escalating Phase II Clinical Trial on the Safety and Efficacy of Tadekinig Alfa (IL-18BP) in Adult-Onset Still's Disease," *Annals of the Rheumatic Diseases* 77 (2018): 840–847, https://doi.org/10.1136/annrheumdis-2017-212608.

8. Apollo Therapeutics Ltd, "A Phase 1b, Multicenter, Open-Label Study to Evaluate the Safety and Tolerability, Efficacy, Pharmacokinetics, and Pharmacodynamics of Camoteskimab in Subjects With Adult Onset Still's Disease," (2023), clinicaltrials.gov.

9. K. H. G. Mills, "IL-17 and IL-17-Producing Cells in Protection Versus Pathology," *Nature Reviews. Immunology* 23 (2023): 38–54, https://doi.org/10.1038/s41577-022-00746-9.

10. W. Hueber, B. E. Sands, S. Lewitzky, et al., "Secukinumab, a Human Anti-IL-17A Monoclonal Antibody, for Moderate to Severe Crohn's Disease: Unexpected Results of a Randomised, Double-Blind Placebo-Controlled Trial," *Gut* 61 (2012): 1693–1700, https://doi.org/10.1136/gutjnl-2011-301668.

11. T. Arkachaisri, K. L. Teh, S. Vilaiyuk, et al., "The Asia-Pacific League of Associations for Rheumatology Consensus Recommendations on the Management of Juvenile Idiopathic Arthritis (JIA): Polyarticular Course JIA, Temporomandibular Joint Arthritis, Imaging, and Non-Pharmacologic Therapies," *International Journal of Rheumatic Diseases* 29 (2026): e70640, https://doi.org/10.1111/1756-185x.70640.

12. T.-C. Hsu and J. C.-C. Wei, "Breakthrough Biologics: Charting the Course for Sjögren's Syndrome Treatment in 2024," *International Journal of Rheumatic Diseases* 29 (2026): e70650, https://doi.org/10.1111/1756-185x.70650.

International Journal of Rheumatic Diseases

WILEY

International Journal of Rheumatic Diseases

ORIGINAL ARTICLE

Global Pattern, Trend, and Cross-Country Inequality of Low Bone Mineral Density From 1990 to 2021: Findings From the Global Burden of Disease Study

Ying Lv[1] | Yan Chen[2] | Dongze Wu[2] | Jing Zhu[2]

[1]School of Clinical Medicine, Hospital of North Sichuan Medical College, North Sichuan Medical College, Nanchong, China | [2]Department of Rheumatology and Immunology, Sichuan Provincial People's Hospital, School of Medicine, University of Electronic Science and Technology of China, Chengdu, China

Correspondence: Dongze Wu (dongze_wu@163.com) | Jing Zhu (zhujingys@sina.com)

Received: 8 January 2026 | **Revised:** 19 April 2026 | **Accepted:** 12 May 2026

Keywords: disease burden | inequality | low bone mineral density | pattern | trend

ABSTRACT

Objectives: Low bone mineral density (LBMD), a major osteoporotic fracture risk factor, disproportionately affects females globally. This study analyzing its burden through trends, health inequities, and predictive modeling.

Methods: Data from the Global Burden of Disease (GBD) 2021 were used to extract summary exposure values (SEV), mortality, and disability-adjusted life years (DALYs) for LBMD. Temporal trends, demographic and epidemiological changes, health inequalities, and projections were analyzed.

Results: In 2021, the global age-standardized rate of SEV was 23.51 (0–100 scale), declining at an AAPC of −0.16 since 1990. The age-standardized mortality rate (ASMR) and age-standardized DALY rate (ASDR) were 5.65 (95% UI: 4.71, 6.40) and 204.99 (95% UI: 168.92, 242.95) per 100 000 population, respectively, and both declined from 1990 to 2021. SEV was higher in females than males (28.56 vs. 18.08), while ASMR (4.99 vs. 6.45) and ASDR (196.37 vs. 211.01) were higher in males. Inequality slope indices in DALYs showed widening gaps between highest and lowest SDI countries, from −26.31 in 1990 to −53.34 in 2021. The absolute burden was mainly driven by population growth and aging, and ASMR and ASDR are expected to continue declining through 2050.

Conclusion: Although the age-standardized burden of LBMD declined from 1990 to 2021, the absolute burden remained substantial and was largely driven by population growth and aging. The burden was concentrated in low-SDI regions, while some high-SDI regions showed unfavorable trends. Females had higher exposure levels, whereas males bore a greater overall disease burden. Reducing the global LBMD burden requires improved nutrition and care in low-SDI regions, targeted prevention in postmenopausal women, and earlier detection and treatment in men.

1 | Introduction

Osteoporosis is a chronic degenerative metabolic bone disease caused by an imbalance between osteoclasts and osteoblasts, characterized by low bone mineral density (LBMD). The progressive deterioration of bone microarchitecture and the concurrent reduction in bone strength increase bone fragility and fracture susceptibility [1, 2]. Bone mineral density (BMD) is usually measured with dual-energy x-ray absorptiometry (DXA) at the hip, lumbar spine, or femoral neck, which is most often

Ying Lv and Yan Chen contributed equally to this study.

described as a T-score [3]. A T-score between −1.0 and −2.5 is defined as LBMD, and T-score at or below −2.5 is defined as osteoporosis [4]. For each one SD decrement in BMD, the risk of fracture increases by a factor of 2–3 [5].

Osteoporosis is a highly prevalent disease and leads to massive costs to both the individual and society through associated fragility fractures [6]. As life expectancy increases and the population ages, the burden of osteoporosis and associated fractures is expected to grow rapidly [7]. It is estimated that one in three females and one in five males over the age of 50 worldwide will sustain an osteoporotic fracture [8]. In France, Germany, Italy, Spain, Sweden, and the United Kingdom alone, 2.68 million new fragility fractures occurred in 2017, leading to a loss of over one million quality-adjusted life years, costing an estimated €37.5 billion in healthcare [9, 10]. In 2030, over 3.3 million new fractures are anticipated across the same six countries, with accompanying total fracture-related costs approximating €47.4 billion [10]. The lifetime fracture risk of a patient with osteoporosis is as high as 40% [11] and adverse fracture consequences include functional impairment, chronic pain, reduced quality of life, loss of independence, and premature mortality, especially after hip and vertebral fractures [12]. Therefore, LBMD should be identified early to mitigate future fracture risk and enable clinical intervention in high-risk patients prior to fracture occurrence.

Although previous studies have described the global, regional, and national burden of LBMD, little is known about the drivers of temporal changes, cross-country inequality, and future burden trends [13, 14]. Using GBD 2021 data, the present study extends prior analyses by not only updating long-term trends from 1990 to 2021 but also incorporating decomposition analysis, cross-country inequality assessment, and forecasting burden until 2050. In addition, we examined sex- and age-specific patterns of LBMD burden, providing a more comprehensive understanding of how demographic change, epidemiological patterns, and socioeconomic disparities shape the global burden of LBMD.

2 | Methods

2.1 | Data Sources and Data Collection

The GBD 2021 study synthesizes epidemiological data from 21 GBD regions and 204 countries/territories from 1990 to 2021. The GBD network utilized DisMod-MR 2.1 within a Bayesian disease modeling meta-regression tool to leverage all available data to generate disease estimates, including LBMD [15]. According to the comparative risk assessment conceptual framework, the GBD 2021 study established a causal relationship between LBMD and Levels 1–4 causes. Level 1 cause is injuries. Level 2 causes include unintentional injuries, transport injuries, self-harm, and interpersonal violence. Level 3 causes include animal contact, road injuries, other transport injuries, falls, interpersonal violence, and exposure to mechanical forces. Level 4 causes include physical violence by other means, other road injuries, non-venomous animal contact, motor vehicle road injuries, pedestrian road injuries, cyclist road injuries, motorcyclist road injuries, and other exposure to mechanical forces. Summary exposure values (SEVs) of LBMD, deaths, and disability-adjusted life years (DALYs) attributable to LBMD with 95% uncertainty interval (UI) were extracted from the Global Health Data Exchange (GHDx).

2.2 | Sociodemographic Index (SDI) and SEV

The SDI evaluates the socio-demographic status of a country or region based on its average income, educational attainment, and fertility rates [16]. The World Bank categorizes 204 countries and territories into five categories in terms of SDI: low SDI (< 0.46), low-middle SDI (0.46, 0.60), middle SDI (0.60, 0.70), high-middle SDI (0.70, 0.81), and high SDI (> 0.81). SEV is a population-level metric to quantify how far a population's exposure to a modifiable risk factor lies from the theoretical minimum-risk exposure distribution (TMRED) with a scale from 0 to 100. Zero indicates that the entire population is at the TMRED (no excess risk) but 100 indicates that the entire population is at the highest observed (or counterfactual) risk level [15].

2.3 | Cross-Country Inequality Analysis

Countries and territories were ranked by SDI from lowest to highest. The slope index of inequality (SII) and relative concentration index (RCI) were used to assess absolute and relative cross-country inequality in LBMD burden, respectively. The SII was estimated by regressing country-level age-standardized DALY and mortality rates on the relative SDI rank, defined by the midpoint of the cumulative population distribution. The RCI was derived from the concentration curve, which relates the cumulative proportion of age-standardized DALY and mortality rates to the cumulative proportion of the population ranked by SDI. Negative SII or RCI values indicated that the burden was concentrated in lower-SDI countries, whereas positive values indicated a greater burden in higher-SDI countries [17].

2.4 | Decomposition Analysis

To quantify the factors contributing to changes in the absolute burden of LBMD over the past 30 years, we conducted a decomposition analysis. The change in DALYs or deaths was partitioned into population growth, population aging, and epidemiological change, reflecting changes in population size, age structure, and age-specific rates, respectively. This approach was used to estimate the relative contribution of each component to changes in LBMD burden at the global level and across regions.

2.5 | Predictive Analysis

To forecast the global LBMD burden from 2021 to 2050, we applied a Bayesian age-period-cohort (BAPC) model with integrated nested Laplace approximation (INLA). Based on GBD 2021 data on SEV, mortality, and DALYs from 1990 to 2021, the model incorporated age, period, and cohort effects to estimate future numbers and age-standardized rates (ASRs) through 2050. Uncertainty was summarized as UIs within the Bayesian framework. The future standard population was derived from GBD 2017 population projections [18].

2.6 | Statistical Analysis

To determine trends in various epidemiological indicators over time, the Joinpoint Regression Program (version 5.1.0.0; National Cancer Institute, Rockville, MD, USA) was used. The average annual percent change (AAPC) and its accompanying 95% confidence interval (CI) from 1990 to 2021 were calculated for a comprehensive appraisal of the observed trends. All procedures for analysis and graphic representation were performed utilizing the open-source software R (version 4.3.3).

3 | Results

3.1 | Global and Regional SEV of Low Bone Mineral Density

Globally, the ASR of SEV for LBMD was 23.51 (95% UI: 18.01, 30.26) per 100 population in 2021. However, the ASR of SEV decreased from 1990 to 2021 (AAPC = −0.16, 95% CI: −0.17, −0.15). Gender disparities were evident, with females (28.56, 95% UI: 22.77, 35.30) showing a higher SEV rate than males (18.08, 95% UI: 12.86, 24.68) in 2021 (Table 1).

By SDI category, the highest SEV rate was observed in low-SDI regions (29.01, 95% CI: 23.22, 36.06) (Table 1, Figure 1). Of note, all SDI regions demonstrated declining trends of SEV, with the quickest in the middle SDI (AAPC = −0.31, 95% CI: −0.24, −0.47) (Table 1).

Substantial regional variations were also observed, with the highest SEV rate recorded in Western Sub-Saharan Africa (31.50, 95% UI: 25.54, 38.35), followed closely by Central Sub-Saharan Africa (30.81, 95% UI: 24.56, 38.21) and the lowest in Western Europe (17.61, 95% UI: 12.50, 24.03). The SEV rate declined in all regions except High-income North America, where it slightly increased (AAPC = 0.06, 95% CI: 0.02, 0.10), driven primarily by females (AAPC = 0.26, 95% CI: 0.23, 0.29) (Table 1).

At the national level, Guinea, Togo, and Sierra Leone had the highest SEV rates, with Guinea (35.45, 95% UI: 28.91, 42.57) showing the peak value. While most countries exhibited decreasing trends since 1990, some (e.g., Afghanistan, Nauru, Northern Mariana Islands, and United States) showed increases, with Afghanistan experiencing the most pronounced rise (AAPC = 0.24, 95% CI: 0.23, 0.25) (Table S1, Figure 2).

3.2 | Global and Regional DALYs and Deaths of Low Bone Mineral Density

In 2021, the global DALYs and deaths attributable to LBMD were approximately 17 310 085 and 459 661, respectively, with an ASDR of 204.99 and an ASMR of 5.65 per 100 000 population. Although both ASDR and ASMR showed decreasing trends from 1990 to 2021, with AAPCs of −0.51 and −0.28, respectively, the absolute numbers remained high worldwide (Tables S2 and S3; Figure S1). Females accounted for a higher number of DALYs and deaths, whereas males had higher ASDR and ASMR (ASDR: 211.01 vs. 196.37; ASMR: 6.45 vs. 4.99) (Tables S2 and S3).

At the SDI, regional, and national levels, the patterns and trends in DALYs and deaths were generally similar to those of SEV. Higher ASDR and ASMR were predominantly observed in low-SDI regions and countries, particularly in Central Africa, the Middle East, and South Asia. In contrast, several high-SDI regions and countries, such as High-income North America and Australia, showed worsening trends over time (AAPC > 0) (Tables S2–S5; Figures S2–S5).

3.3 | The Age Effect of Low Bone Mineral Density

In 2021, the SEV rate increased progressively with age, peaking in the 85–89 age group (26.09, 95% UI: 17.75, 34.75) before declining. Negative AAPCs were observed across all age groups, demonstrating that the SEV rate declined over the past 30 years in every cohort. Notably, the rate of decline accelerated with age, reaching its maximum in the 70–74 age group (AAPC = −0.24, 95% CI: −0.26, −0.23) (Table S6; Figure S6). Relative to SEV, the ASDR and ASMR increased sharply with age, reaching a peak at 95 plus group (ASDR: 5945.32; ASMR: 418.11). From 1990 to 2021, the decline in ASDR and ASMR gradually diminished with age, and over 85–89 age group, the AAPC became positive, suggesting an increasing trend in both ASDR and ASMR (Tables S7 and S8; Figure S8).

Regarding sex differences, females consistently exhibited higher SEV rates than males across all age groups (Figure S6). Conversely, males demonstrated higher ASMR across all age groups and higher ASDR years (Tables S7 and S8; Figure S7).

3.4 | The Association Between ASR, SDI, and AAPC

In 2021, there was a negative correlation between the SDI level and the ASR of SEV across both 21 GBD regions and 204 countries and territories ($\rho = -0.808$, $p < 0.001$) (Figure S9). Similar negative correlations were observed in ASDR and ASMR (Figures 3A,B and S10). In 1990, AAPC showed a positive correlation with ASR of SEV in 1990 ($\rho = 0.21$, $p = 0.003$) (Figure S9), whereas both ASDR and ASMR demonstrated negative correlations with AAPC (Figures 3C and S10). Furthermore, a significant negative correlation was found between the AAPC of SEV and the SDI in 2021 ($\rho = -0.395$, $p < 0.001$) (Figure S9). Notably, regions with SDI below 0.80 maintained negative correlations between SDI and both ASDR and ASMR, but this relationship gradually reversed in regions with SDI above 0.80 (Figures 3D and S10).

3.5 | The Disease Burden Attributable to Low Bone Mineral Density

Falls from unintentional injuries showed the strongest correlation with LBMD-related disability and mortality, followed by road injuries from transport injuries (Figures S11 and S12).

From 1990 to 2021, the ASR of LBMD-related disability due to falls remained above 120 per 100 000 population, while that attributed to road injuries fluctuated around 55 per 100 000. All six causes showed a downward trend over this period, with falls exhibiting the least pronounced reduction

TABLE 1 | Global and regional age-standardized rate and absolute number of summary exposure value attributable to low bone mineral density in 2021 and the temporal trends from 1990 to 2021.

	Both sexes		Female		Male	
Location	**2021 (95% UI)**	**AAPC (95% CI)**	**2021 (95% UI)**	**AAPC (95% CI)**	**2021 (95% UI)**	**AAPC (95% CI)**
Global	23.51 (18.01 to 30.26)	−0.16 (−0.17 to −0.15)	28.56 (22.77 to 35.30)	−0.07 (−0.07 to −0.06)	18.08 (12.86 to 24.68)	−0.30 (−0.32 to −0.29)
SDI regions						
High SDI	20.39 (15.09 to 26.93)	−0.14 (−0.15 to −0.12)	24.05 (18.42 to 30.81)	−0.04 (−0.05 to −0.03)	16.46 (11.35 to 22.90)	−0.20 (−0.22 to −0.19)
High-middle SDI	22.00 (16.69 to 28.60)	−0.16 (−0.17 to −0.14)	27.09 (21.43 to 33.84)	−0.06 (−0.06 to −0.05)	16.32 (11.18 to 22.75)	−0.26 (−0.28 to −0.23)
Middle SDI	24.11 (18.67 to 30.79)	−0.31 (−0.32 to −0.30)	29.67 (23.61 to 36.29)	−0.24 (−0.24 to −0.23)	18.14 (12.93 to 24.79)	−0.47 (−0.49 to −0.45)
Low-middle SDI	25.51 (19.74 to 32.45)	−0.19 (−0.20 to −0.18)	30.49 (24.42 to 37.30)	−0.18 (−0.19 to −0.17)	20.26 (14.68 to 27.29)	−0.28 (−0.29 to −0.26)
Low SDI	29.01 (23.22 to 36.06)	−0.14 (−0.15 to −0.13)	34.91 (28.99 to 41.63)	−0.14 (−0.15 to −0.14)	22.96 (17.09 to 30.08)	−0.20 (−0.21 to −0.19)
GBD regions						
Eastern Europe	18.12 (12.86 to 24.27)	−0.28 (−0.29 to −0.26)	22.99 (17.37 to 29.69)	−0.20 (−0.22 to −0.19)	11.68 (6.96 to 17.54)	−0.29 (−0.35 to −0.25)
Oceania	23.93 (17.92 to 30.61)	−0.05 (−0.06 to −0.04)	30.67 (24.05 to 37.53)	−0.07 (−0.09 to −0.07)	17.59 (12.04 to 24.46)	0.01 (0.00 to 0.03)
Southeast Asia	26.71 (21.25 to 33.45)	−0.23 (−0.24 to −0.22)	34.56 (28.47 to 41.46)	−0.17 (−0.18 to −0.17)	17.93 (12.64 to 24.55)	−0.35 (−0.37 to −0.33)
East Asia	24.59 (18.95 to 31.40)	−0.35 (−0.37 to −0.34)	30.06 (24.23 to 36.84)	−0.22 (−0.23 to −0.21)	18.75 (13.36 to 25.71)	−0.54 (−0.56 to −0.52)
Central Asia	18.11 (12.80 to 24.17)	−0.31 (−0.32 to −0.29)	22.69 (16.79 to 29.32)	−0.27 (−0.28 to −0.26)	12.82 (8.07 to 19.18)	−0.31 (−0.34 to −0.29)
South Asia	25.26 (19.66 to 32.26)	−0.20 (−0.21 to −0.18)	29.87 (24.09 to 36.60)	−0.20 (−0.21 to −0.19)	20.57 (14.86 to 27.81)	−0.27 (−0.29 to −0.25)
High-income North America	21.69 (16.08 to 28.34)	0.06 (0.02 to 0.10)	25.05 (19.11 to 31.80)	0.26 (0.23 to 0.29)	17.94 (12.40 to 24.76)	−0.18 (−0.23 to −0.13)
Central Europe	17.90 (12.78 to 24.30)	−0.37 (−0.38 to −0.35)	24.76 (18.92 to 31.31)	−0.32 (−0.32 to −0.31)	10.51 (5.64 to 17.38)	−0.38 (−0.41 to −0.34)
Australasia	19.50 (13.51 to 26.41)	−0.41 (−0.42 to −0.40)	21.07 (14.65 to 27.73)	−0.39 (−0.39 to −0.38)	17.77 (11.98 to 25.21)	−0.41 (−0.42 to −0.40)
Western Europe	17.61 (12.50 to 24.03)	−0.28 (−0.29 to −0.26)	20.71 (15.39 to 27.39)	−0.22 (−0.23 to −0.21)	14.23 (9.27 to 20.65)	−0.29 (−0.32 to −0.27)

(Continues)

TABLE 1 | (Continued)

Location	Both sexes		Female		Male	
	2021 (95% UI)	AAPC (95% CI)	2021 (95% UI)	AAPC (95% CI)	2021 (95% UI)	AAPC (95% CI)
High-income Asia Pacific	22.60 (17.24 to 29.40)	−0.29 (−0.35 to −0.26)	26.71 (20.57 to 33.54)	−0.23 (−0.27 to −0.20)	18.19 (12.91 to 24.96)	−0.29 (−0.36 to −0.23)
North Africa and Middle East	22.41 (16.80 to 28.95)	−0.22 (−0.24 to −0.21)	25.68 (20.07 to 32.14)	−0.23 (−0.24 to −0.22)	19.28 (13.77 to 26.07)	−0.22 (−0.23 to −0.20)
Caribbean	19.17 (13.68 to 25.51)	−0.33 (−0.34 to −0.32)	22.29 (16.50 to 28.75)	−0.29 (−0.30 to −0.28)	15.77 (10.61 to 22.40)	−0.42 (−0.43 to −0.41)
Central Latin America	21.23 (15.89 to 27.85)	−0.27 (−0.28 to −0.26)	27.30 (21.35 to 33.79)	−0.21 (−0.22 to −0.20)	14.35 (9.48 to 20.69)	−0.48 (−0.50 to −0.46)
Andean Latin America	18.77 (13.10 to 25.18)	−0.41 (−0.42 to −0.39)	23.39 (16.98 to 30.18)	−0.35 (−0.36 to −0.34)	13.86 (8.75 to 19.88)	−0.55 (−0.57 to −0.52)
Southern Latin America	21.14 (15.66 to 27.69)	−0.27 (−0.28 to −0.26)	24.96 (19.07 to 32.15)	−0.25 (−0.26 to −0.24)	16.66 (11.19 to 23.75)	−0.30 (−0.32 to −0.29)
Tropical Latin America	22.12 (16.61 to 28.91)	−0.44 (−0.45 to −0.43)	27.09 (20.87 to 33.92)	−0.41 (−0.42 to −0.40)	16.49 (11.23 to 22.97)	−0.53 (−0.55 to −0.52)
Western Sub-Saharan Africa	31.50 (25.54 to 38.35)	−0.16 (−0.17 to −0.15)	39.51 (33.44 to 46.29)	−0.21 (−0.22 to −0.21)	22.67 (16.86 to 29.78)	−0.30 (−0.31 to −0.29)
Southern Sub-Saharan Africa	26.35 (20.45 to 33.26)	−0.21 (−0.22 to −0.19)	29.73 (23.44 to 36.53)	−0.16 (−0.16 to −0.15)	22.20 (16.42 to 29.19)	−0.29 (−0.32 to −0.28)
Central Sub-Saharan Africa	30.81 (24.56 to 38.21)	−0.09 (−0.10 to −0.08)	36.12 (29.41 to 43.13)	−0.07 (−0.08 to −0.06)	24.90 (18.67 to 32.39)	−0.10 (−0.11 to −0.10)
Eastern Sub-Saharan Africa	30.14 (24.22 to 37.04)	−0.22 (−0.23 to −0.21)	36.07 (29.95 to 42.87)	−0.20 (−0.20 to −0.19)	23.80 (17.95 to 30.93)	−0.30 (−0.31 to −0.29)

Abbreviations: AAPC, average annual percent change; CI, confidence interval; SDI, sociodemographic index; UI, uncertainty interval.

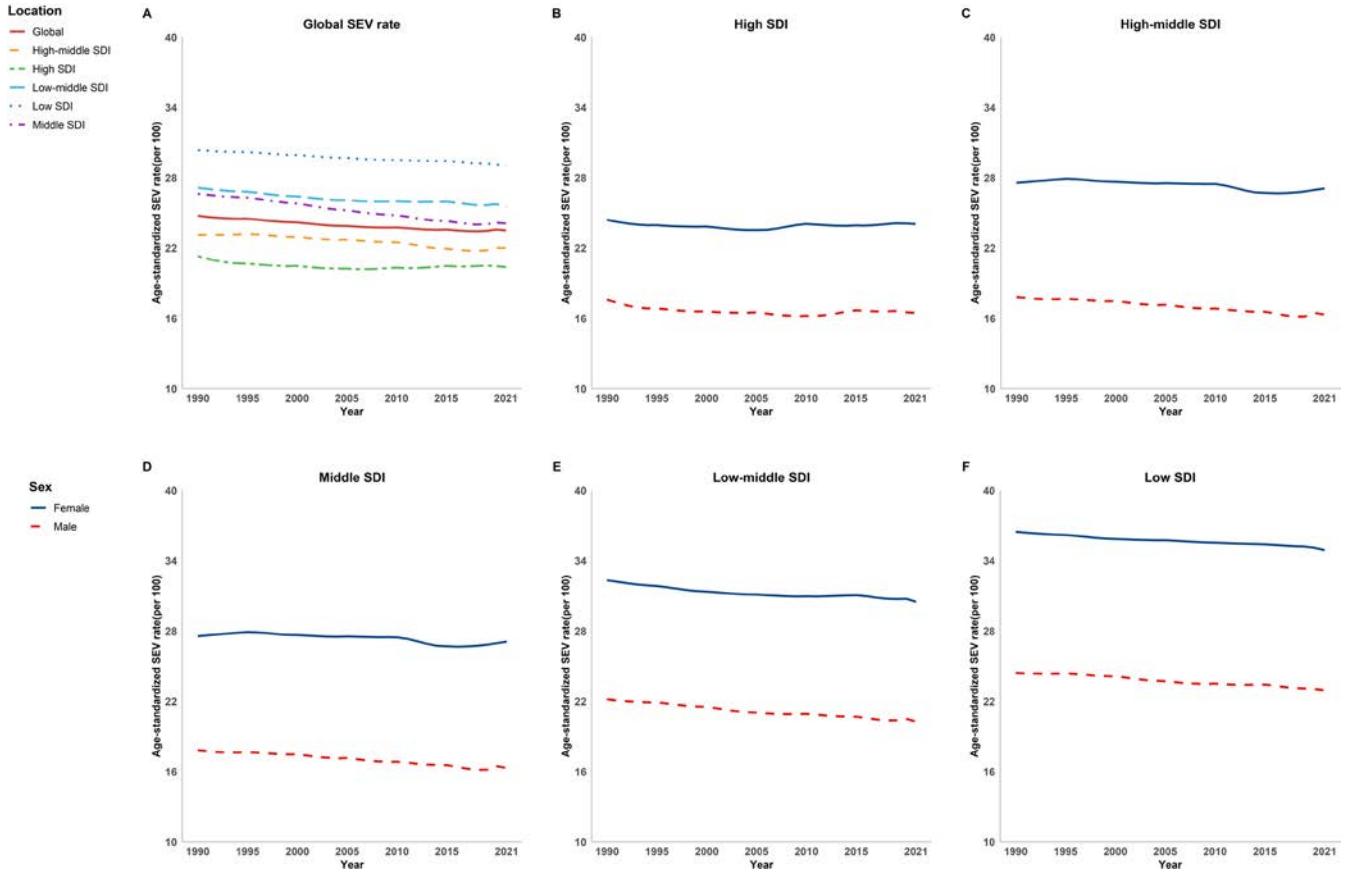

FIGURE 1 | Age-standardized rate of summary exposure value attributable to low bone mineral density by five SDI regions at global level, from 1990 to 2021. (A) Age-standardized rate of summary exposure value attributable to low bone mineral density by five SDI regions at global level, for both sexes. (B) Age-standardized rate of summary exposure value attributable to low bone mineral density between males and females in regions with high SDI. (C) Age-standardized rate of summary exposure value attributable to low bone mineral density between males and females in regions with high-middle SDI. (D) Age-standardized rate of summary exposure value attributable to low bone mineral density between males and females in regions with middle SDI. (E) Age-standardized rate of summary exposure value attributable to low bone mineral density between males and females in regions with low-middle SDI. (F) Age-standardized rate of summary exposure value for low bone mineral density between males and females in regions with low SDI. SDI, sociodemographic index.

(AAPC = −0.12, 95% CI: −0.14, −0.11). With respect to gender, females had a higher ASR of LBMD-related disability due to falls, while males showed a higher ASR of LBMD-related disability caused by road injury (Table S2; Figure S12). Across all age groups, the proportion of disability cases attributable to falls from unintentional injuries increased with age, in contrast to the decreasing trend observed in road injuries from transport injuries (Figures S13 and S14).

A similar pattern in sex distribution and temporal trends was observed in LBMD-related mortality, although certain differences were noted. Specifically, mortality due to falls (AAPC = 0.03, 95% CI: −0.02, 0.06) exhibited an increasing trend over the past 30 years, while the other five causes declined. Additionally, males showed a slight predominance in LBMD-related mortality attributed to falls (Table S3; Figures S11–S14).

3.6 | The SII and RCI of Low Bone Mineral Density in 1990 and 2021

As indicated by the SII, the absolute gap in ASDR between the highest and lowest SDI countries increased from −26.31 (95% CI: −59.10, 6.48) in 1990 to −53.34 (95% CI: −76.88, −29.80) in 2021, highlighting that countries with lower SDI bore disproportionately higher burdens. In contrast, the relative gradient inequality, measured by the RCI, was −0.04 (95% CI: −0.07, −0.02) in 1990 and −0.06 (95% CI: −0.09, −0.04) in 2021, indicating a consistent concentration of the burden among the poorer populations (Table S9, Figure 4). Between 1990 and 2021, both the SII and the RCI of mortality were negative, exhibiting only modest changes over time (Table S9, Figure S15).

3.7 | The Decomposition Analysis of Low Bone Mineral Density

The last 30 years have experienced a substantial increase in DALYs globally, with the most pronounced increase found in middle-SDI. Aging, population, and epidemiological changes contributed 14.67%, 113.59%, and −28.26%, respectively, to this overall increase. The impact of population was particularly prominent in high-middle SDI (147.41%) and low SDI (118.30%) regions, while the contributions of aging and epidemiological changes were most notable in high SDI (34.62%) and high-middle SDI regions (−70.80%), respectively (Tables S10–S12;

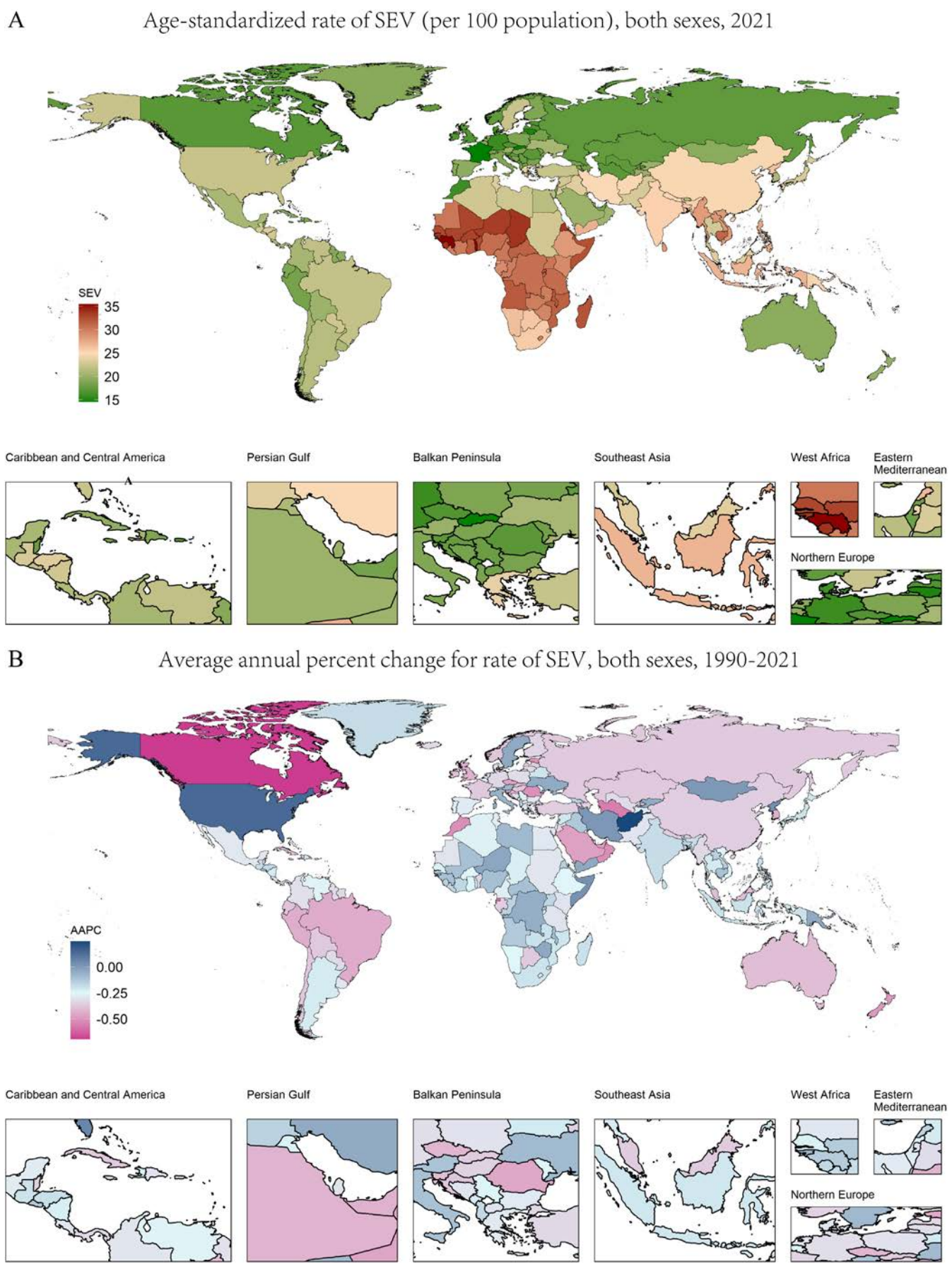

FIGURE 2 | Legend on next page.

FIGURE 2 | Global map of summary exposure value for low bone mineral density in 204 countries and territories for both sexes. (A) Global map in age-standardized rate of summary exposure value attributable to low bone mineral density, 2021. (B) Global map in average annual percent change in age-standardized rate of summary exposure value attributable to LBMD, 1990–2021. SEV, summary exposure value.

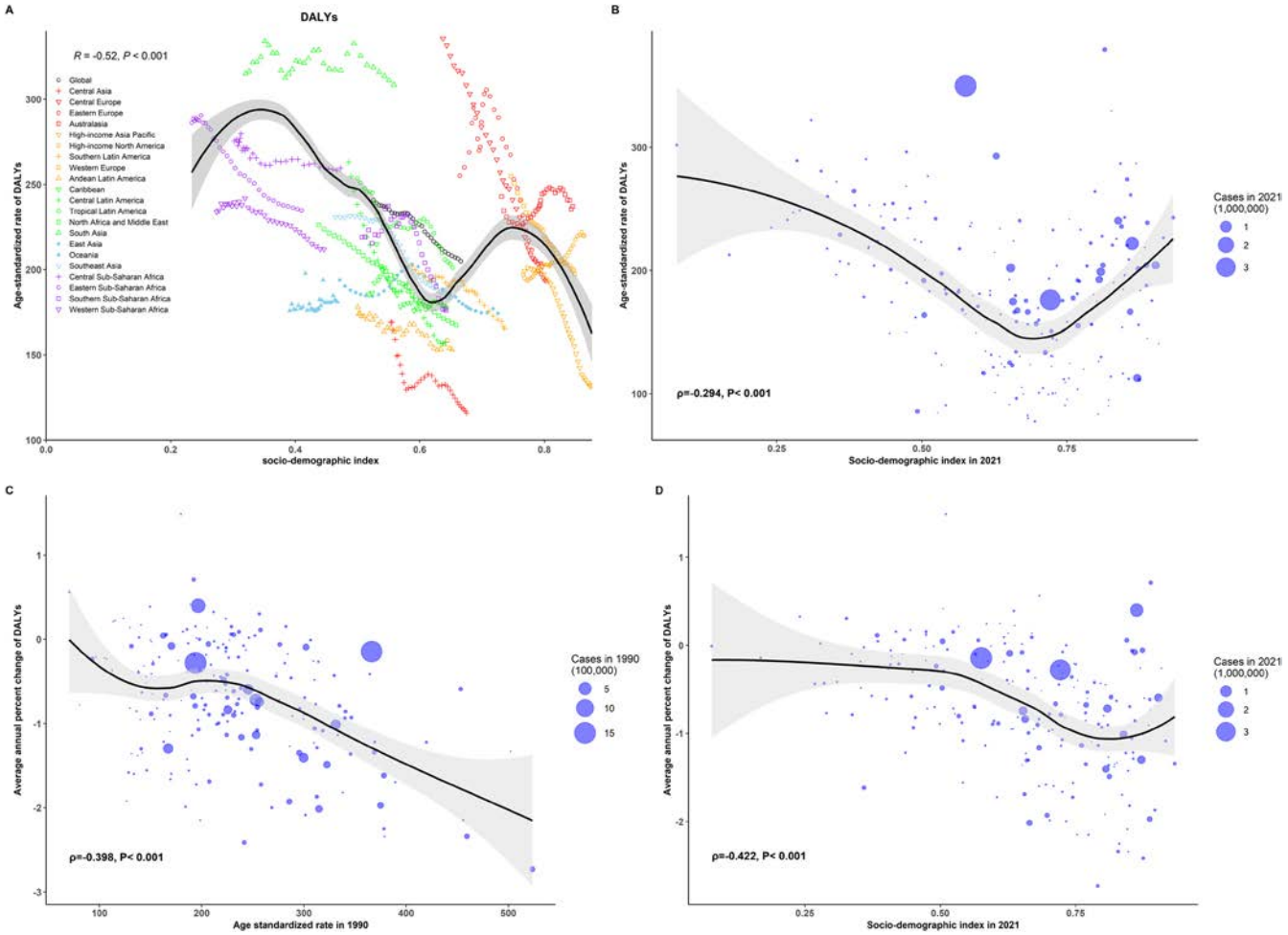

FIGURE 3 | The association between age standardized rate of disability-adjusted life years, sociodemographic index, average annual percent change across global burden of disease regions and countries and territories. (A) ASR of DALYs attributable to LBMD per 100 000 persons for SDI by 21 global burden of disease regions, 2021. Black line represents expected values based on SDI and disease rates across 21 GBD regions; each point shows observed ASR of DALYs for specified region in 2021. (B) ASR of DALYs attributable to LBMD per 100 000 persons for SDI by 204 countries and territories, 2021. Black line represents expected values based on SDI and disease across 204 countries and territories, each point shows observed ASR of DALYs for specified country in 2021. (C) The correlation between AAPC and ASR of DALYs attributable to LBMD in 1990 across 204 countries and territories. The size of circle is increased with the absolute number of LBMD. The ρ indices and p values were derived from Pearson correlation analysis. (D) The correlation between AAPC and SDI attributable to LBMD in 2021 across 204 countries and territories. The size of circle is increased with the absolute number of LBMD. The ρ indices and p values were derived from Pearson correlation analysis. AAPC, average annual percent change; ASR, age-standardized rate; DALYs, disability-adjusted life years; GBD, global burden of disease; LBMD, low bone mineral density.

Figure S16). Similar contribution patterns were observed in mortality as well (Tables S13–S15; Figure S17).

3.8 | The Predictive Analysis of Low Bone Mineral Density Through 2050

Globally, the ASDR and ASMR attributable to LBMD are projected to continue declining until 2050, whereas the absolute numbers of DALYs and deaths are expected to increase steadily over the same period (Figures S18 and S19).

4 | Discussion

LBMD remains a substantial and growing public health challenge, yet it has received insufficient attention over the past three decades. In this study, we provide an updated and more

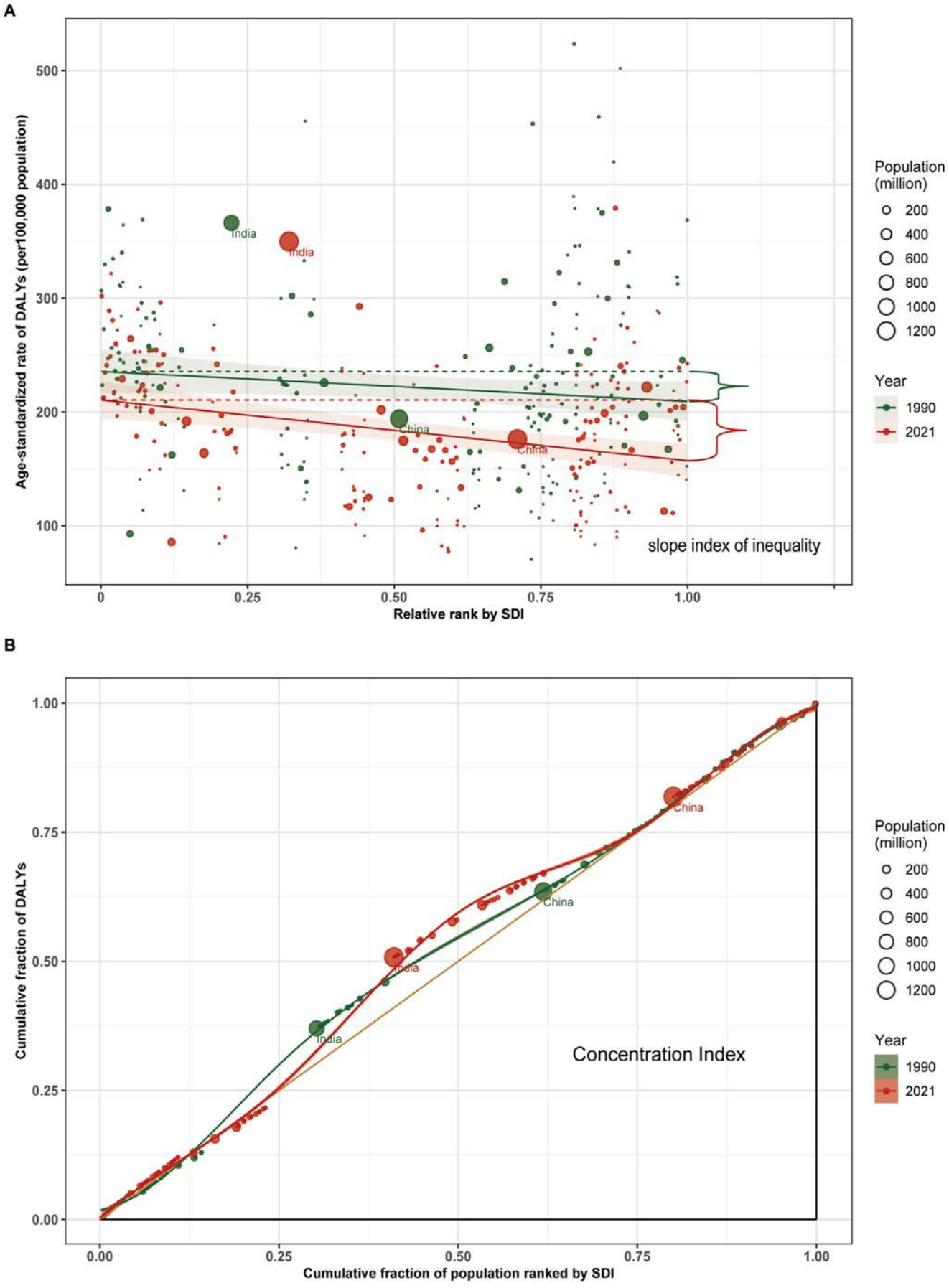

FIGURE 4 | Legend on next page.

FIGURE 4 | Health inequality regression curves and concentration curves for low bone mineral density in terms of disability-adjusted life years. (A) Health inequality regression curves of disability-adjusted life years for low bone mineral density worldwide, 1990 and 2021. (B) Concentration curves of disability-adjusted life years for low bone mineral density worldwide, 1990 and 2021. DALYs, disability-adjusted life years; SDI, sociodemographic index.

comprehensive assessment of temporal trends, inequality, future projections, and sex- and age-specific differences in LBMD burden. Five major findings emerge from our analysis.

Our findings showed that although the age-standardized burden of LBMD declined over the past three decades, the absolute burden still increased and was largely driven by population growth and aging.

First, the global population will grow to 8.5 billion by 2030 and 9.7 billion by 2050 and the share of global population at ages 65 and above is projected to rise from 10% in 2022 to 16% in 2050 [19]. Given LBMD is an age-related degenerative disease, population growth and aging are expected to increase the burden of LBMD. Second, glucocorticoids, longstanding anti-inflammatory or immunosuppressive agents, might be another key factor [20]. Approximately 1% of UK and USA adults receive long-term oral glucocorticoids [21], yet excess exposure inhibits osteoblast formation, leading to reduced BMD and fragility fracture [22]. A meta-analysis showed glucocorticoid use with a nearly threefold higher risk of vertebral fracture and doubled hip fracture risk [21]. Third, the widespread adoption of DXA has facilitated earlier detection of LBMD [23]. Fourth, non-pharmaceutical interventions, such as smoking cessation, weight maintenance, regular physical activity, and moderation of alcohol intake, have been widely advocated [24, 25]. Particularly, regular physical activity may prevent bone mass loss during old age [26]. The decline in ASR might be attributed to the promotion of physical activity, increased awareness of calcium and vitamin D supplementation [8], and a growing number of governments have identified osteoporosis prevention as a national health priority [27].

Our findings indicate that the burden of LBMD is not only concentrated in poor areas, but also increasing in rich areas. On the one hand, smoking prevalence and excessive alcohol consumption rates are markedly higher in lower socioeconomic groups [28]. Nicotine exposure and alcohol misuse can affect the activity of osteoblasts, diminish calcium absorption, and thus impair bone formation [24]. In persons with chronic alcoholism, fractures are four times as common as in healthy controls [29], while smokers face 16%–20% elevated fracture risk relative to non-smokers [30]. Populations in low SDI regions commonly have inadequate intake of calcium, vitamin D, and protein, which triggers systemic bone homeostasis imbalances. Low vitamin D and protein intake reduce intestinal calcium absorption, inducing secondary hyperparathyroidism that heightens bone remodeling and compromises skeletal health [31]. Among low body mass index (BMI) individuals, insufficient body fat reduces estrogen levels, accelerating bone resorption [32]. This challenge is compounded by a severe shortage of medical resources in less-developed countries, with fewer than one DXA machine per million population [27]. As a result, individuals with LBMD were less likely to undergo BMD measurements and to receive timely bone-protective medications [33]. On the other hand, the increased burden of LBMD in high SDI may stem from a more serious aging population and longer life expectancy, which leads to a higher proportion of elderly females [34]. Additionally, the lower prevalence of manual labor and unemployment among high SDI might imply a higher proportion of white-collar professionals, whose work typically involves more sedentary behaviors [35]. Such sedentary work patterns have already been reported as a risk factor for hip fracture [36], as they increased bone resorption and decreased bone formation [37].

Our study also highlights an important sex disparity in LBMD, with higher exposure levels in females but a greater attributable disease burden in males. Among males, age-related bone loss and androgen deficiency after age 50 contribute to trabecular thinning and muscle mass loss, which increase the propensity to falls and thus fractures [38]. Fractures in males most commonly occur in the hip and spine [39], both strongly associated with osteoporosis-related disability and mortality [40]. Moreover, males with fractures tend to have more comorbidities (e.g., cardiovascular disease, chronic obstructive pulmonary disease) and higher rates of infection (e.g., pneumonia, septicaemia) [41]. A prospective observational cohort study showed that males with a hip fracture have an increased mortality risk of dying from cardiovascular disease and pneumonia at fivefold and 2.4-fold, respectively [42]. Another contributing factor is the widespread misconception that osteoporosis affects only females [43], compounded by inadequate physician awareness, as experts have not yet reached a consensus regarding screening guidelines in males [44]. These factors lead to early underdiagnosis and consequent undertreatment of osteoporosis in males. In addition, males frequently have secondary osteoporosis caused by medications (e.g., glucocorticoids), diseases (e.g., hypogonadism), or unhealthy lifestyle factors (e.g., alcoholism, smoking, sedentary lifestyle) [45], further complicating treatment and increasing the risk of disability and mortality. On the female side, the higher prevalence of osteoporosis is partly due to their longer life expectancy [46], leading to a greater proportion of females in the elderly population where the disease is most common [47]. Postmenopausal estrogen deficiency further accelerates bone resorption by osteoclast overactivation, resulting in bone mineral loss [48]. Moreover, females accumulate less bone mass during a shorter pubertal growth period, leading to lower peak bone mass which is a key risk factor for osteoporosis [49]. To mitigate this gender disparity in LBMD burden, postmenopausal women are advised to increase calcium, vitamin D, and protein intake [49], while high-risk males should improve osteoporosis awareness [43] and strengthen postfracture care and prognosis [50].

Our study has several limitations beyond the inherent weaknesses of the GBD methodology. First, the burden of LBMD in lower-income countries is likely underestimated due to

insufficient awareness of LBMD and the relative inadequacy of screening equipment. Besides, in this study, the TMRED of LBMD was derived from the age- and sex-specific 99th percentile of the NHANES 1988–2014. This approach may underestimate LBMD exposure in older populations compared to definitions established by the WHO, NOF, and ISCD guidelines. Finally, the temporal scope of our study was limited by data availability, leading to the omission of recent LBMD statistics. Subsequent research efforts should prioritize incorporating the most up-to-date data to ensure a more accurate description of the changing global trends in LBMD.

Author Contributions

Ying Lv: writing – original draft, writing – review and editing, methodology, formal analysis, data curation, visualization. **Yan Chen:** writing – review and editing, formal analysis, methodology. **Dongze Wu:** software, writing – review and editing, visualization, methodology, conceptualization, project administration, supervision. **Jing Zhu:** funding acquisition, resources, writing – review and editing, project administration, supervision.

Acknowledgments

We thank the staff at the Institute for Health Metrics and Evaluation and its collaborators who prepared publicly available and impactful data. This study is based on publicly available data and solely reflects the opinion of its authors and not that of the Institute for Health Metrics and Evaluation.

Funding

The authors have nothing to report.

Conflicts of Interest

The authors declare no conflicts of interest.

Data Availability Statement

The data underlying this article are available in the Institute of Health Metrics and Evaluation, at https://vizhub.healthdata.org/gbd-results/.

References

1. K. Redlich and J. S. Smolen, "Inflammatory Bone Loss: Pathogenesis and Therapeutic Intervention," *Nature Reviews Drug Discovery* 11, no. 3 (2012): 234–250.

2. J. E. Compston, M. R. McClung, and W. D. Leslie, "Osteoporosis," *Lancet* 393, no. 10169 (2019): 364–376.

3. W. K. Nicholson, M. Silverstein, J. B. Wong, et al., "Screening for Osteoporosis to Prevent Fractures: US Preventive Services Task Force Recommendation Statement," *JAMA* 333, no. 6 (2025): 498–508.

4. J. J. Fenton, J. A. Robbins, A. L. Amarnath, and P. Franks, "Osteoporosis Overtreatment in a Regional Health Care System," *JAMA Internal Medicine* 176, no. 3 (2016): 391–393.

5. D. M. Black and C. J. Rosen, "Clinical Practice. Postmenopausal Osteoporosis," *New England Journal of Medicine* 374, no. 3 (2016): 254–262.

6. N. Harvey, E. Dennison, and C. Cooper, "Osteoporosis: Impact on Health and Economics," *Nature Reviews Rheumatology* 6, no. 2 (2010): 99–105.

7. D. Bliuc, T. Tran, W. Chen, et al., "The Association Between Multimorbidity and Osteoporosis Investigation and Treatment in High-Risk Fracture Patients in Australia: A Prospective Cohort Study," *PLoS Medicine* 20, no. 1 (2023): e1004142.

8. S. N. Morin, W. D. Leslie, and J. T. Schousboe, "Osteoporosis: A Review," *JAMA* 334 (2025): 894–907.

9. E. Toth, J. Banefelt, K. Åkesson, A. Spångeus, G. Ortsäter, and C. Libanati, "History of Previous Fracture and Imminent Fracture Risk in Swedish Women Aged 55 to 90 Years Presenting With a Fragility Fracture," *Journal of Bone and Mineral Research* 35, no. 5 (2020): 861–868.

10. J. Adams, N. Wilson, E. Hurkmans, et al., "2019 EULAR Points to Consider for Non-Physician Health Professionals to Prevent and Manage Fragility Fractures in Adults 50 Years or Older," *Annals of the Rheumatic Diseases* 80, no. 1 (2021): 57–64.

11. T. D. Rachner, S. Khosla, and L. C. Hofbauer, "Osteoporosis: Now and the Future," *Lancet* 377, no. 9773 (2011): 1276–1287.

12. K. E. Ensrud and C. J. Crandall, "Osteoporosis," *Annals of Internal Medicine* 177, no. 1 (2024): Itc1–ITC16.

13. J. Li, H. Jia, Z. Liu, and K. Xu, "Global, Regional and National Trends in the Burden of Low Bone Mineral Density From 1990 to 2030: A Bayesian Age-Period-Cohort Modeling Study," *Bone* 189 (2024): 117253.

14. Y. Shen, X. Huang, J. Wu, et al., "The Global Burden of Osteoporosis, Low Bone Mass, and Its Related Fracture in 204 Countries and Territories, 1990-2019," *Frontiers in Endocrinology* 13 (2022): 882241.

15. GBD 2021 Risk Factors Collaborators, "Global Burden and Strength of Evidence for 88 Risk Factors in 204 Countries and 811 Subnational Locations, 1990–2021: A Systematic Analysis for the Global Burden of Disease Study 2021," *Lancet* 403, no. 10440 (2024): 2162–2203.

16. GBD 2021 Risk Factors Collaborators, "Global Age-Sex-Specific Mortality, Life Expectancy, and Population Estimates in 204 Countries and Territories and 811 Subnational Locations, 1950-2021, and the Impact of the COVID-19 Pandemic: A Comprehensive Demographic Analysis for the Global Burden of Disease Study 2021," *Lancet* 403, no. 10440 (2024): 1989–2056.

17. P. Ordunez, R. Martinez, P. Soliz, G. Giraldo, O. J. Mujica, and P. Nordet, "Rheumatic Heart Disease Burden, Trends, and Inequalities in the Americas, 1990-2017: A Population-Based Study," *Lancet Global Health* 7, no. 10 (2019): e1388–e1397.

18. Institute for Health Metrics and Evaluation (IHME), "Global Fertility, Mortality, Migration, and Population Forecasts 2017–2100," June 27, 2025, https://ghdx.healthdata.org/record/ihme-data/global-population-forecasts-2017-2100.

19. United Nations Population Division (UNPD), "World Population Prospects 2022," https://population.un.org/wpp/.

20. J. Vandewalle, A. Luypaert, K. De Bosscher, and C. Libert, "Therapeutic Mechanisms of Glucocorticoids," *Trends in Endocrinology and Metabolism* 29, no. 1 (2018): 42–54.

21. P. Chotiyarnwong and E. V. McCloskey, "Pathogenesis of Glucocorticoid-Induced Osteoporosis and Options for Treatment," *Nature Reviews Endocrinology* 16, no. 8 (2020): 437–447.

22. P. R. Ebeling, H. H. Nguyen, J. Aleksova, A. J. Vincent, P. Wong, and F. Milat, "Secondary Osteoporosis," *Endocrine Reviews* 43, no. 2 (2022): 240–313.

23. K. J. Chun, "Bone Densitometry," *Seminars in Nuclear Medicine* 41, no. 3 (2011): 220–228.

24. K. Zhu and R. L. Prince, "Lifestyle and Osteoporosis," *Current Osteoporosis Reports* 13, no. 1 (2015): 52–59.

25. I. R. Reid, "Short-Term and Long-Term Effects of Osteoporosis Therapies," *Nature Reviews Endocrinology* 11, no. 7 (2015): 418–428.

26. S. K. Papadopoulou, K. Papadimitriou, G. Voulgaridou, et al., "Exercise and Nutrition Impact on Osteoporosis and Sarcopenia-The Incidence of Osteosarcopenia: A Narrative Review," *Nutrients* 13, no. 12 (2021): 4499.

27. N. C. Harvey, E. V. McCloskey, P. J. Mitchell, et al., "Mind the (Treatment) Gap: A Global Perspective on Current and Future Strategies for Prevention of Fragility Fractures," *Osteoporosis International* 28, no. 5 (2017): 1507–1529.

28. G. Valentin, M. B. Ravn, E. K. Jensen, et al., "Socio-Economic Inequalities in Fragility Fracture Incidence: A Systematic Review and Meta-Analysis of 61 Observational Studies," *Osteoporosis International* 32, no. 12 (2021): 2433–2448.

29. D. B. Maurel, N. Boisseau, C. L. Benhamou, and C. Jaffre, "Alcohol and Bone: Review of Dose Effects and Mechanisms," *Osteoporosis International* 23, no. 1 (2012): 1–16.

30. C. Rogmark, A. Fedorowski, and V. Hamrefors, "Physical Activity and Psychosocial Factors Associated With Risk of Future Fractures in Middle-Aged Men and Women," *Journal of Bone and Mineral Research* 36, no. 5 (2021): 852–860.

31. R. Rizzoli, E. Biver, and T. C. Brennan-Speranza, "Nutritional Intake and Bone Health," *Lancet Diabetes & Endocrinology* 9, no. 9 (2021): 606–621.

32. B. L. Riggs, S. Khosla, and L. J. Melton, 3rd, "Sex Steroids and the Construction and Conservation of the Adult Skeleton," *Endocrine Reviews* 23, no. 3 (2002): 279–302.

33. E. Guilley, F. Herrmann, C. H. Rapin, P. Hoffmeyer, R. Rizzoli, and T. Chevalley, "Socioeconomic and Living Conditions Are Determinants of Hip Fracture Incidence and Age Occurrence Among Community-Dwelling Elderly," *Osteoporosis International* 22, no. 2 (2011): 647–653.

34. O. Karlsson, A. Y. Chang, O. F. Norheim, W. Mao, S. Bolongaita, and D. T. Jamison, "Priority Health Conditions and Global Life Expectancy Disparities," *JAMA Network Open* 8, no. 5 (2025): e2512198.

35. C. Reyes, M. García-Gil, J. M. Elorza, et al., "Socioeconomic Status and Its Association With the Risk of Developing Hip Fractures: A Region-Wide Ecological Study," *Bone* 73 (2015): 127–131.

36. M. J. LaMonte, J. Wactawski-Wende, J. C. Larson, et al., "Association of Physical Activity and Fracture Risk Among Postmenopausal Women," *JAMA Network Open* 2, no. 10 (2019): e1914084.

37. A. J. Pinto, A. Bergouignan, P. C. Dempsey, et al., "Physiology of Sedentary Behavior," *Physiological Reviews* 103, no. 4 (2023): 2561–2622.

38. R. A. Adler, "Osteoporosis in Men: A Review," *Bone Research* 2 (2014): 14001.

39. J. S. Walsh and R. Eastell, "Osteoporosis in Men," *Nature Reviews Endocrinology* 9, no. 11 (2013): 637–645.

40. S. E. Sattui and K. G. Saag, "Fracture Mortality: Associations With Epidemiology and Osteoporosis Treatment," *Nature Reviews Endocrinology* 10, no. 10 (2014): 592–602.

41. R. S. Sterling, "Gender and Race/Ethnicity Differences in Hip Fracture Incidence, Morbidity, Mortality, and Function," *Clinical Orthopaedics and Related Research* 469, no. 7 (2011): 1913–1918.

42. J. J. Roche, R. T. Wenn, O. Sahota, and C. G. Moran, "Effect of Comorbidities and Postoperative Complications on Mortality After Hip Fracture in Elderly People: Prospective Observational Cohort Study," *BMJ (Clinical Research ed)* 331, no. 7529 (2005): 1374.

43. The Lancet Diabetes Endocrinology, "Osteoporosis: Overlooked in Men for Too Long," *Lancet Diabetes & Endocrinology* 9, no. 1 (2021): 1.

44. N. R. Fuggle, C. Beaudart, O. Bruyère, et al., "Evidence-Based Guideline for the Management of Osteoporosis in Men," *Nature Reviews Rheumatology* 20, no. 4 (2024): 241–251.

45. G. Rinonapoli, C. Ruggiero, L. Meccariello, M. Bisaccia, P. Ceccarini, and A. Caraffa, "Osteoporosis in Men: A Review of an Underestimated Bone Condition," *International Journal of Molecular Sciences* 22, no. 4 (2021): 2105.

46. S. N. Austad and K. E. Fischer, "Sex Differences in Lifespan," *Cell Metabolism* 23, no. 6 (2016): 1022–1033.

47. J. A. Kanis, C. Cooper, R. Rizzoli, and J. Y. Reginster, "European Guidance for the Diagnosis and Management of Osteoporosis in Postmenopausal Women," *Osteoporosis International* 30, no. 1 (2019): 3–44.

48. S. Khosla, M. J. Oursler, and D. G. Monroe, "Estrogen and the Skeleton," *Trends in Endocrinology and Metabolism* 23, no. 11 (2012): 576–581.

49. T. Chevalley and R. Rizzoli, "Acquisition of Peak Bone Mass," *Best Practice & Research Clinical Endocrinology & Metabolism* 36, no. 2 (2022): 101616.

50. M. S. LeBoff, S. L. Greenspan, K. L. Insogna, et al., "The Clinician's Guide to Prevention and Treatment of Osteoporosis," *Osteoporosis International* 33, no. 10 (2022): 2049–2102.

Supporting Information

Additional supporting information can be found online in the Supporting Information section. **Figure S1:** Total number and age-standardized rate of disability-adjusted life years and mortality attributable to low bone mineral density from 1990 to 2021. **Figure S2:** Global map of disability-adjusted life years attributable to low bone mineral density in 204 countries and territories for both sexes. **Figure S3:** Global map of mortality attributable to low bone mineral density in 204 countries and territories for both sexes. **Figure S4:** Age-standardized rate of disability-adjusted life years attributable to low bone mineral density by five sociodemographic index regions at global level, from 1990 to 2021. **Figure S5:** Age-standardized rate of mortality attributable to low bone mineral density by five sociodemographic index regions at global level, from 1990 to 2021. **Figure S6:** Age-standardized rate and average annual percent change of summary exposure value attributable to low bone mineral density throughout 44–95 plus years old. **Figure S7:** Age-standardized rate and number of disability-adjusted life years and mortality attributable to low bone mineral density throughout 44–95 plus years old in 2021, by sexes. **Figure S8:** Average annual percent change in number and age-standardized rate of mortality and disability-adjusted life years attributable to low bone mineral density from 44 years old to 95 plus years old, for both sexes, 1990–2021. **Figure S9:** The association between age standardized rate of summary exposure value, sociodemographic index, average annual percent change across 21 GBD regions and 204 countries and territories. **Figure S10:** The association between age standardized rate of mortality, sociodemographic index, average annual percent change across 21 GBD regions and 204 countries and territories. **Figure S11:** Age standardized rate of low bone mineral density-related disability-adjusted life years and mortality attributable to Level 2 causes from 1990 to 2021 in global, by sexes. **Figure S12:** Age standardized rate of low bone mineral density-related disability-adjusted life years and mortality attributable to Level 3 causes from 1990 to 2021 in global, by sexes. **Figure S13:** Percentage in number of low bone mineral density-related disability-adjusted life years and mortality attributable to Level 2 causes from 44 to 95 plus years old in global, by sexes, 2021. **Figure S14:** Percentage in number of low bone mineral density-related disability-adjusted life years and mortality attributable to Level 3 causes from 44 to 95 plus years old in global, by sexes, 2021. **Figure S15:** Health inequality regression curves and concentration curves for low bone mineral density in terms of mortality. **Figure S16:** The changes in disability-adjusted life years of low bone mineral density according to aging, population growth and epidemiological change from 1990 to 2021 at global level by sociodemographic index quintile and by regions stratified and sexes. **Figure S17:** The changes in mortality of low bone mineral density according to aging, population growth and epidemiological change from 1990 to 2021 at global level by sociodemographic index quintile and by regions

stratified and sexes. **Figure S18:** The predicted absolute number and age-standardized rate of disability-adjusted life years to 2050, by sexes. **Figure S19:** The predicted absolute number and age-standardized rate of mortality to 2050, by sexes. **Table S1:** Age-standardized rate of summary exposure value attributable to low bone mineral density according to 204 countries and territories and its temporal trends from 1990 to 2021. **Table S2:** Global and regional age-standardized rate and absolute number of disability-adjusted life years attributable to low bone mineral density in 2021 and the temporal trends from 1990 to 2021. **Table S3:** Global and regional age-standardized rate and absolute number of mortality attributable to low bone mineral density in 2021 and the temporal trends from 1990 to 2021. **Table S4:** Age-standardized rate and absolute number of disability-adjusted life years attributable to low bone mineral density according to 204 countries and territories and its temporal trends from 1990 to 2021. **Table S5:** Age-standardized rate and absolute number of mortality attributable to low bone mineral density according to 204 countries and territories and its temporal trends from 1990 to 2021. **Table S6:** Age-standardized rate of summary exposure value attributable to low bone mineral density according to ages and its temporal trends from 1990 to 2021. **Table S7:** Absolute number and age-standardized rate of disability-adjusted life years attributable to low bone mineral density according to ages and its temporal trends from 1990 to 2021 for both sexes, females and males. **Table S8:** Absolute number and age-standardized rate of mortality attributable to low bone mineral density according to ages and its temporal trends from 1990 to 2021. **Table S9:** Health inequality regression curves and concentration curves attributable to low bone mineral density in terms of disability-adjusted life years and mortality. **Table S10:** The contribution of aging, population, and epidemiological change to number of disability-adjusted life years attributable to low bone mineral density in both sexes, according to global, SDI regions, and GBD regions. **Table S11:** The contribution of aging, population, and epidemiological change to number of disability-adjusted life years attributable to low bone mineral density in female, according to global, SDI regions, and GBD regions. **Table S12:** The contribution of aging, population, and epidemiological change to number of disability-adjusted life years attributable to low bone mineral density in male, according to global, SDI regions, and GBD regions. **Table S13:** The contribution of aging, population, and epidemiological change to number of mortality attributable to low bone mineral density in both sexes, according to global, SDI regions, and GBD regions. **Table S14:** The contribution of aging, population, and epidemiological change to number of mortality attributable to low bone mineral density in female, according to global, SDI regions, and GBD regions. **Table S15:** The contribution of aging, population, and epidemiological change to number of mortality attributable to low bone mineral density in male, according to global, SDI regions, and GBD regions.

International Journal of Rheumatic Diseases

WILEY

International Journal of Rheumatic Diseases

LETTER TO THE EDITOR

Identifying Antigen-Specific Autoreactive B Cells in Sjögren's Disease: Methodological Challenges and Emerging Strategies

Ranjeet Singh Mahla[1,2]

[1]Medical Science Division, Kennedy Institute of Rheumatology, University of Oxford, Oxford, UK | [2]Vaccine and Infectious Disease Division, Fred Hutchinson Cancer Centre, Seattle, Washington, USA

Correspondence: Ranjeet Singh Mahla (rmahla@fredhutch.org)

Received: 18 December 2025 | **Revised:** 21 April 2026 | **Accepted:** 13 May 2026

Dear Editor,

In Sjogren's disease (SjD), the immune system targets the salivary and lacrimal glands, causing chronic inflammation, glandular dysfunction, and reduced tear and saliva production, leading to xerostomia and keratoconjunctivitis sicca [1, 2]. Key immune mechanisms include B cell hyperactivity, characterized by elevated circulating anti-SSA (Ro60 and Ro52), anti-SSB (La), and rheumatoid factors (RFs: IgM-RF, IgA-RF, and IgG-RF), increased expression activation and proliferation markers (e.g., CD86, CD38, HLA-DR, and Ki67), and enhanced secretion of IL6, BAFF, along with $CD4^+$ T cell-driven inflammation and the formation of ectopic lymphoid structures due to immune infiltration, all contributing to sustained autoimmunity [1, 2].

To fully understand the role of autoreactive B cells in SjD, it is essential to determine whether they exhibit dynamic changes or persist along specific developmental trajectories in response to inflammatory cues from $CD4^+$ T cells [3]. Key factors to explore include B cell subpopulation dynamics, BCR repertoire evolution [4], gene usage patterns, and autoreactive antibody production, alongside interactions with T cells and antigen-presenting cells (APCs) subsets. CD40-CD40L signaling and T follicular helper (Tfh) cells sustain B cell activation, driving the formation of ectopic lymphoid structures (ELSs) within salivary glands. These structures facilitate germinal center-like reactions, fostering clonal selection, somatic hypermutation (SHM), and affinity maturation, which may sustain persistent autoreactivity. Additionally, BAFF, APRIL, IFN-γ, and IL-21 play crucial roles in autoreactive B cell survival and dysregulation. Leveraging single-cell RNA sequencing (scRNA-seq), BCR repertoire analysis, and multi-omics approaches will be key to mapping B cell trajectories and designing targeted SjD therapies.

Recently, Lee et al., have characterized self-reactive clones from five major B cell subsets; transitional (Tr; IgD^-, $CD27^-$, $CD10^+$, $CD38^+$), mature naïve (MN; IgD^+, $CD27^-$, $CD10^-$), switched memory (Mem; IgD^-, $CD27^+$, IgM^-, $CD38^-$), double negative (DN; IgD^-, $CD27^-$), and plasmablasts (PB; IgD^-, $CD27^+$, IgM^-, $CD38^{hi}$) B cells from SjD patients and healthy controls [1]. B cell sorting followed by in vitro culture and expansion is a standard approach for discovering antigen-specific B cells. This study opens new avenues for the discovery and validation of autoreactive B cell clones and antigen-specific antibodies, particularly anti-Ro52, anti-Ro60, anti-La, and anti-RF antibodies, which play a crucial role in SjD pathogenesis. Discovering and validating these antigen-specific clones is essential. However, Lee et al. observed that none of the IgG-positive supernatants were reactive to Ro52, Ro60, or La antigens, highlighting the challenges in identifying specific autoreactive clones (Figure 1). Even after a robust immune response, antigen-specific B cells typically represent only 0.01%–0.1% of the total B cell population at any given time, posing a significant challenge in identifying autoreactive clones within the immune repertoire. This challenge may be addressed through selective enrichment techniques such as MACS/FACS using antigen-specific tetramers or multimers, single-cell RNA sequencing to profile individual cells, and affinity selection to isolate autoreactive B cells with high affinity for self-antigens. Additionally, performing longitudinal analysis can provide deeper insights into autoreactive B cell dynamics. However, antigen-specific enrichment approaches such as tetramer or dextramer-based isolation have inherent limitations,

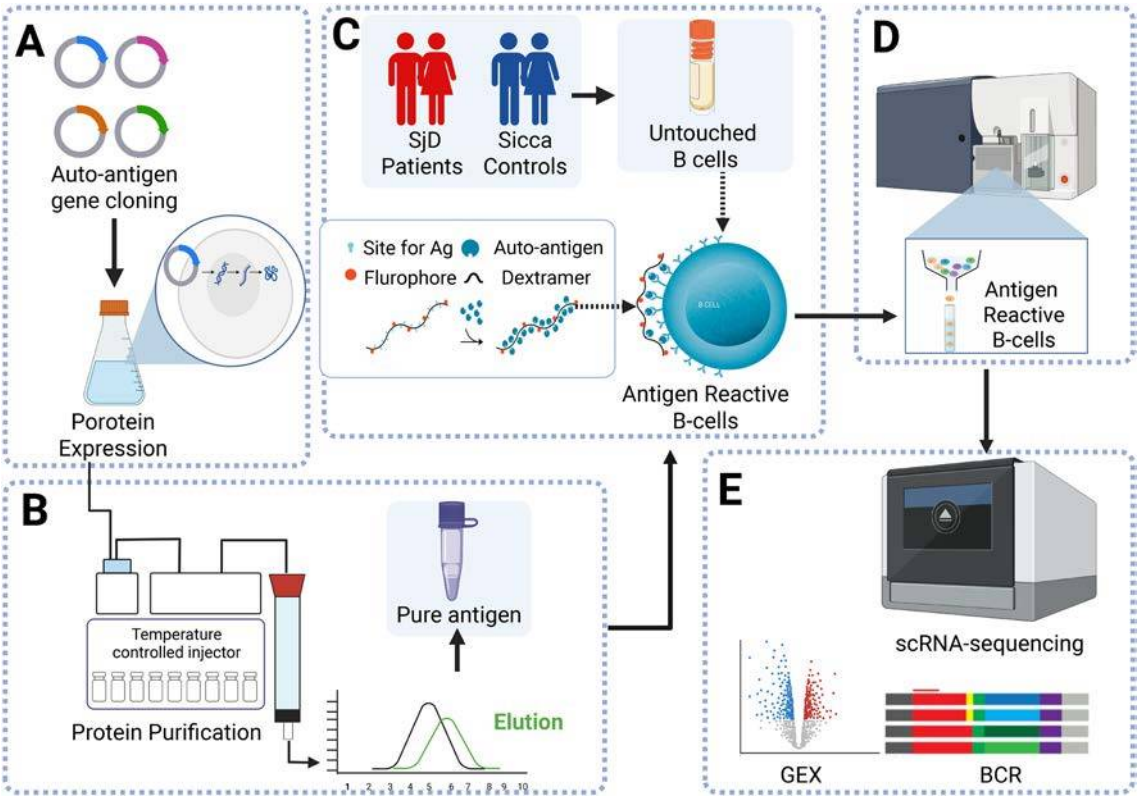

FIGURE 1 | Workflow for analysis of antigen-specific autoreactive B cells in Sjögren's disease (SjD). (A) Genes encoding autoantigens (e.g., Ro60, Ro52, and La) are cloned into expression vectors for protein production in insect (BEVS), mammalian (pCDNA3.1, pCEP4), and bacterial (pET21/pET32a/pET28a) systems. These vectors enable expression in Sf9, Sf21, High Five, Expi293, HEK293F, Rosetta-DE3, and BL21-DE3 cells. For high-yield expression, genes are placed under strong promoters, and an AviTag is incorporated for biotinylation. (B) HA-tagged proteins are purified using Ni^{2+}/Co^{2+} affinity chromatography columns on an HPLC system. (C) Blood samples from SjD patients and sicca controls are processed to isolate peripheral blood mononuclear cells (PBMCs), followed by isolation of untouched B cells via negative selection. Autoantigens are loaded onto dextramers for specific labeling. (D) Dextramer-labeled antigen-reactive B cells are identified and flow-sorted. (E) Flow-sorted antigen-specific autoreactive B cells are subjected to single-cell RNA sequencing, and their clonal and transcriptomic profiles are analyzed. Subpopulation-specific differences between SjD patients and sicca controls are further evaluated for antibody discovery and validation of disease-associated clones.

including potential alterations in antigen conformation affecting epitope recognition, affinity thresholds that may exclude low-affinity but biologically relevant clones, and the risk of non-specific binding. In the case of SjD, a more effective approach for discovering autoreactive B cells would involve selecting Ro60, Ro52, and La antigen-specific B cells from the Tr, MN, Mem, DN, and PB B cell populations of both SjD patients and healthy controls [5]. To isolate antigen-specific B cells from SjD patients, Ro60, La, and Ro52 antigen tetramers and multimers can be used. These antigens are generally produced in bacterial, insect, and mammalian cells, with HA tags for protein purification and AviTags for biotinylation. Biotinylated antigens are then assembled into tetramers and multimers (such as Dextramer). Longitudinal analysis of these antigen-specific B cells using dual fluorophore-conjugated antigen dextramers assemblies can provide insights into the dynamics of autoreactive B cells in SjD patients and enable the discovery of rare low-affinity antigen specific B cells [3]. According to Lee et al., none of the 34 self-reactive B cell clones (8 from healthy controls and 26 from SjD patients) identified via Sanger sequencing were reactive to Ro60, Ro52, and La. This suggests that other antigens beyond Ro60, Ro52, La, and RF play a role in SjD pathogenesis. The presence of autoreactive clones in healthy controls indicates that such clones are not specific to SjD, pointing to ambiguity in defining self-tolerance breaches [6]. The 34 clones are not clonally expanded, nor do they overlap with bulk RNA sequencing, though DN B cells and PB cell clones exhibit longer CDRH3 regions. The processes of V(D)J recombination, somatic hypermutation, class switch recombination, positive/negative selection, self-tolerance mechanism, cross-reactivity, and clonal expansion generate diversity in the B cell repertoire [7]. In autoimmune conditions like SjD, lupus, systemic sclerosis, the self-tolerance mechanisms are dysregulated, and breach of self-tolerance mechanism can contribute to the development of autoreactive B cells. Therefore, isolating and characterizing antigen-specific B cells is critical for identifying SjD-specific autoreactive clones [8]. It is crucial to accurately define reference controls for studying autoreactive B cells in SjD patients. Rather than using healthy controls, sicca controls—individuals with dry eye symptoms but without SjD—are more appropriate. These controls help better differentiate autoreactive B cells specific to SjD, providing a clearer understanding of the disease's pathogenesis [1, 2, 4, 8]. Apart from sorting antigen-specific B cells, quantitative and qualitative analyses of B cell subsets in SjD patients have greater implications for understanding SjD pathogenesis.

In summary, a comprehensive B cell subpopulation analysis of autoreactive B cells in SjD is crucial for characterizing

antigen-specific B cells. Flow cytometry enrichment of antigen-specific B cells using a dextramer backbone enables binding of multiple antigens and facilitates low-affinity BCR binding to autoantigens by flow cytometry (Figure 1). Flow-sorted cells are processed by paired single-cell gene expression and B cell receptor sequencing analysis for discovery and validation of antigen-specific autoreactive clones.

Author Contributions

Ranjeet Singh Mahla: conceptualization and writing the manuscript.

Conflicts of Interest

The author declares no conflicts of interest.

Data Availability Statement

The author has nothing to report.

References

1. A. Y. Lee, Z. Qi, K. J. Jackson, and J. H. Reed, "Self-Reactive B Cells Are Increased in All Major Stages of Peripheral Development in Sjogren's Disease," *Immunology and Cell Biology* 103 (2025): 401–410, https://doi.org/10.1111/imcb.70005.

2. S. Negrini, G. Emmi, M. Greco, et al., "Sjogren's Syndrome: A Systemic Autoimmune Disease," *Clinical and Experimental Medicine* 22 (2022): 9–25, https://doi.org/10.1007/s10238-021-00728-6.

3. L. Scharf, H. Axelsson, A. Emmanouilidi, et al., "Longitudinal Single-Cell Analysis of SARS-CoV-2-Reactive B Cells Uncovers Persistence of Early-Formed, Antigen-Specific Clones," *JCI Insight* 8 (2023): e165299, https://doi.org/10.1172/jci.insight.165299.

4. R. Wilbrink, L. van der Weele, A. J. P. L. Spoorenberg, et al., "B Cell Receptor Repertoire Analysis of the CD21(Lo) B Cell Compartment in Healthy Individuals, Patients With Sjogren's Disease, and Patients With Radiographic Axial Spondyloarthritis," *European Journal of Immunology* 55 (2025): e202451398, https://doi.org/10.1002/eji.202451398.

5. A. Mahendra, A. Haque, P. Prabakaran, et al., "Honing-In Antigen-Specific Cells During Antibody Discovery: A User-Friendly Process to Mine a Deeper Repertoire," *Communications Biology* 5 (2022): 1157, https://doi.org/10.1038/s42003-022-04129-7.

6. X. Hou, W. Wei, J. Zhang, et al., "Characterisation of T and B Cell Receptor Repertoire in Patients With Systemic Lupus Erythematosus," *Clinical and Experimental Rheumatology* 41 (2023): 2216–2223, https://doi.org/10.55563/clinexprheumatol/1rjr4s.

7. X. Chi, Y. Li, and X. Qiu, "V(D)J Recombination, Somatic Hypermutation and Class Switch Recombination of Immunoglobulins: Mechanism and Regulation," *Immunology* 160 (2020): 233–247, https://doi.org/10.1111/imm.13176.

8. R. S. Mahla, E. L. Jones, and L. B. Dustin, "Ro60-Roles in RNA Processing, Inflammation, and Rheumatic Autoimmune Diseases," *International Journal of Molecular Sciences* 25 (2024): 7705, https://doi.org/10.3390/ijms25147705.

International Journal of Rheumatic Diseases

WILEY

International Journal of Rheumatic Diseases

LETTER TO THE EDITOR

From Algorithm Performance to Clinical Impact: Reframing Artificial Intelligence in Rheumatology

Saumya Rawat[1] | Ved Prakash Chathurvedi[1] | Hemalatha Shanmugam[2]

[1]Sir Gangaram Hospital, New Delhi, India | [2]PanScience Innovations, New Delhi, India

Correspondence: Hemalatha Shanmugam (hemalatha@parchaa.com)

Received: 6 March 2026 | **Revised:** 8 May 2026 | **Accepted:** 1 June 2026

Dear Editor,

Rheumatology represents one of the most complex domains in internal medicine. Diseases such as rheumatoid arthritis, systemic lupus erythematosus, and spondyloarthritis are characterized by heterogeneous immune mechanisms, fluctuating inflammatory activity, delayed structural manifestations, and variable therapeutic response [1]. Despite advances in imaging, biomarkers, and targeted biologics, routine care remains episodic, data-fragmented, and often reactive. The increasing volume of multimodal data—from radiographs and Magnetic Resonance Imaging (MRI) to laboratory markers and electronic health records (EHRs)—has exceeded the limits of unaided clinical cognition [2, 3]. Artificial intelligence (AI) has therefore emerged not merely as a technical innovation but as a structural necessity.

This perspective is based on a narrative synthesis of contemporary literature on artificial intelligence applications in rheumatology, with emphasis on translational validity, implementation barriers, and clinical utility rather than algorithmic development alone. Current literature demonstrates rapid expansion of AI applications across rheumatology [3, 4]. Machine learning models have been developed for diagnostic classification, radiographic scoring, prediction of therapeutic response, flare forecasting, and risk stratification [3, 5, 6]. Deep learning systems have achieved high performance in automated detection of joint damage and inflammatory features on radiographs [7]. Natural language processing approaches have successfully extracted disease phenotypes from unstructured EHR data, demonstrating improved case identification from routine clinical documentation [8]. Large language models (LLMs) have been evaluated for treatment-related information delivery and vignette-based decision support [9]. Collectively, these studies establish technical feasibility and an existing persistent translational gap between algorithmic performance in controlled environments and measurable impact on real-world clinical outcomes. However, the central limitation remains fragmentation. Most investigations report algorithmic performance in controlled settings, typically expressed through AUROC (Area Under the Receiver Operating Characteristic curve) or accuracy metrics, yet stop short of examining how such tools alter clinical pathways, improve longitudinal outcomes, or integrate into routine workflow. The field risks accumulating high-performing models without achieving systemic transformation.

This editorial aims to reframe the evaluation of artificial intelligence in rheumatology from isolated performance metrics toward its ability to influence clinical decision-making, workflow integration, and longitudinal patient outcomes. This editorial proposes a pathway-centered framework for AI integration in rheumatology, structured across five interdependent domains: early detection, diagnostic augmentation, prognostic stratification, precision therapeutics, and continuous monitoring. Figure 1 represents an overview of the AI-enabled pathway in Rheumatology Care.

2 | Early Detection and Referral Optimization

Delayed diagnosis remains a major contributor to irreversible structural damage, particularly in inflammatory arthritis where early therapeutic intervention alters long-term disease trajectory [1]. Machine learning models applied to EHR data have demonstrated potential to identify at-risk individuals prior to overt radiographic change [10]. The translational priority, however, is not discrimination performance alone, but embedding such systems within primary care and referral networks to reduce diagnostic latency and inappropriate referral burden.

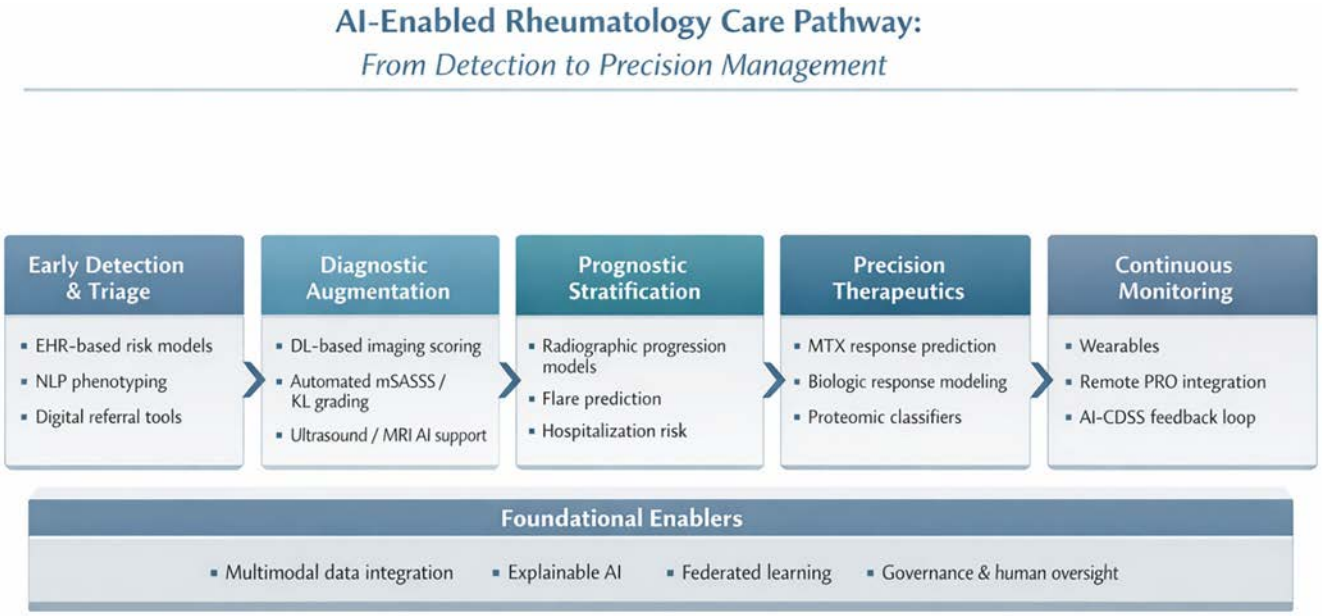

FIGURE 1 | Conceptual framework illustrating the integration of artificial intelligence across the rheumatology care continuum, spanning early detection, diagnosis, prognostication, therapeutic decision-making, and continuous monitoring.

3 | Diagnostic Augmentation Through Imaging AI

Radiographic scoring remains labor-intensive and subject to interobserver variability. Deep learning systems and automated mSASSS (Modified Stoke Ankylosing Spondylitis Spinal Score) scoring models have shown strong concordance with expert assessments in osteoarthritis, inflammatory arthritis and ankylosing spondylitis classification, and further demonstrate feasibility for longitudinal structural monitoring [11]. Yet evaluation must extend beyond agreement metrics to include reproducibility across imaging protocols, interoperability with PACS infrastructure (Picture Archiving and Communication System), and impact on treat-to-target strategies. Without workflow integration, imaging AI remains parallel rather than embedded within clinical systems.

A pertinent example is the RBknee algorithm; while it demonstrates expert-level accuracy in structural radiographic grading, its clinical utility is limited by a significant 'actionability gap,' as structural severity frequently fails to correlate with symptomatic disease, and the model exhibits technical fragility (e.g., 13%–22% disagreement upon image flipping) that can erode clinician trust and disrupt established diagnostic workflows [10].

4 | Prognostic Stratification

Predicting structural progression, hospitalization risk, or flare probability represents a core objective of precision rheumatology. Machine learning models using longitudinal EMR data have achieved moderate predictive performance for structural progression in ankylosing spondylitis and hospitalization in systemic lupus erythematosus [11, 12]. Flare prediction systems incorporated into clinical tools have demonstrated promising AUROC values and improved clinician confidence [13]. Nonetheless, external validation and calibration across heterogeneous populations remain limited [5]. Prognostic AI must evolve from retrospective modeling toward prospective trials demonstrating outcome modification.

A concrete illustration of this gap is found in Rheumatoid Arthritis flare prediction models; for instance, a machine-learning-based decision support tool achieved high predictive accuracy (AUROC 0.80) but led to a decline in physician acceptance (NPS dropped from +40% to −20%) because it prioritized data points that differed from clinical priorities. Such tools often provide structurally accurate but clinically non-actionable outputs, failing to synchronize with the complex, shared decision-making process required to change prescribing habits in real-world rheumatology practice [13].

5 | Precision Therapeutics

Treatment-response heterogeneity in rheumatoid arthritis persists despite biologic advances. Multiple studies have applied machine learning to predict methotrexate or biologic response, with AUROC values commonly ranging from 0.72 to 0.84 [14]. Registry-based models incorporating explainable AI approaches have identified drug-specific predictors of non-response [9]. These findings suggest feasibility of individualized therapeutic selection by considering clinical and genetic characteristics of patients using AI [15]. However, predictive models must be operationalized within prescribing workflows and shared decision-making contexts to reduce ineffective drug exposure and healthcare expenditure.

6 | Continuous Monitoring and Digital Phenotyping

Wearable-derived physical activity metrics correlate with functional outcomes in rheumatic diseases [8]. AI-enabled clinical

decision support systems that integrate longitudinal patient-reported outcomes and laboratory trends can enhance flare detection and guide dose tapering strategies [13]. Such tools represent a shift from episodic clinic-based assessment toward dynamic disease management.

7 | Structural Imperatives for Integration

Three structural priorities should define the next phase of AI development in rheumatology. Table 1 provides the implementation priorities for AI in various domains of Rheumatology.

TABLE 1 | From algorithm performance to clinical impact: Implementation priorities for AI in rheumatology.

Domain	Predominant focus of current evidence	Key methodological and translational gaps	Strategic priorities for clinical integration
Diagnosis	Discriminative performance metrics (AUROC, sensitivity, specificity) derived from structured datasets and imaging cohorts	Limited external validation; spectrum bias; underrepresentation of early or atypical disease; minimal assessment of calibration and clinical utility	Multicenter external validation across heterogeneous populations; calibration reporting; decision-curve analysis; integration into referral and triage workflows with real-world impact assessment
Prognosis	Retrospective modeling of radiographic progression, flare risk, or hospitalization using registry or EHR data	Inadequate temporal validation; limited calibration and risk stratification thresholds; absence of prospective outcome evaluation	Prospective cohort validation; dynamic risk updating models; evaluation of impact on treatment escalation decisions; pragmatic trials assessing outcome modification
Treatment Response Prediction	Biomarker-driven or clinical-variable–based prediction of response to methotrexate or biologics	Poor interoperability with prescribing systems; limited explainability; lack of head-to-head comparison with clinician judgment	Embedding predictive tools within EHR prescribing interfaces; explainable AI outputs supporting shared decision-making; randomized or quasi-experimental evaluation of therapeutic optimization
Flare Prediction & Monitoring	Supervised learning models predicting flare events using longitudinal clinical data	Limited real-world deployment; low integration with patient-reported outcomes (PROs) and remote monitoring; insufficient implementation science evidence	Integration with digital PRO platforms and wearable data streams; adaptive monitoring systems; cluster-randomized implementation studies assessing reduction in preventable flares
Large Language Models (LLMs)	Evaluation of informational accuracy and question-answering performance in rheumatology contexts	Hallucination risk; lack of domain-specific fine-tuning; absence of governance frameworks; unclear medico-legal accountability	Development of rheumatology-specific benchmark datasets; standardized evaluation and human-in-loop frameworks for hallucination detection; domain-specific fine-tuning and validation against curated clinical datasets. Institutional governance policies; formal evaluation of impact on clinician workload and patient education quality

7.1 | First, Data Harmonization and Interoperability

Rheumatology datasets are inherently multimodal, spanning imaging, serology, transcriptomics, and narrative documentation. Heterogeneous diagnostic criteria and evolving disease definitions complicate generalizability [3]. Beyond structural variability, there is a restricted scope and representativeness of training datasets. Models developed on narrow or homogeneous data are more likely to encode systematic bias and show performance degradation when applied to broader clinical populations. Addressing this requires not only standardized ontologies and harmonized data capture, but also deliberate efforts to aggregate data across institutions through well-defined data-sharing frameworks. Building datasets that reflect variation in ethnicity, geography, and clinical practice patterns is essential to ensure that model outputs remain reliable, generalizable, and clinically applicable across diverse real-world settings [15].

7.2 | Second, Interpretability and Clinical Trust

Black-box models hinder adoption in chronic immune-mediated diseases requiring nuanced clinical reasoning. Explainable AI techniques enhance transparency and facilitate clinician engagement [14]. Interpretability should be considered foundational to implementation.

7.3 | Third, Outcome-Centered Validation

High AUROC values do not guarantee improved patient outcomes. In this context, a truly actionable output refers to a prediction that directly informs or alters a clinical decision—such as anticipating response to a specific biologic therapy—rather than merely identifying a state already evident to the clinician, such as high disease activity. Future investigations should prioritize clinically meaningful endpoints, including reduced diagnostic delay, decreased flare frequency, improved functional status, optimized drug persistence, and lower hospitalization rates. Implementation science—not algorithmic novelty alone—should define progress.

8 | Generative AI and Governance

While diagnostic and predictive AI applications continue to face challenges related to real-world integration and clinical impact, administrative and generative AI tools are currently demonstrating more immediate utility in supporting clinician workflows. The rapid emergence of LLMs underscores the need for disciplined integration. GPT-based systems can provide generally accurate treatment-related responses [9, 16]. However, limitations including hallucinated citations and outdated training data necessitate strict human oversight [17, 18]. In rheumatology, where therapeutic decisions often depend on subtle immunologic interpretation, generative systems must remain adjunctive rather than authoritative.

From a regulatory perspective, the clinical deployment of AI aligns with the framework of Software as a Medical Device (SaMD), which follows a total product lifecycle approach encompassing development, validation, deployment, and continuous monitoring. Guidance from regulatory agencies such as the U.S. Food and Drug Administration (FDA), along with international SaMD frameworks, emphasizes adherence to Good Machine Learning Practice (GMLP), including data quality, model transparency, reproducibility, and rigorous clinical validation. A key emerging concept is the Predetermined Change Control Plan (PCCP), which allows for predefined, regulator-approved modifications to machine learning models post-deployment while maintaining safety and effectiveness. This is particularly relevant for adaptive AI systems, enabling controlled model updates without requiring repeated full regulatory submissions. In parallel, these frameworks mandate structured post-market surveillance to monitor real-world performance, detect algorithmic drift, and generate real-world evidence across diverse populations [19]. The European Union Artificial Intelligence Act further introduces a risk-based classification system, requiring high-risk clinical AI systems to meet stringent standards for human oversight, technical robustness, auditability, and data governance [20]. Alignment with these evolving regulatory principles is essential to ensure that generative AI systems are deployed in a manner that safeguards patient privacy, maintains clinical accountability, and supports reliable integration into healthcare workflows.

9 | Conclusion

AI in rheumatology has progressed from exploratory experimentation to proof-of-concept validation across diagnosis, prognosis, and therapeutic optimization [3, 4]. The specialty now stands at a strategic inflection point. The central question is no longer whether algorithms can detect erosions or predict treatment response, but whether rheumatology can systematically integrate these tools to redesign care pathways.

Transitioning from model-level innovation to system-level implementation will determine whether AI meaningfully reduces diagnostic delay, enhances therapeutic precision, and improves long-term outcomes. A pathway-centered, governance-aware, outcome-driven framework provides a structured direction for achieving that transformation.

Author Contributions

Saumya Rawat: conceptualization, literature review, manuscript drafting, critical revision of intellectual content. **Ved Prakash Chathurvedi:** literature review, content development, manuscript review, critical revision of intellectual content. **Hemalatha Shanmugam:** conceptualization, literature review, manuscript drafting, manuscript editing, supervision, and correspondence. All authors contributed to the interpretation of the literature, reviewed and approved the final manuscript, and agree to be accountable for all aspects of the work.

Funding

The authors have nothing to report.

Conflicts of Interest

The authors declare no conflicts of interest.

Data Availability Statement

The authors have nothing to report.

References

1. J. S. Smolen, D. Aletaha, A. Barton, et al., "Rheumatoid Arthritis," *Nature Reviews Disease Primers* 4 (2018): 18001.

2. J. Kedra, T. Radstake, A. Pandit, et al., "Current Status of Use of Big Data and Artificial Intelligence in RMDs: A Systematic Literature Review Informing EULAR Recommendations," *RMD Open* 5, no. 2 (2019): e001004.

3. S. Dubey, A. Chan, A. O. Adebajo, D. Walker, and M. Bukhari, "Artificial Intelligence and Machine Learning in Rheumatology," *Rheumatology (Oxford, England)* 63, no. 8 (2024): 2040–2041.

4. S. Momtazmanesh, A. Nowroozi, and N. Rezaei, "Artificial Intelligence in Rheumatoid Arthritis: Current Status and Future Perspectives: A State-of-the-Art Review," *Rheumatology and Therapy* 9, no. 5 (2022): 1249–1304.

5. V. Bouget, J. Duquesne, S. Hassler, et al., "Machine Learning Predicts Response to TNF Inhibitors in Rheumatoid Arthritis: Results on the ESPOIR and ABIRISK Cohorts," *RMD Open* 8, no. 2 (2022): e002442.

6. J. Duquesne, V. Bouget, P. H. Cournède, et al., "Machine Learning Identifies a Profile of Inadequate Responder to Methotrexate in Rheumatoid Arthritis," *Rheumatology (Oxford, England)* 62, no. 7 (2023): 2402–2409.

7. J. Baloun, L. A. Cerezo, T. Kropáčková, et al., "Machine Learning-Assisted Screening of Clinical Features for Predicting Difficult-to-Treat Rheumatoid Arthritis," *Scientific Reports* 15, no. 1 (2025): 34747.

8. H. Ocagli, R. Agarinis, D. Azzolina, et al., "Physical Activity Assessment With Wearable Devices in Rheumatic Diseases: A Systematic Review and Meta-Analysis," *Rheumatology (Oxford, England)* 62, no. 3 (2023): 1031–1046.

9. B. N. Coskun, B. Yagiz, G. Ocakoglu, E. Dalkilic, and Y. Pehlivan, "Assessing the Accuracy and Completeness of Artificial Intelligence Language Models in Providing Information on Methotrexate Use," *Rheumatology International* 44, no. 3 (2024): 509–515.

10. A. Lenskjold, M. W. Brejnebøl, M. H. Rose, et al., "Artificial Intelligence Tools Trained on Human-Labeled Data Reflect Human Biases: A Case Study in a Large Clinical Consecutive Knee Osteoarthritis Cohort," *Scientific Reports* 14 (2024): 26782, https://doi.org/10.1038/s41598-024-75752-z.

11. B. S. Koo, M. Jang, J. S. Oh, et al., "Machine Learning Models With Time-Series Clinical Features to Predict Radiographic Progression in Patients With Ankylosing Spondylitis," *Journal of Rheumatic Diseases* 31, no. 2 (2024): 97–107.

12. A. M. Jorge, D. Smith, Z. Wu, et al., "Exploration of Machine Learning Methods to Predict Systemic Lupus Erythematosus Hospitalizations," *Lupus* 31, no. 11 (2022): 1296–1305.

13. H. Labinsky, D. Ukalovic, F. Hartmann, et al., "An AI-Powered Clinical Decision Support System to Predict Flares in Rheumatoid Arthritis: A Pilot Study," *Diagnostics (Basel)* 13, no. 1 (2023): 148.

14. D. Ukalovic, B. F. Leeb, B. Rintelen, et al., "Prediction of Ineffectiveness of Biological Drugs Using Machine Learning and Explainable AI Methods: Data From the Austrian Biological Registry BioReg," *Arthritis Research & Therapy* 26, no. 1 (2024): 44.

15. O. Koker, S. Sahin, M. Yildiz, A. Adrovic, and O. Kasapcopur, "The Emerging Paradigm in Pediatric Rheumatology: Harnessing the Power of Artificial Intelligence," *Rheumatology International* 44, no. 11 (2024): 2315–2325, https://doi.org/10.1007/s00296-024-05661-x.

16. S. S. Zhao, C. Hong, T. Cai, et al., "Incorporating Natural Language Processing to Improve Classification of Axial Spondyloarthritis Using Electronic Health Records," *Rheumatology (Oxford, England)* 59, no. 5 (2020): 1059–1065.

17. K. Can Demirbaş, M. Yıldız, S. Saygılı, N. Canpolat, and Ö. Kasapçopur, "Artificial Intelligence in Pediatrics: Learning to Walk Together," *Turkish Archives of Pediatrics* 59, no. 2 (2024): 121–130, https://doi.org/10.5152/TurkArchPediatr.2024.24002.

18. T. Dave, S. A. Athaluri, and S. Singh, "ChatGPT in Medicine: An Overview of Its Applications, Advantages, Limitations, Future Prospects, and Ethical Considerations," *Frontiers in Artificial Intelligence* 4, no. 6 (2023): 1169595.

19. Center, *AI-Enabled Device Software Functions [Internet]* (U.S. Food and Drug Administration, 2025), https://www.fda.gov/regulatory-information/search-fda-guidance-documents/artificial-intelligence-enabled-device-software-functions-lifecycle-management-and-marketing.

20. European Union, *Regulation—EU—2024/1689—EN—EUR-Lex [Internet]* (Europa.eu, 2024), https://eur-lex.europa.eu/eli/reg/2024/1689/oj/eng.

International Journal of Rheumatic Diseases

WILEY

International Journal of Rheumatic Diseases

LETTER TO THE EDITOR

Development and Validation of Data-Driven, Rule-Based Algorithms for Identifying Antineutrophil Cytoplasmic Antibody-Associated Vasculitis in Administrative Claims Databases

Ken-ei Sada | Research Group Developing Japanese Claims-Based Algorithms for Connective Tissue Diseases

Department of Clinical Epidemiology, Kochi Medical School, Nankoku, Japan

Correspondence: Ken-ei Sada (sadak@kochi-u.ac.jp)

Received: 20 December 2025 | **Revised:** 3 April 2026 | **Accepted:** 27 May 2026

Dear Editor,

Antineutrophil cytoplasmic antibody (ANCA)-associated vasculitis (AAV) consists of three major subtypes: microscopic polyangiitis (MPA), granulomatosis with polyangiitis (GPA), and eosinophilic granulomatosis with polyangiitis (EGPA). Because of rarity and heterogeneity, randomized control trials are difficult to conduct.

Administrative claims databases are widely used in epidemiologic and health services research, including studies of AAV on disease frequency, healthcare utilization, and medical costs [1, 2]. A key limitation of administrative claims data is the lack of detailed clinical information; although the validity of identifying AAV using International Classification of Diseases (ICD) codes alone has been examined overseas, rigorous algorithm development and validation against chart review remain essential. Because healthcare systems and data structures differ substantially between Japan and other countries, algorithms created abroad cannot be directly applied. This study aimed to develop and validate practical, reliable algorithms for identifying patients with AAV in Japanese claims data using decision tree methods.

This retrospective cross-sectional study was conducted at six tertiary care institutions (Table S1). We focused on outpatients because outpatient and inpatient populations may represent different clinical contexts of AAV and may therefore require different identification algorithms. We identified outpatients who had at least one visit between 1 November and 31 December 2023 and extracted their administrative claims data for the preceding 12 months. The study population was randomly divided into training ($n = 8199$) and testing ($n = 3512$) sets, and an independent external validation cohort ($n = 1827$) was obtained from Kyoto Prefectural University Hospital.

In this study, we adopted the *all possible cases* approach. In this approach, the population defined by the International Classification of Diseases, 10th revision (ICD-10) for MPA (M31.7), GPA (M31.3), EGPA (M30.1), or other specified necrotizing vasculopathies (M31.8) was regarded as the candidate universe. All potential cases underwent chart review to confirm the diagnosis. AAV was considered present if any of the following applied: (1) prior participation in a clinical study, (2) fulfillment of established AAV classification criteria [3–6], or (3) clinical confirmation by two independent physicians.

A decision tree model was used to identify patients with AAV. The analysis was performed for the overall AAV cohort as well as separately for the MPA/GPA and EGPA subgroups to examine disease-specific discriminative features. When applied to the training set, the decision tree primarily split on AAV-related ICD-10 codes. Therefore, to improve subtype discrimination, an additional tree was constructed using only patients with these codes.

Group Members: The Research Group Developing Japanese Claims-Based Algorithms for Connective Tissue Diseases consisted of Ken-ei Sada, Yoshia Miyawaki, Ryo Yanai, Takashi Kida, Akira Onishi, Ryusuke Yoshimi, Kunihiro Ichinose, and Yasuhiro Shimojima. Detailed affiliations of the group members are provided in Table S1.

A total of 30 predictor variables were evaluated (Table S2), and only variables retained by all three selection methods (least absolute shrinkage and selection operator [LASSO], Boruta, and recursive feature elimination [RFE]) were included.

The diagnostic performance of the simplified classification rules derived from the decision tree was assessed by comparison with chart-confirmed AAV diagnoses in the testing and external validation sets. Model performance was evaluated using accuracy, sensitivity, specificity, positive predictive value (PPV), and negative predictive value (NPV). The F1 score was also calculated as a summary metric of precision and recall. All analyses were conducted using R version 4.4.1 (R Foundation for Statistical Computing, Vienna, Austria) and Stata version 17.0 (StataCorp, College Station, TX, USA).

Of enrolled patients, 3%–5% of patients in each dataset were confirmed to have AAV by chart review, with similar proportions across the training, testing, and external validation sets (Table S3). Fifteen candidate variables were consistently selected (Table S2) and used to construct a decision tree.

When the model was restricted to patients with AAV diagnosis codes in the training set ($n=413$), ANCA testing emerged as the primary split. Among patients without ANCA testing ($n=170$), classification was further determined by the presence of bronchial asthma, whereas among those with ANCA testing ($n=243$), the next split was anti-double-stranded DNA (anti-dsDNA) antibody testing (Figure 1). In the full decision tree, additional lower-level splits included CRP, tacrolimus use, and ICD-10 code for SLE; however, these were not included in the final simplified rule-based algorithms, which were constructed to improve interpretability and practical applicability. Three simplified classification rules derived from the decision tree were evaluated (Table 1). Across both the testing and external validation datasets, Rule 3 showed the most favorable overall performance (Table S4).

From 27 candidate variables, excluding AAV diagnosis codes other than EGPA, six were selected to contract the MPA/GPA model. Among 242 patients with diagnosis codes for MPA/GPA in the training set, ANCA testing emerged as the primary split, followed by the absence of an EGPA diagnosis code among those with ANCA testing (Figure S1). The three derived rules were shown in Table 1. For the MPA/GPA model, Rule 3 performed best in testing, whereas Rule 2 showed the most favorable balance on external validation (Table S5).

Among 28 candidate variables (excluding AAV codes other than MPA/GPA), five were selected for decision tree construction for EGPA. Among 110 patients with EGPA codes in the training set, bronchial asthma emerged as the primary split, followed by the absence of MPA/GPA codes among those without asthma (Figure S2). The three simplified rules were shown in Table 1. For EGPA, Rule 1 performed best in testing, whereas Rules 2 and 3 showed the most favorable balance on external validation (Table S6).

In this study, to improve the PPV for identifying AAV cases, we incorporated additional criteria beyond disease codes, specifically ANCA testing, bronchial asthma, and anti-dsDNA antibody testing. The inclusion of ANCA testing appears particularly appropriate in Japan, where a high proportion of patients with AAV are myeloperoxidase-ANCA-positive [7] and routine ANCA monitoring is recommended [8]. In contrast, approximately half of patients with EGPA are ANCA-negative [9]; thus, incorporating bronchial asthma likely improved sensitivity by capturing EGPA cases without ANCA testing. Anti-dsDNA antibodies are highly specific for systemic lupus erythematosus (SLE), in which ANCA positivity occurs in about 10% of patients [10]. Therefore, excluding patients undergoing ANCA monitoring for SLE effectively increased PPV in our algorithm.

The algorithms may undercapture patients with mild disease or those managed outside specialist care, who are underrepresented in tertiary hospital claims data. However, reliance on diagnosis codes and laboratory tests, rather than medications, may reduce bias related to treatment intensity. Nevertheless, this study was limited to outpatients, and the findings may not be directly generalizable to inpatient settings, where patients

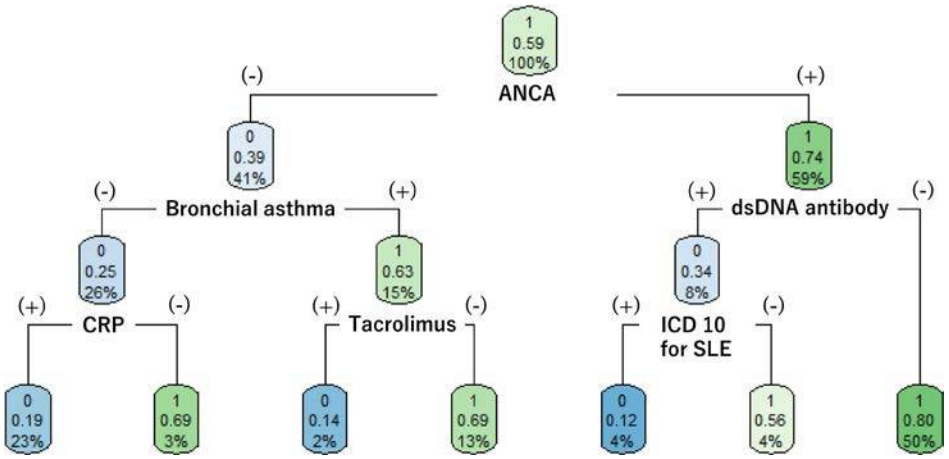

FIGURE 1 | Decision tree for case identification of ANCA-associated vasculitis Each node is labeled with the predicted class (0 = negative, 1 = positive), the proportion of positive cases within the node, and the percentage of the total cohort classified into the node. Node color indicates the predicted class and node purity: Green shades indicate nodes classified as positive, blue shades indicate nodes classified as negative, and darker shades indicate greater purity. ANCA, antineutrophil cytoplasmic antibody; CRP, C-reactive protein; dsDNA, double-stranded DNA; ICD, International Classification of Diseases; SLE, systemic lupus erythematosus.

TABLE 1 | Rule-based algorithms for ANCA associated vasculitis, microscopic polyangiitis/granulomatosis with polyangiitis, and eosinophilic granulomatosis with polyangiitis.

AAV	Rule 1	AAV diagnosis codes only
	Rule 2	Rule 1 and ANCA testing
	Rule 3	Rule 1 and ((ANCA testing and no anti-dsDNA antibody testing) or (no ANCA testing and bronchial asthma))
MPA/GPA	Rule 1	MPA/GPA diagnosis codes only
	Rule 2	Rule 1 and ANCA testing
	Rule 3	Rule 2 and no diagnosis code for EGPA
EGPA	Rule 1	EGPA diagnosis codes only
	Rule 2	Rule 1 and bronchial asthma
	Rule 3	Rule 1 and (bronchial asthma or no MPA/GPA diagnosis code)

may more often be in the remission-induction phase and may require a separate identification algorithm.

In conclusion, this study demonstrates that simple rule-based algorithms, developed through a systematic and data-driven approach integrating disease codes, ANCA testing, bronchial asthma, and anti-dsDNA antibody testing, can reliably and validly identify patients with AAV in Japanese claims data.

Author Contributions

K.-e.S. had full access to all of the data in the study. He took responsibility for the data's integrity and the data analysis's accuracy. K.-e.S., Y.M., R.Y., T.K., A.O., R.Y., K.I., and Y.S. Study conception and design; K.-e.S., Y.M., R.Y., T.K., A.O., R.Y., K.I., and Y.S. Interpretation of data and manuscript writing support; All authors read and approved the final manuscript.

Acknowledgments

The authors thank Honyaku Center Inc. for assistance with English language editing.

Funding

This study was supported by JSPS KAKENHI (grant number JP23H03128). The funder had no role in the study design, data collection, analysis, interpretation, manuscript preparation, or the decision to submit the manuscript for publication.

Ethics Statement

The study complied with the principles of the Declaration of Helsinki and the Ethical Guidelines for Medical and Health Research Involving Human Subjects in Japan. Ethical approval was obtained from the Ethics Committee of Kochi Medical School (approval number: 2023-054).

Consent

Informed consent was obtained through an opt-out approach, with each participating department publicly disclosing the study protocol and offering patients the opportunity to decline participation via institutional websites.

Conflicts of Interest

K.S. received an honorarium for lectures from GlaxoSmithKline K.K. These financial interactions were unrelated to the present study.

Data Availability Statement

The data that support the findings of this study are available from the corresponding author upon reasonable request.

References

1. L. Degli Esposti, M. Dovizio, V. Perrone, et al., "Profile, Healthcare Resource Consumption and Related Costs in ANCA-Associated Vasculitis Patients: A Real-World Analysis in Italy," *Advances in Therapy* 40, no. 12 (2023): 5338–5353.

2. J. K. Ahn, J. Hwang, C. B. Choi, and G. H. Seo, "Risk of Acute Myocardial Infarction, Stroke, and Venous Thromboembolism Among Patients With Anti-Neutrophil Cytoplasmic Antibody-Associated Vasculitis in South Korea: A Nationwide Population-Based Study," *Joint, Bone, Spine* 90, no. 2 (2023): 105498.

3. R. Watts, S. Lane, T. Hanslik, et al., "Development and Validation of a Consensus Methodology for the Classification of the ANCA-Associated Vasculitides and Polyarteritis Nodosa for Epidemiological Studies," *Annals of the Rheumatic Diseases* 66, no. 2 (2007): 222–227.

4. R. Suppiah, J. C. Robson, P. C. Grayson, et al., "2022 American College of Rheumatology/European Alliance of Associations for Rheumatology Classification Criteria for Microscopic Polyangiitis," *Annals of the Rheumatic Diseases* 81, no. 3 (2022): 321–326.

5. J. C. Robson, P. C. Grayson, C. Ponte, et al., "2022 American College of Rheumatology/European Alliance of Associations for Rheumatology Classification Criteria for Granulomatosis With Polyangiitis," *Annals of the Rheumatic Diseases* 81, no. 3 (2022): 315–320.

6. P. C. Grayson, C. Ponte, R. Suppiah, et al., "2022 American College of Rheumatology/European Alliance of Associations for Rheumatology Classification Criteria for Eosinophilic Granulomatosis With Polyangiitis," *Annals of the Rheumatic Diseases* 81, no. 3 (2022): 309–314.

7. K. E. Sada, M. Yamamura, M. Harigai, et al., "Classification and Characteristics of Japanese Patients With Antineutrophil Cytoplasmic Antibody-Associated Vasculitis in a Nationwide, Prospective, Inception Cohort Study," *Arthritis Research & Therapy* 16, no. 2 (2014): R101.

8. M. Casal Moura, P. Gauckler, H. J. Anders, et al., "Management of Antineutrophil Cytoplasmic Antibody-Associated Vasculitis With Glomerulonephritis as Proposed by the ACR 2021, EULAR 2022 and KDIGO 2021 Guidelines/Recommendations," *Nephrology, Dialysis, Transplantation* 38, no. 11 (2023): 2637–2651.

9. K. E. Sada, K. Amano, R. Uehara, et al., "A Nationwide Survey on the Epidemiology and Clinical Features of Eosinophilic Granulomatosis With Polyangiitis (Churg-Strauss) in Japan," *Modern Rheumatology* 24, no. 4 (2014): 640–644.

10. M. Galeazzi, G. Morozzi, G. D. Sebastiani, et al., "Anti-Neutrophil Cytoplasmic Antibodies in 566 European Patients With Systemic Lupus Erythematosus: Prevalence, Clinical Associations and Correlation With Other Autoantibodies. European Concerted Action on the Immunogenetics of SLE," *Clinical and Experimental Rheumatology* 16, no. 5 (1998): 541–546.

Supporting Information

Additional supporting information can be found online in the Supporting Information section. **Figure S1:** Decision tree for case identification of microscopic polyangiitis/granulomatosis with polyangiitis. Each node is labeled with the predicted class (0 = negative, 1 = positive),

the proportion of positive cases within the node, and the percentage of the total cohort classified into the node. Node color indicates the predicted class and node purity: green shades indicate nodes classified as positive, blue shades indicate nodes classified as negative, and darker shades indicate greater purity. ANCA, antineutrophil cytoplasmic antibody; EGPA, eosinophilic granulomatosis with polyangiitis; ICD, International Classification of Diseases. **Figure S2:** Decision tree for case identification of eosinophilic granulomatosis with polyangiitis. Each node is labeled with the predicted class (0 = negative, 1 = positive), the proportion of positive cases within the node, and the percentage of the total cohort classified into the node. Node color indicates the predicted class and node purity: green shades indicate nodes classified as positive, blue shades indicate nodes classified as negative, and darker shades indicate greater purity. GPA, granulomatosis with polyangiitis; ICD, International Classification of Diseases; MPA, microscopic polyangiitis. **Table S1:** Research group developing Japanese claims-based algorithms for connective tissue diseases. **Table S2:** Candidate variables selected for analysis. **Table S3:** Distribution of ICD-10-based and chart-confirmed cases in the training, testing, and external validation datasets. **Table S4:** Diagnostic performance of rule-based algorithms for ANCA-associated vasculitis in the testing and external validation datasets. **Table S5:** Diagnostic performance of rule-based algorithms for microscopic polyangiitis/granulomatosis with polyangiitis in the testing and external validation datasets. **Table S6:** Diagnostic performance of rule-based algorithms for eosinophilic granulomatosis with polyangiitis in the testing and external validation datasets.

International Journal of Rheumatic Diseases

WILEY

International Journal of Rheumatic Diseases

ORIGINAL ARTICLE

Reciprocal Regulation of GLI1 and GLI3 Fine Tunes the Pathogenic Behavior of Synovial Fibroblasts in Rheumatoid Arthritis

Motohiko Sato[1] | Tetsuya Saito[1] | Yoji Komiya[1] | Seiji Noda[1] | Yasuhiro Tagawa[1] | Akio Yamamoto[1] | Hideyuki Iwai[1] | Kentaro Endo[2] | Hideyuki Koga[3] | Yasuhiro Takahara[4] | Kazutaka Sugimoto[5] | Ichiro Sekiya[2] | Eiryo Kawakami[6,7,8,9] | Tadashi Hosoya[1] | Shinsuke Yasuda[1]

[1]Department of Rheumatology, Graduate School of Medical and Dental Sciences, Institute of Science Tokyo (IST), Tokyo, Japan | [2]Center for Stem Cell and Regenerative Medicine, Institute of Science Tokyo (IST), Tokyo, Japan | [3]Department of Joint Surgery and Sports Medicine, Graduate School of Medical and Dental Sciences, Institute of Science Tokyo (IST), Tokyo, Japan | [4]Department of Orthopedic Surgery, Nippon Kokan Fukuyama Hospital, Hiroshima, Japan | [5]Department of Orthopedics, Sonodakai Joint Replacement Center Hospital, Tokyo, Japan | [6]Department of Artificial Intelligence Medicine, Graduate School of Medicine, Chiba University, Chiba, Japan | [7]Advanced Data Science Project (ADSP), RIKEN Information R&D and Strategy Headquarters, Kanagawa, Japan | [8]NEXT-Ganken Program, Japanese Foundation for Cancer Research (JFCR), Tokyo, Japan | [9]Institute for Advanced Academic Research (IAAR), Chiba University, Chiba, Japan

Correspondence: Tetsuya Saito (saito.rheu@tmd.ac.jp) | Shinsuke Yasuda (syasuda.rheu@tmd.ac.jp)

Received: 18 December 2025 | **Revised:** 10 April 2026 | **Accepted:** 27 April 2026

Keywords: fibroblast | GLI1 | GLI3 | hedgehog signaling pathway | rheumatoid arthritis

ABSTRACT

Objective: We investigated the role of GLI3, a transcription factor highly expressed in the pathogenic THY1$^+$CD34$^-$ sublining subset of rheumatoid arthritis synovial fibroblasts (RASFs), in regulating their pathogenic behavior.

Methods: GLI3 protein levels were quantified in freshly isolated RASF subsets by Western blotting. Bulk RASFs were subjected to siRNA-mediated knockdown (KD) of GLI3 or GLI1, followed by RNA sequencing. The effects of GANT61 on RASF proliferation, cell-cycle progression, migration, viability, and apoptosis were assessed using EdU/PI analysis, scratch assays, CCK-8 assays, and Annexin V/PI flow cytometry.

Results: GLI3 expression was enriched in THY1$^+$CD34$^-$ RASFs at both mRNA and protein levels. GLI3 KD increased GLI1 expression and upregulated genes involved in inflammation, matrix remodeling, and cell cycle regulation, including IL6, IL11, IL24, IL33, MMP3, PLAU, CCNA2, and E2F1. Pathway enrichment analysis revealed activation of ECM–receptor interaction, PI3K–Akt, and TNF signaling. Co-silencing GLI1 with GLI3 blunted the induction of IL11, IL24, IL33, CCNA2, E2F1, and PLAU observed with GLI3 KD alone, indicating that GLI1 mediates a subset of the transcriptional effects induced by GLI3 loss. GANT61 suppressed CCNA2 and E2F1 expression, inhibited RASF proliferation and migration, and did not markedly increase apoptosis.

Conclusion: GLI3 functions as a negative regulator of GLI1 and its downstream targets that drive the pathogenic behavior of RASFs. Targeting the GLI1–GLI3 axis may represent a promising therapeutic strategy to modulate fibroblast-driven inflammation and joint destruction in RA.

Abbreviations: b/tsDMARDs, biologic or targeted synthetic disease-modifying antirheumatic drugs; D2T RA, difficult-to-treat rheumatoid arthritis; DEGs, differentially expressed genes; GLI3-FL, full-length GLI3; GLI3-R, repressor form of GLI3; HH, Hedgehog; KD, knockdown; qPCR, quantitative polymerase chain reaction; RA, rheumatoid arthritis; RASF, rheumatoid arthritis synovial fibroblast; RNA-seq, RNA sequencing; siRNA, small interfering RNA; TNF-α, tumor necrosis factor alpha.

1 | Introduction

Rheumatoid arthritis (RA) is a chronic autoimmune disorder characterized by persistent synovial inflammation, in which pathological interactions between immune and stromal cells—particularly synovial fibroblasts (SFs)—drive progressive joint destruction, including cartilage degradation and bone erosion [1, 2]. The advent of targeted therapies, such as inhibitors of pro-inflammatory cytokines (e.g., TNF-α and IL-6) and small-molecule inhibitors of the JAK–STAT signaling pathway, has markedly improved disease outcomes for many patients. However, a subset of individuals—estimated to be up to 20%—experience inadequate therapeutic responses or drug intolerance despite treatment with multiple classes of biologic or targeted synthetic disease-modifying antirheumatic drugs (b/tsDMARDs), a condition now classified as difficult-to-treat RA (D2T RA) [3–5]. The molecular basis underlying this treatment resistance remains poorly understood, underscoring the urgent need for alternative therapeutic strategies.

Recent advances in transcriptomic profiling, including single-cell RNA sequencing, have revealed substantial inter-patient variability in the cellular composition of the inflamed synovium, which may significantly influence treatment responses. Notably, the R4RA trial—the first precision medicine trial in RA guided by synovial biopsy transcriptomics—unexpectedly highlighted the contribution of synovial fibroblast subsets to therapeutic resistance [6]. Specifically, synovial tissues enriched with fibroblast-associated gene expression signatures were found to respond poorly to conventional immunosuppressive therapies, including IL-6 receptor blockade and B cell–targeted therapies. These findings suggest that strategies directly targeting SF activity may complement current immunomodulatory approaches. Pathogenic rheumatoid arthritis synovial fibroblasts (RASFs) exhibit tumor-like properties, such as unchecked proliferation, enhanced migratory and invasive potential, angiogenic support, and the secretion of inflammatory mediators that perpetuate chronic synovitis and joint destruction. Despite their pivotal role in RA pathogenesis, no approved therapies to date specifically target SFs, emphasizing the need to elucidate the molecular pathways governing their pathogenic behavior [7, 8].

To identify transcription factors (TFs) that drive the pathological features of SF subsets—including excessive proliferation, invasion, angiogenesis, and cytokine production—we previously performed microarray-based transcriptomic profiling of the three major RASF subsets: $THY1^{-}CD34^{-}$ lining cells, $THY1^{+}CD34^{-}$ sublining cells, and $THY1^{+}CD34^{+}$ sublining cells [9–13]. These subsets are anatomically and functionally distinct, with $THY1^{-}CD34^{-}$ lining RASFs enriched for tissue-destructive programs, $THY1^{+}CD34^{-}$ sublining RASFs showing prominent inflammatory and immune-interacting features, and $THY1^{+}CD34^{+}$ sublining RASFs exhibiting a comparatively less inflammatory, stromal-supportive phenotype [9–13]. More recent single-cell and spatial studies suggest that these major subsets are further diversified by inflammation-associated states, including HLA-DRA^{high} RASFs with inflammatory and antigen-presentation-related features, $ITGA5^{+}$ RASFs linked to proinflammatory niche formation, and $COMP^{hi}$ fibrogenic RASFs associated with treatment resistance [14–16]. Against this evolving framework, GLI3 emerged as one of the most highly expressed transcription factors in the $THY1^{+}CD34^{-}$ sublining subset, which is consistently associated with aggressive fibroblast phenotypes.

The Hedgehog (HH)–GLI signaling pathway is an evolutionarily conserved regulatory cascade that orchestrates embryonic development, tissue patterning, and cellular proliferation, differentiation, and oncogenesis [17]. In mammals, the three GLI transcription factors—GLI1, GLI2, and GLI3—mediate the transcriptional outputs of HH signaling. GLI1 primarily acts as a transcriptional activator, whereas GLI2 and GLI3 may function as either full-length activators (FL) or as truncated repressors (R), depending on their post-translational processing. In the absence of HH ligands, GLI3 is phosphorylated and partially degraded to yield GLI3-R, which acts as a repressor by competitively binding to GLI target sequences and antagonizing GLI1 activity. Upon HH ligand stimulation, this repression is relieved through the degradation of GLI3-R and/or the stabilization of GLI3-FL, thereby enabling transcriptional activation of HH target genes [17, 18] (Figure 1A).

While previous studies have demonstrated upregulated expression of HH pathway components—particularly GLI1—in RA synovial tissue [19–24], the role of GLI3 in RASFs remains largely unexplored. Intriguingly, recent studies in cancer have revealed that GLI3 can regulate cellular proliferation and invasion through non-canonical, HH-independent pathways, suggesting that its effects are context-dependent [25]. In the present study, we aimed to elucidate the functional role of GLI3, the most highly expressed TF in the aggressive $THY1^{+}CD34^{-}$ sublining RASF subsets. Our findings uncover a reciprocal GLI3–GLI1 regulatory axis and suggest that targeting this pathway may represent a promising strategy to suppress fibroblast-driven inflammation and joint damage in RA.

2 | Materials and Methods

2.1 | Patient Recruitment

This study was conducted in accordance with the Declaration of Helsinki and approved by the Medical Research Ethics Committee of the Institute of Science Tokyo (M2000-979); synovial tissue was obtained from RA patients undergoing arthroplasty after written informed consent [13].

2.2 | Synovial Cell Isolation and Culture

After mincing, synovial tissues were enzymatically digested in DMEM at 37°C using 2 mg/mL collagenase type IV (Worthington, NJ, USA), 0.8 mg/mL dispase II, and 0.1 mg/mL DNase I (Roche, Basel, Switzerland) with gentle agitation. The supernatant was collected every 15 min and replaced with fresh enzyme solution four times. After ACK lysis, cells were processed along two predefined routes:

Subset-sorted SFs (ex vivo) for Western blotting and microarray: Live $CD45^{-}CD235a^{-}CD31^{-}PDPN^{+}$ cells were sorted into $THY1^{-}CD34^{-}$, $THY1^{+}CD34^{-}$, and $THY1^{+}CD34^{+}$ subsets

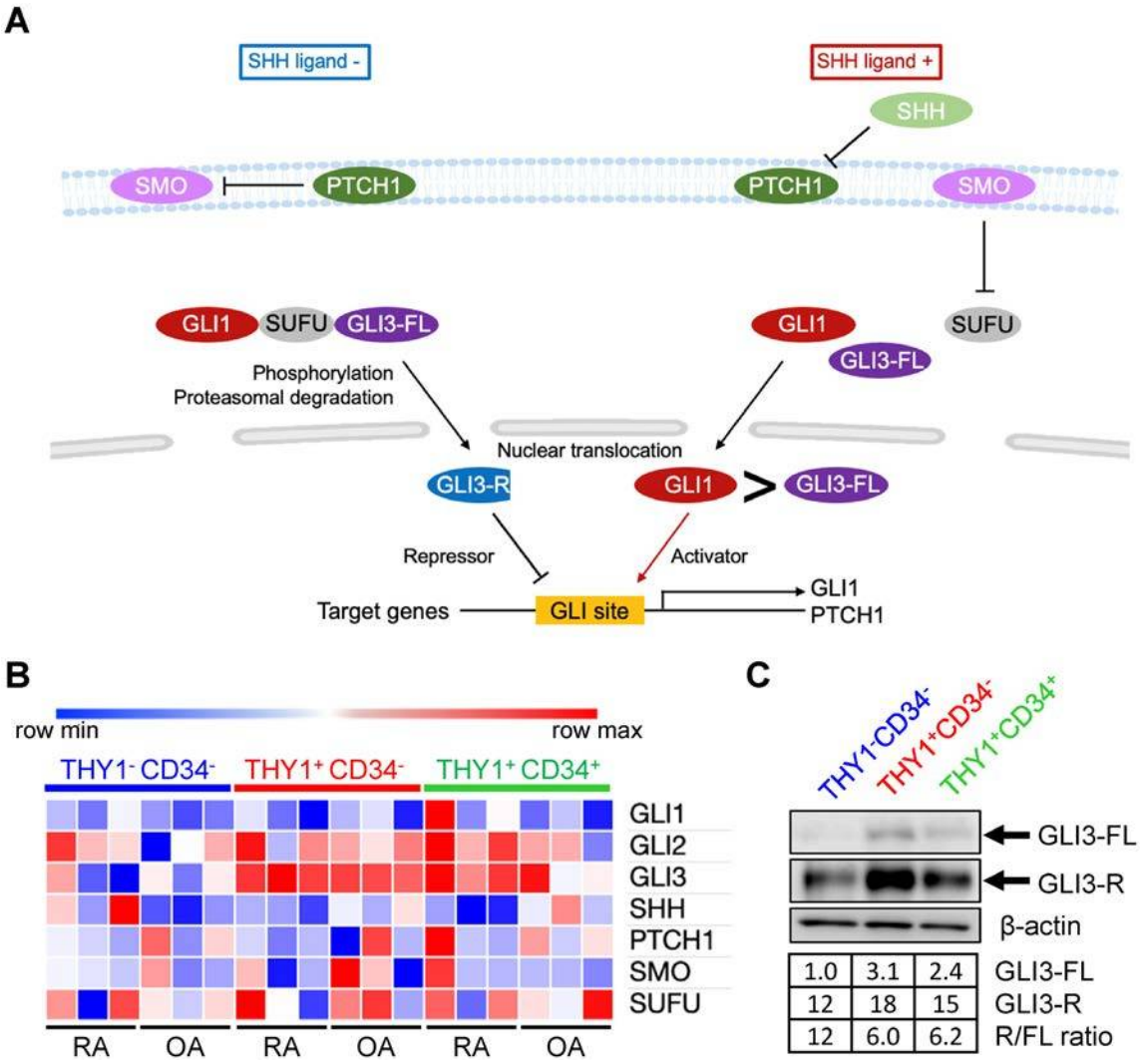

FIGURE 1 | Expression of GLI3 protein in RASF subsets. (A) Schematic diagram of the Hedgehog–GLI signaling pathway. Canonical SHH–PTCH1 signaling promotes the nuclear translocation of the transcriptional activators GLI1, GLI2, and full-length GLI3 (GLI3-FL). In contrast, in the absence of ligand, GLI3-FL undergoes proteolytic processing into the truncated repressor form GLI3-R, thereby maintaining a balance between activation and repression within the HH–GLI pathway. (B) Heat map showing the expression of HH/GLI-related components in three RASF subsets. Microarray data from $THY1^{-}CD34^{-}$, $THY1^{+}CD34^{-}$, and $THY1^{+}CD34^{+}$ subsets derived from three RA and three OA patients were previously published [9, 13]. Among the components, only GLI3 was significantly upregulated in the $THY1^{+}CD34^{-}$ subset ($\log_2 FC > 0.5$, $p < 0.05$, FDR < 0.01). (C) Western blotting analysis of GLI3 in freshly isolated RASF subsets. Full-length GLI3 (GLI3-FL, 190 kDa) and repressor GLI3 (GLI3-R, 83 kDa) are indicated by arrows. β-Actin was used as a loading control. Band intensities were quantified using ImageJ, normalized to β-Actin, and expressed as fold changes relative to the $THY1^{-}CD34^{-}$ subset, whose GLI3-FL level was set to 1.0.

using FACSAria III (BD Biosciences, CA, USA) as previously described [9, 12, 13], and the gating strategy of SF subsets was shown in Figure S1. These cells were used without in vitro passaging for Western blotting. Microarray data from our previous work [9, 13] were reanalyzed for the expression of HH-GLI pathway component genes.

Bulk RASFs (cultured) for RNA-seq and functional assays: Cell suspensions were plated in DMEM supplemented with 10% FBS and penicillin/streptomycin and passaged weekly to avoid overconfluence. Cells at passages 6–10 were used for RNA-seq and functional assays, including scratch migration, EdU incorporation, and cell cycle analysis, Annexin V/PI apoptosis assays, and cell viability assays.

2.3 | Antibodies and Reagents

The following reagents and antibodies were used for the analysis of synovial cells with flow cytometry, cell sorting, and several in vitro assays: anti-CD45-APC-H7 (2D1, BD Biosciences, CA, USA), anti-CD235a-APC-Alexa Fluor750 (11E4B-7-6, Beckman Coulter, FL, USA), anti-CD31-PE-Cyanine7 (WM-59, eBioscience, CA, USA), anti-CD146-APC (P1H12, eBioscience), anti-CD34-PE (4H11, eBioscience), anti-PDPN-PerCP-eFluor710 (NZ-1.3, eBioscience), anti-THY1-FITC (5E10, BD Biosciences), anti-CD73-PE-CF594 (AD2, BD Biosciences), anti-CD271-APC (ME20.4, eBioscience), anti-CD54-PE-CF594 (HA58, BioLegend, CA, USA), anti-CD44-APC (G44-26, BD Biosciences), anti-CD29-APC (TS2/16,

BioLegend), human TruStain FcX (BioLegend), Live/Dead fixable aqua dead cell stain kits (Molecular Probes, Thermo Fisher Scientific, MA, USA), anti-GLI3 (AF3690, R&D Systems, Minneapolis, MN, USA), anti-β-actin (AC-15, Sigma-Aldrich, St. Louis, MO, USA), horseradish peroxidase (HRP)-conjugated mouse IgG and HRP-conjugated rabbit IgG (7074 and 7076, Cell Signaling Technology, Danvers, MA, USA), and the GLI1 inhibitor GANT61 (HY-13901, MedChemExpress, Monmouth Junction, NJ, USA).

2.4 | Gene Knockdown by siRNA

Bulk RASFs were seeded onto plates and transfected with siRNA using Lipofectamine RNAiMAX (Thermo Fisher Scientific, Waltham, MA, USA) according to the manufacturer's instructions. After 72 h, the transfected cells were stimulated with 10 ng/mL TNF-α for 24 h. The siRNAs used were siGLI1 (Thermo Fisher Scientific, Silencer Select: s5815), siGLI3 (Thermo Fisher Scientific, Silencer Select: s5822), and siCtrl (Thermo Fisher Scientific, Silencer Select Negative Control siRNA No. 2). The siRNA knockdown efficiencies are shown in Figure S2.

2.5 | RNA-Sequencing Analysis

Poly(A)$^+$ RNA was extracted from siGLI3-, siGLI1- and siCtrl-transfected bulk RASF derived from three independent RA donors ($n = 3$ biological replicates per group) using the RNeasy Mini Kit (Qiagen, Hilden, Germany). Strand-specific mRNA libraries were prepared with the BGI Optimal Dual-mode mRNA Library Prep Kit according to the manufacturer's protocol. In brief, poly(A)$^+$ RNA was captured with oligo(dT) beads, fragmented, converted to cDNA, and second-strand synthesis incorporated dUTP to preserve strandedness. After end repair, A-tailing, adaptor ligation, PCR amplification, and quality control with an Agilent 2100 Bioanalyzer, double-stranded libraries were circularized, amplified by Φ29 rolling-circle replication to generate DNA nanoballs (~300 copies each), and sequenced as paired-end 100-bp reads on a DNBSEQ-G400 platform (BGI, Hong Kong). Raw reads were filtered with SOAPnuke v2.2.1 to remove adaptors and low-quality or ambiguous bases, and clean reads were aligned to the GRCh38.p12 human reference genome using Bowtie2 v2.4.5, and gene-level read counts and expression values (TPM, FPKM) were obtained with RSEM v1.3.1. For differential expression analysis, the gene-by-sample read-count matrix from RSEM was imported into DESeq2 v1.34.0, and genes with a false discovery rate (FDR) ≤ 0.05 were considered significantly differentially expressed. TPM and FPKM values were used only for descriptive purposes (e.g., visualization). The full read-count matrix used as DESeq2 input is provided in Table S1. Volcano plots were generated using GraphPad Prism 10. Functional enrichment of differentially expressed genes (DEGs) for Gene Ontology (GO) and KEGG categories was assessed using the hypergeometric test (R function phyper), and Benjamini–Hochberg–adjusted Q-values ≤ 0.05 were considered significant. RNA-seq data is provided in Table S1.

2.6 | Real-Time Quantitative Polymerase Chain Reaction

RNA was extracted from bulk RASFs using the RNeasy Mini Kit (Qiagen, Hilden, Germany), and complementary DNA (cDNA) was synthesized using the QuantiTect Reverse Transcription Kit (Qiagen). Quantitative polymerase chain reaction (qPCR) was performed on a LightCycler 96 (Roche) using SYBR Green PCR Master Mix (Qiagen). Primer sequences for all genes analyzed are listed in Table S2.

2.7 | Western Blotting

Freshly isolated RASF subsets were lysed in 2% SDS sample buffer containing complete mini protease inhibitor (Roche) and phosphatase inhibitor cocktail (Sigma-Aldrich). Cell lysates were boiled with 5% 2-mercaptoethanol at 95°C for 5 min and subjected to SDS-PAGE. The PVDF membrane was blocked with 5% bovine serum albumin in TBS-T for 1 h at room temperature, incubated overnight at 4°C with primary antibodies (GLI3: 1:1000, β-actin: 1:5000) in Can Get Signal Solution 1 (NKB-301, TOYOBO, Osaka, Japan), and then incubated with HRP-conjugated secondary antibody (1:5000) in Can Get Signal Solution 2 (NKB-301, TOYOBO). Signals were detected using ECL Prime Western blotting Detection Reagent (Amersham Biosciences, GE Healthcare, Little Chalfont, UK) and ImageQuant LAS-4000 (FUJIFILM Life Science, Tokyo, Japan). Band intensities of GLI3-FL and GLI3-R were quantified using ImageJ (NIH, Bethesda, MD, USA) following a standard protocol. Mean gray values were background-corrected, normalized to β-actin in the same lane, and expressed as fold changes relative to the THY1$^-$CD34$^-$ subset, whose GLI3-FL level was set to 1.0.

2.8 | Scratch Assay

To assess cell migration ability, bulk RASFs (1.0×10^5 cells/mL) were plated in 1 mL DMEM in a 12-well plate. After overnight incubation in 5% CO_2 at 37°C, a sterile 1000 μL pipette tip was used to create a scratch in the cell monolayer. The cells were washed with PBS to remove debris, and fresh DMEM was added. Two days before harvest, the cells were pretreated with 0, 5, or 10 μM GANT61, followed by stimulation with 0 or 10 ng/mL TNF-α for 24 h. Images were captured using BZ-9000 All-in-One Fluorescence Microscope (KEYENCE, Osaka, Japan), and the closure rate was analyzed using ImageJ (NIH, Bethesda, MD, USA).

2.9 | EdU Incorporation and Cell Cycle Analysis

To evaluate DNA synthesis and cell cycle distribution, bulk RASFs were cultured under the same conditions and treatment schedule as described for the scratch assay. 20 μM EdU was added together with TNF-α for the final 24 h. Cells were then harvested and stained using the Click-iT Plus EdU Alexa Fluor 647 Flow Cytometry Assay Kit (C10634, Invitrogen, Carlsbad, CA, USA)

and FxCycle PI/RNase Staining Solution (F10797, Invitrogen, Carlsbad, CA, USA). Flow cytometric data were acquired using FACSLyric (BD Biosciences, CA, USA) and analyzed to determine EdU incorporation and cell cycle distribution (G0/G1, S, and G2/M phases) based on EdU incorporation and DNA content. Relative EdU incorporation was calculated by normalizing to the untreated control and used for figure presentation.

2.10 | Annexin V/PI Apoptosis Assay

To assess apoptosis, bulk RASFs were cultured under the same conditions and treatment schedule as described for the scratch assay, and apoptosis was evaluated in TNF-α-stimulated cells with or without GANT61. Untreated cells served as a negative control, and cells treated with 10 μg/mL actinomycin D plus 10 ng/mL TNF-α for 24 h served as a positive control. Cells were then harvested and stained using the Dead Cell Apoptosis Kit with Annexin V Alexa Fluor 488 and Propidium Iodide (PI) (Thermo Fisher Scientific, Waltham, MA, USA). Flow cytometric data were acquired using FACSLyric and analyzed to determine the proportions of viable, apoptotic, and necrotic cells.

2.11 | Cell Viability Assay

To evaluate cell viability, bulk RASFs were cultured under the same treatment schedule as described for the scratch assay, except that cells were seeded in 96-well plates. Cell viability was assessed using the Cell Counting Kit-8 (Dojindo Molecular Technologies, Rockville, MD, USA). Relative viability was calculated by normalizing to the untreated control and used for figure presentation.

2.12 | Statistical Analysis

Data in bar graphs are presented as mean ± standard deviation (SD). For comparisons between two matched groups, paired *t*-tests were used. For comparisons among three or more matched groups, one-way ANOVA followed by Bonferroni's multiple-comparison test was performed. A $p < 0.05$ was considered statistically significant. Statistical analyses were performed using Prism 10 (GraphPad Software).

3 | Results

3.1 | GLI3 Is Preferentially Expressed in the THY1$^+$CD34$^-$ RASF Subset

We previously compared the mRNA expression levels of TFs across three major SF subsets obtained from 3 RA and 3 osteoarthritis (OA) patients—THY1$^-$CD34$^-$, THY1$^+$CD34$^-$, and THY1$^+$CD34$^+$—to identify regulators involved in IL-6 production [13]. Among 65 differentially expressed TFs, GLI3 was significantly upregulated in the THY1$^+$CD34$^-$ sublining subset, which is associated with aggressive pathogenic behavior (Figure 1B). GLI3 is a transcription factor functioning downstream of the Hedgehog (HH)–GLI signaling pathway and can act either as a full-length activator (GLI3-FL) or as a truncated repressor (GLI3-R), depending on the presence of HH ligands (Figure 1A) [17]. Consistent with these findings, re-analysis of a publicly available single-cell RNA-seq dataset of RA synovial tissue [11] showed that GLI3 expression was preferentially enriched in the THY1$^+$ sublining RASF subsets from patients with clinically active RA, whereas those in sustained remission exhibited lower GLI3 expression (Figure S3).

Interestingly, in our microarray dataset, other HH–GLI pathway components—including SHH, SMO, SUFU, PTCH1, and other GLI family members (GLI1, GLI2)—showed no statistically significant differences in expression among the SF subsets (Figure 1B). This suggests that the upregulation of GLI3 in the THY1$^+$CD34$^-$ subset may occur largely independently of canonical HH pathway activation.

We further evaluated GLI3 protein expression in freshly isolated RASF subsets from RA synovial tissue (Figure 1C and Figure S6). Because GLI3-R (83 kDa) is generated by post-translational, PKA/GSK3β-dependent proteolysis of GLI3-FL (190 kDa), its abundance cannot be inferred from transcriptomic analysis. We therefore assessed the expression of GLI3-FL and GLI3-R by Western blotting with an antibody recognizing the common N-terminal domain of both forms. Both GLI3-FL and GLI3-R were more abundantly expressed in the THY1$^+$CD34$^-$ subset compared to the THY1$^-$CD34$^-$ and THY1$^+$CD34$^+$ subsets. Notably, GLI3-R was the predominant detectable form in all subsets, while both GLI3-FL and GLI3-R were most abundant in the THY1$^+$CD34$^-$ subset. These results indicate that both GLI3-FL and GLI3-R were highly expressed in the pathogenic THY1$^+$CD34$^-$ subset.

3.2 | GLI3 Represses Pro-Inflammatory and Proliferative Gene Programs in RASFs

To investigate the functional role of GLI3 in RASFs treated with TNF-α, we performed siRNA-mediated knockdown (KD) of GLI3 followed by RNA-seq analysis. Among the genes upregulated upon GLI3 KD, GLI1, a canonical target and effector of the HH–GLI pathway, exhibited one of the largest fold changes (Figure 2A). In addition, genes associated with the pathogenic behavior of RASFs—including IL6, IL11, IL24, IL33, CCNA2, E2F1, MMP3, and PLAU—were also significantly upregulated in GLI3-deficient cells (Figure 2A).

KEGG pathway enrichment analysis of the upregulated gene set revealed significant enrichment in pathways involved in ECM–receptor interaction, PI3K–Akt signaling, focal adhesion, TNF signaling, and cytokine–cytokine receptor interaction (Figure 2B).

qPCR analysis in an independent set of samples confirmed the same directional changes in selected DEGs identified by RNA-seq (Figure 2C). These results suggest that GLI3 functions primarily as a transcriptional repressor in RASFs, suppressing

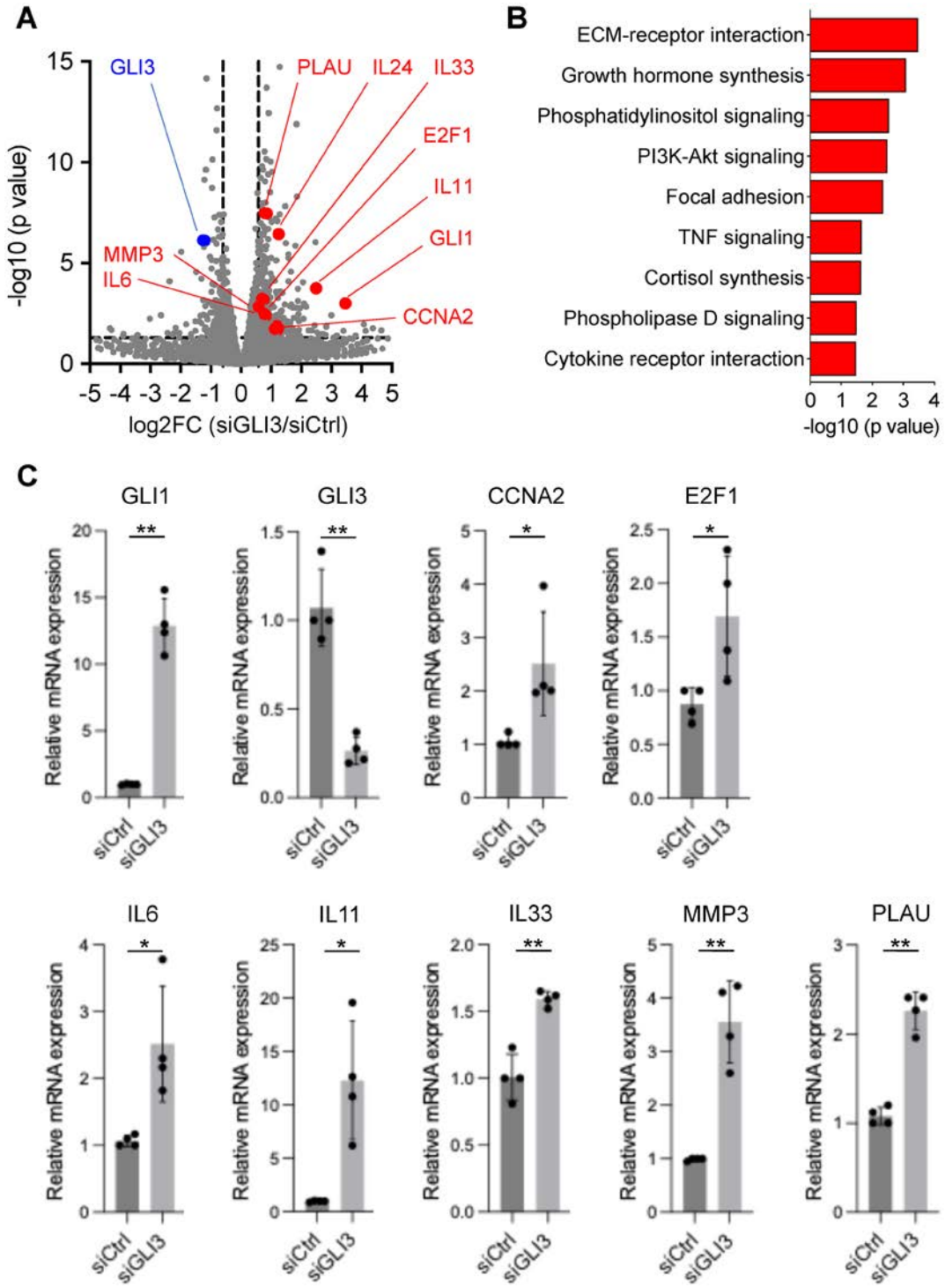

FIGURE 2 | Identification of GLI3 target genes by RNA-seq in RASFs. (A) Volcano plot showing differentially expressed genes between siCtrl- and siGLI3-transfected RASFs ($\log_2$FC > 0.5, FDR < 0.05). Bulk RASFs derived from three independent RA donors were transfected with siCtrl or siGLI3, followed by stimulation with 10 ng/mL TNF-α for 24 h after 72 h of transfection. Total RNA was subjected to bulk RNA-seq, and differential expression was assessed using DESeq2 v1.34.0 on the RSEM-derived read-count matrix ($n = 3$). (B) KEGG pathway enrichment analysis of genes up-regulated by siGLI3 (DESeq2, siGLI3 vs. siCtrl). The top nine significantly enriched pathways (Benjamini–Hochberg–adjusted $Q < 0.05$) are shown. (C) qPCR validation of selected differentially expressed genes identified by RNA-seq in an independent set of bulk RASF samples ($n = 4$ biological replicates). Gene expression levels were normalized to the internal control and are presented relative to the siCtrl group. Data represent mean ± SD. *$p < 0.05$, **$p < 0.01$ by paired t-test.

genes associated with inflammatory, proliferative, and migratory behavior.

3.3 | GLI1 Mediates a Subset of Gene Induction Following GLI3 Knockdown

Given the strong upregulation of GLI1 and multiple pathogenic genes upon GLI3 KD, we hypothesized that GLI1 may mediate the transcriptional effects induced by GLI3 loss. To test this, we performed RNA-seq following siRNA knockdown of GLI1 alone, and dual knockdown of GLI3 and GLI1. Knockdown of GLI1 alone had minimal impact on gene expression, likely due to its low basal expression in RASFs (Figure 3). In contrast, the co-silencing of GLI1 with GLI3 significantly attenuated the induction of IL11, IL24, IL33, CCNA2, E2F1, and PLAU observed with GLI3 KD alone (Figure 3), suggesting that these genes are positively regulated by GLI1. In contrast, the expression of IL6 and MMP3, while elevated upon GLI3 KD, remained unaffected by the additional knockdown of GLI1, indicating a GLI1-independent regulatory mechanism.

These findings indicate that GLI1 acts as a transcriptional activator for a subset of GLI3-repressed genes, and that the GLI3–GLI1 axis plays a selective role in the regulation of inflammatory and proliferative genes in RASFs.

3.4 | Pharmacological Inhibition of GLI1 Suppresses RASF Proliferation and Migration

The observation that GLI1 KD showed a modest suppressive effect on CCNA2, E2F1, and PLAU—genes involved in cell proliferation and migration—suggested a role for GLI1 in promoting the aggressive phenotype of RASFs. To evaluate whether pharmacological inhibition of GLI activity could reproduce these effects, we treated RASFs with GANT61, a small-molecule inhibitor of GLI1 transcriptional activity [26]. Scratch assays showed that GANT61 significantly impaired RASF migration (Figure 4A). Consistently, EdU/PI cell-cycle analysis demonstrated a dose-dependent reduction in EdU incorporation and in the S-phase fraction, indicating suppressed proliferative activity (Figure 4B and Figure S4). At 5 μM, GANT61 did not significantly reduce cell viability in CCK-8 assays (Figure 4C). In parallel, GANT61 decreased the expression of the cell-cycle–associated genes CCNA2 and E2F1 (Figure 4D). Moreover, Annexin V/PI analysis showed no significant increase in total apoptosis under these conditions (Figure 4E and Figure S5).

Taken together, these results suggest that GLI1—normally repressed by GLI3 in RASFs—contributes to the proliferative and migratory phenotype of RASFs, and that pharmacological GLI inhibition suppresses these pathogenic properties without marked apoptosis induction.

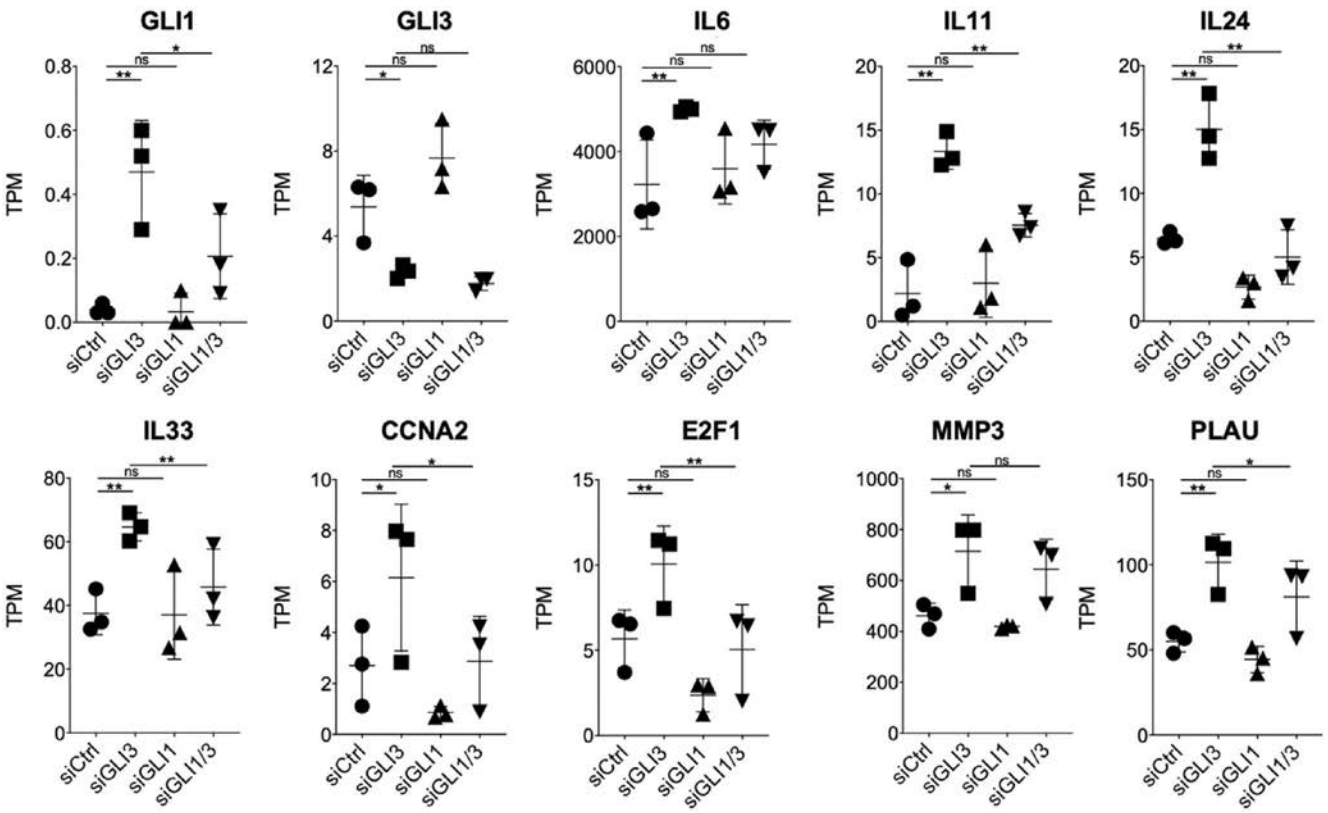

FIGURE 3 | Involvement of GLI1 in GLI3-mediated gene regulation in RASFs. Bulk RASFs derived from three independent RA donors were transfected with siCtrl, siGLI3, siGLI1, or a combination of siGLI3 and siGLI1, followed by stimulation with 10 ng/mL TNF-α for 24 h after 72 h of transfection. Total RNA was analyzed by bulk RNA-seq, and gene expression was quantified as TPM using RSEM v1.3.1. Bar graphs summarize RSEM-derived TPM values (mean ± SD; $n = 3$) for selected GLI3-mediated genes identified in the RNA-seq analysis. Statistical significance was determined by one-way ANOVA with Bonferroni's multiple comparison test. *$p < 0.05$, **$p < 0.01$; ns, not significant.

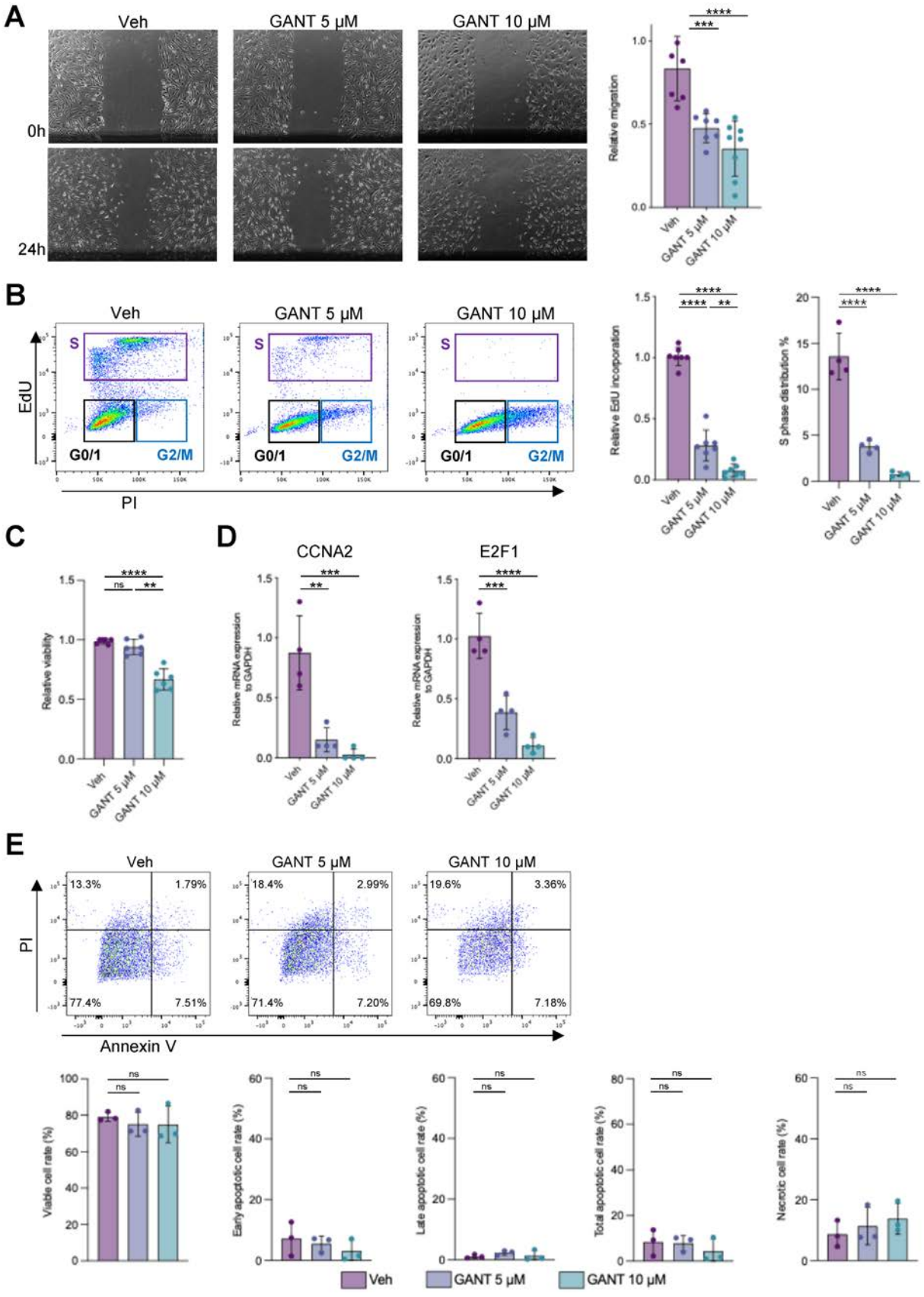

FIGURE 4 | Legend on next page.

FIGURE 4 | Suppression of RASF proliferation and migration by the GLI1 inhibitor GANT61. (A) Scratch assay of bulk RASFs treated with GANT61. Representative images and quantification of relative migration are shown ($n = 4$ biological replicates). (B) EdU incorporation and cell cycle analysis of bulk RASFs treated with GANT61. Representative plots and quantification of relative EdU incorporation and S-phase fraction are shown ($n = 4$ biological replicates). (C) Cell viability of bulk RASFs treated with GANT61, as assessed by CCK-8 assay ($n = 3$ biological replicates). (D) qPCR analysis of CCNA2 and E2F1 expression in bulk RASFs treated with GANT61 ($n = 4$ biological replicates). (E) Annexin V/PI apoptosis assay of bulk RASFs treated with GANT61. Representative plots and quantification of viable, early apoptotic, late apoptotic, total apoptotic, and necrotic cell fractions are shown ($n = 3$ biological replicates). Data are presented as mean ± SD. Statistical significance was assessed by one-way ANOVA followed by Bonferroni's multiple comparison test. *$p < 0.05$, **$p < 0.01$, ***$p < 0.001$, ****$p < 0.0001$.

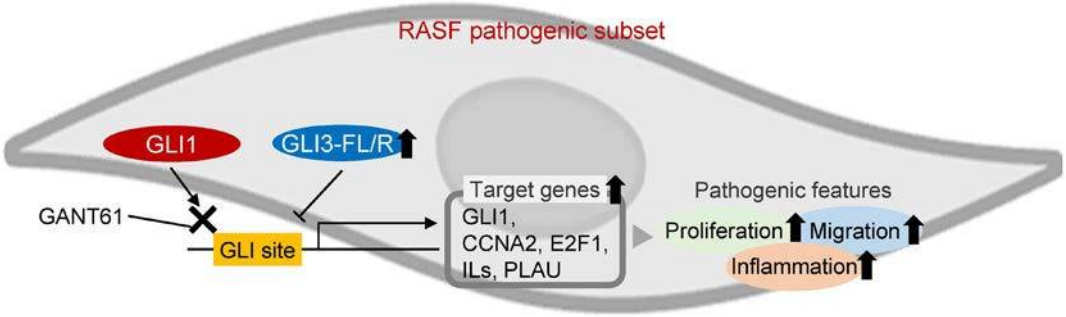

FIGURE 5 | Hypothetical model of the reciprocal regulation between GLI1 and GLI3 in pathogenic RASFs. In the pathogenic RASF subset, GLI3-FL/R is highly expressed and inhibits GLI1 activity via competitive binding to GLI sites, thereby suppressing the transcription of GLI1 target genes involved in proliferation, migration, and inflammation. GANT61 inhibits GLI1-DNA binding and may serve as a therapeutic agent targeting RASF-mediated pathology.

4 | Discussion

In this study, we identified a reciprocal regulatory relationship between GLI1 and GLI3 in the aggressive behaviors of RASFs. While previous studies have demonstrated that GLI1 promotes the inflammatory and invasive characteristics of RASFs, and that its inhibition ameliorates RA pathology in both in vitro and in vivo models [27–29], our findings identify GLI3—which is highly expressed in the pathogenic subset—as a negative regulator of GLI1 activity in RASFs. These results expand our understanding of GLI family transcriptional dynamics and suggest that dysregulated GLI1–GLI3 interactions may contribute to RASF pathogenicity, presenting a potential therapeutic target (Figure 5).

Among the transcription factors identified by microarray-based profiling across SF subsets, GLI3 was one of the few significantly upregulated in the THY1$^+$CD34$^-$ population, a subset particularly associated with inflammatory pathogenic features in RA. This interpretation should be integrated with the current view that the pathogenic sublining RASF subsets contain multiple functionally distinct states, including inflammatory, immune-interacting, and fibrogenic populations [14–16]. While GLI1 expression is well known to be induced by canonical HH/GLI signaling, the regulatory mechanisms governing GLI3 expression are far less understood. Recent studies have reported elevated GLI3 expression in various cancer cell types, driven by epigenetic mechanisms such as promoter methylation and post-transcriptional regulation by specific microRNAs [25]. Additionally, developmental studies have implicated Wnt/β-catenin/Tcf and Notch/RBPJ signaling pathways in the transcriptional activation of GLI3 during neural differentiation [30–32]. Given that both Wnt and Notch signaling are involved in the differentiation and activation of RASF subsets, it is plausible that these pathways contribute to the elevated GLI3 expression observed in the pathogenic THY1$^+$CD34$^-$ subset. Moreover, recent work in innate immune cells has shown that GLI3 can be induced by LPS via the TLR4–TRIF–IRF3 axis [33]. It remains possible that pro-inflammatory cytokines and growth factors involved in RASF activation contribute to GLI3 upregulation. These observations raise the possibility that elevated GLI3 expression in the pathogenic subset reflects a negative feedback mechanism aimed at restraining excessive GLI1-driven transcriptional activity. It is also possible that the GLI1–GLI3 axis is not uniform within the broader THY1$^+$CD34$^-$ RASF subset, which may encompass functionally distinct fibroblast states. Further subdivision of this subset may therefore help clarify whether GLI3-mediated regulation differs among pathogenic RASF subpopulations.

GLI3 can function either as a transcriptional activator (GLI3-FL) or repressor (GLI3-R), depending on the presence or absence of HH ligands. In the context of canonical HH signaling, its primary role is to repress HH target genes under basal conditions, and GLI3 is preferentially processed into the repressor form under ligand-poor conditions. Although this study did not directly determine the mechanism underlying the predominance of GLI3-R over GLI3-FL in the THY1$^+$CD34$^-$ subset, our results are compatible with a state in which canonical HH ligand input is limited. However, recent evidence from cancer research suggests that GLI3 may also exhibit oncogenic functions, promoting tumor cell proliferation and invasion [25]. For instance, in prostate cancer cells,

GLI3-R has been shown to promote proliferation through interaction with the androgen receptor [34]. According to our siRNA experiments in RASFs, GLI3 acted predominantly as a transcriptional repressor of GLI1 target genes, consistent with its canonical function. This suggests that the $THY1^{+}CD34^{-}$ subset may retain responsiveness to HH ligands. In addition to canonical HH signaling, several other pathways—including PKA, GSK3β, and Notch—have been shown to regulate GLI3 processing and shift the balance between its repressor and activator forms [25]. These non-canonical inputs may also contribute to fibroblast activation by modulating the GLI1–GLI3 axis. Although GLI2 expression did not differ significantly among SF subsets in our data, previous studies have shown that GLI2 mediates fibroblast activation and tissue fibrosis, particularly in response to TGF-β signaling, suggesting that GLI2 may modulate RASF behavior under specific inflammatory or fibrotic conditions.

Our data using GANT61, a selective GLI1 inhibitor, further support the critical role of GLI1 in regulating RASF proliferation and migration. In our in vitro system, GANT61 suppressed migration, EdU incorporation, S-phase entry, and the expression of CCNA2 and E2F1, without marked apoptosis induction. The lack of a significant viability decrease at 5 μM further suggests that these inhibitory effects were not merely due to nonspecific toxicity. GANT61 has been shown to reduce disease severity in collagen-induced arthritis (CIA) models by inhibiting cell proliferation and inducing apoptosis [35], partly consistent with our in vitro findings. Similarly, cyclopamine, a classical HH pathway inhibitor, has been reported to suppress SHH, PTCH1, SMO, and GLI1 expression, induce G1 cell cycle arrest, and inhibit RhoA/Rac1 signaling and cyclin D1 expression in RASFs [36, 37]. These effects contribute to impaired RASF migration and enhanced cartilage protection in antigen-induced arthritis (AIA) models [19]. Currently, a range of HH/GLI pathway inhibitors—including HH ligand blockers, PTCH and SMO antagonists, and GLI transcriptional inhibitors—are under investigation in oncology [38]. Our findings support the translational relevance of the GLI1–GLI3 regulatory axis in RA and provide a rationale for exploring GLI1-specific inhibition as a novel therapeutic approach targeting fibroblast-driven pathology.

This study has several limitations. First, the precise molecular mechanisms underlying GLI3 upregulation in specific RASF subsets remain incompletely defined. Second, due to interpatient heterogeneity in RA, the relatively small sample size may not fully capture the diversity of disease subtypes. Third, functional assays were performed using cultured bulk RASFs, which may obscure subset-specific effects and limit the extrapolation to in vivo contexts. Lastly, although our findings are consistent with non-canonical regulation of GLI3, we did not directly examine the effects of canonical Hedgehog (HH) ligand stimulation and therefore cannot fully exclude its potential involvement. It is also possible that GLI1 is upregulated in the pathogenic subset via HH signaling in certain RA cases. Future studies incorporating single-cell analyses and ligand-based perturbations will be necessary to further clarify the regulation and function of GLI3 in RA pathogenesis.

5 | Conclusion

We identified GLI3 as a negative regulator of GLI1 in RASFs. Dysregulated activity of GLI family transcription factors contributes to the overproduction of inflammatory mediators, as well as to the aberrant proliferation and migration of RASFs. These findings highlight the GLI1–GLI3 reciprocal regulatory axis as a novel pathogenic mechanism and a promising therapeutic target in RA.

Author Contributions

Motohiko Sato, Yoji Komiya, Fumitaka Mizoguchi, Tetsuya Saito, and Shinsuke Yasuda conceived the study aims and design. Motohiko Sato, Yoji Komiya, and Tetsuya Saito performed experiments. Motohiko Sato, Yoji Komiya, Seiji Noda, Yasuhiro Tagawa, Akio Yamamoto, and Hideyuki Iwai contributed to synovial specimen processing as part of the core research team. Kentaro Endo, Hideyuki Koga, Yasuhiro Takahara, Kazutaka Sugimoto, and Ichiro Sekiya served as site investigators responsible for clinical synovial specimen provision. Eiryo Kawakami conducted statistical analyses. Motohiko Sato, Tadashi Hosoya, Tetsuya Saito, and Shinsuke Yasuda analyzed and interpreted the data. Motohiko Sato, Tetsuya Saito, and Shinsuke Yasuda drafted the manuscript; all authors contributed to discussion, critically reviewed the manuscript for important intellectual content, and approved the final version. (All authors meet ICMJE authorship criteria).

Acknowledgments

We gratefully acknowledge the late Dr. Fumitaka Mizoguchi (d. 2020) for his contributions to the formulation of the study aims and design, and for his valuable discussions with the core research team.

Funding

This work was supported by the Japan Agency for Medical Research and Development (AMED) under grant number 21ek0410061h0003 and by the Japan Society for the Promotion of Science (JSPS) KAKENHI under grant numbers 21K20755 and 22K08519.

Disclosure

T.S. received research funding from Eli Lilly, speaking fees from Abbvie, Asahi Kasei Pharma, Chugai Pharmaceutical, Eisai, Eli Lilly, GlaxoSmithKline, Mitsubishi Tanabe Pharma, Ono Pharmaceutical, Taisho Pharmaceutical, and Astellas Pharma. S.Y. received research funding from Asahi Kasei Pharma, Ayumi Pharmaceutical Corporation, Chugai Pharmaceutical, Nippon Boehringer Ingelheim Co. Ltd., and Taisho Pharmaceutical Co. Ltd., speaking fees from Abbvie, Asahi Kasei Pharma, Chugai Pharmaceutical, Eisai, Eli Lilly, GlaxoSmithKline, Mitsubishi Tanabe Pharma, and Ono Pharmaceutical, and consultant fees from Eisai, ImmunoForge, Novartis, and Otsuka Pharmaceutical Co. Ltd.

Ethics Statement

Ethics approval and consent to participate. We have confirmed the ethics approval from the medical research ethics committee of Institute of Science Tokyo (approval number: M2000-979).

Consent

We have obtained written informed consent for publication from all the patients.

Conflicts of Interest

The authors declare no conflicts of interest.

Data Availability Statement

The microarray dataset analyzed in this study is publicly available in the Gene Expression Omnibus under accession number GSE109450. The bulk RNA-seq dataset generated in this study has been deposited in the Gene Expression Omnibus under accession number GSE329806. The gene-by-sample bulk RNA-seq read-count matrix generated in this study is provided in Table S1. Additional data supporting the findings of this study are available from the corresponding author upon reasonable request.

References

1. J. S. Smolen, D. Aletaha, A. Barton, et al., "Rheumatoid Arthritis," *Nature Reviews. Disease Primers* 4 (2018): 18001.

2. E. M. Gravallese and G. S. Firestein, "Rheumatoid Arthritis—Common Origins, Divergent Mechanisms," *New England Journal of Medicine* 388, no. 6 (2023): 529–542.

3. N. M. T. Roodenrijs, M. J. H. de Hair, M. C. van der Goes, et al., "Characteristics of Difficult-to-Treat Rheumatoid Arthritis: Results of an International Survey," *Annals of the Rheumatic Diseases* 77, no. 12 (2018): 1705–1709.

4. G. Nagy, N. M. T. Roodenrijs, P. M. Welsing, et al., "EULAR Definition of Difficult-To-Treat Rheumatoid Arthritis," *Annals of the Rheumatic Diseases* 80, no. 1 (2021): 31–35.

5. M. J. H. de Hair, J. W. G. Jacobs, J. M. van Laar, et al., "Difficult-To-Treat Rheumatoid Arthritis: An Area of Unmet Clinical Need," *Rheumatology (Oxford, England)* 57, no. 7 (2018): 1135–1144.

6. F. Rivellese, A. E. A. Surace, K. Goldmann, et al., "Rituximab Versus Tocilizumab in Rheumatoid Arthritis: Synovial Biopsy-Based Biomarker Analysis of the Phase 4 R4RA Randomized Trial," *Nature Medicine* 28, no. 6 (2022): 1256–1268.

7. S. Davidson, M. Coles, T. Thomas, et al., "Fibroblasts as Immune Regulators in Infection, Inflammation and Cancer," *Nature Reviews. Immunology* 21, no. 11 (2021): 704–717.

8. G. Nygaard and G. S. Firestein, "Restoring Synovial Homeostasis in Rheumatoid Arthritis by Targeting Fibroblast-Like Synoviocytes," *Nature Reviews Rheumatology* 16, no. 6 (2020): 316–333.

9. F. Mizoguchi, K. Slowikowski, K. Wei, et al., "Functionally Distinct Disease-Associated Fibroblast Subsets in Rheumatoid Arthritis," *Nature Communications* 9, no. 1 (2018): 789.

10. F. Zhang, K. Wei, K. Slowikowski, et al., "Defining Inflammatory Cell States in Rheumatoid Arthritis Joint Synovial Tissues by Integrating Single-Cell Transcriptomics and Mass Cytometry," *Nature Immunology* 20, no. 7 (2019): 928–942.

11. S. Alivernini, L. MacDonald, A. Elmesmari, et al., "Distinct Synovial Tissue Macrophage Subsets Regulate Inflammation and Remission in Rheumatoid Arthritis," *Nature Medicine* 26, no. 8 (2020): 1295–1306.

12. S. Noda, T. Hosoya, Y. Komiya, et al., "CD34 + THY1+ Synovial Fibroblast Subset in Arthritic Joints Has High Osteoblastic and Chondrogenic Potentials In Vitro," *Arthritis Research & Therapy* 24, no. 1 (2022): 45.

13. Y. Tagawa, T. Saito, H. Iwai, et al., "ARID5B Is a Negative Modulator of IL-6 Production in Rheumatoid Arthritis Synovial Fibroblasts," *Immunological Medicine* 47, no. 3 (2024): 176–185.

14. M. H. Smith, V. R. Gao, P. K. Periyakoil, et al., "Drivers of Heterogeneity in Synovial Fibroblasts in Rheumatoid Arthritis," *Nature Immunology* 24, no. 7 (2023): 1200–1210.

15. L. Zheng, M. Gu, X. Li, et al., "ITGA5+ Synovial Fibroblasts Orchestrate Proinflammatory Niche Formation by Remodelling the Local Immune Microenvironment in Rheumatoid Arthritis," *Annals of the Rheumatic Diseases* 84, no. 2 (2025): 232–252.

16. K. Bhamidipati, A. B. R. McIntyre, S. Kazerounian, et al., "Spatial Patterning of Fibroblast TGFβ Signaling Underlies Treatment Resistance in Rheumatoid Arthritis," *Nature Immunology* 27 (2026): 556–571.

17. J. Briscoe and P. P. Thérond, "The Mechanisms of Hedgehog Signalling and Its Roles in Development and Disease," *Nature Reviews Molecular Cell Biology* 14, no. 7 (2013): 416–429.

18. E. W. Humke, K. V. Dorn, R. Rohatgi, et al., "The Output of Hedgehog Signaling Is Controlled by the Dynamic Association Between Suppressor of Fused and the Gli Proteins," *Genes & Development* 24, no. 7 (2010): 670–682.

19. R. Li, L. Cai, J. Ding, X. Y. Hu, C. M. Hu, and T. N. Wu, "Inhibition of Hedgehog Signal Pathway by Cyclopamine Attenuates Inflammation and Articular Cartilage Damage in Rats With Adjuvant-Induced Arthritis," *Journal of Pharmacy and Pharmacology* 67, no. 7 (2015): 963–971.

20. S. L. Zhu, M. Q. Luo, W. X. Peng, et al., "Sonic Hedgehog Signalling Pathway Regulates Apoptosis Through Smo Protein in Human Umbilical Vein Endothelial Cells," *Rheumatology (Oxford, England)* 54, no. 6 (2015): 1093–1102.

21. S. Zhu, J. Dang, Y. Shi, et al., "Sonic Hedgehog Promotes Synovial Inflammation and Articular Damage Through p38 Mitogen-Activated Protein Kinase Signaling in Experimental Arthritis," *Journal of Autoimmunity* 132 (2022): 102902.

22. R. Li, L. Cai, J. Li, C. M. Hu, and T. N. Wu, "Expression of Hedgehog Signal Pathway in Articular Cartilage Is Associated With the Severity of Cartilage Damage in Rats With Adjuvant-Induced Arthritis," *Journal of Inflammation (London)* 12 (2015): 24.

23. Y. Su, H. Xing, L. Zhang, J. Kang, and L. Bai, "Role of the Hedgehog Signaling Pathway in Rheumatic Diseases: An Overview," *Frontiers in Immunology* 13 (2022): 940455.

24. Y. Li, M. Ming, C. Li, et al., "The Emerging Role of the Hedgehog Signaling Pathway in Immunity Response and Autoimmune Diseases," *Autoimmunity* 56, no. 1 (2023): 2259127.

25. S. J. Matissek and S. F. Elsawa, "GLI3: A Mediator of Genetic Diseases, Development and Cancer," *Cell Communication and Signaling: CCS* 18, no. 1 (2020): 54.

26. M. Lauth, A. Bergström, R. Toftgård, et al., "Inhibition of GLI-Mediated Transcription and Tumor Cell Growth by Small-Molecule Antagonists," *Proceedings of the National Academy of Sciences of the United States of America* 104, no. 20 (2007): 8455–8460.

27. S. Qin, D. Sun, H. Li, et al., "The Effect of SHH-Gli Signaling Pathway on the Synovial Fibroblast Proliferation in Rheumatoid Arthritis," *Inflammation* 39, no. 2 (2016): 503–512.

28. G. Ge, Q. Guo, Y. Zhou, et al., "GLI1 Facilitates Collagen-Induced Arthritis in Mice by Collaborative Regulation of DNA Methyltransferases," *eLife* 12 (2023): e92142.

29. M. Wang, S. Zhu, W. Peng, et al., "Sonic Hedgehog Signaling Drives Proliferation of Synoviocytes in Rheumatoid Arthritis: A Possible Novel Therapeutic Target," *Journal of Immunology Research* 2014 (2014): 401903.

30. R. Alvarez-Medina, J. Cayuso, E. Martí, et al., "Wnt Canonical Pathway Restricts Graded Shh/Gli Patterning Activity Through the Regulation of Gli3 Expression," *Development* 135, no. 2 (2008): 237–247.

31. K. Hasenpusch-Theil, D. Magnani, T. Theil, E. M. Amaniti, L. Han, and D. Armstrong, "Transcriptional Analysis of Gli3 Mutants Identifies

Wnt Target Genes in the Developing Hippocampus," *Cerebral Cortex* 22, no. 12 (2012): 2878–2893.

32. Y. Li, M. A. Hibbs, K. Yun, A. L. Gard, and N. A. Shylo, "Genome-Wide Analysis of N1ICD/RBPJ Targets In Vivo Reveals Direct Transcriptional Regulation of Wnt, SHH, and Hippo Pathway Effectors by Notch1," *Stem Cells* 30, no. 4 (2012): 741–752.

33. S. J. Matissek, M. Karbalivand, W. Han, et al., "A Novel Mechanism of Regulation of the Oncogenic Transcription Factor GLI3 by Toll-Like Receptor Signaling," *Oncotarget* 13 (2022): 944–959.

34. J. B. Kaushal, P. Raut, S. Halder, et al., "Oncogenic Potential of Truncated-Gli3 via the Gsk3β/Gli3/AR-V7 Axis in Castration-Resistant Prostate Cancer," *Oncogene* 44, no. 15 (2025): 1007–1023.

35. S. Qin, D. Sun, X. Li, et al., "GANT61 Alleviates Arthritic Symptoms by Targeting Fibroblast-Like Synoviocytes in CIA Rats," *Journal of Orthopaedic Science* 24, no. 2 (2019): 353–360.

36. S. L. Zhu, J. L. Huang, W. X. Peng, et al., "Inhibition of Smoothened Decreases Proliferation of Synoviocytes in Rheumatoid Arthritis," *Cellular & Molecular Immunology* 14, no. 2 (2017): 214–222.

37. Z. Hu, Y. Chen, J. Huang, S. Zhu, X. Feng, and B. Zhang, "Sonic Hedgehog Promotes Proliferation and Migration of Fibroblast-Like Synoviocytes in Rheumatoid Arthritis via Rho/ROCK Signaling," *Journal of Immunology Research* 2022 (2022): 3423692.

38. X. Wang, T. Wang, X. Song, et al., "Current Status of Hedgehog Signaling Inhibitors," *Current Topics in Medicinal Chemistry* 24, no. 3 (2024): 243–258.

Supporting Information

Additional supporting information can be found online in the Supporting Information section. **Figure S1:** The gating strategy of RASF subsets. **Figure S2:** siRNA knockdown efficiencies. **Figure S3:** scRNA-seq Heatmap. **Figure S4:** Full cell-cycle distribution of bulk RASFs treated with GANT61 and TNF-α. **Figure S5:** Negative and positive control results for Annexin V/PI apoptosis analysis in bulk RASFs. **Figure S6:** Uncropped Western blot images for GLI3 detection in freshly isolated RASF subsets. **Table S1:** Gene-by-sample RNA-seq read-count matrix of bulk RASFs used for differential expression analyses in Figures 2 and 3. **Table S2:** qPCR primer sequences.

International Journal of Rheumatic Diseases

WILEY

International Journal of Rheumatic Diseases

ORIGINAL ARTICLE

Efficacy and Safety of Secukinumab in Enthesitis-Related Arthritis: A Retrospective Study in China

Xinwei Shi | Junmei Zhang | Fengqiao Gao | Weiying Kuang | Jianghong Deng | Xiaohua Tan | Chao Li | Shipeng Li | Jing Gao | Xuanyi Liu | Baixu Sun | Caifeng Li

Department of Rheumatology, Beijing Children's Hospital, Capital Medical University, National Center for Children's Health, Beijing, China

Correspondence: Caifeng Li (caifeng_li@yeah.net)

Received: 5 March 2026 | **Revised:** 20 May 2026 | **Accepted:** 24 May 2026

Keywords: biological therapy | enthesitis-related arthritis | IL-17 inhibitor | prognosis | secukinumab

ABSTRACT

Objectives: Enthesitis-related arthritis (ERA) is a form of chronic inflammatory arthritis. Even when administered with a combination of non-steroidal anti-inflammatory drugs (NSAIDs), disease-modifying anti-rheumatic drugs (DMARDs), and biologics, some patients remain in an active disease state. Antecedent studies have revealed that interleukin-17 (IL-17) plays an important role in the pathogenesis of ERA and have demonstrated the efficacy of IL-17 inhibitors. This real-world, retrospective study aimed to assess the efficacy and safety of secukinumab in patients with ERA.

Methods: This was a retrospective, single-center cohort study of 31 Chinese patients who had been diagnosed with ERA and treated with secukinumab for at least 3 months. The primary outcomes were the proportion of patients achieving JIA ACR 30/50/70/90/100 response criteria and ACR inactive disease, as well as the change in Juvenile Spondyloarthritis Disease Activity (JSpADA) Index from baseline. Secondary outcomes included changes in the number of joints with active arthritis and enthesitis, C-reactive protein (CRP), and erythrocyte sedimentation rate (ESR). Outcomes were assessed every 3 months after secukinumab initiation. The Wilcoxon signed-rank test and paired t-test were used to analyze the data.

Results: Male predominance (24/31, 77.4%), late disease onset, HLA-B27 positivity (13/31, 41.9%), and enthesitis (10/31, 32.3%) were the key characteristics of our cohort. The median follow-up duration was 0.9 years (ranging from 0.4 to 2.7 years). At the last follow-up, ACR 30/50/70/90/100 response rates were 87% (27/31), 68% (21/31), 65% (20/31), 32.3% (10/31) and 12.9% (4/31); 25.8% (8/31) of patients achieved ACR inactive disease. JSpADA scores decreased from baseline (median 5.0, IQR: 3.5–5.0) to month 3 (median 3.5, IQR: 2.5–4.0; median difference = 1.25, $Z = -4.26$, $p < 0.001$, 95% CI: 0.8 to 2.0), to month 6 to 3.0 (IQR: 2.0–4.0; median difference = 1.5, $Z = -3.85$, $p < 0.001$, 95% CI: 1.0 to 2.3), month 9 to 3.0 (IQR: 1.0–3.0; median difference = 2.3, $Z = -3.09$, $p = 0.002$, 95% CI: 1.5 to −3.0) and month 12 to 2.5 (IQR: 1.0–3.0; median difference = 2.25, $Z = -2.95$, $p = 0.003$, 95% CI: 1.5 to 3.3). The mean active joint count decreased from 9.3 ± 0.7 at baseline to 3.3 ± 0.5 at 12 months. Normalization of C-reactive protein (CRP) and erythrocyte sedimentation rate (ESR) was observed.

Conclusion: In this retrospective, single-center study, secukinumab appears to be associated with improvement in arthritis and disease activity in Chinese children with ERA. Further studies are needed to investigate the correlation between IL-17 and ERA.

Abbreviations: ACR, American College of Rheumatology; AE, adverse event; AS, ankylosing spondylitis; CHAQ, Childhood Health Assessment Questionnaire; CI, confidence intervals; CRP, C-reactive protein; DMARDs, disease-modifying anti-rheumatic drugs; ERA, enthesitis-related arthritis; ESR, erythrocyte sedimentation rate; FDA, Food and Drug Administration; HIMRISS, Hip Inflammation MRI Scoring System; HLA-B27, Human Leukocyte Antigen-B27; IL-17, interleukin-17; ILAR, International League of Associations for Rheumatology; IQR, interquartile range; JADAS27, Juvenile Arthritis Disease Activity Score with 27 Joints; JIA, Juvenile idiopathic arthritis; JSpADA, Juvenile Spondyloarthritis Disease Activity; MRI, magnetic resonance imaging; nr-axSpA, non-radiographic axial spondyloarthritis; NSAIDs, non-steroidal anti-inflammatory drugs; PhGA, physician's global assessment; RF, rheumatoid factor; SAE, serious adverse event; SD, standard deviation; SPARCC, Spondyloarthritis Research Consortium of Canada; TNFi, tumor necrosis factor inhibitors.

1 | Introduction

Juvenile idiopathic arthritis (JIA) is a chronic inflammatory arthritis affecting patients under 16 years of age, with a disease course lasting more than 6 weeks and an unknown exact cause. Enthesitis-related arthritis (ERA) is a subgroup of JIA [1] and accounts for 30% of pediatric patients with JIA in Asia [2]. ERA is more common in patients older than six. Characteristic manifestations of ERA include involvement of the peripheral joints, entheses, and axial skeleton, and it is considered a similar disease to adult-onset spondyloarthropathies [3]. Other manifestations include acute anterior uveitis, fever, gastrointestinal symptoms, seronegativity for rheumatoid factor (RF), human leukocyte antigen-B27 (HLA-B27) positivity, and a familial aggregation tendency. Compared with other subtypes of JIA, patients with ERA have higher pain intensity, a longer disease course, and poorer health status. Additionally, ERA patients are more difficult to reach and maintain clinical remission [4–6].

In accordance with the 2019 treatment recommendations from the American College of Rheumatology (ACR), non-steroidal anti-inflammatory drugs (NSAIDs) are recommended as first-line therapy [7]. Disease-modifying anti-rheumatic drugs (DMARDs) such as methotrexate or sulfasalazine are also used. Methotrexate is preferred, and sulfasalazine is effective in peripheral arthritis but has shown limited efficacy in axial disease [8]. Tumor necrosis factor inhibitors (TNFi) have demonstrated improvements in active arthritis. Adalimumab yielded 65% ACR 30 response and 53% ACR 70 response after 12 weeks of treatment. Etanercept showed 93% ACR 30 response and 93% ACR 50 response at Week 24 [9, 10]. However, a number of patients remain in an active disease state. Thus, more intensive treatment options are called for.

Recently, there has been an emerging interest in the role of interleukin (IL)-17A in the pathogenesis of ERA. IL-17 is essential in arthritis as well as cartilage and bone destruction. The serum level of IL-17 in JIA is significantly higher than that of healthy controls. Moreover, the level of IL-17 is positively correlated with disease activity and inflammatory markers [11]. Secukinumab, a monoclonal antibody targeting IL-17A, has yielded satisfactory responses in the treatment of adult-onset ankylosing spondylitis (AS). In a phase 3 clinical trial of AS, 58.3% of patients reached ASAS20 response after 16 weeks of treatment [12]. In a phase 3 double-blind, placebo-controlled clinical trial in ERA and juvenile psoriatic arthritis, 67.4% of patients achieved ACR70 response, 34.9% achieved clinical inactive disease and there was a notable reduction in Juvenile Arthritis Disease Activity Score with 27 Joints (JADAS27) scores [13]. Although secukinumab has demonstrated efficacy in ERA, real-world evidence, particularly in Chinese children, remains limited. Moreover, it remains unclear whether the efficacy observed in clinical trials translates directly into Chinese clinical practice, where disease phenotypes, HLA-B27 prevalence and prior treatment exposures may differ. A total of 31 ERA patients were included herein. This retrospective study aimed to: (1) evaluate the efficacy of secukinumab in Chinese ERA patients; (2) describe the safety profile in this population; and (3) provide real-world clinical data to support the use of secukinumab in Chinese pediatric rheumatology practice.

2 | Method

2.1 | Study Population

This study was a single-center, retrospective cohort study conducted from April 1 to December 31 in the year of 2024. Inclusion criteria were: (1) diagnosed of ERA based on the 2001 JIA criteria of the International League of Associations for Rheumatology (ILAR) [1]; (2) received at least 3 months of secukinumab treatment; and (3) regularly followed up at Beijing Children's Hospital, Capital Medical University. Exclusion criteria were: (1) received less than 3 months of secukinumab treatment; (2) had other rheumatic diseases or secondary arthritis. Consecutive patients meeting eligibility criteria were included to minimize selection bias. Indication for starting secukinumab was persistent disease activity for more than 6 months without response to one or more DMARDs, NSAIDs, or biologics. Prior biologic exposure was defined as inadequate response (failure to achieve ACR30 after 3 months of treatment) or intolerance to at least one TNFi. Both TNFi-naïve and TNFi-experienced patients were included.

2.2 | Secukinumab Dosing Regimen

Secukinumab was administered subcutaneously. The loading regimen was 75 mg for body weight < 50 kg and 150 mg for body weight ≥ 50 kg, once weekly for 4 weeks (Weeks 0, 1, 2, 3, 4), followed by a maintenance regimen of the same dose every 4 weeks thereafter. The dose was increased from 150 mg to 300 mg when an inadequate response was observed after at least 3 months of treatment.

2.3 | Concomitant Therapies

Concomitant medications, including NSAIDs, DMARDs and, corticosteroids, were permitted. Doses of concomitant therapies were required to be stable for at least 4 weeks prior to secukinumab initiation and remained unchanged throughout the study period, unless clinically indicated for safety reasons. Any changes in concomitant medications during follow-up were recorded.

2.4 | Ethics Statement

This study has gained approval from the Ethics Committee of Beijing Children's Hospital on April 22, 2025 ([2025]-E-060-R). Written informed consent was obtained from patients and their legal guardians.

2.5 | Data Collection, Outcomes and Assessments

Clinical information regarding disease onset, disease course, clinical manifestations, laboratory tests and previous treatment was collected. Laboratory tests such as complete blood count, C-reactive protein (CRP), erythrocyte sedimentation rate (ESR), urinalysis, liver function, kidney function and coagulation profile were performed. HLA-B27 and autoantibody

(e.g., RF and antinuclear antibody) testing were performed. Primary outcomes were: proportion of patients achieving JIA ACR 30/50/70/90/100 response [14], ACR inactive disease [15] and change from baseline in Juvenile Spondyloarthritis Disease Activity (JSpADA) score [16] at each follow-up timepoint. Secondary outcomes were: (1) reduction in active arthritis joint count and enthesitis count; (2) change from baseline in laboratory parameters (CRP, ESR) at each follow-up timepoint; (3) safety outcomes (adverse events) throughout the study period. Assessment timepoints were baseline (secukinumab initiation) and at 3, 6, 9, 12, 15 and 18 months after treatment initiation; long-term follow-up up to 32 months. Ocular involvement was investigated through intraocular pressure measurement, slit lamp examination and fundus photography. Nasopharyngitis, nausea, diarrhea, cough, headache, and injection-site reaction were common adverse effects of secukinumab and were monitored carefully at each 3-month follow-up.

2.6 | Statistical Analysis

All data in the study were analyzed using SPSS 27.0. Normality of the continuous variable data was tested using the Shapiro–Wilk test. Continuous variables with a normal distribution were presented as mean ± standard deviation (SD) and compared using the parametric test (paired *t*-test), while those with a non-normal distribution were reported as median with interquartile range (IQR) and compared using the non-parametric test (Wilcoxon signed-rank test). Categorical variables were presented as numbers (percentages), where appropriate. Missing data were handled using complete-case analysis. As an exploratory and hypothesis-generating study, no formal sample size calculation was performed. A two-sided p-value < 0.05 indicated a significant difference; 95% confidence intervals (CI) were reported.

3 | Results

3.1 | Baseline Information

Of all cases assessed, 24 were male and the ratio of male-to-female was 3.43:1, indicating male predominance. All cases were Han Chinese. Six patients (19.4%) had a first-degree relative with a history of rheumatic disease. Table 1 summarizes the general information at baseline. The mean age at disease onset was 10.0 ± 0.5 years (ranging from 4.3 to 15.8 years). At the time of the first prescription, the hip was the most frequently involved joint (24/31, 83.9%) followed by the ankle (25/31, 80.6%) and sacroiliac joint (24/31, 77.4%). JSpADA scores ranged from 3 to 6, with a median score of 5.0 (IQR: 3.5–5.0). JSpADA scores did not differ significantly between HLA-B27-positive and HLA-B27-negative patients (median difference = 0.0, $Z = -0.46$, $p = 0.695$, 95% CI: −1.0 to 0.5). The mean number of joints with active arthritis was 9.3 ± 0.7. The median number of enthesitis cases was 3 (IQR: 2–4). One patient (3.2%) was diagnosed with anterior uveitis accompanied by decreased visual acuity. All patients were tested for HLA-B27 and 13 (41.9%) were tested positive. Regarding inflammatory markers, the mean serum levels of CRP and ESR were 17.03 ± 3.71 mg/L and 21.4 ± 2.9 mm/h.

TABLE 1 | General information at baseline.

Feature	Number (%) or mean ± SD or median [IQR]
Sex	
Male	24 (77.4%)
Female	7 (22.6%)
Ethnicity	
Han Chinese	31 (100%)
Family history	6 (19.4%)
Mean age at disease onset	10.0 ± 0.5 years
Mean age at first prescription	11.4 ± 0.5 years
Manifestation	
Arthritis	31 (100%)
Hip	26 (83.9%)
Ankle	25 (80.6%)
Sacroiliac joint	24 (77.4%)
Knee	23 (74.2%)
Spine	12 (38.7%)
Enthesitis	10 (32.3%)
MCP/PIP	9 (29.0%)
Shoulder	6 (19.4%)
Elbow	5 (16.1%)
Wrist	4 (12.9%)
Mean number of active arthritis	9.3 ± 0.7
Median number of enthesitis	3 [2, 4]
Median JSpADA score	5 [3.5, 5]
Pulmonary involvement	7 (22.6%)
Uveitis	1 (3.2%)
HLA-B27 positivity	13 (41.9%)
Mean serum level of CRP mg/L	17.03 ± 3.71
Mean serum level of ESR mm/h	21.4 ± 2.9

Note: Data were presented as *n* (%), mean ± SD, or median [IQR] as appropriate. Abbreviations: CRP, C-reactive protein; ESR, erythrocyte sedimentation rate; HLA-B27, human leukocyte antigen B27; IQR, interquartile range; JSpADA, Juvenile Spondyloarthritis Disease Activity Index; MCP, metacarpophalangeal joint; PIP, proximal interphalangeal joint; SD, standard deviation.

3.2 | Prior Treatments

All patients received a combination of NSAIDs and DMARDs as first-line treatment. A total of 24 patients (77.4%) had used TNFi as therapy. Eight of them (25.8%) had been treated with more than one type of TNFi. Two patients switched to a JAK inhibitor (baricitinib) owing to TNFi ineffectiveness (Table 2).

TABLE 2 | Medication at baseline, before the start and during secukinumab.

Treatment	Treatment at first prescription	Treatment before the start of Secukinumab	Treatment during follow-up visit
Glucocorticoid	2 (6.5%)	3 (9.7%)	1 (3.2%)
NSAIDs	31 (100%)	20 (64.5%)	16 (51.6%)
Methotrexate	4 (12.9%)	5 (16.1%)	5 (16.1%)
Sulfasalazine	28 (90.3%)	28 (90.3%)	26 (83.9%)
Leflunomide		1 (3.2%)	3 (9.7%)
Iguratimod		6 (19.4%)	6 (19.4%)
Hydroxychloroquine		1 (3.2%)	
Baricitinib		2 (6.5%)	
Thalidomide		3 (9.7%)	4 (12.9%)
Tumor necrosis factor inhibitor			
Etanercept	5 (16.1%)	12 (38.7%)	
Adalimumab	4 (12.9%)	10 (32.3%)	
Infliximab	5 (16.1%)	13 (41.9%)	

Note: Data were presented as *n* (%). Patients could receive more than one concomitant medication.
Abbreviation: NSAIDs, non-steroidal anti-inflammatory drugs.

3.3 | Secukinumab Efficacy

Indication of starting secukinumab was sustained active arthritis for more than 6 months and failure of previous treatment with NSAIDs, DMARDs, and biologics. The mean disease duration before secukinumab initiation and mean treatment duration with secukinumab were 1.7 ± 0.3 years (ranging from 0 to 5.2 years) and 0.9 ± 0.1 years (ranging from 0.4 to 2.7 years), respectively. One patient received secukinumab at the first prescription due to a long disease history and high disease activity. The dose of secukinumab was increased from 150 mg to 300 mg in 2 patients (6.5%) due to high disease activity.

All 31 patients were followed up every 3 months after secukinumab initiation. Follow-up patient numbers were as follows: 31 at 3 months, 24 at 6 months, 19 at 9 months, 17 at 12 months, 8 at 15 months, 3 at 18 months, and 1 at 32 months. At baseline, the median JSpADA score was 5.0 (IQR: 3.5–5.0), and it decreased significantly at month 3 to 3.5 (IQR: 2.5–4.0; median difference = 1.25, $Z = -4.26$, $p < 0.001$, 95% CI: 0.8 to 2.0), month 6 to 3.0 (IQR: 2.0–4.0; median difference = 1.5, $Z = -3.85$, $p < 0.001$, 95% CI: 1.0 to 2.3), month 9 to 3.0 (IQR: 1.0–3.0; median difference = 2.3, $Z = -3.09$, $p = 0.002$, 95% CI: 1.5 to −3.0) and month 12 to 2.5 (IQR: 1.0–3.0; median difference = 2.25, $Z = -2.95$, $p = 0.003$, 95% CI: 1.5 to 3.3; Figure 1). As for joints with active arthritis, a significant decrease was observed at month 3 (4.7 ± 0.5, mean difference = 4.6, t = 3.37, $p = 0.002$, 95% CI: 3.4 to 5.8), month 6 (4.4 ± 0.5, mean difference = 5.4, t = 3.881, $p < 0.001$, 95% CI: 3.7 to 7.1), month 9 (3.26 ± 0.5, mean difference = 6.1, t = 5.90, $p < 0.001$, 95% CI: 4.3 to 7.9) and month 12 (3.29 ± 0.5, mean difference = 6.4, t = 5.72, $p < 0.001$, 95% CI: 4.2 to 8.5; Figure 2). The median number of enthesitis cases dropped from 2 (IQR: 2–3) at secukinumab initiation to 2 (IQR: 0–2) at the last follow-up visit. A significant improvement in enthesitis was observed in month 12 (median difference = 1.5, $Z = -2.23$, $p = 0.026$, 95% CI: 1.0 to 2.0). The patient with anterior uveitis at baseline showed improvement in ocular manifestations. Regarding inflammatory markers, normalization of CRP and ESR was observed. The ESR level was 21.4 ± 2.9 mm/h at month 0 and decreased significantly at 3, 6, 9 and 12 months (Figure 3). At the last follow-up, ACR 30/50/70/90/100 response rates were 87.1% (27/31), 67.7% (21/31), 64.5% (20/31), 32.3% (10/31), and 12.9% (4/31), respectively; 25.8% (8/31) achieved ACR inactive disease (Table 3), including one patient on secukinumab monotherapy.

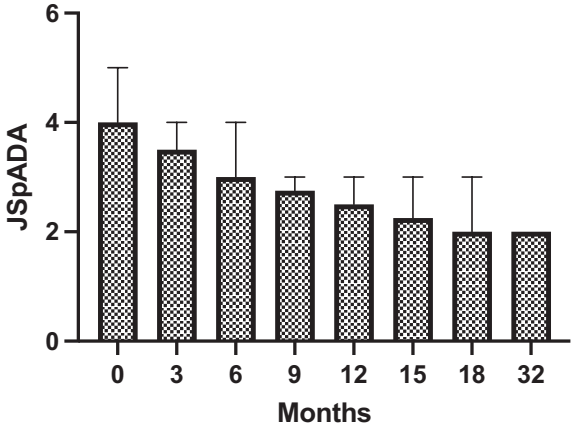

FIGURE 1 | Median JSpADA score at secukinumab initiation and follow-up visit. JSpADA scores were presented as median (IQR). Baseline (Month 0) $n = 31$; (Month 3) $n = 31$; (Month 6) $n = 24$; (Month 9) $n = 19$; (Month 12) $n = 17$; (Month 15) $n = 8$; (Month 18) $n = 3$; (Month 32) $n = 1$. Significant reductions were observed at Months 3 (median difference 1.25, $p < 0.001$), 6 (median difference 1.5, $p < 0.001$), 9 (median difference 2.3, $p = 0.002$), and 12 (median difference 2.25, $p = 0.003$).

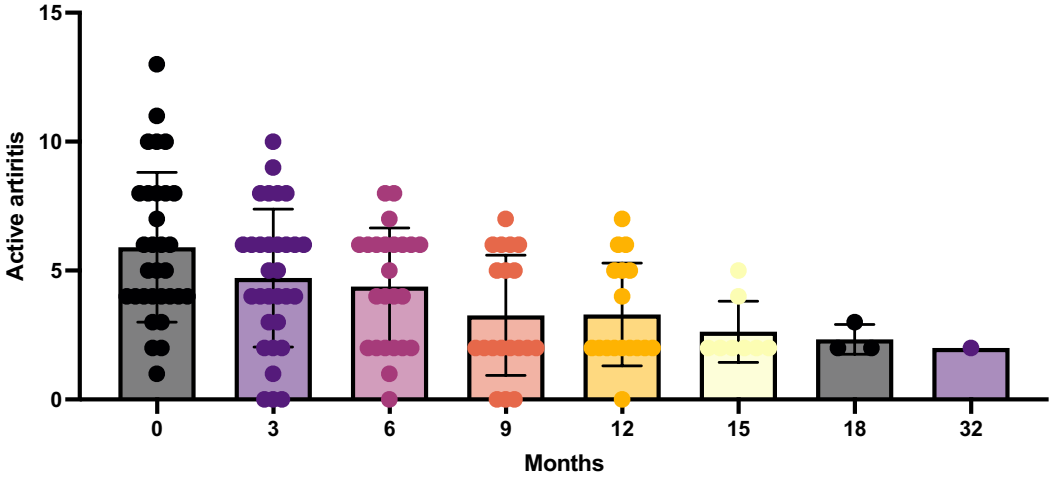

FIGURE 2 | Mean number of joints with active arthritis at secukinumab initiation and follow-up visit. Data were presented as mean ± SD. Significant reductions were observed at Months 3 (mean difference 4.7, $p = 0.002$), 6 (mean difference 5.4, $p < 0.001$), 9 (mean difference 6.1, $p < 0.001$), and 12 (mean difference 6.4, $p < 0.001$).

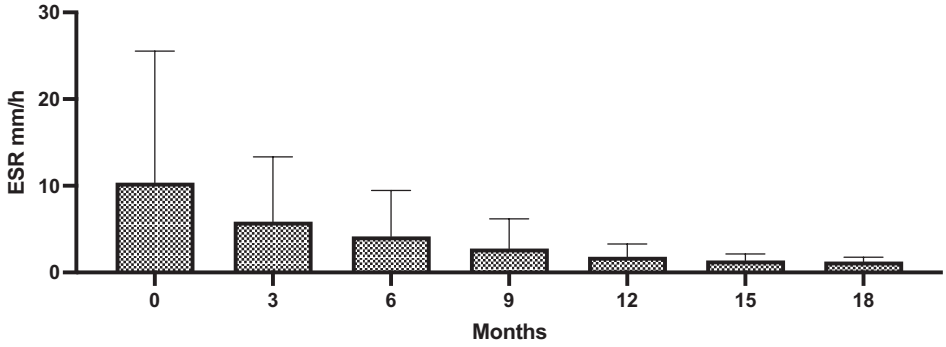

FIGURE 3 | Median value of ESR at secukinumab initiation and follow-up visit. Data were presented as mean (SD). Significant reductions were observed at Months 3 ($p = 0.01$), 6 ($p = 0.008$), 9 ($p = 0.003$), and 12 ($p = 0.004$).

TABLE 3 | ACR 30/50/70/90/100 response and ACR inactive disease at most recent follow-up visit.

ACR response	Number (%)
ACR 30 response	27 (87.1)
ACR 50 response	21 (67.7)
ACR 70 response	20 (62.5)
ACR 90 response	10 (32.3)
ACR 100 response	4 (12.9)
ACR inactive disease	8 (25.8)

Note: Data were presented as *n* (%).

3.4 | Adverse Effect

Over a mean follow-up of 0.9 years, no serious adverse event (SAE) or adverse event (AE) prompting discontinuation of secukinumab was reported. One patient (3.2%) experienced a mild injection-site reaction (redness and itching) which resolved spontaneously. No cases of uveitis, inflammatory bowel disease, or other predefined AEs (nasopharyngitis, nausea, diarrhea, cough, and headache) were observed.

4 | Discussion

This retrospective study included 31 ERA patients with male predominance. Patients' characteristics including late disease onset, HLA-B27 association and enthesitis were consistent with previous reports [1]. The proportion of HLA-B27 positivity in our study (41.9%) falls within the lower range of the 40%–90% reported in other ERA cohorts [17]. No significant differences in JSpADA scores were found between HLA-B27-positive and HLA-B27-negative patients, which may be attributed to the limited sample size. Peripheral arthritis occurs in nearly 90% of ERA patients, with oligoarthritis being the most common pattern. Knees and ankles are the most frequently affected joints. Axial arthritis (e.g., sacroiliac and spine arthritis) is observed in 30%–60% of patients [18]. Among patients with axial involvement, hip involvement is more frequent [19]. In our study, our patients had axial involvement and a high frequency of hip joint involvement. As for peripheral joints, ankles and knees were most frequently involved. Antecedent researchers have uncovered that hip involvement, tarsitis, older age at disease onset, enthesitis, sacroiliitis and HLA-B27 positivity are predictors of poor outcome [20]. Consequently, most patients included in our study were classified as having severe disease at baseline, which was associated with a poor outcome.

After at least 3 months of secukinumab treatment, this real-world retrospective study of ERA confirms that secukinumab delivers meaningful improvement in disease activity, arthritis, enthesitis, and inflammatory markers. ACR30/50/70/90/100 response rates were 87.1%/67.7%/64.5%/32.3%/12.9%, and 25.8% of patients achieved ACR inactive disease. Among patients who achieved ACR inactive disease, one patient received secukinumab monotherapy, suggesting potential efficacy of secukinumab as monotherapy. Inflammatory markers such as CRP and ESR are indicators of disease activity [21]. ESR decreased significantly after secukinumab treatment, indicating reduced disease activity. The treatment was well tolerated, with no SAEs or treatment discontinuation.

IL-17 plays a central role in ERA pathogenesis by mediating synovial inflammation, cartilage damage and bone destruction, with elevated levels detected in patients' serum and synovial fluid [22] and correlated with disease activity [23–25]. Secukinumab has been licensed by the U.S. Food and Drug Administration (FDA) for the treatment of ERA in patients aged 4 years and older, blocks proinflammatory signal and reduces joint and entheseal inflammation. Our work supports this mechanistic framework. However, the precise relationship between IL-17 expression, HLA-B27 status and long-term structural progression in ERA remains incompletely understood and warrants further investigation.

Our findings align well with the phase 3 multinational clinical trial of secukinumab in ERA and pediatric psoriatic arthritis, which reported 67.4% ACR 70 response and 34.9% clinical inactive disease at Week 52, accompanied by significant reduction in JADAS 27 [13]. Despite differences in study design (real-world retrospective versus randomized controlled trial), ethnicity (Chinese versus multinational), and baseline disease severity (our cohort had greater prior biologic exposure and higher activity), our ACR70 response (64.5%) and inactive disease rate (25.8%) are broadly comparable, reinforcing the external validity of secukinumab for ERA across diverse populations. Our results also align with real-world studies in anti-TNF-refractory ERA patients, which showed significant JSpADA and disease activity score reduction [26, 27]. Notably, our study included a high proportion of patients with prior TNFi exposure (77.4%), and 8 had received more than one TNFi. These real-world datasets support secukinumab efficacy in TNFi-insufficient patients, complementing controlled trial evidence and filling gaps in pediatric evidence specific to Chinese cohorts and underscoring secukinumab's practical value as a second-line or later biologic for patients unresponsive to standard therapies.

Secukinumab effectively improved clinical outcomes in ERA patients without severe adverse effects, making it a promising treatment option for ERA patients. However, these findings require validation in larger prospective controlled studies to further clarify ERA pathogenesis and treatment efficacy.

4.1 | Limitations

This study has several limitations. First, due to its retrospective, single-center design without a control or comparator group, causal inference and the ability to compare the relative efficacy of secukinumab against other treatments (e.g., TNF inhibitors) are limited. Second, power calculation was not performed prior to the study. The sample size was determined by the number of patients meeting the inclusion criteria rather than by a priori power estimation. The small sample size, particularly the limited number of patients with long-term follow-up (e.g., only three patients at 18 months), precludes subgroup analyses and reduces the precision of our efficacy and safety estimates. Third, the follow-up duration (median 0.9 years, range 0.4–2.7 years) may be insufficient to fully assess long-term safety events or sustained radiographic outcomes. Fourth, a diagnostic limitation is the use of the 2001 ILAR criteria (widely used clinically) rather than the newer 2019 PRINTO criteria. Finally, the severity of sacroiliac arthritis can be assessed using the Spondyloarthritis Research Consortium of Canada (SPARCC) and Hip Inflammation MRI Scoring System (HIMRISS) scoring systems based on Magnetic Resonance Imaging (MRI). The lack of such MRI scores prevented us from assessing joint involvement radiographically.

5 | Conclusion

In this retrospective study, secukinumab treatment was associated with improvements in arthritis and disease activity in Chinese children with ERA. The treatment was well-tolerated, with no severe adverse reactions reported. Due to the observational design and limited sample size, these findings are exploratory. Larger and controlled prospective studies are needed to confirm long-term efficacy and safety.

Author Contributions

X.S. and J.Z. contributed equally to this study. X.S. collected the data, conducted data analysis and drafted the manuscript. J.Z. coordinated and supervised data collection, conducted data analysis and drafted the manuscript of this study. F.G., W.K., J.D., X.T., C.L., S.L., J.G., X.L., and B.S. collected the data. C.L. provided critical comments and revised the manuscript.

Acknowledgments

We thank all the participants and their parents for the study.

Funding

The authors have nothing to report.

Disclosure

The authors have nothing to report.

Conflicts of Interest

The authors declare no conflicts of interest.

Data Availability Statement

Condensed anonymized data are available from the corresponding author on reasonable request.

References

1. R. E. Petty, T. R. Southwood, P. Manners, et al., "International League of Associations for Rheumatology Classification of Juvenile Idiopathic

Arthritis: Second Revision, Edmonton, 2001," *Journal of Rheumatology* 31, no. 2 (2004): 390–392.

2. A. Consolaro, G. Giancane, A. Alongi, et al., "Phenotypic Variability and Disparities in Treatment and Outcomes of Childhood Arthritis Throughout the World: An Observational Cohort Study," *Lancet. Child & Adolescent Health* 3, no. 4 (2019): 255–263.

3. P. F. Weiss, R. C. Fuhlbrigge, E. von Scheven, et al., "Children With Enthesitis-Related Arthritis and Possible Benefits From Treatments for Adults With Spondyloarthritis," *Arthritis Care & Research* 74, no. 7 (2022): 1058–1064.

4. Y. J. Shih, Y. H. Yang, C. Y. Lin, C. L. Chang, and B. L. Chiang, "Enthesitis-Related Arthritis Is the Most Common Category of Juvenile Idiopathic Arthritis in Taiwan and Presents Persistent Active Disease," *Pediatric Rheumatology* 17, no. 1 (2019): 58.

5. L. Berntson, E. Nordal, K. Aalto, et al., "HLA-B27 Predicts a More Chronic Disease Course in an 8-Year Follow-Up Cohort of Patients With Juvenile Idiopathic Arthritis," *Journal of Rheumatology* 40, no. 5 (2013): 725–731.

6. P. F. Weiss, T. Beukelman, L. E. Schanberg, Y. U. K. I. K. O. Kimura, and R. O. B. E. R. T. A. Colbert, "Enthesitis-Related Arthritis Is Associated With Higher Pain Intensity and Poorer Health Status in Comparison With Other Categories of Juvenile Idiopathic Arthritis: The Childhood Arthritis and Rheumatology Research Alliance Registry," *Journal of Rheumatology* 39, no. 12 (2012): 2341–2351.

7. S. Ringold, S. T. A. Angeles-Han, T. Beukelman, et al., "2019 American College of Rheumatology/Arthritis Foundation Guideline for the Treatment of Juvenile Idiopathic Arthritis: Therapeutic Approaches for Non-Systemic Polyarthritis, Sacroiliitis, and Enthesitis," *Arthritis and Rheumatology* 71, no. 6 (2019): 846–863.

8. J. Guzman, A. Henrey, T. Loughin, et al., "Predicting Which Children With Juvenile Idiopathic Arthritis Will Not Attain Early Remission With Conventional Treatment: Results From the ReACCh-Out Cohort," *Journal of Rheumatology* 46, no. 6 (2019): 628–635.

9. G. Horneff, S. Fitter, I. Foeldvari, et al., "Double-Blind, Placebo-Controlled Randomized Trial With Adalimumab for Treatment of Juvenile Onset Ankylosing Spondylitis (JoAS): Significant Short Term Improvement," *Arthritis Research & Therapy* 14, no. 5 (2012): R230.

10. G. Horneff, I. Foeldvari, K. Minden, et al., "Efficacy and Safety of Etanercept in Patients With the Enthesitis-Related Arthritis Category of Juvenile Idiopathic Arthritis: Results From a Phase III Randomized, Double-Blind Study," *Arthritis and Rheumatology* 67, no. 8 (2015): 2240–2249.

11. G. Vijatov-Djuric, A. Doronjski, I. Mitic, et al., "Interleukin-17A Levels Increase in Serum of Children With Juvenile Idiopathic Arthritis," *Archives of Rheumatology* 32, no. 3 (2017): 234–243.

12. F. Huang, F. Sun, W. G. Wan, et al., "Secukinumab Provided Significant and Sustained Improvement in the Signs and Symptoms of Ankylosing Spondylitis: Results From the 52-Week, Phase III China-Centric Study, MEASURE 5," *Chinese Medical Journal* 133, no. 21 (2020): 2521–2531.

13. H. I. Brunner, I. Foeldvari, E. Alexeeva, et al., "Secukinumab in Enthesitis-Related Arthritis and Juvenile Psoriatic Arthritis: A Randomised, Double-Blind, Placebo-Controlled, Treatment Withdrawal, Phase 3 Trial," *Annals of the Rheumatic Diseases* 82, no. 1 (2023): 154–160.

14. E. H. Giannini, N. Ruperto, A. Ravelli, D. J. Lovell, D. T. Felson, and A. Martini, "Preliminary Definition of Improvement in Juvenile Arthritis," *Arthritis & Rheumatism* 40, no. 7 (1997): 1202–1209.

15. C. A. Wallace, E. H. Giannini, B. Huang, L. Itert, and N. Ruperto, "American College of Rheumatology Provisional Criteria for Defining Clinical Inactive Disease in Select Categories of Juvenile Idiopathic Arthritis," *Arthritis Care & Research* 63, no. 7 (2011): 929–936.

16. P. F. Weiss, R. A. Colbert, R. Xiao, et al., "Development and Retrospective Validation of the Juvenile Spondyloarthritis Disease Activity Index," *Arthritis Care and Research* 66, no. 12 (2014): 1775–1782.

17. Z. Zuber, D. Turowska-Heydel, M. Sobczyk, Z. Żuber, and J. Chudek, "Prevalence of HLA-B27 Antigen in Patients With Juvenile Idiopathic Arthritis," *Reumatologia* 53, no. 3 (2015): 125–130.

18. S. Di Gennaro, G. Di Matteo, G. Stornaiuolo, et al., "Advances in the Diagnosis and Treatment of Enthesitis-Related Arthritis," *Children (Basel)* 10, no. 10 (2023): 1647.

19. Y. Guo, Y. Fang, T. Zhang, et al., "Axial Involvement in Enthesitis-Related Arthritis: Results From a Single-Center Cohort," *Pediatric Rheumatology* 21, no. 1 (2023): 13.

20. R. Naveen, S. Guleria, and A. Aggarwal, "Recent Updates in Enthesitis-Related Arthritis," *Rheumatology International* 43, no. 3 (2023): 409–420.

21. B. Flatø, A. M. Hoffmann-Vold, A. Reiff, et al., "Long-Term Outcome and Prognostic Factors in Enthesitis-Related Arthritis: A Case-Control Study," *Arthritis and Rheumatism* 54, no. 11 (2006): 3573–3582.

22. S. Agarwal, R. Misra, and A. Aggarwal, "Interleukin 17 Levels Are Increased in Juvenile Idiopathic Arthritis Synovial Fluid and Induce Synovial Fibroblasts to Produce Proinflammatory Cytokines and Matrix Metalloproteinases," *Journal of Rheumatology* 35, no. 3 (2008): 515–519.

23. A. Mahendra, R. Misra, and A. Aggarwal, "Th1 and Th17 Predominance in the Enthesitis-Related Arthritis Form of Juvenile Idiopathic Arthritis," *Journal of Rheumatology* 36, no. 8 (2009): 1730–1736.

24. B. Olivito, G. Simonini, S. Ciullini, et al., "Th17 Transcription Factor RORC2 Is Inversely Correlated With FOXP3 Expression in the Joints of Children With Juvenile Idiopathic Arthritis," *Journal of Rheumatology* 36, no. 9 (2009): 2017–2024.

25. S. A. Wu, K. W. Yeh, W. I. Lee, T. C. Yao, and J. L. Huang, "Persistent Improper Upregulation of Th17 and TReg Cells in Patients With Juvenile Idiopathic Arthritis," *Journal of Microbiology, Immunology, and Infection* 49, no. 3 (2016): 402–408.

26. J. Baer, J. Klotsche, and I. Foeldvari, "Secukinumab in the Treatment for Patients With Juvenile Enthesitis Related Arthritis Non-Responsive to Anti-TNF Treatment According the Juvenile Spondyloarthritis Disease Activity Index," *Clinical and Experimental Rheumatology* 40, no. 3 (2022): 620–624.

27. S. Papailiou, M. Onoufriou, L. Mentesidou, A. Syggelou, M. N. Tsolia, and D. N. Maritsi, "Achieving Inactive Disease in Enthesitis-Related Arthritis With Secukinumab Following TNF-Inhibitor Failure," *Rheumatology (Oxford, England)* 63 (2023): e297–e298.

International Journal of Rheumatic Diseases

WILEY

International Journal of Rheumatic Diseases

ORIGINAL ARTICLE

Global Burden, Trends, and High-BMI-Attributable Risk of Hip Osteoarthritis: An Analysis of GBD 2021 Data

Xueming Shi[1,2] | Chen Lin[1,2] | Jiaying Yang[3] | Zhiwei Cao[3] | Xiaoning Duan[4]

[1]Department of Orthodontics, Tianjin Stomatological Hospital, School of Medicine, Nankai University, Tianjin, China | [2]Tianjin Key Laboratory of Oral and Maxillofacial Function Reconstruction, Tianjin, China | [3]School of Clinical Stomatology, Tianjin Medical University, Tianjin, China | [4]School of Medicine, Nankai University, Tianjin, China

Correspondence: Chen Lin (linchen2119@qq.com)

Received: 29 October 2025 | **Revised:** 12 April 2026 | **Accepted:** 27 May 2026

Keywords: global burden diseases | hip osteoarthritis | mendelian randomization | prediction | risk factors

ABSTRACT

Background: The purpose of this study is to evaluate the global burden of hip osteoarthritis (OA) and investigate its risk factors using Global Burden of Disease (GBD) 2021 data and Mendelian randomization (MR).

Methods: Hip OA burden was assessed by region, age, sex, and Socio-Demographic Index (SDI). Temporal trends were evaluated using Joinpoint regression-derived average annual percentage change (AAPC). Two-sample MR and mediation analysis explored causal risk factors. Future burden from 2022 to 2050 was primarily projected using a Bayesian age-period-cohort (BAPC) model, with autoregressive integrated moving average (ARIMA) analysis used as a sensitivity comparison.

Results: The global age-standardized hip OA prevalence was 416.01/100000 in 2021. The incidence and prevalence varied widely across countries. Males who were above 70 years old had a greater incidence of hip OA. The incidence and prevalence positively correlated with SDI, with the largest rise in incident cases occurring in middle SDI regions. Joinpoint analysis showed that the global burden of hip OA increased significantly from 1990 to 2021, with AAPCs of 0.2206 for incidence, 0.1879 for prevalence, and 0.1846 for DALYs. The most pronounced increases were observed in low-middle and middle SDI regions. High body mass index (BMI) contributed to a 21.2% increase in disability-adjusted life years (DALYs) from 1990 to 2021. MR mediation supported a positive association between higher BMI and hip OA and suggested that palmitoyl sphingomyelin may represent a potential mediator. The primary BAPC model suggested that the burden of hip OA would remain substantial through 2050, whereas comparison with ARIMA indicated model-dependent uncertainty in the long-term magnitude of the forecasts.

Conclusions: Our study provides valuable insights into the global epidemiological trends and risk factors of hip OA. These findings can help formulate policies and allocate resources, although long-term projections should be interpreted cautiously because they are sensitive to model choice.

1 | Background

Osteoarthritis (OA) is a chronic degenerative joint disease characterized by the deterioration of articular cartilage, synovial inflammation, and bone remodeling [1]. It most commonly affects the hip, knee, and hand joints and is a leading cause of chronic pain and long-term disability in adults [2, 3]. The dysfunction and reduced quality of life associated with OA impose

Abbreviations: AAPC, Average annual percentage change; ASRs, Age-standardized rates; BAPC, Bayesian Age-period-Cohort; BMI, Body mass index; CI, Concentration index; DALYs, Disability-adjusted life-years; GBD, Global Burden of Diseases Injuries and Risk Factors Study; IVs, Instrumental variables; MR, Mendelian randomization; OA, Osteoarthritis; SDI, Sociodemographic index; SNPs, Single-nucleotide polymorphisms; UI, Uncertainty intervals.

The first two authors contributed equally to this article.

a significant burden on both individuals and society [4, 5]. The disease burden caused by OA demands urgent attention, and research on early intervention and preventive strategies has become a critical focus in public health.

In recent years, the disease burden of OA has been extensively studied [4, 6–8]. OA is a heterogeneous, multifactorial chronic condition, and the progression of joint involvement over time varies among individuals. Hip and knee OA are the leading causes of disability worldwide. Most studies to date have focused on the knee, with results often extrapolated to the hip, which extends to treatment recommendations in clinical guidelines [9, 10]. Extrapolating results from studies of knee OA may limit our understanding of disease characteristics specific to hip OA, thereby limiting the development and implementation of effective treatments [11]. The Global Burden of Disease (GBD), Injury, and Risk Factors Study is the only comprehensive framework for estimating global disease burden, providing metrics such as age-standardized incidence, prevalence, and disability-adjusted life years (DALYs) for hip OA [12]. Fu et al. analyzed the global burden of hip OA using GBD 2019 data but did not explore the causal relationships between risk factors and the disease [13]. Additionally, these studies were based on pre-2021 GBD data and focused on specific age groups and regional or national disease burdens [14–16]. Another study utilized the World Health Organization's disease burden database to report the global burden of OA from 1990 to 2021, but did not specifically address hip OA or examine its burden in relation to country, region, gender, age, or the Socio-demographic Index (SDI) [17]. With the increasing availability of global hip OA health data and updates to the GBD database, a comprehensive analysis of the global burden of hip OA is necessary.

To provide an updated and integrated perspective on hip osteoarthritis burden, we analyzed GBD 2021 data across locations, age groups, sexes, and SDI strata from 1990 to 2021. We systematically examined age-standardized rates (ASRs) in 204 countries and 21 regions and evaluated temporal trends using Joinpoint regression-derived average annual percentage change (AAPC). In addition to describing epidemiological patterns, we examined BMI-attributable burden and included supplementary Mendelian randomization (MR) analyses as genetics-based triangulation evidence for the BMI-hip OA association. Our aim was not to redefine the established burden framework, but to extend the current literature by integrating burden patterns, inequality, BMI-related burden, and complementary genetic evidence.

2 | Methods

2.1 | Data Source

The GBD 2021 study, conducted by the Institute for Health Metrics and Evaluation (IHME) at the University of Washington, comprehensively evaluated the burden of 369 diseases and 88 risk factors across 204 countries and territories from 1990 to 2021 [18]. The Global Health Data Exchange (GHDx, https://www.healthdata.org/) provides interactive access to this wealth of data, allowing researchers and policymakers to explore and analyze the findings. The data regarding hip OA incidence, prevalence, and DALYs, along with the corresponding 95% uncertainty intervals (UIs) and the corresponding ASRs, were obtained from the GBD 2021 [12]. This dataset encompasses all age groups from 45 to 95 years and older, spanning the period from 1990 to 2021.

2.2 | Average Annual Percent Change

Temporal trends in the age-standardized incidence, prevalence, and DALY rates of hip OA were assessed using Joinpoint regression analysis. The annual percent change (APC) for each time segment and the average annual percent change (AAPC) for the overall study period were calculated with 95% confidence intervals. A positive AAPC indicated an overall increasing trend, whereas a negative AAPC indicated an overall decreasing trend.

2.3 | Socio-Demographic Index

The SDI assesses the state of development of an area in relation to health outcomes by measuring factors such as fertility rates, per capita income, and education levels. For the GBD 2021 study, the SDI values were multiplied by 100 to create a scale ranging from 0 to 100 and categorized into five classes (low, low-middle, middle, high-middle, and high).

2.4 | Decomposition Analysis

To examine key drivers behind variations in hip OA metrics between 1990 and 2021, we performed a decomposition analysis. We first divided these metrics by SDI, then used the Das Gupta method to assess the proportional contributions of epidemiological shifts, population growth, and aging to the changes [19].

2.5 | Mendelian Randomization and Mediation Analysis

MR is a statistical method that employs genetic variations (single-nucleotide polymorphisms, SNPs) as instrumental variables (IVs) for investigating causal relationships [20]. Two-step MR was conducted to determine the relation of body mass index (BMI) to the predicted risk of hip OA and whether human blood metabolites could mediate this association. The first step is evaluating the causal effect of BMI and blood metabolite signatures on hip OA with a two-sample MR and screening out blood metabolite signatures highly related to the risk of hip OA. The second step is evaluating the causal effect of BMI on the blood metabolites' signatures and calculating the proportion of mediation of each mediator for BMI's effect on hip OA. We used Inverse Variance Weighted (IVW) as the main analysis method. Sensitivity analyses were conducted employing Cochran's Q statistic and MR-Egger regression to test for heterogeneity among SNPs ($p < 0.05$ indicating heterogeneity), and MR-Egger regression to detect horizontal pleiotropy ($p < 0.05$ indicating pleiotropy). Leave-one-out sensitivity analysis was employed to assess whether any single SNP disproportionately influenced the causal relationship between exposure and outcome.

Data for BMI was derived from finngen_R10_BMI_IRN. Data for hip OA (ebi-a-GCST007091) were from the GWAS Catalog

TABLE 1 | The regions ranked the highest and lowest in ASRs in 1990 and 2021, along with the AAPC.

	Location	ASR (95% UI) 1990	ASR (95% UI) 2021	AAPC (95% UI)
Prevalence	Global	391.66 (303.26–496.51)	416.01 (321.23–529.74)	0.19 (0.15–0.23)
	High-income	794.20 (600.76–1014.57)	901.22 (679.89–1166.61)	0.40 (0.27–0.54)
	North America	202.95 (155.63–260.08)	259.20 (199.36–334.02)	0.85 (0.81–0.88)
	East Asia			
Incidence	Global	19.27 (14.72–24.41)	20.67 (15.76–26.19)	0.22 (0.18–0.26)
	High-income	39.79 (29.95–51.20)	45.62 (34.22–58.44)	0.40 (0.27–0.54)
	North America	10.66 (8.02–13.63)	13.81 (10.39–17.59)	0.85 (0.81–0.88)
	East Asia			
DALYs	Global	12.43 (5.86–25.21)	13.19 (6.20–26.65)	0.18 (0.15–0.22)
	High-income	25.27 (12.05–51.60)	28.34 (13.46–57.59)	0.32 (0.26–0.38)
	North America	6.54 (3.01–13.11)	8.32 (3.85–16.56)	0.78(0.76–0.81)
	East Asia			

Abbreviations: AAPC, Average annual percent change; ASR, age-standardized rate per 100 000 people; UI, uncertainty intervals.

(Genome-wide association studies, https://gwas.mrcieu.ac.uk/) [21], featuring 15 704 cases and 378 169 controls. All participants in the study were from Europe. Data for 486 human blood metabolites were also from the GWAS Catalog [22]. The research objects should not overlap, meaning the SNP represented exposure and outcome should be from different research sources.

2.6 | Bayesian Age-Period-Cohort (BAPC) and ARIMA Projection Analyses

The BAPC model is a statistical approach widely used in epidemiological and biostatistical research to examine temporal trends in disease burden [23, 24]. By integrating sample data with prior knowledge, this method generates reliable parameter estimates, ensuring statistically robust results. In this study, we stratified the population by gender and employed the BAPC package to project hip OA incidence trends from 2022 to 2050.

To assess the stability of long-term forecasting results, we additionally performed an autoregressive integrated moving average (ARIMA) analysis as a sensitivity analysis based on the same annual time series. For ARIMA model validation, data from 1990 to 2015 were used as the training set, and data from 2016 to 2021 were used as the test set. Forecasting agreement between ARIMA and BAPC was further evaluated by comparing projected values for 2022–2050 using Pearson correlation coefficients, mean absolute percentage error (MAPE), and root mean square error (RMSE). Because BAPC explicitly models age-period-cohort structure and demographic change, it was retained as the primary forecasting framework, whereas ARIMA was used as a complementary time-series model to evaluate model-dependent uncertainty.

3 | Results

3.1 | Global Burden Analysis From 1990 to 2021

Globally, the burden of hip OA increased from 1990 to 2021. Specifically, the age-standardized prevalence rate (ASPR) increased from 391.66 (95% UI 303.26–496.51) cases per 100 000 individuals in 1990 to 416.01 (95% UI 321.23–529.74) cases per 100 000 individuals in 2021, showing an overall upward trend with an AAPC of 0.19 (95% CI 0.15–0.23). Similarly, the incident cases of hip OA in 2021 were around 1.8 million (95% UI 1.4–2.3), with an age-standardized incidence rate (ASIR) increased from 19.27 per 100 000 (95% UI 14.72–24.41) to 20.67 per 100 000 (95% UI 15.76–26.19) over the same period, showing an overall upward trend with an AAPC of 0.22 (95% CI 0.18–0.26). Moreover, the number of DALYs as a result of hip OA was 1.14 million (95% UI 0.54–2.31), with an age-standardized DALYs rate (ASDR) of 13.19 (95% UI 6.20–26.65) per 100 000 population. The ASDR also showed a significant overall increase from 1990 to 2021, with an AAPC of 0.18 (95% CI 0.15–0.22) (Table 1).

At the regional level in 2021, the highest ASIR, ASPR, and ASDR were recorded in high-income North America (ASIR: 45.62 per 100 000, ASPR: 901.22 per 100 000, ASDR: 28.34 per 100 000), while East Asia demonstrated comparatively lower epidemiological metrics (ASIR: 13.81 per 100 000, ASPR: 259.20 per 100 000, ASDR: 8.32 per 100 000) (Table 1 and Figure S1). Notably, although East Asia demonstrated comparatively lower epidemiological levels across all three parameters, it showed one of the most pronounced upward temporal patterns over the study period (Table 1).

In GBD 2021, China, the United States of America, India, and Japan had the largest numbers of hip OA cases, which were approximately 5.47 million (95% UI 4.19–7.11 million), 5.20 million (95% UI 3.95–6.73 million), 3.70 million (95% UI 2.80–4.70 million), and 1.42 million (95% UI 1.08–1.79 million), respectively. In addition, the United States of America (ASIR: 47.32; ASPR: 937; ASDR: 29.42), Iceland (44.24; 850; 27.39), and the United Kingdom (41.80; 810; 25.89) demonstrated the highest age-standardized incidence, prevalence, and DALYs rates per 100 000 population among 204 countries and territories, maintaining consistent ranking patterns across all three metrics (Figure 1A). Among these nations, the United Arab Emirates and Qatar need special attention because of the significantly increasing burden of hip OA observed from 1990 to 2021 (Figure 1B).

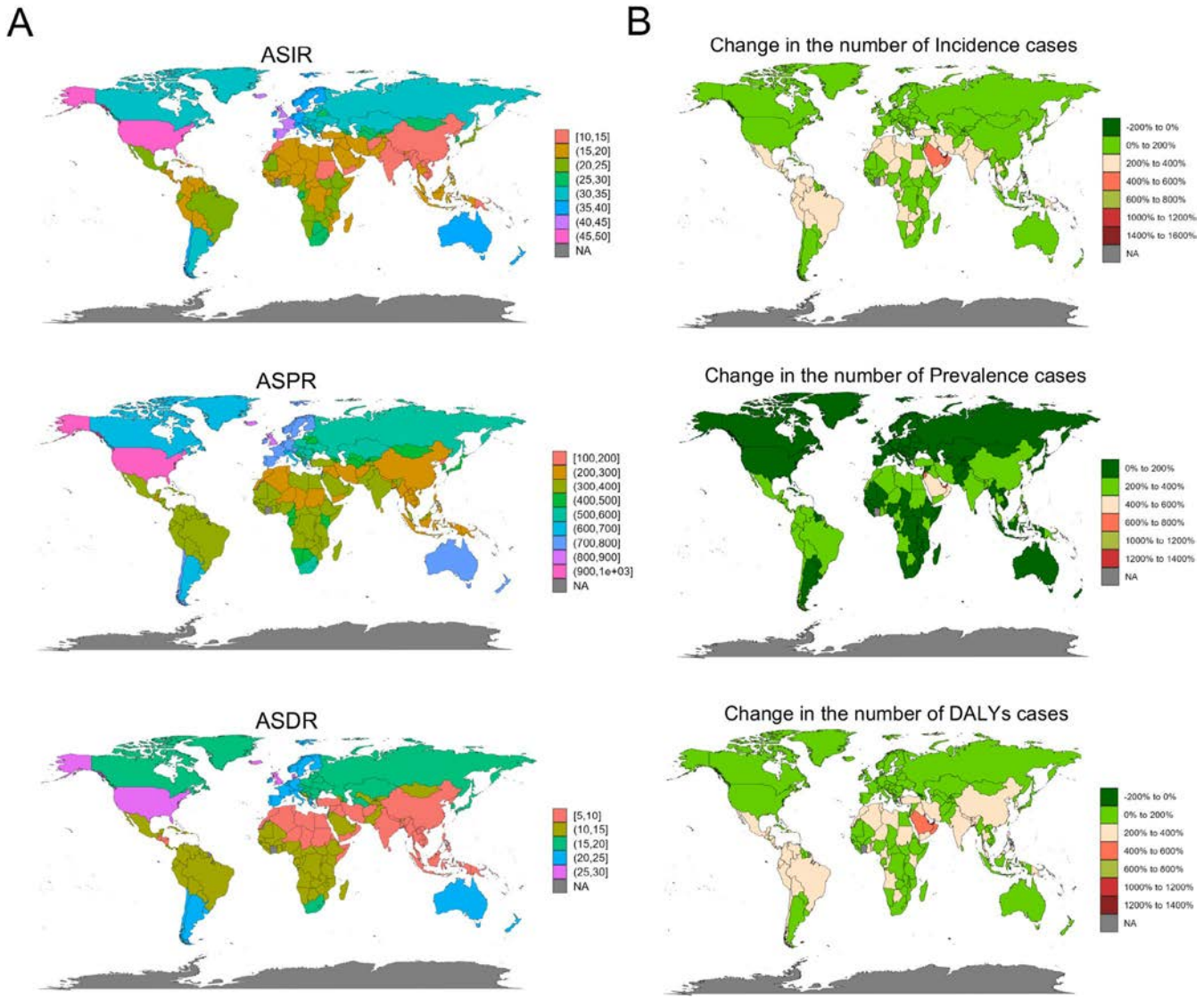

FIGURE 1 | Global burden analysis of hip osteoarthritis from 204 countries and territories. (A) The age-standardized incidence, prevalence, and DALYs rates of hip osteoarthritis in 2021; (B) The percent of the change in the number of incidence, prevalence, and DALYs cases from 1990 to 2021. DALYs, disability-adjusted life years.

3.2 | Age and Sex Patterns

Globally in 2021, hip OA incidence increased with age, with a peak in both sexes within the age range of 55–59 years. Concurrently, the prevalence of hip OA had a parallel temporal pattern, peaking in both sexes at ages 65–69 years (Figure S2). Among patients who were below 70 years old, the ASIR of female patients was greater than that of male patients, but the opposite pattern was found for patients who were above 70 years old (Figure 2A). Yet, there was no notable difference in the prevalence of hip OA between the two sexes or across age groups (Figure 2B).

The DALYs of hip OA in both men and women were unimodally distributed across different age groups; both sexes within the age range of 65–69 years had the highest number of DALYs (83 228 female cases vs. 76 855 male cases) (Figure 2C). Both genders experienced a consistent surge in ASIR, ASPR, and ASDR between 1990 and 2019, followed by a gradual decline through 2021 (Figure S3).

3.3 | Burden by Sociodemographic Index

From 1990 to 2021, the global burden of hip OA was significantly influenced by the SDI. In 2021, the ASIR and ASPR attributable to hip OA were higher in the high SDI quintiles than in the high–middle, middle, low-middle, and low SDI quintiles, with an ASIR of 35.05 cases per 100 000 people and an ASPR of 687.17 per 100 000 people (Figure 3A). However, Joinpoint analysis showed that the most rapid increases over time were observed in low-middle and middle SDI regions rather than in high SDI regions. For incidence, the AAPC was 0.6577 (95% CI 0.6460–0.6694) in low-middle SDI regions and 0.6470 (95% CI 0.6321–0.6619) in middle SDI regions, compared with 0.3683 (95% CI 0.2681–0.4687) in high SDI regions. Similar patterns were observed for prevalence and DALYs. For prevalence, the AAPCs were 0.6500 (95% CI 0.6336–0.6664) in low-middle SDI regions and 0.6322 (95% CI 0.6188–0.6456) in middle SDI regions. For DALYs, the corresponding AAPCs were 0.6519 (95% CI 0.6338–0.6699) and 0.6270 (95% CI 0.6121–0.6420),

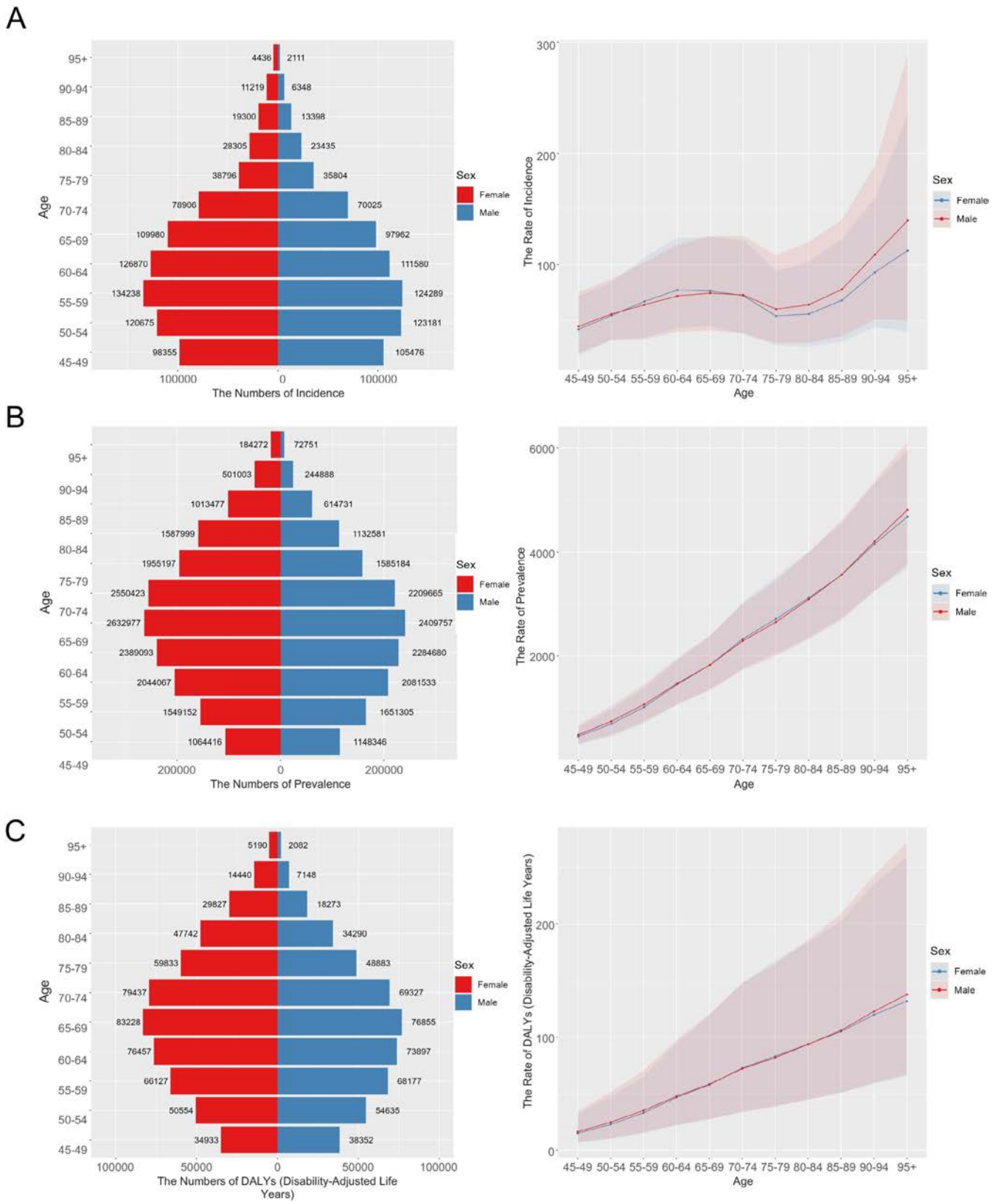

FIGURE 2 | Gender disparities in the burden of hip osteoarthritis in different age groups. (A) Global number and age-standardized rates of incidence (A), prevalence (B), and DALYs (C) of hip osteoarthritis by age and sex, from 1990 to 2021. DALYs, disability-adjusted life-years.

respectively (Figure 3B and Supplementary Table 1). These findings indicate that although the absolute burden remained highest in high SDI settings, the most pronounced long-term increases occurred in transitional SDI regions.

Decomposition analyses for the global population indicated that population growth was the predominant factor behind the increased burden of hip OA. Specifically, population growth contributed 85.37%, 84.87%, and 85.18% to the increase of global

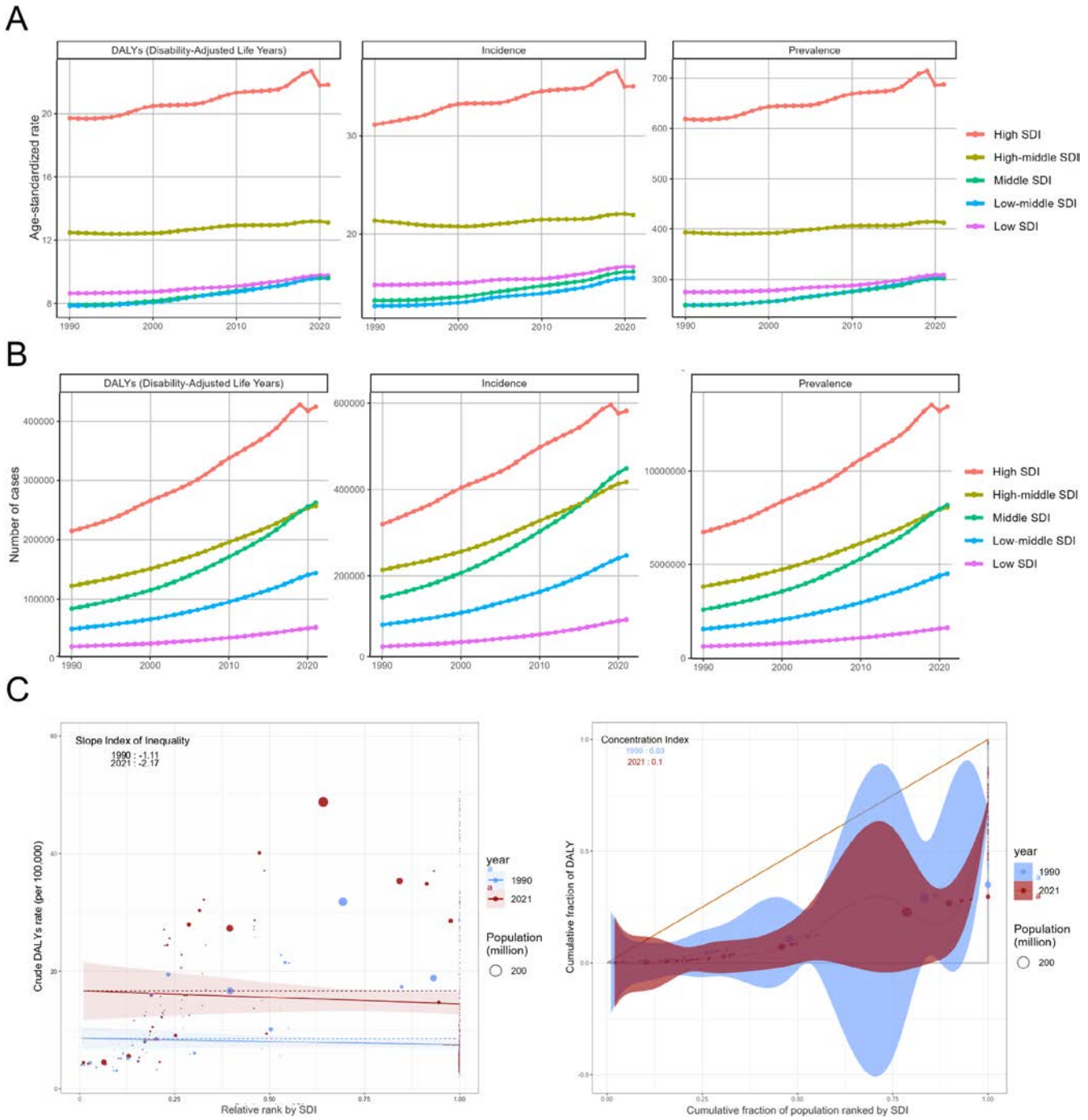

FIGURE 3 | Temporal trend for the burden of hip osteoarthritis by Sociodemographic Index from 1990 to 2021. (A, B) Age-standardized rates (A) and numbers (B) of DALYs, incidence, and prevalence of hip osteoarthritis grouped by different Sociodemographic Index from 1990 to 2021; (C) Health inequality regression curves and concentration curves of DALYs in hip osteoarthritis globally. DALYs, disability-adjusted life-years.

incidence, prevalence, and DALYs during 1990–2021, respectively. Notably, in disparate SDI regions, the trends exhibited consistency with the global trend across the majority of region groups. However, the situation in middle SDI regions diverged from the global trend, with the aging exerting a facilitating effect on the hip OA burden (Figure S4). This may be attributed to the relatively elderly population in middle SDI regions and the insufficient medical support for the aging population.

The hip OA health inequalities during 1990–2021 were further analyzed. For DALYs, the slope index changed from −1.11 to −2.17, and the concentration index increased from 0.03 to 0.1 (Figure 3C). These data suggest that during this period, the health inequalities of hip OA burden continued to aggravate. This increased inequality may be related to inadequate health care resources in low SDI areas.

3.4 | Influence of Risk Factors on Burden of Hip OA

Globally in 2021, 35.5% of DALYs resulting from hip OA were attributable to high BMI, an increase of 21.2% between 1990

and 2021. For sex Patterns, the risk factor in terms of risk-attributable DALYs globally was high BMI in females (risk-attributable DALYs = 36.9%), especially the largest increase in percentage (by 8.8%) was recorded in Southern Sub-Saharan Africa. Regionally, high-income North America, North Africa and the Middle East, and Southern Latin America showed the highest percentages of age-standardized DALYs due to high BMI, which were 46.2%, 45.1%, and 44.6%, respectively (Figure 4A). The most significant increase in percentage increase (by 13.1%) was recorded in East Asia. Nationally, Kuwait, Qatar, and Tonga showed the highest percentages of age-standardized DALYs attributed to high BMI, which were 52.0%, 50.7%, and 50.5%.

3.5 | Mendelian Randomization Mediation Analysis

The two-sample MR analysis was further conducted to assess the relationships between higher BMI and hip OA. Both IVW method and Weighted median method revealed that higher BMI was associated with an increased risk of hip OA (IVW: OR = 1.44, 95% CI: 1.31–1.58; Weighted median: OR = 1.47, 95% CI: 1.29–1.68) (Figure 4B). Further, no single SNP seriously violated GM's overall impact on hip OA in the leave-one-out sensitivity analysis. Next, we performed a reverse MR analysis. Results proved that no obvious causal effect of hip OA on BMI (OR = 1.043, 95% CI: 0.962, 1.132) was detected (Figure 4C).

Studies indicate that changes in BMI are significantly associated with levels of multiple metabolites in plasma, which are involved in lipid metabolism, amino acid metabolism, energy metabolism, and inflammatory pathways, among others. We next detected mediation effects of the blood metabolites between BMI and hip OA. Analysis revealed the total effect of elevated BMI on hip OA risk was $\beta = 0.3719$ (95% CI: 0.2737–0.4701). Mediation testing identified blood metabolite palmitoyl sphingomyelin (PSM) as the significant mediator ($\beta = 0.0183$, 95% CI: 0.0002–0.0365), accounting for 4.9% of the total effect, while the direct effect remained statistically significant ($\beta = 0.3536$, 95% CI: (0.2537–0.4534)) (Figure 4D and Table S2). Product of coefficients tests supported result robustness ($p = 0.041$), suggesting that dysregulation of palmitoyl sphingomyelin may represent a key biological pathway linking BMI to hip OA (Table S2).

3.6 | Projections of Hip OA-Related Disease Burden Using BAPC and ARIMA

The BAPC model was used as the primary approach to project the future burden of hip OA from 2022 to 2050. Under the BAPC framework, the age-standardized incidence and prevalence of hip OA were projected to remain at relatively high levels through 2050, with only modest declines over time and a persistently greater burden in males than in females (Figure 5A,B).

As a sensitivity analysis, ARIMA models were additionally constructed. Temporal validation using data from 1990 to 2015 for training and 2016–2021 for testing showed that ARIMA did not fully reproduce the observed fluctuations in later years (Figure S5). Long-term ARIMA forecasts also differed substantially from the BAPC projections, generally yielding much lower values (Figure S6). These results suggest that the precise magnitude of future burden is model-dependent, although the overall burden is expected to remain substantial.

4 | Discussion

In this study, we presented an updated global assessment of the incidence, prevalence, and DALYs of hip OA from 1990 to 2021, and conducted a comprehensive assessment of the disease burden through comparative, trend, decomposition, health inequality, and predictive analyses. Our findings revealed that the burden of hip OA increased over time globally and in most regions and countries. High-income North America shows the greatest burden of disease in 2021, while China and Thailand need special attention because of the increasing burden of hip OA observed from 1990 to 2021. Additionally, the incidence and prevalence of hip OA increased with age and revealed female preponderance and geographic diversity. High BMI was a risk factor for numerous diseases, including hip OA. In this study, we additionally performed MR analyses as supplementary genetics-based triangulation, which supported the positive association between higher BMI and hip OA. The primary BAPC model suggested that the burden of hip OA would remain substantial through 2050, although model comparison indicated uncertainty in the precise long-term magnitude of the forecasts.

Most cases of hip OA occur in older adults [25]. The primary reason for this phenomenon may be attributed to age-related degenerative changes in joint cartilage, which are strongly associated with epigenetic alterations, telomere attrition, mitochondrial dysfunction, and changes in the mechanical properties of the cell [26, 27]. Researchers have also proposed a potential link between the elevated prevalence in aging populations and lifelong mechanical stress from obesity or occupational joint loading [28, 29]. Additionally, early joint injuries or developmental abnormalities, such as hip dysplasia, were found to significantly increase the likelihood of developing hip OA in later life [30, 31]. Studies on interventions to delay cartilage degeneration and improve functional outcomes in hip OA patients need to be prioritized for these reasons.

The study revealed a marked positive association between SDI and both ASIR and ASPR of hip osteoarthritis, contrasting with an inverse relationship observed between SDI and ASDR. This epidemiological pattern may be potentially driven by optimized health system performance and expanded access to therapeutic interventions in high-SDI settings, effectively mitigating disease-related mortality risks. Notably, middle-SDI regions demonstrated the most pronounced increase in incident cases, where aging emerged as a key amplifier of OA burden. These populations face critical challenges, including underdeveloped healthcare infrastructure, limited social safety nets for chronic musculoskeletal conditions, and constrained capacity to manage treatment-related expenditures. Addressing these disparities through targeted health policy

A

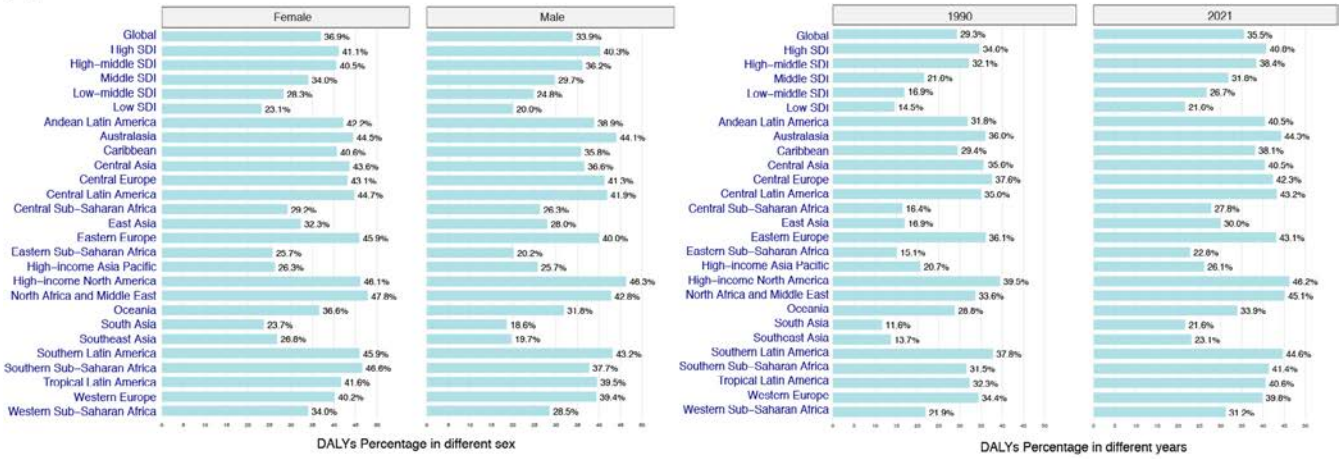

B

Exposure	Outcome	nSNP	Method	OR (95% CI)	P-value
Body mass index	Osteoarthritis (hip)	267	Inverse variance weighted	1.45(1.31 to 1.60)	1.14e-13
		267	MR Egger	1.62(1.22 to 2.13)	0.00080837
		267	Simple mode	1.63(1.06 to 2.50)	0.02618213
		267	Weighted median	1.55(1.35 to 1.77)	4.12e-10
		267	Weighted mode	1.81(1.33 to 2.46)	0.00019428

C

Exposure	Outcome	nSNP	Method	OR (95% CI)	P-value
Osteoarthritis (hip)	Body mass index	21	Inverse variance weighted	1.00(0.97 to 1.02)	0.780999975
Osteoarthritis (hip)	Body mass index	21	MR Egger	1.02(0.95 to 1.11)	0.55591113
Osteoarthritis (hip)	Body mass index	21	Simple mode	1.00(0.97 to 1.03)	0.999384158
Osteoarthritis (hip)	Body mass index	21	Weighted median	1.00(0.98 to 1.02)	0.986778154
Osteoarthritis (hip)	Body mass index	21	Weighted mode	0.99(0.97 to 1.02)	0.614205658

D

Exposure	Outcome	nSNP	Method	OR (95% CI)	P-value
Palmitoyl sphingomyelin	Osteoarthritis (hip)	42	Inverse variance weighted	0.53(0.34 to 0.80)	0.00282667
		42	MR Egger	0.08(0.02 to 0.33)	0.00131563
		42	Simple mode	0.43(0.12 to 1.56)	0.20358454
		42	Weighted median	0.60(0.33 to 1.07)	0.08408907
		42	Weighted mode	0.41(0.14 to 1.17)	0.10291809
Body mass index	Palmitoyl sphingomyelin	118	Inverse variance weighted	0.97(0.95 to 0.99)	0.00512128
		118	MR Egger	0.98(0.91 to 1.05)	0.54095839
		118	Simple mode	0.96(0.90 to 1.04)	0.31262221
		118	Weighted median	0.96(0.94 to 0.99)	0.02088174
		118	Weighted mode	0.96(0.91 to 1.02)	0.19390425

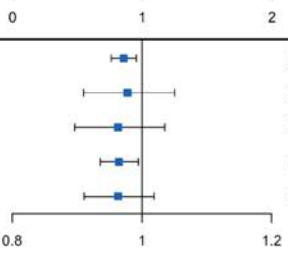

FIGURE 4 | Influence and Mendelian randomization analysis of BMI on the burden of hip OA. (A) Proportion of hip osteoarthritis DALYs attributable to high BMI in 1990 and 2021 from different regions and sex. (B) The associations of BMI with risk of hip osteoarthritis; (C) A reverse MR analysis showed no causal role of hip osteoarthritis on BMI. (D) MR mediation analysis showed the mediation effect of palmitoyl sphingomyelin between BMI and hip osteoarthritis. DALYs, disability-adjusted life years; BMI, body mass index.

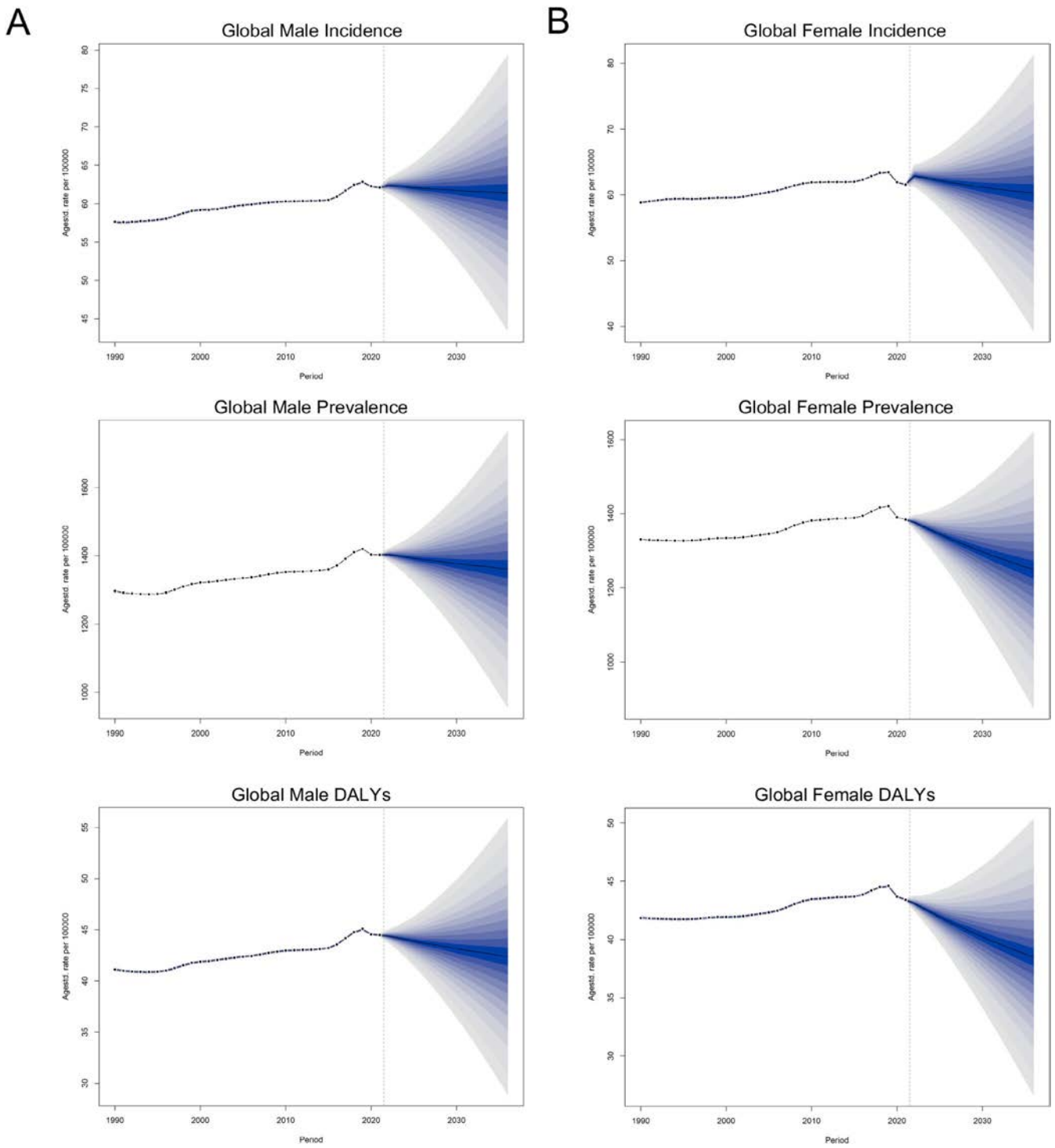

FIGURE 5 | Projection of age-standardized incidence, prevalence, and DALYs of hip osteoarthritis from 2022 to 2050 based on the primary BAPC model. (A) Male; (B) Female. DALYs, disability-adjusted life years. Blue shades are the corresponding confidence intervals.

interventions should constitute a priority in global OA management strategies, particularly within transitional socioeconomic development gradients.

Obesity is considered to be the primary risk factor for OA [32, 33]. Our study established that high BMI is also associated with an increase in the risk of hip OA, accounting for around 35.5% of the DALYs attributable to hip OA, and we further evaluated this association with MR analysis. Some studies have indicated that obesity is more prevalent in high-income countries or regions [34, 35]. This explains why the disease burden is greater in high-SDI areas as well. Our study also revealed that the most significant impact of high BMI on DALYs was in high-income North America, North Africa, and the Middle East, exceeding 45% in these regions, indicating the importance of obesity control programs. These findings not only enhance our understanding of the complexity of the disease but also provide a strong foundation for developing more effective public health measures,

optimizing resource allocation, fostering international cooperation, and advancing scientific research. These efforts aim to improve the quality of life of patients with hip OA and reduce the overall burden of the disease.

Emerging evidence highlights a significant association between elevated BMI and perturbations in sphingolipid metabolism [36]. Asano et al. demonstrated that sphingomyelin synthases modulate lipid raft composition, with sphingomyelin enrichment reducing responsiveness to CXCL12/CXCR4 signaling pathways critical for cell migration and inflammatory regulation [37]. Meanwhile, the CXCL12/CXCR4 axis is a critical mediator in OA progression, primarily through its roles in inflammation, cartilage degradation, and subchondral bone remodeling [38, 39]. However, the causal directionality of the BMI–sphingomyelin relationship remains debated. Future research should prioritize tissue-specific analyses to investigate the tripartite relationship among obesity, phospholipid metabolism, and osteoarthritis. We recommend employing an approach that integrates population-based studies with animal experiments. This dual strategy will not only validate and corroborate our Mendelian randomization findings but also provide mechanistic insights into how lipid metabolic pathways modulate joint degeneration. Such multidisciplinary investigation could ultimately facilitate the development of targeted therapeutic interventions for metabolic osteoarthritis.

The comparison between BAPC and ARIMA forecasts provides additional Insight into the uncertainty of long-term disease burden prediction. In our analysis, ARIMA-based projections diverged substantially from BAPC projections, with nearly inverse forecast trajectories and markedly lower ARIMA estimates in later years. This discrepancy is likely attributable to the different statistical assumptions underlying the two models. BAPC explicitly incorporates age-period-cohort structure and is therefore better suited to long-term epidemiological forecasting in settings where demographic transition and population aging are major drivers of disease burden. In contrast, ARIMA relies primarily on autocorrelation and recent time-series behavior, making it more sensitive to short-term fluctuations and recent changes in the observed data. Therefore, although ARIMA served as a useful sensitivity analysis and short-term validation framework, BAPC was considered more appropriate as the primary model for long-term burden projection in this study.

This study has several limitations. First, as with all GBD-based analyses, the estimates depend on the quality and completeness of the underlying data sources and modeling framework. Second, some descriptive burden analyses overlap with recently published GBD 2021-based hip OA studies; therefore, the present work should be interpreted as an integrative extension rather than a wholly novel epidemiological description. Third, because the GWAS datasets used for MR were primarily derived from individuals of European ancestry, the generalizability of the genetic findings to other populations is limited. Fourth, although high BMI was identified as an important contributor to hip OA burden, other relevant risk factors, such as hip dysplasia, occupational loading, and a history of hip injury or surgery, could not be quantitatively assessed within the current GBD framework. Finally, the mediation effect explained by palmitoyl sphingomyelin was modest, suggesting that additional mediators are likely involved; therefore, this finding should be interpreted as exploratory rather than definitive.

5 | Conclusions

Our study provides an updated overview of the global epidemiological trends and risk factors for hip osteoarthritis. These findings help formulate policies and allocate resources. Further research is necessary to investigate additional risk factors to inform early prevention strategies at the earliest stages of the disease.

Author Contributions

X.S. contributed to project administration, drafting, and data analysis. C.L. contributed to validation, data analysis, and visualization. J.Y. and Z.C. contributed to data collection and collation. X.D. contributed to supervision, drafting, and editing. All authors read and approved the final manuscript.

Acknowledgments

We thank those who provided GWAS data for the study. We thank them for obtaining GWAS data from various studies.

Funding

This work was financially supported by the Scientific Research Project of Tianjin Education Commission (Natural Science) [2024ZX016].

Ethics Statement

The requirement of ethical approval for the study was approved by the Institutional Review Board of Tianjin Stomatological Hospital of Nankai University. All methods were performed in accordance with the relevant guidelines and regulations.

Consent

The study did not need ethics approval because it used publicly available data. This study followed the Guidelines for Accurate and Transparent Health Estimates Reporting Guidelines for cross-sectional studies.

Conflicts of Interest

The authors declare no conflicts of interest.

Data Availability Statement

The data that support the findings of this study are available in the GWAS Catalog at https://www.ebi.ac.uk/gwas/. These data were derived from the following resources available in the public domain: -Genome-wide association studies, https://gwas.mrcieu.ac.uk/.

References

1. S. Glyn-Jones, A. J. Palmer, R. Agricola, et al., "Osteoarthritis," *Lancet* 386 (2015): 376–387.

2. G.B.D.O. Collaborators, "Global, Regional, and National Burden of Osteoarthritis, 1990-2020 and Projections to 2050: A Systematic Analysis for the Global Burden of Disease Study 2021," *Lancet Rheumatology* 5 (2023): e508-e522.

3. I. N. Ackerman, R. Buchbinder, and L. March, "Global Burden of Disease Study 2019: An Opportunity to Understand the Growing Prevalence and Impact of Hip, Knee, Hand and Other Osteoarthritis in Australia," *Internal Medicine Journal* 53 (2023): 1875–1882.

4. Q. Weng, Q. Chen, T. Jiang, et al., "Global Burden of Early-Onset Osteoarthritis, 1990-2019: Results From the Global Burden of Disease Study 2019," *Annals of the Rheumatic Diseases* 83 (2024): 915–925.

5. V. P. Leifer, J. N. Katz, and E. Losina, "The Burden of OA-Health Services and Economics," *Osteoarthritis and Cartilage* 30 (2022): 10–16.

6. H. Long, Q. Liu, H. Yin, et al., "Prevalence Trends of Site-Specific Osteoarthritis From 1990 to 2019: Findings From the Global Burden of Disease Study 2019," *Arthritis and Rheumatology* 74 (2022): 1172–1183.

7. R. Giorgino, D. Albano, S. Fusco, G. M. Peretti, L. Mangiavini, and C. Messina, "Knee Osteoarthritis: Epidemiology, Pathogenesis, and Mesenchymal Stem Cells: What Else Is New? An Update," *International Journal of Molecular Sciences* 24 (2023): 6405.

8. S. Safiri, A. A. Kolahi, E. Smith, et al., "Global, Regional and National Burden of Osteoarthritis 1990-2017: A Systematic Analysis of the Global Burden of Disease Study 2017," *Annals of the Rheumatic Diseases* 79 (2020): 819–828.

9. A. Cui, H. Li, D. Wang, J. Zhong, Y. Chen, and H. Lu, "Global, Regional Prevalence, Incidence and Risk Factors of Knee Osteoarthritis in Population-Based Studies," *EClinicalMedicine* 29-30 (2020): 100587.

10. G. Yang, J. Wang, Y. Liu, et al., "Burden of Knee Osteoarthritis in 204 Countries and Territories, 1990-2019: Results From the Global Burden of Disease Study 2019," *Arthritis Care & Research (Hoboken)* 75 (2023): 2489–2500.

11. M. Hall, M. van der Esch, R. S. Hinman, et al., "How Does Hip Osteoarthritis Differ From Knee Osteoarthritis?," *Osteoarthritis and Cartilage* 30 (2022): 32–41.

12. G.B.D. Diseases, and C. Injuries, "Global Incidence, Prevalence, Years Lived With Disability (YLDs), disability-Adjusted Life-Years (DALYs), and Healthy Life Expectancy (HALE) for 371 Diseases and Injuries in 204 Countries and Territories and 811 Subnational Locations, 1990-2021: A Systematic Analysis for the Global Burden of Disease Study 2021," *Lancet* 403 (2024): 2133–2161.

13. M. Fu, H. Zhou, Y. Li, H. Jin, and X. Liu, "Global, Regional, and National Burdens of Hip Osteoarthritis From 1990 to 2019: Estimates From the 2019 Global Burden of Disease Study," *Arthritis Research & Therapy* 24 (2022): 8.

14. A. A. Kiadaliri, L. S. Lohmander, M. Moradi-Lakeh, I. F. Petersson, and M. Englund, "High and Rising Burden of Hip and Knee Osteoarthritis in the Nordic Region, 1990-2015," *Acta Orthopaedica* 89 (2018): 177–183.

15. S. J. Nho, S. M. Kymes, J. J. Callaghan, and D. T. Felson, "The Burden of Hip Osteoarthritis in the United States: Epidemiologic and Economic Considerations," *Journal of the American Academy of Orthopaedic Surgeons* 21, no. Suppl 1 (2013): S1–S6.

16. A. H. Hoveidaei, A. Nakhostin-Ansari, S. H. Hosseini-Asl, et al., "Increasing Burden of Hip Osteoarthritis in the Middle East and North Africa (MENA): An Epidemiological Analysis From 1990 to 2019," *Archives of Orthopaedic and Trauma Surgery* 143 (2023): 3563–3573.

17. H. Z. Li, X. Z. Liang, Y. Q. Sun, H. F. Jia, J. C. Li, and G. Li, "Global, Regional, and National Burdens of Osteoarthritis From 1990 to 2021: Findings From the 2021 Global Burden of Disease Study," *Frontiers in Medicine (Lausanne)* 11 (2024): 1476853.

18. G.B.D.R.F. Collaborators, "Global Burden and Strength of Evidence for 88 Risk Factors in 204 Countries and 811 Subnational Locations, 1990-2021: A Systematic Analysis for the Global Burden of Disease Study 2021," *Lancet* 403 (2024): 2162–2203.

19. Y. Wang, Y. Wang, L. Fan, and Y. Yu, "The Burden of Severe Periodontitis in China From 1990 to 2021, With Projections to 2050: A Comprehensive Analysis From the Global Burden of Disease Study 2021," *International Dental Journal* 75 (2025): 32–44.

20. Z. Cao, Y. Wu, Q. Li, Y. Li, and J. Wu, "A Causal Relationship Between Childhood Obesity and Risk of Osteoarthritis: Results From a Two-Sample Mendelian Randomization Analysis," *Annals of Medicine* 54 (2022): 1636–1645.

21. I. Tachmazidou, K. Hatzikotoulas, L. Southam, et al., "Identification of New Therapeutic Targets for Osteoarthritis Through Genome-Wide Analyses of UK Biobank Data," *Nature Genetics* 51 (2019): 230–236.

22. S. Y. Shin, E. B. Fauman, A. K. Petersen, et al., "An Atlas of Genetic Influences on Human Blood Metabolites," *Nature Genetics* 46 (2014): 543–550.

23. G.B.D.F. Collaborators, "Burden of Disease Scenarios for 204 Countries and Territories, 2022-2050: A Forecasting Analysis for the Global Burden of Disease Study 2021," *Lancet* 403 (2024): 2204–2256.

24. E. Kiyoshige, S. Ogata, M. O'Flaherty, et al., "Projections of Future Coronary Heart Disease and Stroke Mortality in Japan Until 2040: A Bayesian Age-Period-Cohort Analysis," *Lancet Regional Health - Western Pacific* 31 (2023): 100637.

25. W. Hu, Y. Chen, C. Dou, and S. Dong, "Microenvironment in Subchondral Bone: Predominant Regulator for the Treatment of Osteoarthritis," *Annals of the Rheumatic Diseases* 80 (2021): 413–422.

26. S. Wakale, X. Wu, Y. Sonar, et al., "How Are Aging and Osteoarthritis Related?," *Aging and Disease* 14 (2023): 592–604.

27. L. Zheng, Z. Zhang, P. Sheng, and A. Mobasheri, "The Role of Metabolism in Chondrocyte Dysfunction and the Progression of Osteoarthritis," *Ageing Research Reviews* 66 (2021): 101249.

28. T. Wang and C. He, "Pro-Inflammatory Cytokines: The Link Between Obesity and Osteoarthritis," *Cytokine & Growth Factor Reviews* 44 (2018): 38–50.

29. C. Lewis, J. A. Jackson, A. Stjernbrandt, et al., "Occupational Risk Factors for Thumb Carpometacarpal Joint Osteoarthritis: A Register-Based Study of Construction Workers," *Occupational and Environmental Medicine* 82 (2025): 14–20.

30. Y. Sun, Y. You, Q. Wu, R. Hu, and K. Dai, "Genetically Inspired Organoids Prevent Joint Degeneration and Alleviate Chondrocyte Senescence via Col11a1-HIF1alpha-Mediated Glycolysis-OXPHOS Metabolism Shift," *Clinical and Translational Medicine* 14 (2024): e1574.

31. C. L. Peters, "Mild to Moderate Hip OA: Joint Preservation or Total Hip Arthroplasty?," *Journal of Arthroplasty* 30 (2015): 1109–1112.

32. A. Batushansky, S. Zhu, R. K. Komaravolu, S. South, P. Mehta-D'souza, and T. M. Griffin, "Fundamentals of OA. An Initiative of Osteoarthritis and Cartilage. Obesity and Metabolic Factors in OA," *Osteoarthritis and Cartilage* 30 (2022): 501–515.

33. Z. Yao, W. Qi, H. Zhang, et al., "Down-Regulated GAS6 Impairs Synovial Macrophage Efferocytosis and Promotes Obesity-Associated Osteoarthritis," *eLife* 12 (2023): e83069.

34. G.B.D.O. Collaborators, A. Afshin, M. H. Forouzanfar, et al., "Health Effects of Overweight and Obesity in 195 Countries Over 25 Years," *New England Journal of Medicine* 377 (2017): 13–27.

35. G. A. Hawker and L. K. King, "The Burden of Osteoarthritis in Older Adults," *Clinics in Geriatric Medicine* 38 (2022): 181–192.

36. C. D. Green, M. Maceyka, L. A. Cowart, and S. Spiegel, "Sphingolipids in Metabolic Disease: The Good, the Bad, and the Unknown," *Cell Metabolism* 33 (2021): 1293–1306.

37. S. Asano, K. Kitatani, M. Taniguchi, et al., "Regulation of Cell Migration by Sphingomyelin Synthases: Sphingomyelin in Lipid Rafts Decreases Responsiveness to Signaling by the CXCL12/CXCR4 Pathway," *Molecular and Cellular Biology* 32 (2012): 3242–3252.

38. A. Hildebrandt, T. Dietrich, J. Weber, et al., "The Dual Pro-Inflammatory and Bone-Protective Role of Calcitonin Gene-Related Peptide Alpha in Age-Related Osteoarthritis," *Arthritis Research & Therapy* 25 (2023): 244.

39. J. Li, H. Chen, D. Zhang, J. Xie, and X. Zhou, "The Role of Stromal Cell-Derived Factor 1 on Cartilage Development and Disease," *Osteoarthritis and Cartilage* 29 (2021): 313–322.

Supporting Information

Additional supporting information can be found online in the Supporting Information section. **Figure S1:** Regional distribution of the burden of hip osteoarthritis. Age-standardized incidence, DALY, and prevalence rates of hip osteoarthritis across different GBD regions. Bars indicate estimated age-standardized rates, and error bars indicate the corresponding 95% uncertainty intervals. **Figure S2:** Age-specific burden of hip osteoarthritis. Numbers and age-standardized rates of hip osteoarthritis-related incidence, DALYs, and prevalence across different age groups. The left panels show the number of cases, and the right panels show the corresponding age-standardized rates. Error bars indicate 95% uncertainty intervals. **Figure S3:** Temporal trends in the sex-specific burden of hip osteoarthritis from 1990 to 2021. Age-standardized incidence, DALY, and prevalence rates of hip osteoarthritis are shown by sex from 1990 to 2021. Lines represent estimates for both sexes combined, females, and males. **Figure S4:** Decomposition analysis of changes in the hip osteoarthritis burden from 1990 to 2021. Changes in the number of incident cases, prevalent cases, and DALYs attributable to hip osteoarthritis were decomposed into the contributions of population growth, population aging, and epidemiological change across global and SDI regions. Stacked bars indicate the contribution of each component, and black dots indicate the overall net change. **Figure S5:** Temporal validation of ARIMA models for hip osteoarthritis burden estimates. ARIMA models were trained using age-standardized rates from 1990 to 2015 and validated against observed data from 2016 to 2021. The panels show validation results for incidence, prevalence, and DALYs stratified by sex. Blue dashed lines indicate ARIMA-predicted values, and black solid lines indicate observed values. **Figure S6:** Robustness comparison between BAPC and ARIMA projections for hip osteoarthritis burden. Projected age-standardized rates of hip osteoarthritis-related incidence, prevalence, and DALYs from 2022 to 2050 were compared between Bayesian age-period-cohort and ARIMA models by sex. Red solid lines indicate BAPC projections, and blue dashed lines indicate ARIMA projections. **Table S1:** Change in the number of incidence cases among different SDI regions, with the AAPC from 1990 to 2021. **Table S2:** Mediation effect of BMI on hip OA via blood metabolites.

International Journal of Rheumatic Diseases

WILEY

International Journal of Rheumatic Diseases

CLINICAL IMAGE

Pericaval Fat Collection in a Patient With Systemic Juvenile Idiopathic Arthritis

Masaki Shimizu[1] | Chinatsu Kaneko[2] | Maho Hatano[2] | Hitoshi Irabu[2] | Yuko Hayashi[1] | Taku Ishii[1]

[1]Department of Pediatrics, Perinatal and Maternal Medicine, Graduate School of Medical and Dental Sciences, Institute of Science Tokyo, Tokyo, Japan | [2]Department of Pediatrics and Developmental Biology, Graduate School of Medical and Dental Sciences, Institute of Science Tokyo, Tokyo, Japan

Correspondence: Masaki Shimizu (mshimizu.ped@tmd.ac.jp)

Received: 26 December 2025 | **Revised:** 13 May 2026 | **Accepted:** 24 May 2026

Keywords: obesity | pericaval fat collection | systemic juvenile idiopathic arthritis

A 3-year-old girl presented fever, rash and polyarthritis, and was diagnosed with systemic juvenile idiopathic arthritis (s-JIA). She exhibited resistance to tocilizumab, canakinumab, tacrolimus, cyclosporine (CyA), colchicine and iguratimod following a glucocorticoids (GCs)-dependent course with frequent relapses complicated with macrophage activation syndrome (MAS). At the age of 11 years, she developed MAS refractory to high-dose GCs and CyA was referred to us. Cardiac ultrasound examination performed at admission showed pericardial effusion. The patient received treatment with ruxolitinib in combination with high-dose GCs and CyA and achieved remission. Echocardiography for pericardial effusion reassessment 4 months later showed no effusion but revealed a new, non-mobile, adhesive, hyperechoic lesion measuring 1.2 cm × 1.2 cm in the inferior vena cava (IVC) distal to the hepatic vein junction (Figure 1a). Blood tests indicated no significant abnormal findings. Contrast-enhanced computed tomography revealed no thrombosis but showed low density adipose tissue with no contrast enhancement surrounding the IVC protruding into the IVC at the level of the liver (Figure 1b). From these findings,

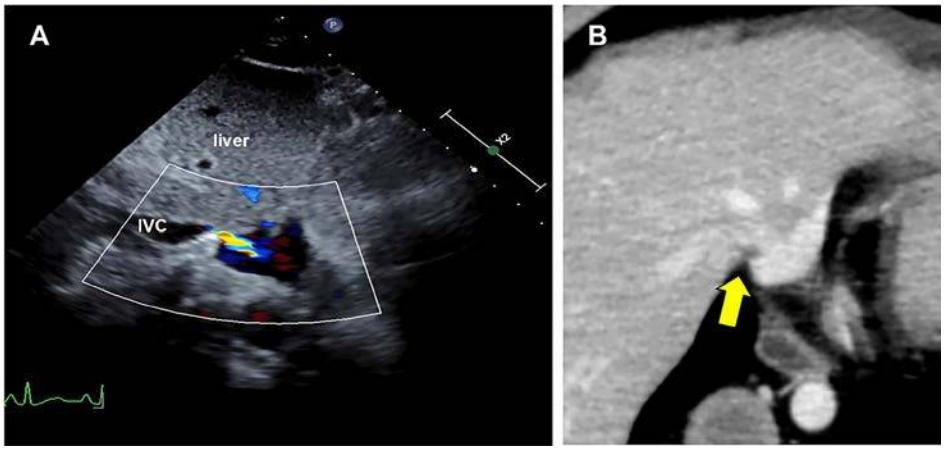

FIGURE 1 | Cardiac ultrasound finding. A non-mobile, adhesive, hyperechoic lesion measuring 1.2 cm × 1.2 cm was found in the inferior vena cava (IVC) distal to the hepatic vein junction. Contrast-enhanced computed tomography finding. Low density adipose tissue with no contrast enhancement surrounding the inferior vena cava was observed protruding into the inferior vena cava at the level of the liver (yellow arrow).

Abbreviation: IVC, inferior vena cava.

the diagnosis of pericaval fat collection was made. The patient's height, weight, and body mass index were 108.3 cm, 31.3 kg, and 26.7, respectively.

Pericaval fat collection is a normal variant in which fatty tissues surrounding the IVC protrude into the IVC at the level of the liver, and fat from around the esophagus or stomach may extend into the IVC, resembling a tumor or thrombus. They are most commonly located at the confluence of the hepatic veins and can be oval, round, or linear in shape [1–4]. Pericaval fat collection is observed in 0.5%–5% of normal individuals but is more common in patients with chronic liver disease, cirrhosis, and obesity [1–4]. Pericaval fat collection may be rare in children, but it should be considered in pediatric patients with rheumatic diseases receiving high-dose GCs.

Author Contributions

All authors contributed to the study conception and design. Material preparation, data collection were performed by M.S., C.K., M.H., H.I. and Y.H. and supervision by T.I. The first draft of the manuscript was written by M.S. All authors read and approved the final manuscript.

Acknowledgments

We would also like to thank Dr. Yuko Akutsu, Dr. Futaba Miyaoka, and Dr. Shuya Kaneko for a helpful discussion.

Funding

The authors have nothing to report.

Ethics Statement

Ethical approval was not required for this case report. The work was conducted in accordance with ethical standards and patient confidentiality was fully respected.

Consent

Written informed consent was obtained from the patient and the patient's parents.

Conflicts of Interest

The authors declare no conflicts of interest.

Data Availability Statement

The data that support the findings of this study are available on request from the corresponding author. The data are not publicly available due to privacy or ethical restrictions.

References

1. B. K. Han, J. G. Im, J. W. Jung, M. J. Chung, and K. M. Yeon, "Pericaval Fat Collection That Mimics Thrombosis of the Inferior Vena Cava: Demonstration With Use of Multi-Directional Reformation CT," *Radiology* 203 (1997): 105–108, https://doi.org/10.1148/radiology.203.1.9122375.

2. J. Hines, D. S. Katz, L. Goffner, and G. D. Rubin, "Fat Collection Related to the Intrahepatic Inferior Vena Cava on CT," *AJR. American Journal of Roentgenology* 172 (1999): 409–411, https://doi.org/10.2214/ajr.172.2.9930793.

3. N. L. Raju and J. H. Austin, "Case 37: Juxtacaval Fat Collection—Mimic of Lipoma in the Subdiaphragmatic Inferior Vena Cava," *Radiology* 220 (2001): 471–473, https://doi.org/10.1148/radiology.220.2.r01au12471.

4. H. Miyake, K. Suzuki, S. Ueda, Y. Yamada, H. Takeda, and H. Mori, "Localized Fat Collection Adjacent to the Intrahepatic Portion of the Inferior Vena Cava: A Normal Variant on CT," *AJR. American Journal of Roentgenology* 158 (1992): 423–425, https://doi.org/10.2214/ajr.158.2.1729801.

International Journal of Rheumatic Diseases

WILEY

International Journal of Rheumatic Diseases

CORRECTION

Correction to "The Asia-Pacific League of Associations for Rheumatology Consensus Recommendations on the Management of Juvenile Idiopathic Arthritis (JIA): Polyarticular Course JIA, Temporomandibular Joint Arthritis, Imaging, and Non-Pharmacologic Therapies"

T. Arkachaisri, K. L. Teh, S. Vilaiyuk, et al., "The Asia-Pacific League of Associations for Rheumatology Consensus Recommendations on the Management of Juvenile Idiopathic Arthritis (JIA): Polyarticular Course JIA, Temporomandibular Joint Arthritis, Imaging, and Non-Pharmacologic Therapies," *International Journal of Rheumatic Diseases* 29, no. 4 (2026): e70640, https://doi.org/10.1111/1756-185x.70640.

The above article was published as "Review". It should be "Guideline".

The online article has been corrected.